LATVIJAS UNIVERSITĀTE

ĶĪMIJAS FAKULTĀTE

Artis Kons

PULVERA RENTGENDIFRAKCIJAS UN APRĒĶINU METOŽU IZMANTOŠANA IZVĒLĒTU FARMACEITISKI AKTĪVU VIELU POLIMORFO FORMU STRUKTURĀLAJIEM PĒTĪJUMIEM

PROMOCIJAS DARBS

Doktora grāda iegūšanai ķīmijas nozarē

Apakšnozare: fizikālā ķīmija

Darba vadītājs

asoc. prof. *Dr. chem.* Agris Bērziņš

RĪGA, 2021

Promocijas darbs izstrādāts Latvijas Universitātes Ķīmijas fakultātes Fizikālās ķīmijas katedrā laika posmā no 2014. gada līdz 2020. gadam.

LATVIJAS
UNIVERSITĀTE

Darbs sastāv no kopsavilkumiem latviešu un angļu valodā un no piecām zinātniskajām publikācijām. Darba forma: publikāciju kopa ķīmijā, fizikālajā ķīmijā.

Darba vadītājs:
asoc. prof. *Dr. chem.* **Agris Bērziņš**

Darba recenzenti:
1) prof. *Dr. chem.* **Donāts Erts** (Latvijas Universitāte)
2) *Dr. chem.* **Mihails Arhangelskis** (Varšavas Universitāte)
3) prof. *Dr. chem.* **Fabrīcija Grepioni** (Boloņas Universitāte)

Promocijas darba aizstāvēšana notiks 2021. gada 23. augustā plkst. 14.00 Latvijas Universitātes Ķīmijas nozares promocijas padomes atklātā sēdē, Latvijas Universitātē, Ķīmijas fakultātē, Jelgavas ielā 1, Rīgā.

Ar promocijas darbu var iepazīties LU Bibliotēkas daudznozaru bibliotēkā: datorika, juridiskās zinātnes, teoloģija (Rīgā, Raiņa bulvārī 19).

ISBN 978-9934-18-693-6
ISBN 978-9934-18-694-3 (PDF)

ANOTĀCIJA

Darbā pētītas vairākas farmaceitiski aktīvas vielas, kas izvēlētas, pamatojoties uz to spēju veidot daudzas sīkkristāliskas polimorfās formas. Izpētīta šo savienojumu kristālisko cietfāžu daudzveidība, veicot polimorfo formu un solvātu/hidrātu iegūšanu no dažādiem šķīdinātājiem. Iegūtās kristāliskās cietfāzes raksturotas ar rentgendifraktometriju, termiskās analīzes metodēm un dažādiem fāžu stabilitātes raksturošanas paņēmieniem. No pulvera rentgendifrakcijas datiem noteiktas 33 mikrokristālisku polimorfu un saistītu solvātu struktūras. Kristālisko struktūru optimizācijai, validācijai un enerģijas aprēķiniem pielietota dispersijas koriģēta blīvuma funkcionāļa teorija. Kristāliskās struktūras informācija izmantota, lai racionalizētu iegūto polimorfu veidošanos, fāžu pārejas un savstarpējo termodinamisko stabilitāti.

Atslēgvārdi: *polimorfisms, termodinamiskā stabilitāte, mikrokristālisks pulveris, pulvera rentgendifraktometrija, struktūru noteikšana, dispersijas koriģēta blīvuma funkcionāļa teorija*

SATURS / CONTENTS

IEVADS

Daudzas organiskas vielas, tai skaitā farmaceitiski aktīvās cietvielas (FAV), veido vairākas polimorfās modifikācijas (t. i., fāzes ar identisku ķīmisko sastāvu, bet atšķirīgu kristālisko struktūru). Lai gan šis fenomens ir zināms jau vismaz 180 gadus, tieši pēdējās divās desmitgadēs šajā jomā ir novērojams būtisks pētnieciskās aktivitātes pieaugums, ko virza gan fundamentāla zinātnes attīstība, gan rūpnieciskā nepieciešamība.

Polimorfām formām ir iespējama atšķirīga stabilitāte[1], mehāniskās īpašības[2] un biopiejamība[3], kas ir īpaši svarīgi FAV. Tādējādi svarīgākie polimorfisma izpētes aspekti ir formu atklāšana, fizikāli ķīmisko īpašību izpratne, struktūras raksturojums, kā arī uzticamas un reproducējamas metodes izstrāde katras specifiskās formas iegūšanai.

Tiecoties izprast polimorfisma parādību, ir ļoti svarīgi atrast un izpētīt tādas sistēmas, kas demonstrē daudzskaitlīgu polimorfismu un sastāv no vairākiem labi raksturotiem polimorfiem. Lai gan lielākajai daļai publicēto polimorfo sistēmu ir tikai divi zināmi polimorfi, savienojumi ar lielāku polimorfo formu daudzveidību sniedz labākas iespējas izpētīt polimorfisma parādības pamata aspektus. Atklājot un raksturojot jaunas sistēmas ar lielu polimorfo formu daudzveidību, tiek uzlabota izpratne par polimorfismu.

Cietvielu fāžu daudzveidība var būt ļoti atšķirīga. Eksistē savienojumi, kas veido tikai monomorfus[4], bet ir arī vielas, kurām ir zināmas vairāk nekā 10 polimorfās formas. Ja ņem vērā arī solvātu (t. i., fāzes, kurām kristālrežģī ir šķīdinātāja molekulas) veidošanos, tad kopējais vienas FAV veidotais fāžu skaits var sasniegt pat vairāk nekā 100 formas[5]. Pašlaik lielākais publicēto polimorfo formu skaits ir savienojumam 5-metil-2-[(2-nitrofenil)amino]-3-tiofēnkarbonitrils (ROY)[1,6–10] ar 13 strukturāli raksturotiem polimorfiem, tālāk seko R-enceniklīna hidrogēnhlorīds[11,12] un galunisertibs[13] ar 10 noteiktām kristāliskajām struktūrām, tad aripriprazols[14] un nikotīnamīds[15] ar 9 struktūrām, flufenamīnskābe[16] un tolfenamīnskābe[17,18] ar 8 struktūrām. Jāuzsver, ka Kembridžas strukturālajā datubāzē ir atrodams, ka savienojumi ar vairāk nekā 3 strukturāli raksturotiem polimorfiem ir ļoti reti sastopami.

Vielas tendence veidot solvātus var ierobežot iespēju kristalizēt nesolvatētas fāzes, taču tajā pašā laikā tā paver iespēju desolvatācijas ceļā iegūt tādus jaunus polimorfus, kurus nav iespējams iegūt ar standarta kristalizācijas metodēm[19]. Lai gan jaunu polimorfu iegūšana, desolvatējot solvātus, nav nekas jauns, informācija par šādi iegūtu fāžu kristāliskajām struktūrām bieži paliek nezināma, jo šīs formas tiek iegūtas nevis monokristālu, bet gan sīkkristālisku pulveru veidā. Tomēr kristāliskai struktūrai ir nozīmīga loma, lai spētu izprast vielas fizikālķīmiskās īpašības, tādēļ struktūras noteikšana, izmantojot pulvera rentgendifrakcijas datus, veiksmīgi ir pielietojama kā tuvākā alternatīva monokristāla rentgendifrakcijai.

Šī pētījuma **mērķis** ir izpētīt izteikti polimorfiskas farmaceitiski aktīvu vielu sistēmas, izmantojot integrētu eksperimentālās un datormodelēšanas pētīšanas metodikas pieeju, lai noteiktu šo formu veidošanās strukturālos un termodinamiskos aspektus.

Izvirzīti šādi **uzdevumi**:

1) noteikt hifenadīna hidrogēnhlorīda, sehifenadīna hidrogēnhlorīda, enceniklīna hidrogēnhlorīda un datrolēna kristālisko fāžu daudzveidību ar kristalizācijas un cietfāžu pārejas eksperimentiem;
2) ar rentgendifrakcijas un termiskās analīzes metodēm raksturot iegūtās kristāliskās formas;
3) noteikt iegūto nesolvatēto polimorfo formu un saistīto solvātu (ja ir) struktūras no pulvera vai monokristāla rentgendifrakcijas datiem;
4) veikt vienīgā molekulārā savienojuma – dantrolēna polimorfu kristālisko struktūru paredzēšanas aprēķinus;
5) veikt iegūto cietfāžu kristālisko struktūru analīzi un kvantu ķīmiskos aprēķinus, racionalizējot polimorfo formu veidošanos, stabilitāti un fāžu pārejas.

Zinātniskā novitāte

1. Enceniklīna hidrogēnhlorīda spēja veidot dažādās starpmolekulārās mijiedarbības, kas nodrošina iespējas efektīvam pakojumam pie dažāda jonu novietojuma kristāliskajā stāvoklī, ļauj šim savienojumam veidot rekordlielu (10) pakojuma polimorfu skaitu, kas ir unikāls gadījums, jo citu literatūrā publicētu savienojumu augsto polimorfo formu daudzveidību nodrošina tieši konformāciju atšķirības.
2. Iegūto polimorfo formu stabilitātes noteikšanai izmantota pieeja, apvienojot teorētiskos aprēķinus ar nepilnīgu informāciju par stabilitāti no eksperimentālajiem datiem. Izmantojot šādu pieeju, var iegūt uzticamākus secinājumus par stabilitāti visā temperatūras intervālā sistēmām, kurām dažādu iemeslu dēļ nav to iespējams noteikt tikai ar eksperimentālām metodēm.
3. Darbā racionalizētas polimorfo formu rašanās iespējas, stabilitāte un fāžu pārejas, izmantojot struktūras, kas noteiktas no sīkkristāliskām fāzēm ar pulvera rentgendifrakciju, kas nebūtu paveicams, izmantojot tradicionālās struktūras noteikšanas metodes.

Praktiskā nozīme

1. Attīstīta vairāku FAV polimorfo formu iegūšanas metodika, desolvatējot solvātus, kas apstiprināta ar teorētiskajiem aprēķiniem. Šo metodiku iespējams pielietot jaunu stabilu, tai skaitā patentējamu, formu iegūšanai, kas ļauj lielākam skaitam farmācijas uzņēmumu ražot izteikti polimorfiskus preperātus, tādējādi paplašinot pieeju tirgum un samazinot to cenu gala patērētājam.
2. Gūta vispārīga izpratne par polimorfo formu rašanās iemesliem, kas sekmē ātru un uzticamu jaunu formu iegūšanu un to stabilitātes paredzēšanu konkrētos apstākļos.
3. Detalizēti raksturotas sistēmas, ieskaitot stabilitātes pētījumus, ļauj veikt pamatotāku komerciālās formas izvēli, tai skaitā, nodrošinot garāku derīguma termiņu vielām, kurām tas ir ierobežots formas nestabilitātes dēļ.

PUBLICĒTIE REZULTĀTI

Publikācijas

1. Kons, A.; Mishnev, A.; Mukhametzyanov, T.; Buzyurov, A.; Semen, L.; Bērziņš, A. Hexamorphism of Dantrolene: Insight into the Crystal Structures, Stability, and Phase Transformations *Cryst. Growth Des.* **2021,** 21, 1190–1201. (IF = **4.17**)

   A. Kons izstrādāja 90 % no eksperimentālā darba apjoma, izstrādāja plānu un uzrakstīja publikāciju, noformēja pētījuma rezultātus atbilstoši žurnāla prasībām, kā arī sagatavoja atbildes uz recenzentu jautājumiem un aizrādījumiem.
2. Kons, A.; Bērziņš, A.; Actiņš, A.; Rekis, T.; van Smaalen, S.; Mishnev, A. Polymorphism of R-Encenicline Hydrochloride: Access to the Highest Number of Structurally Characterized Polymorphs Using Desolvation of Various Solvates. *Cryst. Growth Des.* **2019**, 19, 4765–4773. (IF = **4.17**)

   A. Kons izstrādāja 90 % no eksperimentālā darba apjoma, izstrādāja plānu un uzrakstīja publikāciju, noformēja pētījuma rezultātus atbilstoši žurnāla prasībām, kā arī sagatavoja atbildes uz recenzentu jautājumiem un aizrādījumiem.
3. Bobrovs, R.; Kons, A.; Bērziņš, A.; Rekis, T.; Actiņš, A. Formation and Transformations of Organic Salt Hydrates: Four Encenicline Hydrochloride Monohydrates and Respective Isostructural Desolvates. *Cryst. Growth Des.* **2018**, 18, 2100–2111. (IF = **4.21**)

   A. Kons izstrādāja 90 % no eksperimentālā darba apjoma, sniedza ieguldījumu publikācijas rakstīšanā (50 %), noformēja pētījuma rezultātus atbilstoši žurnāla prasībām, kā arī sniedza ieguldījumu, sagatavojot atbildes uz recenzentu jautājumiem un aizrādījumiem.
4. Kons, A.; Bērziņš, A.; Actiņš, A. Polymorphs and Hydrates of Sequifenadine Hydrochloride: Crystallographic Explanation of Observed Phase Transitions and Thermodynamic Stability. *Cryst. Growth Des.* **2017**, 17, 1146–1158. (IF = **4.17**).

   A. Kons izstrādāja 90 % no eksperimentālā darba apjoma, izstrādāja plānu un uzrakstīja publikāciju, noformēja pētījuma rezultātus atbilstoši žurnāla prasībām, kā arī sagatavoja atbildes uz recenzentu jautājumiem un aizrādījumiem.
5. Kons, A.; Rutkovska, L.; Bērziņš, A.; Bobrovs, R.; Actiņš, A. Three anhydrous forms and a dihydrate form of quifenadine hydrochloride: a structural study of the thermodynamic stability and dehydration mechanism. *CrystEngComm.* **2015**, 17, 3627–3635. (IF = **3.97**)

   A. Kons izstrādāja 70 % no eksperimentālā darba apjoma, izstrādāja plānu un uzrakstīja publikāciju, noformēja pētījuma rezultātus atbilstoši žurnāla prasībām, kā arī sagatavoja atbildes uz recenzentu jautājumiem un aizrādījumiem.

Konferences

1. A. Kons, A. Mishnev, T. A. Mukhametzyanov, A. V. Buzyurov, S. E. Lapuk, A. Bērziņš, Hexamorphism of Dantrolene Insight into the Crystal Structures Stability and Phase Transformations. *University of Latvia 79th conference*, Rīga, Latvija, **2021.**
2. A. Kons, A. Bērziņš, Decamorphism of R-Encenicline hydrochloride. *University of Latvia 78th conference*, Rīga, Latvija, **2020.**

3. A. Kons, A. Bērziņš, T. Rekis, Polimorphism of R-Encenicline hydrochloride: Access to the highest number of structurally characterized polymorphs using desolvation of varius solvates. *The 32nd European Crystallographic Meeting*, Vīne, Austrija, **2019.**
4. A. Kons, A. Actiņš, Access to several crystalline forms of R-Encenicline hydrochloride using desolvation of various solvates. *The 31st European Crystallographic Meeting,*, Ovjedo, Spānija, **2018.**
5. A. Kons, A. Actiņš, Polymorphs and Solvates of Encenicline Hydrochloride. *24th Congress and General Assembly of the International Union of Crystallography*, Haidarābādu, Indija, **2017.**
6. A. Kons, A. Actiņš, Sekvifenadīna hidrogēnhlorīda 6 polimorfās formas: termodinamiskās stabilitātes un struktūru salīdzinājums. *University of Latvia 74th conference*, Rīga, Latvija, **2016.**
7. A. Kons, A. Actiņš, Anhydrous and hydrated crystalline forms of sequifenadine hydrochloride: comparison of thermodynamic stability and crystal structures. *14th European Powder Diffraction Conference (EPDIC 2016)*, Bari, Itālija, **2016.**
8. A. Kons, L. Rutkovska, A. Bērziņš, R. Bobrovs, A. Actiņš, Three anhydrous forms and a dihydrate form of quifenadine hydrochloride: a structural study of the thermodynamic stability and dehydration mechanism. *8th Crystal Forms @ Bologna*, Boloņa, Itālija, **2015.**

Darbā neiekļautās publikācijas

1. Bērziņš, A.; Kons, A.; Saršūns, K.; Belyakov, S.; Actiņš, A. On the Rationalization of Formation of Solvates: Experimental and Computational Study of Solid Forms of Several Nitrobenzoic Acid Derivatives. *Cryst. Growth Des.* **2020**, 20, 5767–5784.
2. Rekis, T.; Bērziņš, A.; Sarceviča I.; Kons, A.; Balodis, M.; Orola, L.; Lorenz, H.; Actiņš, A. A Maze of Solid Solutions of Pimobendan Enantiomers: An Extraordinary Case of Polymorph and Solvate Diversity. *Cryst. Growth Des.* **2018**, 18, 264–273.
3. Bērziņš, A.; Trimdale, A.; Kons, A.; Zvaniņa, D. On the formation and desolvation mechanism of organic molecule solvates: A structural study of methyl cholate solvates. *Cryst. Growth Des.* **2017**, 17, 5712–5724.
4. Bērziņš, K.; Kons, A.; Grante, I.; Dzabijeva, D.; Nakurte, I.; Actiņš, A. Multitechnique approach for qualitative and quantitative characterization of furazidin degradation kinetics under alkaline conditions. *J. Pharm. Biomed. Anal.* **2016**, 129, 433–440.
5. Sarceviča, I.; Kons, A.; Orola, L. Isoniazid cocrystallisation with dicarboxylic acids: vapochemical, mechanochemical and thermal methods. *CrystEngComm,* **2016**, 18, 1625–1635.
6. Orola, L.; Sarceviča, I.; Kons, A.; Actiņš, A.; Veidis, M.V. Conformation of the umifenovir cation in the molecular and crystal structures of four carboxylic acid salts. *J. Mol. Struct.* **2014**, 1056, 6369.
7. Kons, A.; Bērziņš, A.; Krūkle–Bērziņa, K.; Actiņš A. Characterization and physicochemical evaluation of molecular complexes formed between umifenovir and dicarboxylic acids. *Latvian Journal of Chemistry,* **2014**, 52, 28–40.

1. PROMOCIJAS DARBA TEORĒTISKIE PAMATI UN PĒTĪTĀS SISTĒMAS

1.1. Farmaceitiski aktīvu vielu polimorfisms un tā pētīšanas metodes

Farmaceitiski aktīvās cietvielas (FAV) var eksistēt kristāliskā vai retāk amorfā stāvoklī. Kristāliskā stāvoklī molekulas elementāršūnā ir periodiski sakārtotas trīs dimensijās, savukārt amorfām vielām nav šī periodiskā molekulu sakārtojuma un tās ir izvietotas haotiski, taču ir iespējams lokāls periodiskums dažu molekulu garumā[20]. Kristāli var būt veidoti no viena vai vairākiem komponentiem. Daudzkomponentu kristāli sīkāk iedalās solvātos/hidrātos (satur šķīdinātāja/ūdens molekulas kristālrežģī stehiometriskā vai nestehiometrikā attiecībā), sāļos (cietvielas, kas sastāv no katjoniem un anjoniem) un kokristālos (sastāv no divu vai vairāku normālos apstākļos cietu vielu neitrālām molekulām). Savukārt **polimorfi** var būt gan kristāliskas vienkomponenta, gan arī daudzkomponentu fāzes, kurām ir dažāda molekulu konformācija un/vai sakārtojums kristāliskajā režģī, skatīt 1.1. att. Nereti sāls vai kokristāls veido dažādas polimorfās un solvatētās formas, vai amorfo fāzi. Ir iegūstami arī sāls kokristāli un pat sāls kokristālu solvāti/hidrāti[21].

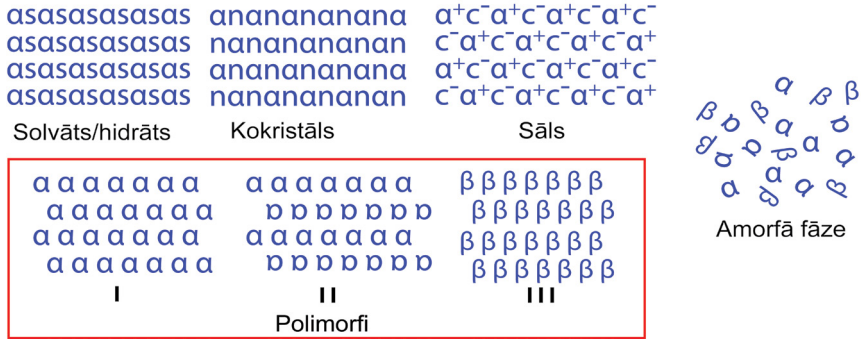

1.1. att. **Vispārīgs farmaceitisku aktīvu cietvielu iedalījums, kur α un β ir molekulas ar atšķirīgu konformāciju; s – šķīdinātājs; n – neitrāla cietviela; α^+ – katjons un c^- – anjons[22]**

Tiek uzskatīts, ka vairāk nekā 80 % organisko savienojumu[23] un vismaz puse FAV[24] ir spējīgi eksistēt vairāk nekā vienā polimorfajā formā. Pie noteiktas temperatūras un spiediena ir tikai viens termodinamiski stabils polimorfs, kuru ir ieteicams izmantot gatavajā zāļu vielā, tomēr nereti izmanto arī metastabilus polimorfus to labākas šķīdības vai stabilā polimorfa izmantošanas aizlieguma dēļ[25,26].

Izšķir divu veidu polimorfismu: sakārtojuma un konformācijas. Sakārtojuma polimorfismā, molekulas galvenokārt ir konformacionāli neelastīgas, kā rezultātā konformācija ir vienāda, bet to izvietojums elementāršūnā ir atšķirīgs. Konformācijas polimorfismā molekulas ir lokanākas un tās eksistē kā atšķirīgi konformēri, bet ar vienādu

izvietojumu elementāršūnā. Daudzas FAV ir konformacionāli elastīgas, jo tām ir iespējama rotācija ap C–C, C–N un C–O saitēm[27,28]. Visbiežāk praksē novēro jauktā tipa polimorfās formas, jo molekulas ar atšķirīgu konformāciju tiecas arī sapakoties atšķirīgi[29]. Molekulu pakojums un konformācija ir atkarīga no iekšmolekulārām un starpmolekulārām mijiedarbībām, tādām kā ūdeņraža saites, halogēnu saites, van der Valsa mijiedarbības, π-π mijiedarbības u. c.[30,31]

Polimorfās formas iespējams iedalīt, arī balstoties uz to termodinamiskajām īpašībām atkarībā no tā, vai viens polimorfs var apgriezeniski pārvērsties otrā vai nē. Starp jebkuriem diviem polimorfiem eksistē enantiotropa vai monotropa saistība. Enantiotropā polimorfo formu sistēmā eksistē tāda abu fāžu līdzsvara temperatūra, kura atrodas zem abu polimorfo formu kušanas temperatūras. Līdzsvara temperatūrā abu polimorfo formu stabilitāte ir vienāda. Monotropa sistēma savukārt ir tad, ja viena polimorfā forma ir stabila visā temperatūras apgabalā līdz pat kušanas temperatūrai[22]. Lai noskaidrotu, vai polimorfu pāris ir enantiotropi vai monotropi saistīts, ir iespējams lietot četrus empīriskus likumus: fāžu pārejas siltuma likumu, kušanas siltuma likumu, blīvuma likumu un infrasarkano likumu[32], kas apraksta saistību starp eksperimentālajiem novērojumiem un polimorfu sistēmas veidu. Tiesa, praksē parasti tiek izmantoti tikai pirmie divi likumi, jo gan blīvuma, gan arī infrasarkanajam likumam dažādu starpmolekulāru mijiedarbību dēļ ir izņēmumi.

1.1. tabula

Metožu pielietojums FAV cietvielu polimorfu pētījumiem[33]

	SC-XRD	PXRD	IR/ Raman	ssNMR	DSC	TG	DVS	HSM
Kristāliskas fāzes identifikācija	✓	✓	✓	✓	✓	✓	✓	✓
Kristāliskā struktūra	✓	✓[a]		✓[a]				
Molekulārā struktūra				✓				
Molekulu ģeometrija	✓	✓[a]		✓				
Ūdeņraža saišu mijiedarbības	✓	✓[a]		✓[a]				
Vājās mijiedarbības	✓	✓[a]						
Cietvielu fāzes dinamika				✓				
Termiskā stabilitāte		✓	✓	✓	✓	✓		✓
Mehāniskā stabilitāte	✓	✓	✓					
Fāžu pārejas		✓	✓	✓	✓	✓	✓	✓
Kušanas temperatūra					✓			✓
De-/hidratācija		✓	✓	✓	✓	✓	✓	✓
Higroskopitāte		✓	✓			✓	✓	
Morfoloģija								✓
Heterogēni maisījumi		✓	✓[a]	✓	✓	✓	✓	✓
Jonizācijas stāvokļi	✓	✓	✓	✓				
In situ procesu mērīšana		✓	✓	✓				

[a] Nepieciešama advancēta metodika

Farmaceitiski aktīvu cietvielu polimorfo formu identifikācijai, raksturošanai un kvantificēšanai ir pieejamas daudzas analītiskās metodes un to kombinācijas, no kurām visbiežāk izmantotās ir pulvera rentgendifrakcija (PXRD), monokristālu rentgendifrakcija (SC–XRD), diferenciāli skenējošā kalorimetrija (DSC), termogravimetrija (TG), termomikroskopija (HSM), molekulāro svārstību sprektroskopija (IR/ Raman), cietvielu kodolmagnētiskās rezonances spektroskopija (ssNMR) un mitruma sorbcijas/desorbcijas analīze (DVS). Lai pilnvērtīgi raksturotu polimorfās formas, ir nepieciešams izmantot vairākas metodes, jo katra no tām sniedz unikālu, bet ierobežotu informāciju par fāzi. Kopsavilkums par analītisko metožu pielietojumu polimorfo sistēmu pētījumiem redzams 1.1. tabulā.

1.2. Pulvera rentgendifrakcijas izmantošana struktūru noteikšanai

Kristāliskās struktūras noteikšana var sniegt būtisku informāciju, izstrādājot cietās farmaceitiskās vielas, dodot iespēju sasaistīt kristālisko struktūru ar dažādām fizikālķīmiskajām īpašībām, piemēram, stabilitāti, biopieejamību un daļiņu morfoloģiju. Lai gan monokristāla rentgendifraktometrija viennozīmīgi ir precīza un vēlama metode struktūras noteikšanai, bieži piemērota izmēra un kvalitātes monokristālus nav iespējams iegūt. Piemēram, tādas farmācijas industrijā izmantotas kristālisko formu iegūšanas metodes, kā ātras metastabilas formas kristalizēšana, solvātu/hidrātu desolvatācija vai mehanoķīmiska iegūšana, rada pulverveida paraugus. Šādos gadījumos arvien biežāk izmanto struktūras noteikšanu no pulvera difrakcijas datiem, pielietojot globālās optimizēšanas metodes jeb struktūras noteikšanu tiešajā telpā.

Pulvera rentgendifrakcijā struktūras noteikšanu apgrūtina difrakcijas informācijas zudums, kad no trīs dimensijām informāciju saspiež vienā dimensijā (1.2. att.). Šī iemesla dēļ pulvera rentgendifraktogrammā parādās ievērojams skaits refleksu, kas pārklājas. Signālu pārklāšanās liedz iegūt precīzu informāciju par refleksu pozīcijām un

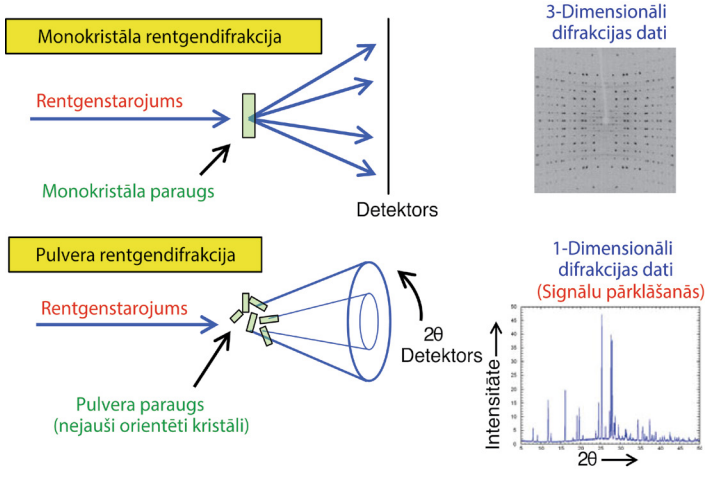

1.2. att. **Pulvera un monokristāla rentgendifrakcijas salīdzinājums**[34]

intensitāšu maksimumiem. Īpaši aktuāli tas ir organiskiem molekulāriem savienojumiem (ieskaitot FAV), kuriem parasti ir relatīvi liela elementāršūna un zema simetrija, kā rezultātā difraktogrammā ir liels pārklājušos refleksu skaits[34].

Lai nodrošinātu, ka strukturālais modelis ir pēc iespējas pareizāks un precīzāks, ir nepieciešams kristālisku paraugu (vēlams, tīras fāzes) iepresēt kapilārā un uzņemt augstas izšķirtspējas datus caurstarojošā režīmā, kapilāru rotējot. Kapilāra rotācija samazina dominējošās orientācijas ietekmi. Lai iegūtu visu strukturāli svarīgo informāciju, eksperimentālo difraktogrammu vēlams uzņemt plašā 2θ diapazonā, parasti līdz 70° vai 80°[35,36].

Struktūras noteikšana no pulvera rentgendifrakcijas datiem sevī ietver piecus vispārīgus soļus: (1) izvēlētu refleksu indeksāciju, lai noteiktu kristālrežģa parametrus, telpisko grupu un asimetrisko vienību; (2) iegūto režģa parametru un telpiskās grupas samērošana ar eksperimentālo difraktogrammu, izmantojot Paulija[37] vai Le Baila[38] metodi, nosakot difrakcijas ainas profila parametrus; (3) ķīmiski pareiza modeļa ievietošanu kristālrežģī; (4) struktūras noteikšanu tiešajā telpā ar globālās optimizēšanas metodēm un (5) struktūras optimizēšanu ar Rietvelda metodi, lai panāktu, ka iegūtais strukturālais modelis maksimāli atbilstu eksperimentālajiem datiem. No visiem procesa posmiem pareiza režģu parametru noteikšana ir vissvarīgākā, jo bez pareiziem režģa parametriem struktūru noteikt nav iespējams, tāpēc ieteicams izmantot dažādu refleksu skaitu indeksēšanu, kā arī pielietot dažādus indeksēšanas algoritmus (Dicvol[39], N-Treor[40], Conograph[41] u. c.). Elementāršūnā ievietojot pareizu ķīmisku modeli (kristalogrāfiski neatkarīgas molekulas, pretjonus, ūdens vai šķīdinātāja molekulas, ko var precizēt ar citām analītiskām metodēm kā NMR, ssNMR, DSC/TG u. c.), tiešajā telpā tiek ģenerētas daudzas kristāliskās struktūras. Tādi globālās optimizēšanas Monte Karlo algoritmi kā simulētā dzesēšana (*simulated annealing*) un paralēlā rūdīšana (*parallel tempering*) kristālrežģī ievietotajam ķīmiskajam modelim maina pozīciju, orientāciju un konformāciju līdz iegūst labāko sakritību starp simulētajiem un eksperimentālajiem datiem. Lai uzlabotu strukturālā modeļa precizitāti, ar Rietvelda metodi optimizē režģa parametrus, atomu pozīcijas, profila un fona parametrus, izotropisko temperatūras faktoru, kā arī 2θ leņķa nobīdes un dominējošās orientācijas parametrus. Lai izvairītos no molekulu ģeometrijas izkropļojumiem, izmanto saišu garuma un leņķa ierobežojumus. Alternatīvi var izmantot arī visu molekulāro fragmentu (izņemot diedrālos leņķus) kā vienu nekustīgu veselumu. Pēc Rietvelda optimizācijas iegūto kristālisko struktūru novērtē, salīdzinot simulēto difraktogrammu ar eksperimentālo, ko vizualizē ar atšķirību līkni (melnā līkne 1.3. a attēlā), svērto pulvera profila R faktoru (*Rwp*), *goodness of fit* (χ^2) un citu parametru vērtībām.

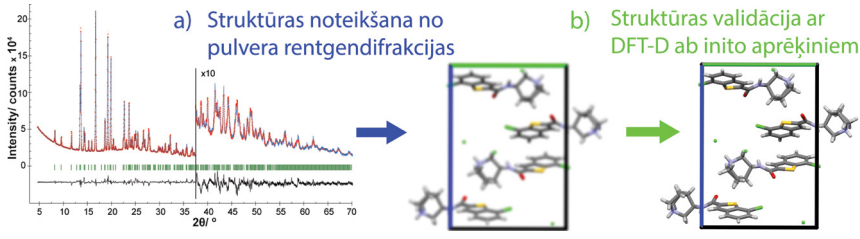

1.3. att. **Shematisks attēlojums precīzas un validētas struktūras noteikšanai no pulvera rentgendifrakcijas datiem**

Pēc Rietvelda optimizācijas pielieto dispersijas koriģētas blīvuma funkcionāļa teorijas (DFT-D) enerģijas minimizēšanu, optimizējot ģeometriju un režģa parametrus (1.3. b attēls). No iegūtajiem rezultātiem ir iespējams validēt struktūras pareizību, salīdzinot atomu koordinašu vidējo kvadrātisko nobīdi (RMSD) pirms un pēc optimizācijas. Par pareizi noteiktām struktūrām uzskata tās, kurām RMSD vērtības ir zemākas par 0,35 Å[42]. Vairāku polimorfo formu gadījumā papildus RMSD vērtībām var iegūt arī pilnās enerģijas (kristālrežģa + konformācijas) vērtības bez termiskās enerģijas ieguldījuma (0 K temperatūrā), kas ļauj novērtēt šo polimorfo formu savstarpējo termodinamisko stabilitāti.

1.3. Pētītās sistēmas

Darba ietvaros pētītas četras farmaceitiski aktīvas vielas, kuras iegūtas no A/S "Olainfarm" (struktūrformulas ar norādītiem diedrāliem leņķu apzīmējumiem dotas 1.4. attēlā).

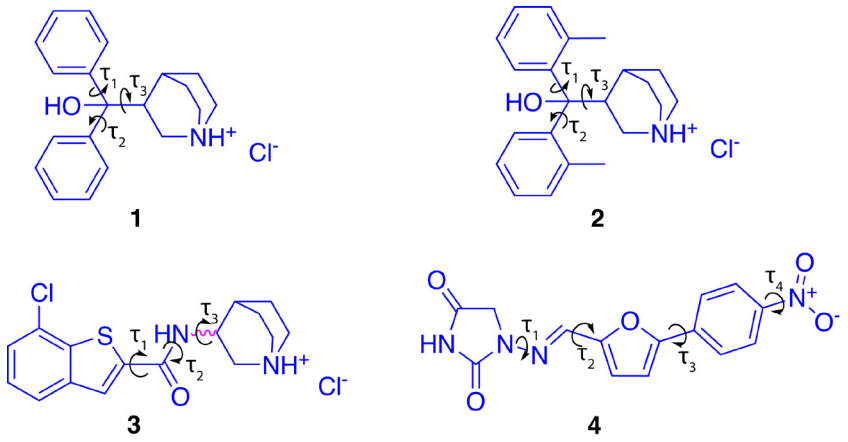

1.4. att. **Pētīto savienojumu struktūrformulas (1 – hifenadīna hidrogēnhlorīds; 2 – sehifenadīna hidrogēnhlorīds; 3 – enceniklīna hidrogēnhlorīds; 4 – dantrolēns)**

Hifenadīna (1-azabiciklo[2.2.2]oktān-3-il(difenil)metanola) **hidrogēnhlorīds** (**1**) jeb fenkarols un **sehifenadīna** (1-azabiciklo [2.2.2]oktān-3-il-bis(2-metilfenil) metanola) **hidrogēnhlorīds** (**2**) jeb bikarfēns ir farmaceitiski aktīvas vielas, kas samazina histamīna iedarbību, bloķējot H1 receptorus ārējos audos, kā arī aktivizē enzīmu diamīnoksidāzi, kas šķeļ endogēno histamīnu, līdz ar to pazemina histamīna daudzumu audos[43,44]. Uzsākot pētījumus, literatūrā nebija pieejama nekāda informācija par šo abu hiduklidilkarbinola atvasinājumu veidotajām cietvielu formām.

Enceniklīna hidrogēnhlorīds (**3**) ((R)-7-hlor-N-hinuklidin-3-il)benztiofēn-2-karboksamīda hidrogēnhlorīds) ir selektīvs α-7 nikotīnskābes acetilholīna receptoru daļējs agonists. Tas tika izstrādāts Alcheimera slimības un šizofrēnijas izraisīto kognitīvo traucējumu ārstēšanai[45]. Par *R* enantiomēra cietvielu formām iepriekš ziņots patentā[46], kurā var atrast informāciju par trīs monohidrātu formām (I, II un X).

Dantrolēns (**4**) (1-[(E)-[5-(4-nitrofenil)furan-2-il]metilidene amino]imidazolidin-2,4-dions) ir muskuļu relaksētājs. Tas ir vienīgais specifiskais un efektīvais līdzeklis ļaundabīgas hipertermijas ārstēšanai, kā arī to izmanto ļaundabīgā neiroleptiskā sindroma, muskuļu spasticitātes (piemēram, pēc insulta, paraplēģijas, cerebrālās triekas vai pacientiem ar multiplo sklerozi) un saindēšanās ar 3,4-metilēndioksi-N-metilamfetamīnu (ekstazī) ārstēšanā[47]. Uzsākot pētījumus, bija pieejama informācija par dantrolēna metanola solvāta kristālisko struktūru, kas noteikta no monokristāla datiem.[48]

2. EKSPERIMENTĀLĀ DAĻA

1. Fāžu identifikācijai pulvera rentgendifraktogrammas uzņemtas ar iekārtu *Bruker D8 Advance* ar 1D pozīcijas jutīgo *Lynxeye* detektoru, izmantojot *Bragg–Brentano* ģeometriju un Cu anoda rentgenstaru avotu. Uzņemšanas režīms: 3–35° 2θ, ātrums 0,2s/0,02° (Latvijas Universitāte, Latvija).
2. Pulvera rentgendifraktogrammas struktūras noteikšanai uzņemtas ar iekārtu *Bruker D8 Discover* ar 1D *Lynxeye* detektoru, izmantojot caurstarojošo ģeometriju un Cu anoda rentgenlampu. Uzņemšanas režīms: 3 vai 4,5–70° 2θ, ātrums 20s/0,01° (Latvijas Universitāte, Latvija).
3. Monokristālu rentgendifraktometri *Rigaku XtaLAB Synergy-S dualflex* ar HyPix6000 detektoru un Cu vai Mo rentgenstaru avotu (Latvijas Organiskās sintēzes institūts, Latvija) un MAR345 ar attēla plāksnes detektoru un Ag rentgenstaru avotu (Baireitas Universitāte, Vācija) izmantoti, lai noteiktu izaudzēto monokristālu kristāliskās struktūras.
3. Diferenciāli skenējošais kalorimetrs/termogravimetrs *Mettler Toledo TGA/DSC2* izmantots iegūto fāžu raksturošanai un solvātos esošā šķīdinātāja stehiometrijas noteikšanai. Uzņemšanas režīms: 25–320 °C, karsēšanas ātrums 10 °C/min, N_2 atmosfērā (Latvijas Universitāte, Latvija).
4. Diferenciāli skenējošais kalorimetrs TA DSC 25 izmantots polimorfo formu kvalitatīvai un kvantitatīvai termisko efektu noteikšanai. Uzņemšanas režīms: 25–320 °C, karsēšanas ātrums 5–20 °C/min, N_2 atmosfērā (Latvijas Universitāte, Latvija).
5. Ultra ātrs skenējošais kalorimetrs *Mettler Toledo Flash DSC1* izmantots, lai atdalītu pārklājušos kušanas un sadalīšanās procesus dantrolēna polimorfiem. Uzņemšanas režīms: 25–350 °C, karsēšanas ātrums 2000 °C/s, N2 atmosfērā (Kazaņas Federālā universitāte, Krievija).
6. Iekārta *Surface Measurement Systems DVS Advantage* izmantota polimorfo formu ūdens tvaika un desorbcijas pētījumiem. Uzņemšanas režīms: 0–95 % RM ar soli 5 % RM, 25 °C (Latvijas Universitāte, Latvija).
7. Automātiskās kristalizācijas iekārta *Technobis Crystal16* izmantota politermiskās šķīdības noteikšanai (Latvijas Universitāte, Latvija).
8. Polarizētās gaismas termomikroskops *Leitz Laborlux 12 PolS* ar *Leica DFC450* kameru izmantots vizuāliem monokristāla dehidratācijas pētījumiem (Rīgas Tehniskā universitāte, Latvija).
9. Kristālisko struktūru noteikšanai no pulvera datiem un Rietvelda optimizācijai izmantotas datorprogrammas *Expo2014* un *Topas5*, periodiskiem DFT-D aprēķiniem izmantotas datorprogrammas *Quantum Espresso* un *Castep*, bet molekulu gāzes fāzes aprēķiniem *Gaussian09.*

3. REZULTĀTI UN TO IZVĒRTĒJUMS

3.1. Hifenadīna hidrogēnhlorīda (1) trimorfisms

Salīdzinot ar pārējiem apskatītajiem savienojumiem, hifenadīna HCl veido vismazāk polimorfo formu, t. i., 3. To daļēji var skaidrot ar faktu, ka hifenadīna HCl nav izteikts solvātu veidotājs un tas liedz iegūt polimorfus, desolvatējot dažādus solvātus, kā to var novērot sehifenadīna HCl, enceniklīna HCl un dantrolēna gadījumā. Vienīgā solvatētā forma, ko veido hifenadīna HCl, ir dihidrāts (DH), ko iegūst, kristalizējot hifenadīna HCl no ūdens, turklāt, dehidratējot šo formu, iegūst metastabilu polimorfu B. Ja šo savienojumu kristalizē no *n*- vai *i*-butanola, iegūst polimorfu C, bet polimorfs A iegūts no citiem 14 ūdeni nesaturošiem šķīdinātājiem. Dihidrāta formai ir iespējams izaudzēt monokristālu, bet visus trīs polimorfus var iegūt vienīgi mikrokristāliska pulvera veidā. Iegūto formu rentgendifraktogrammas redzamas 3.1. attēlā.

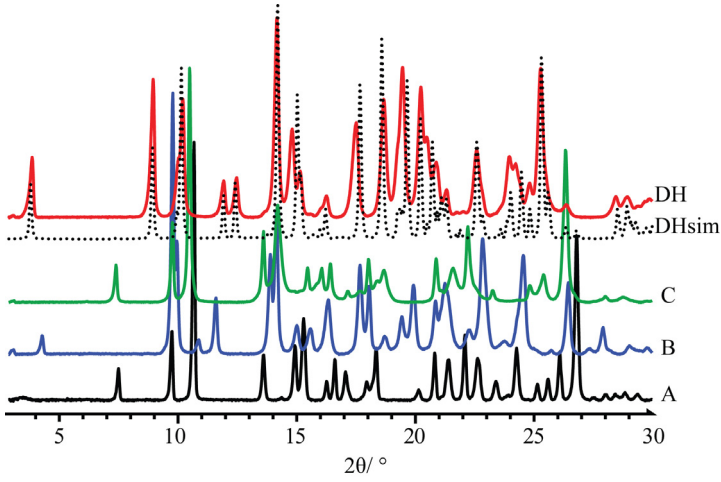

3.1. att. **Hifenadīna hidrogēnhlorīda A, B, C un DH formu rentgendifraktogrammas**

A, B un C polimorfu struktūras noteiktas no pulvera rentgendifrakcijas datiem, bet DH struktūra noteikta no monokristāla datiem. Iegūtā kristalogrāfiskā informācija redzama 3.1. tabulā. Noskaidrots, ka visas iegūtās kristāliskās modifikācijas kristalizējas *P*$\bar{1}$ telpiskajā grupā ar vienu hifenadīna katjonu un vienu hlorīda anjonu asimetriskajā vienībā.

Hifenadīna molekula sastāv no divām fenil, vienas hinuklidīn un vienas hidroksil grupas, kas visas savienotas ar ceturtējo oglekli. Lai gan šajā molekulā ir trīs diedrālie leņķi (skat. 1.4. att. 1), noskaidrots, ka visās struktūrās konformācija ir ļoti līdzīga un pieder pie viena globālā enerģijas minimuma. Hifenadīna HCl struktūrā vienīgais stiprais H saišu akceptors ir Cl^- anjons, bet donori ir NH^+ grupa un hidroksilgrupa.

3.1. tabula

Kristalogrāfiskā informācija hifenadīna HCl formām

	A	B	C	DH
Formula		$C_{20}H_{24}NOCl$		$C_{20}H_{24}NOCl{\cdot}2H_2O$
Molmasa, g·mol^{-1}		329,86		365,88
Parauga tips		Pulverveida		Monokristāls
Temperatūra, K		293(2)		173(2)
Singonija			Triklīnā	
Telpiskā grupa			$P\bar{1}$	
a, Å	6,372(2)	6,408(5)	6,449(2)	6,339(1)
b, Å	12,699(5)	9,281(6)	12,951(3)	8,601(2)
c, Å	10,759(4)	18,356(2)	11,222(2)	18,404(5)
α,°	96,03(2)	113,09(3)	97,60(1)	100,02(2)
β,°	98,88(2)	83,62(3)	106,61(2)	92,32(3)
γ,°	80,68(2)	116,50(3)	75,25(2)	103,45(2)
V, Å^3	845,9(1)	895,8(1)	862,9(1)	957,5(3)
ρ_{calc}, g·cm^3	1,295	1,223	1,270	1,269
Z (Z')	2 (1)	2 (1)	2 (1)	2 (1)
R_{wp} (R_p)/R_1 (wR_2), %	2,81 (1,89)	1,41 (0,99)	3,12 (2,32)	4,8 (14,8)
Pakojuma efektivitāte, %	73,1	71,7	69,1	68,4
Enerģija[a], kJ·mol^{-1}	0	21,2	11,3	N/A

[a] relatīvi pret A polimorfu

Kā redzams 3.2. attēlā, visiem trīs polimorfiem ir vienāds H saišu motīvs (iekrāsots zilā krāsā), kur divi Cl^- anjoni mijiedarbojas ar diviem hifenadīna katjoniem caur N–H···Cl un O–H···Cl ūdeņraža saitēm, veidojot tetramēru $R^2_4(16)$. H saišu tīkls, kas ir novērojams DH struktūrā, ir krietni sarežģītāks divu ūdens molekulu dēļ, kuras darbojas gan kā H saišu donori, gan kā akceptori.

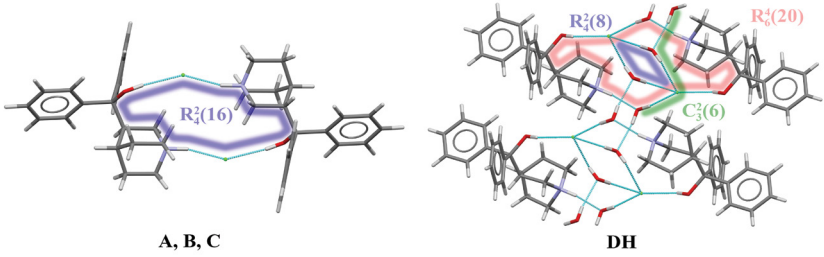

3.2. att. **Hifenadīna HCl polimorfu un dihidrāta struktūrās esošie ūdeņraža saišu motīvi**

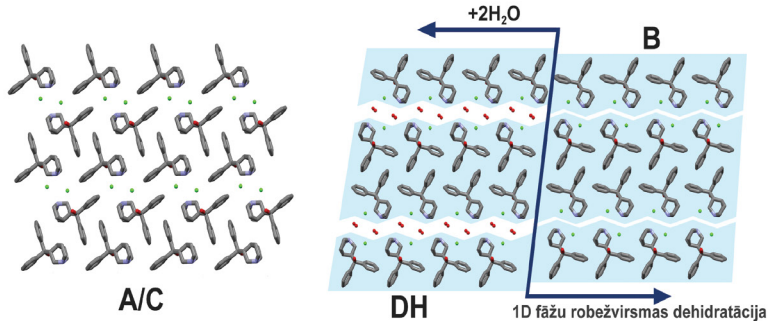

3.3. att. **Hifenadīna HCl A, B, C un DH formu struktūru molekulārais pakojums**

A un C polimorfiem ir vienāds monoslāņains molekulārais pakojums, kur blakus molekulas ir anti paralēlā novietojumā viena pret otru (3.3. att.). Savukārt starp polimorfu A/C un B pakojumu ir redzamas būtiskas atšķirības. B formas struktūrai ir bislāņains molekulārais pakojums, kur blakus molekulas ir vērstas vienā virzienā, bet nākamajā slānī tās ir vērstas pretējā virzienā. B formas struktūrā, salīdzinot ar A un C formu struktūrām, ir vairāk atdalīti hidrofilie un hidrofobie slāņi, kuros tetramēri ir sapakoti ciešāk. Dihidrāta un B formas 2D pakojums sastāv no vienādi orientētiem slāņiem, vienīgā atšķirība ir ūdens molekulas, kuras atrodas starp hidrofilajām hinuklidīna grupām un hlorīda anjoniem. Tas norāda, ka DH ir kanālveida hidrāts, ko apstiprina arī termomikroskopijas novērojumi (3.4. att.), kuros redzams, ka dehidratācija notiek ūdeni saturošo kanālu virzienā. Tā kā ūdens molekulas ir iesaistītas galvenajā H saišu tīklā, šis hidrāts ir arī stehiometrisks.

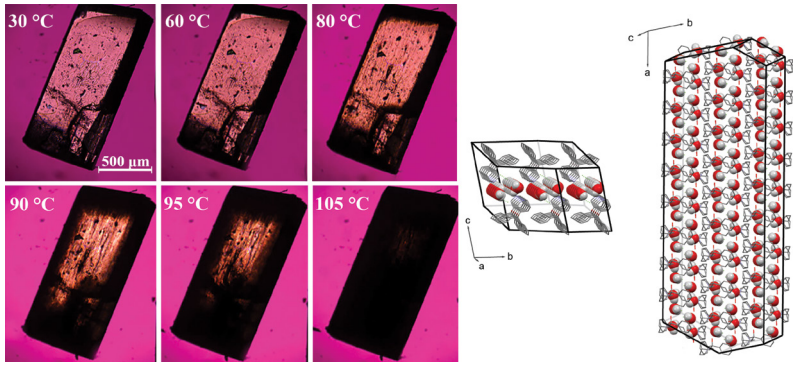

3.4. att. **Termomikroskopijas un simulētie kristāla morfoloģijas dati DH formai**

Augstās strukturālās līdzības dēļ ir skaidrs, kāpēc tieši DH forma dehidratējoties pārvēršas par B polimorfu, nevis par A vai C, jo šī pāreja nemaina hifenadīna katjona paralēlo orientāciju, bet gan tikai palielina attālumu starp tiem. Salīdzinot visu formu pakojuma efektivitāti (2.1.1. tabula), redzams, ka visaugstākā tā ir A formai (73,1 %), tad B (71,7 %) un C (69,1 %), bet viszemākā dihidrātam (68,4 %). Šī pakojuma

efektivitātes rinda polimorfiem atbilst arī novērotajai termodinamiskajai stabilitātei. Dihidrāta zemo pakojuma efektivitāti, bet augsto stabilitāti, skaidro fakts, ka ūdens molekulas kanālos, lai gan neefektīvi sapakotas, stabilizē šo struktūru ar spēcīgām starpmolekulārajām mijiedarbībām, ko sniedz stipru H saišu tīkls.

Lai labāk saprastu atšķirības starp A un C polimorfiem, to struktūras optimizētas, relaksējot atomu pozīcijas un režģa parametrus ar DFT-D metodi, kā rezultātā iegūtas praktiski vienādas struktūras. Tas liecina, ka starp šīm struktūrām ir zema enerģijas barjera un vienīgais izskaidrojums C polimorfa eksistencei ir tas, ka šai formai, kristalizējoties no *n*- vai *i*-butanola, veidojas specifiskas mijiedarbības starp šķīdinātāju un hifenadīna hidrogēnhlorīdu. Molekulas nepaspēj sakārtoties enerģētiski izdevīgākajā pakojumā, un tiek iegūts metastabils polimorfs ar ļoti līdzīgu struktūru termodinamiski stabilajam A polimorfam.

3.2. Sehifenadīna hidrogēnhlorīda (2) heksamorfisms

Meklējot jaunas kristāliskās formas sehifenadīna hifrogēnhlorīdam, iegūti seši nesolvatēti polimorfi (A, B, B', C, D un E), divi dihidrāti (DH un DH-II), monohidrāts (MH), nestehiometrisks hidrāts (NSH). Polimorfus C un E var iegūt tikai desolvatācijas ceļā no attiecīgi metanola un *n*-propanola solvātiem, bet hidrātus MH un NSH iegūst, hidratējot attiecīgi C un E polimorfus. Polimorfu D var iegūt, tikai suspendējot sehifenadīna hidrogēnhlorīdu *n*-propanolā, taču, pārkristalizējot no šī šķīdināja, iegūst *n*-propanola solvātu, kas desolvatējoties izveido E polimorfu. Shematisku formu iegūšanu un fāžu pārejas skatīt 3.5. att.

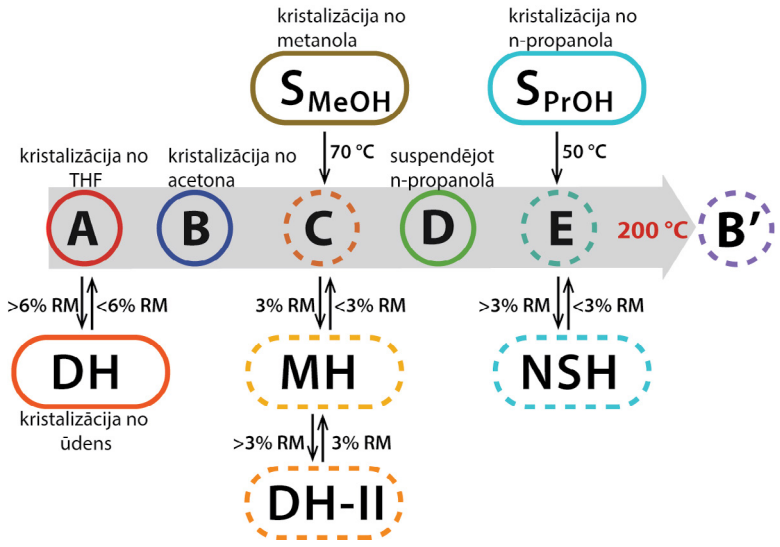

3.5. att. **Shematisks sehifenadīna HCl formu iegūšanas un fāžu pāreju attēlojums. Ar nepārtrauktu līniju apzīmētas formas, kas iegūtas, kristalizējot no šķīduma; ar pārtrauktu līniju parādītas formas, kas iegūtas cietvielu pāreju rezultātā**

Visu sešu polimorfu, kā arī MH un NSH, struktūra noteikta, izmantojot pulvera rentgendifraktometriju, bet DH formas struktūra iegūta no monokristāla datiem. DH-II formai neizdevās iegūt pareizus režģa parametrus un līdz ar to arī noteikt struktūru. A, B, B' polimorfi kristalizējas triklīnajā $P\bar{1}$ telpiskajā grupā ar vienu sehifenadīna katjonu un vienu hlorīda anjonu asimetriskajā vienībā (Z' = 1), bet C, D un E polimorfi kristalizējas attiecīgi monoklīnās singonijas $P2_1/c$, $P2_1/n$ un $C2/c$ telpiskajās grupās ar Z' = 2.

Sehifenadīna un hifenadīna molekulas atšķiras ar divām metil grupām pie benzola gredzeniem un tieši šo metilgrupu iekšmolekulāro mijiedarbību dēļ veidojas vairākas sehifenadīna katjona konformācijas (skat. 3.6. attēlu).

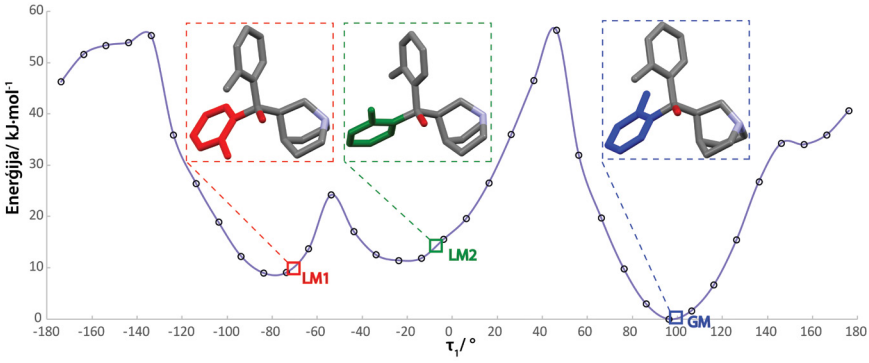

3.6. att. **Potenciālās enerģijas virsmas skenēšanas rezultāts τ_1 leņķim. Eksperimentāli iegūtās konformācijas atzīmētas ar zilo, zaļo un sarkano kvadrātu**

Eksperimentāli ir novērojamas trīs konformācijas, no kurām divas ir lokālā minimuma (LM1 un LM2) un viena globālā minimuma (GM) konformācija. Jāatzīmē, ka katra lokālā minimuma konformācija eksperimentāli novērota tikai vienā gadījumā, respektīvi LM1 ir D polimorfa konformērs, bet LM2 ir C polimorfa konformērs. Veicot ģeometrijas optimizāciju, noskaidrots, ka abiem lokālā minimuma konformēriem ir par 8–10 kJ·mol^{-1} augstāka enerģija nekā GM konformēram. Novērots, ka LM1 un LM2 konformēri veido arī no GM konformēra atšķirīgus H saišu motīvus (3.7. attēls).

Ja A, B, B' un E polimorfos veidojas jau iepriekš hifenadīna HCl gadījumā novērotais tetramērs $R^2_4(16)$, tad D formā ir novērojams katamērs $C^2_4(16)$, bet C polimorfā tetramērs $R^2_4(10)$, kurā OH grupa neveido H saiti. Ja polimorfiem ir atšķirīga konformācija un atšķirīgi H saišu motīvi, tad šādiem polimorfiem ir arī atšķirīgs 3D pakojums, kā tas ir D un C formas gadījumā. Savukārt, A, B un E polimorfiem gan konformācija, gan arī 0D pakojums ir vienāds. A un B formām ir arī kopīgs 2D pakojums, ko nosaka slānis 1 (3.7. attēlā). Šādi blakus esoši slāņi 1 viens pret otru var būt novietoti paralēli kā A formas struktūrā vai arī antiparalēli kā B formas struktūrā. Polimorfu A, E un C struktūrās esošajos slāņos 2, 3 un 4 ūdens ir spējīgs iekļauties, neizmainot pakojumu, un līdz ar to ir iespējams iegūt trīs dažādus hidrātus. Polimorfs A veido dihidrātu, polimorfs C monohidrātu, bet E forma nestehiometrisku hidrātu, kamēr B un D formas neveido strukturāli līdzīgus hidrātus un līdz ar to ir visstabilākās formas paaugstināta mitruma apstākļos.

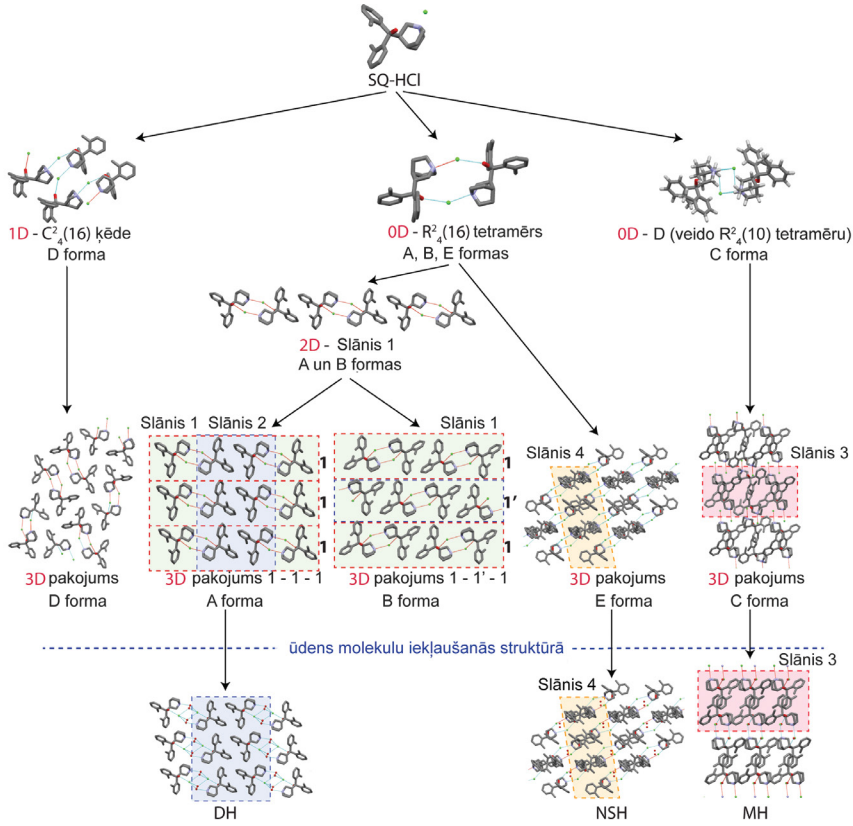

3.7. att. **Sehifenadīna HCl polimorfu struktūrās esošie H saišu motīvi un polimorfu pakojuma līdzības ar hidratētām fāzēm**

3.2. tabula

Polimorfu termodinamiskās stabilitātes rezultāti, kas iegūti, suspendējot polimorfu maisījumus

Maisījums	Fāze pēc suspendēšanas
A/D	D
B/D	D
C/D	D
D/E	D
A/B	B
B/C	B
B/E	B
C/E	B
A/C	A
A/E	A

Polimorfu termodinamiskā stabilitāte salīdzināta, veicot enerģijas aprēķinus ar DFT-D metodi. Iegūtie rezultāti liecina, ka zemākā enerģija un līdz ar to stabilākais polimorfs ir D forma, bet C forma ir visnestabilākā (+20 $kJ \cdot mol^{-1}$), bet pārējo polimorfu stabilitāte ir līdzīga, enerģijas starpībām mainoties +8 – +10 $kJ \cdot mol^{-1}$ intervālā salīdzinājumā ar D formu. Līdzīgu relatīvo stabilitāti polimorfiem apstiprina arī maisījumu suspendēšanas eksperimenti acetonā un etilacetātā 25 °C temperatūrā. Šajos eksperimentos noskaidrots, ka stabilākā ir D forma, kam seko B un A formas. C un E polimorfi savstarpējos maisījumos pārvēršas par B formu (3.2. tabula), kas liecina par šo formu nestabilitāti šajos apstākļos. Līdz ar to, apvienojot eksperimentālos un DFT-D aprēķinu datus, var secināt, ka termodinamiskās stabilitātes rinda 25 °C temperatūrā ir šāda: D > B > A > E > C.

3.3. Enceniklīna hidrogēnhlorīda (3) dekamorfisms

Salīdzinot ar pārējām šeit apskatītajām sistēmām, enceniklīna hidrogēnhlorīds (Enc-HCl) ir visizteiktākais solvātu veidotājs. Kopumā iegūti vairāk nekā 30 solvātu, no kuriem puse kristalizējas kā izostrukturāli solvāti (noteikts pēc režģa parametriem). Vienīgā nesolvatētā fāze, ko iespējams iegūt kristalizējot, ir termodinamiski stabilākais polimorfs IV_D. Šis polimorfs kristalizējas tikai no dimetilforamīda (DMF). Tomēr ir arī vairāki solvāti, kas, zaudējot šķīdinātāju, tiecas pārvērsties par jauniem nesolvatētiem polimorfiem (skat. 3.8. att.), tai skaitā arī četri monohidrāti, kas katrs dehidratējas par jaunu nesolvatētu polimorfu (I_D, II_D, III_D un X_D). Vēl jāpiemin fakts, ka polimorfus VI_D, $VIII_D$, XI_D un XII_D var iegūt, tikai desolvatējot attiecīgi acetonotrila monosolvātu I (S_{ACN-I}), etiķskābes disolvātu (DS_{AA}), skudrskābes monosolvātu (S_{FA}) un acetonitrila monosolvātu II (S_{ACN-II}) eksikatorā virs fosfora pentoksīda ($P_2O)_5$, kas nodrošina 0 % relatīvo mitrumu. Savukārt iepriekš minēto solvātu desolvatācija paaugstinātā temperatūrā noved pie citu polimorfu veidošanās. Kopskaitā, desolvatējot dažādus solvātus, iegūti 12 polimorfi.

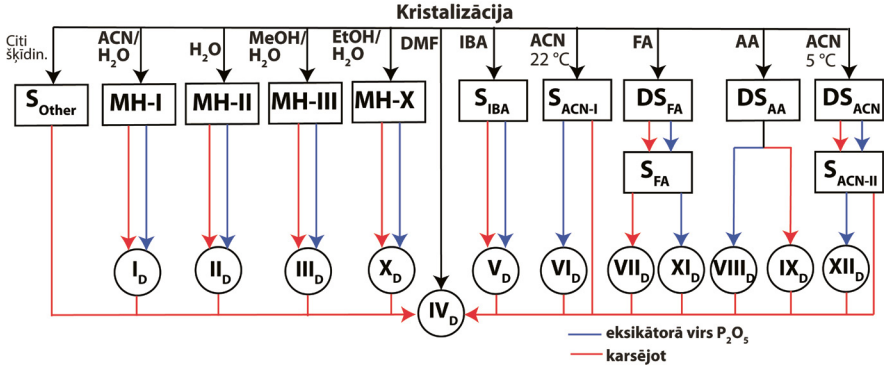

3.8. att. **Shematisks enceniklīna HCl formu iegūšanas un fāžu pārejas attēlojums**

Visu iegūto polimorfu un to attiecīgo prekursoru solvātu/hidrātu rentgendifrakcijas ainas redzamas 3.9. attēlā. Vislielākās līdzības difrakcijas ainās novērojamas starp hidrātiem (MH-I, MH-II, MH-III un MH-X) un starp to dehidratētajām fāzēm (I_D, II_D, III_D un X_D attiecīgi), kas liecina par augstu savstarpējo izostrukturālitāti. Arī starp hidrātiem un dehidrātiem ir līdzīgas difrakcijas ainas, kurās visām fāzēm līdz 15° 2θ skalā signāli novērojami aptuveni tajās pašās pozīcijās. Pārējām prekursoru solvātu fāzēm un to respektīvajiem desolvātiem ir labi izšķiramas difraktogrammas, kuras neliecina par tik augstu savstarpējo strukturālo līdzību. Savukārt trim iegūtajām fāzēm MH-X, X_D un XI_D difrakcijas ainās vienlaikus novēro gan šaurus, gan platus difrakcijas signālus. Tas liecina par nesakārtotību struktūrā, kur molekulas divās dimensijās ir sakārtotas (šaurie refleksi), bet trešajā dimensijā nav (platie refleksi). Šāda veida nesakārtotību var novērot slāņainās struktūrās[49], kur slāņi daļēji ir savstarpēji nobīdīti.

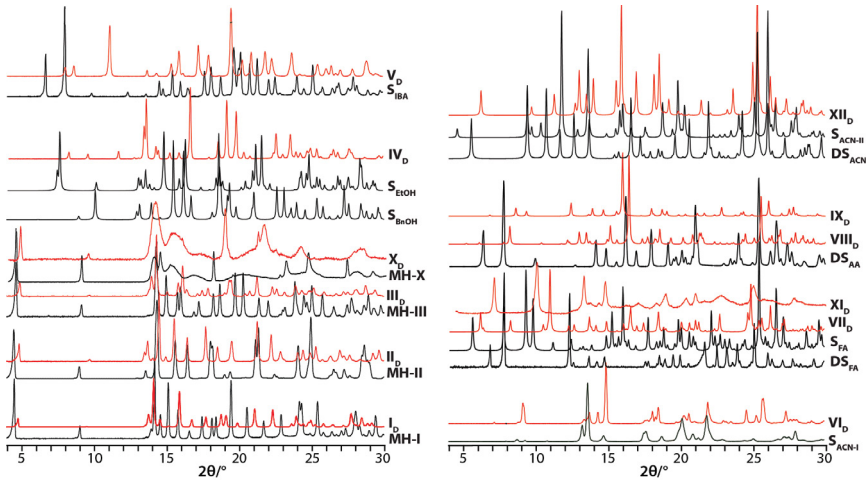

3.9. att. **Enceniklīna solvātu/hidrātu (melnā krāsā) un no tiem iegūto desolvātu (polimorfu, sarkanā krāsā) difraktogrammas**

Kā jau iepriekš minēts, 11 no 12 Enc-HCl polimorfiem ir iespējams iegūt tikai desolvatācijas ceļā, kas nozīmē, ka šīs formas var iegūt tikai mikrokristāliska pulvera veidā un ir nepieciešams izmantot pulvera rentgendifrakciju kristāliskās struktūras noteikšanai. To arī veiksmīgi izdevās veikt 10 polimorfiem. Diemžēl X_D un XI_D formu struktūras palika nenoteiktas to nesakārtotības dēļ. Polimorfa IV_D struktūra vispirms tika noteikta no pulvera datiem, bet vēlāk, kristalizējot no DMF, izdevās izaudzēt arī monokristālu. Abas struktūras sakrita savā starpā. Pēc iegūtajiem struktūras datiem noteikts, ka 7 no 10 polimorfiem kristalizējas divās izplatītākajās Zonkes telpiskajās grupās: $P2_12_12_1$ (IV_D, V_D, VII_D un XII_D) un $P2_1$ (VI_D, $VIII_D$ un IX_D), bet I_D polimorfs – $P3_221$ Zonkes telpiskajā grupā, kamēr II_D un III_D formas ir noteiktas C2 telpiskajā grupā. III_D, VII_D un IX_D formām ir pa divām kristalogrāfiskajām vienībām asimetriskajā vienībā (Z' = 2), bet pārējiem polimorfiem Z' = 1. Lielākoties visiem polimorfiem ir tāda pati telpiskā grupa un arī līdzīgi kristālrežģa parametri kā attiecīgajiem prekursoru solvātiem.

Enceniklīna molekulai ir trīs diedrālie leņķi (skat. 1.4. att.), un dažās struktūrās ir novērojamas konformācijas atšķirības līdz pat 30°, kas rodas, hlorbenzotiofēna grupai rotējot ap C–C (τ1) un hinuklidīna grupai (τ3) rotējot C–N saitēm, tomēr tās visas pieder pie viena globālā enerģijas minimuma, ko apstiprina potenciālās enerģijas virsmas skenēšanas rezultāti visiem diedrālajiem leņķiem. Arī visiem izolētajiem konformēriem gāzes fāzes ģeometrijas optimizācijā vienmēr iegūst identisku konformāciju. Iegūtā konformācijas analīze apliecina, ka Enc-HCl veidotie polimorfi ir pakojuma polimorfi. Šis gadījums ir unikāls, jo, salīdzinot ar citām vielām, kurām ir izteikti liels polimorfu skaits, kā galunisertibam, aripriprazolam, ROY vai flufenamīnskābei[16], Enc-HCl ir vienīgais, kam konformāciju atšķirības nav galvenais polimorfisma virzītājspēks.

Starpmolekulāro mijiedarbību un pakojuma analīze atklāja, ka šīs daudzās polimorfās formas veidojās tāpēc, ka molekulas spēj dažādi sakārtoties kritālrežģī. Šīs dažādās pakojuma iespējas veidojas, jo eksistē pieci dažādi H saišu motīvi, skat. 3.10. attēlu. Tikai vienā struktūrā (I_D) veidojas ciklisks $R^2_4(14)$ tetramērs, sabrūkot heksamēram 1, kad MH-I forma zaudē ūdeni. Lai gan arī heksamērā 2 un 3 ūdens molekulas iesaistās H saišu veidošanā starp enceniklīna katjonu un Cl^- anjonu, dehidratācijas rezultātā izveidojas katamēri 1 un 2 attiecīgi. Pārējos gadījumos šķīdinātāja molekulas ar H saitēm saistās tikai ar Cl^- anjonu un, zaudējot šīs šķīdinātāja molekulas, H saišu motīvs neizmainās. Katamēri 1 C^1_2 (7), 2 C^1_2 (7) un 3 C^1_2 (7), lai gan veido identiskas H saites, tomēr molekulas savstarpēji novietojas atšķirīgi, kas veicina atšķirīga pakojuma veidošanos. Katamērs 1 novērojams polimorfos III_D, IV_D, VI_D un XII_D, katamērs 2 ir atrodams II_D struktūrā, katamērs 3 – VII_D, $VIII_D$ un IX_D struktūrās, un katamērs 4 C^1_1 (7) veido V_D struktūru. Katamērs 4 atšķiras no pārējiem katamēriem, jo H saišu ķēde veidota no N–H···O saitēm nevis no N–H···Cl^-.

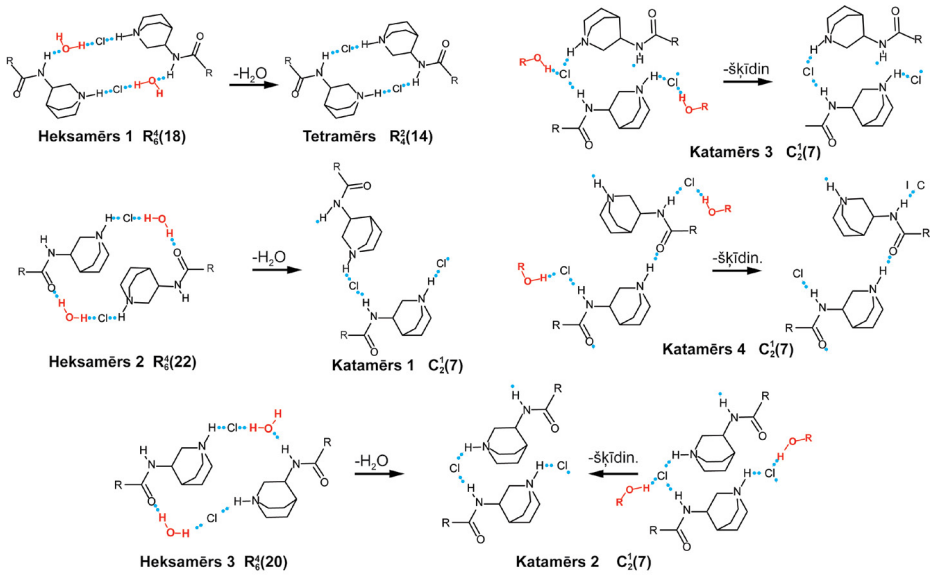

3.10. att. **Enceniklīna HCl formu struktūrās novērotie H saišu motīvi**

Vizuāla pakojuma līdzība starp polimorfiem un attiecīgajiem prekursoru solvātiem/hidrātiem parādīta 3.11. attēlā, savukārt grafisks kvantitatīvs līdzības raksturojums parādīts 3.12. attēlā. Salīdzinot visas struktūras, redzams, ka solvāti/hidrāti, zaudējot šķīdinātāja molekulas, spēj saglābāt savu unikālo pakojumu, kā rezultātā veidojas vairāk vai mazāk strukturāli tuvi desolvāti. Kā jau to varēja nojaust no pulvera rentgendifraktogrammām, tad līdzīgākas struktūras ir starp hidrātiem un to dehidrātiem, ko apstiprina pakojuma līdzības dendogramma (3.12. att. zaļā krāsā). Pārsteidzoši gan ir tas, ka lielāka pakojuma līdzība ir starp MH-I un MH-III hidrātiem un I_D un III_D polimorfiem, nevis starp MH-I/I_D, un MH-III/III_D pāriem. Pārējos gadījumos solvāta un attiecīgā desolvāta strukturālā līdzība ir savstarpēji vistuvākā.

Visu pārējo šeit neminēto solvātu desolvatācijas gadījumā radās IV_D, ko var skaidrot gan ar to, ka šis polimorfs ir termodimamiski stabilākais paaugstinātā temperatūrā, gan arī ar pakojuma līdzībām starp pārējiem solvātiem un IV_D, skatīt S_{EtOH} un IV_D līdzības 3.11. un 3.12. attēlā.

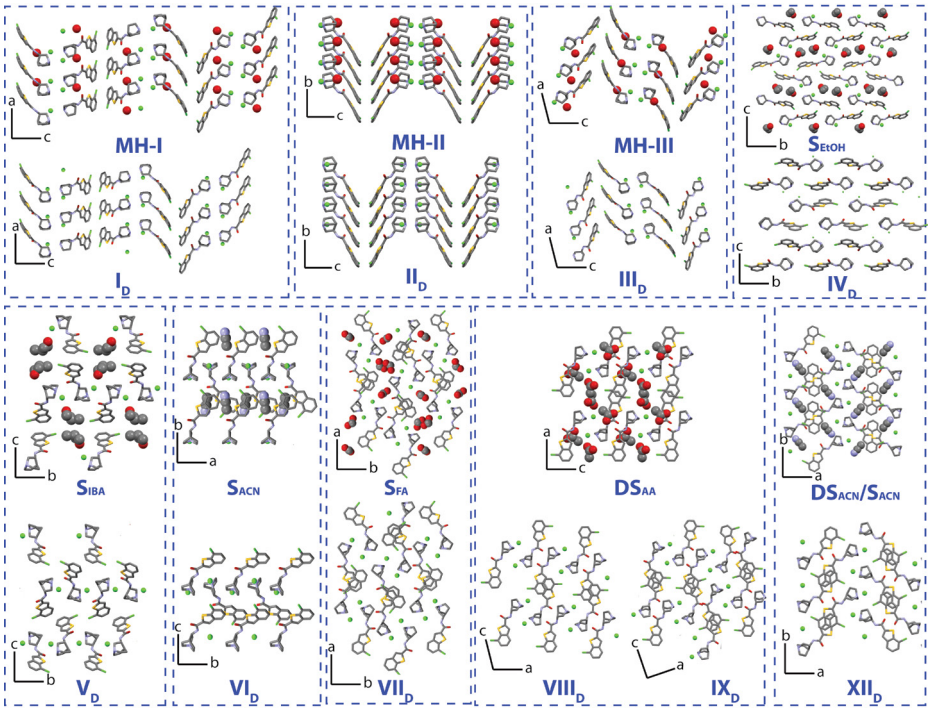

3.11. att. **Enceniklīna HCl polimorfu un atbilstošo solvātu/hidrātu pakojuma līdzības attēlojums**

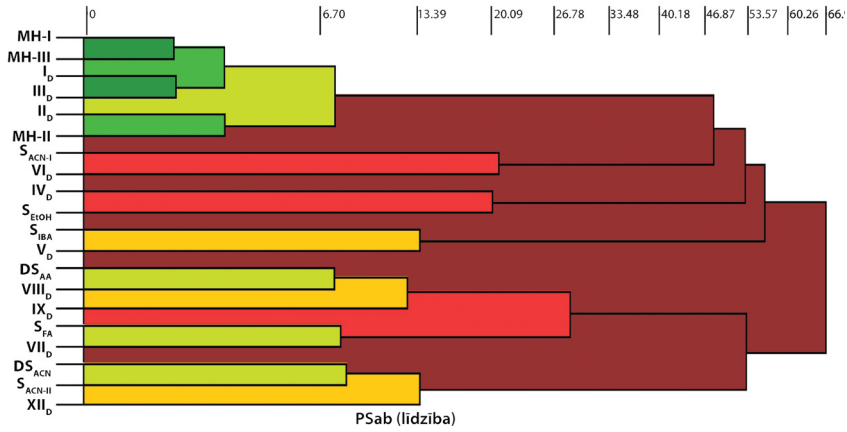

3.12. att. **Enceniklīna HCl polimorfu un atbilstošo solvātu/hidrātu pakojuma līdzības dendogramma**

Diferenciālās skenējošās kalorimetrijas dati (3.13. att. pa kreisi) apstiprināja, ka polimorfam IV_D ir visaugstākā kušanas temperatūra (286 ± 1 °C) un ka, pārējos polimorfus karsējot, tie pārvēršas par IV_D trīs dažādos veidos: 1) endotermiskā fāžu pārejā (V_D), 2) eksotermiskā fāžu pārejā (VI_D un XI_D) vai 3) eksotermiskā pārejā pēc nepilnīgas kušanas/amorfizēšanās, kam atbilst mazais endotermiskais signāls 140–190 °C temperatūrā atkarībā no polimorfa (I_D, II_D, III_D, VII_D, $VIII_D$, IX_D, X_D, un XII_D). Nepilnīgās kušanas/amorfizēšanās entalpija ir pārāk maza (2–7 kJ·mol^{-1}), lai to izmantotu Enc-HCl polimorfu savstarpējās termodinamiskās stabilitātes noteikšanai, līdz ar to, balstoties uz endotermisko/eksotermisko fāžu pārejas likumu[32], ir iespējams noteikt termodinamisko stabilitāti tikai starp trim polimorfu pāriem. IV_D un V_D polimorfi pieder pie enantiotropas sistēmas, savukārt pāri IV_D/VI_D un IV_D/XI_D ir monotropi saistīti. Polimorfo formu maisījumu suspendēšanas rezultāti liecina, ka arī 25 °C temperatūrā termodinamiski stabilākais ir IV_D polimorfs, jo visi maisījumi pārvēršas par IV_D formu. Papildus arī noskaidrota Enc-HCl polimorfu stabilitāte paaugstinātā relatīvajā mitrumā (3.13. att. pa labi). Stabilākais polimorfs ir IV_D forma, kas ir stabila līdz pat 85 % RM, kas pēc tam pārvēršas par MH-I. Relatīvi stabils pret mitrumu ir arī polimorfi V_D, bet pret mitrumu visnestabilākie polimorfi ir I_D, II_D, III_D, $VIII_D$ un IX_D, kas ir stabili tikai tad, ja RM ir mazāks par 5 %.

Lai gan DSK dati un suspendēšanas eksperimenti neatklāj visu polimorfo formu savstarpējo termodinamisko stabilitāti, šī informācija palīdz izvērtēt ticamību enerģijām, kas iegūtas, optimizējot struktūras ar DFD-D metodi, izmantojot dažādus šobrīd aktuālos pseidopontenciālus un/vai dispersijas korekcijas. No eksperimentālajiem rezultātiem izriet, ka V_D formai vajadzētu būt ar viszemāko enerģiju, IV_D vajadzētu būt ar otru zemāko enerģiju un kopējai relatīvās enerģijas starpībai nevajadzētu būt lielākai par ~ 15 kJ·mol^{-1} (tāda ir aptuvenā IV_D formas kušanas entalpija).

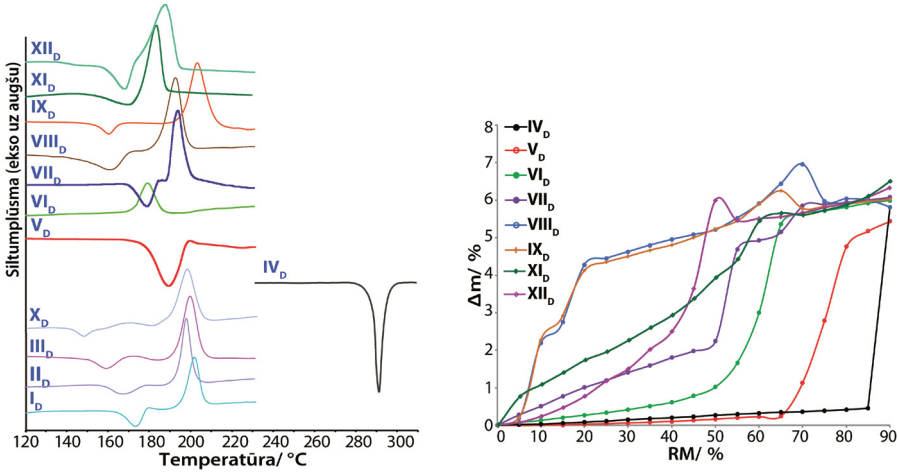

3.13. att. **Enceniklīna HCl polimorfu DSK termogrammas (pa kreisi) un ūdens tvaika sorbcijas izotermas (pa labi)**

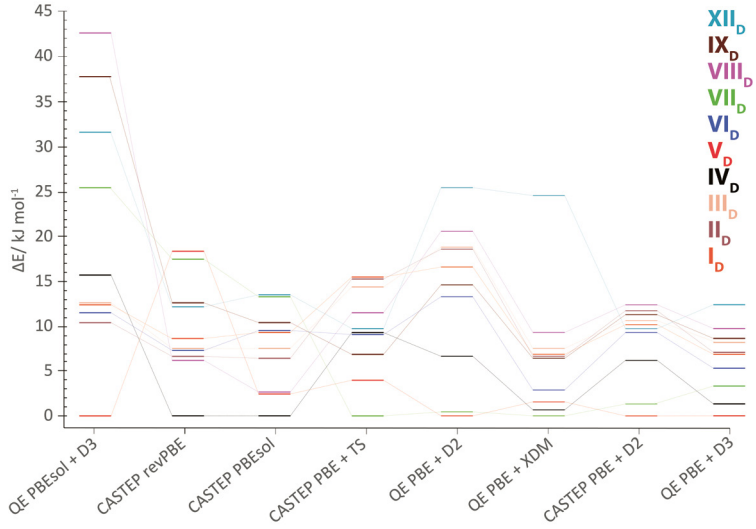

3.14. att. **Enceniklīna HCl polimorfu enerģijas relatīvā attiecība, izmantojot dažādus pseidopotenciālus un/vai dispersijas korekcijas**

No 3.14. attēla var secināt, ka atbilstošākā aprēķinu metode šai sistēmai ir PBE pseidopotenciāls kopā ar D3 dispersijas korekciju, jo ar šo metodi īstenojas visi minētie noteikumi. Līdz ar to aprēķinātā termodinamiskās stabilitātes rinda bez termiskiem ieguldījumiem (0 K) ir $V_D > IV_D$ (+1,5 kJ·mol^{-1}) > VII_D (+3,3 kJ·mol^{-1}) > VI_D (+5,2 kJ·mol^{-1}) > $I_D \approx II_D$ (+7,1 kJ·mol^{-1}) > $III_D \approx IX_D$ (+8,5 kJ·mol^{-1}) > $VIII_D$ (+9,8 kJ·mol^{-1}) > XII_D (+12,2 kJ·mol^{-1}).

3.4. Dantrolēna (4) heksamorfisms

Dantrolēns, atšķirībā no pārējām šajā darbā apskatītajām sistēmām, ir neitrāls molekulārs savienojums. Tomēr arī dantrolēns ir izteikti polimorfisks, un tā polimorfi kristalizējas mikrokristāliska pulvera veidā. Veicot kristalizācijas un suspendēšanas eksperimentus no dažādiem šķīdinātājiem, iegūti trīs polimorfi (I, II un III), trīs monohidrāti (MH-I, MH-II un MH-III) un 16 solvāti. Tālāk, pētot iegūto monohidrātu dehidratāciju, izdevās iegūt vēl trīs dantrolēna polimorfus (IV, V un VI), skat. 3.15. attēlu.

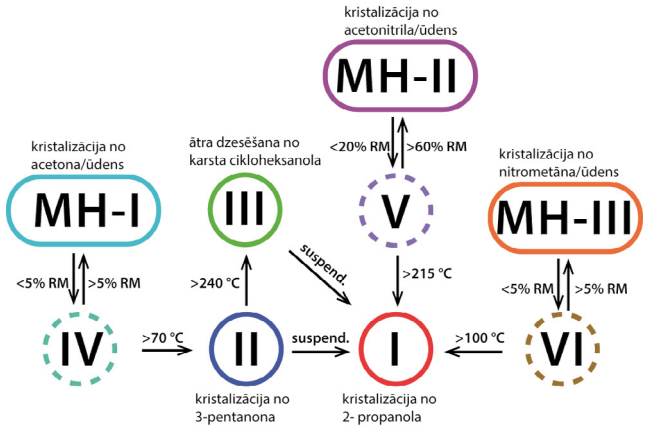

3.15. att. **Shematisks dantrolēna formu iegūšanas un fāžu pāreju attēlojums. Ar nepārtrauktu līniju apzīmētas formas, kas iegūtas, kristalizējot no šķīduma; ar pārtrauktu līniju parādītas formas, kas iegūtas desolvatācijas ceļā**

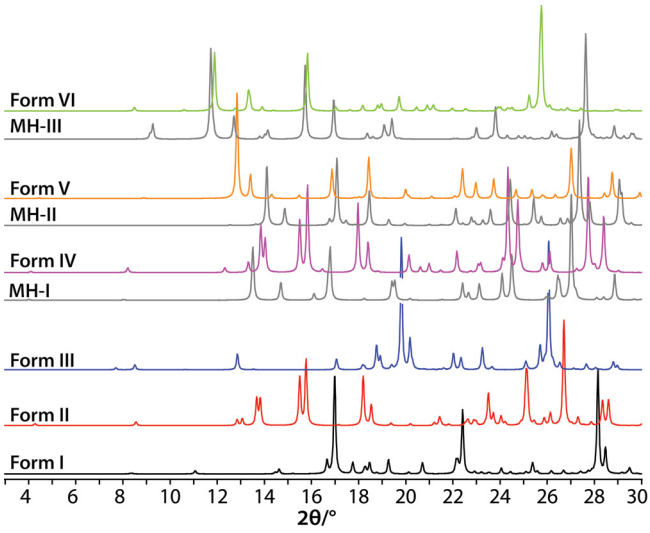

3.16. att. **Dantrolēna polimorfu un monohidrātu difraktogrammas**

Iegūto polimorfu un monohidrātu rentgendifraktogrammas attēlotas 3.16. att., kurā redzams, ka katram polimorfam ir unikāla un viegli atšķirama difrakcijas aina un arī starp polimorfu un atbilstošo monohidrātu difrakcijas ainām ir novērojama pietiekama atšķirība, lai polimorfi netiktu uzskatīti par izomorfiem desolvātiem.

I, II, IV, V, VI, MH-I un MH-III formu kristāliskās struktūras aprēķinātas no pulvera difrakcijas datiem, bet III un MH-II formu struktūras iegūtas no monokristālu rentgenstruktūranalīzes. I, II un III forma kristalizējas centrosimetriskā $P2_1/c$ ($P2_1/n$) telpiskā grupā, bet polimorfi IV un V kristalizējas attiecīgi $P2_1$ un $P2_12_12_1$ necentrosimetriskās telpiskās grupās, bet polimorfs VI centrosimetriskā $P\bar{1}$ grupā. Visās noteiktajās struktūrās asimetriskajā vienībā ir viena dantrolēna molekula ($Z' = 1$). Eksperimentālajās struktūrās ir atrodamas divas atšķirīgas dantrolēna molekulārās konformācijas (A un B), skat. 3.17. a attēlu. Globālā minimuma A konformācija ir novērojama I un III formas kristāliskajā struktūrā, savukārt lokālā minimuma B konformācija visās parējās struktūrās. Galvenā atšķirība starp abām konformācijām ir furilgrupas pagriešanās par 180 ° ap diedrālo leņķi τ2, kas rezultējas ~3 kJ·mol^{-1} enerģijas starpībā (3.17. b att.). Dantrolēna molekulā ir tikai viens ūdeņraža saites donors (N–H grupa) un vairākas vietas, kas var darboties kā potenciālie H saites akceptori. Neskatoties uz to, polimorfu eksperimentālajās struktūrās var novērot trīs atšķirīgus ūdeņraža saišu motīvus, ko veido abi potenciāli spēcīgākie H saišu akceptori (3.17. c att.): $R^2_2(8)$ *a* I un III formā to veido N2–H10···O1 mijiedarbība, $R^2_2(8)$ *b* II un VI formā to veido N2–H10···O2 mijiedarbība, bet $C^1_1(4)$ V formā – N2–H10···O2 mijiedarbība. IV formas struktūrā nav novērojama neviena klasiska ūdeņraža saite, lai gan var novērot $C^1_1(2)$ motīvu, ko veido vāja N2–H10···N2 mijiedarbība.

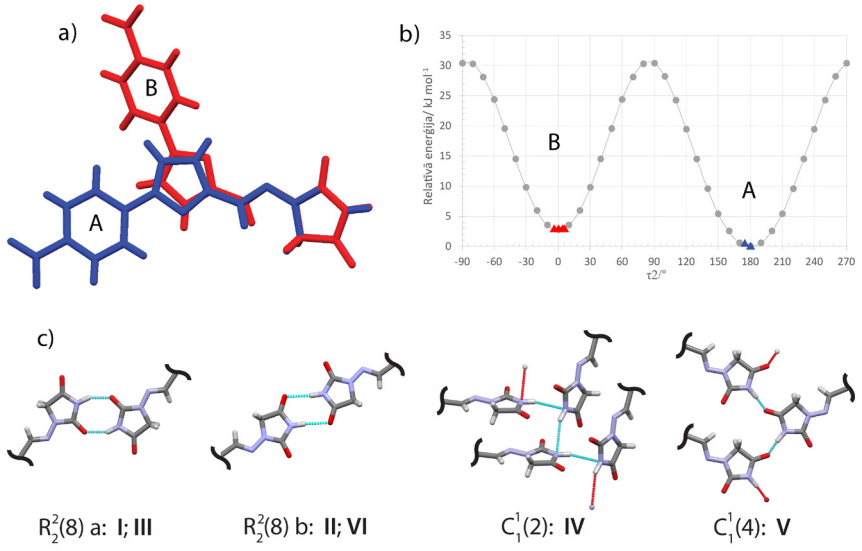

3.17. att. **(a) Dantrolēna kristāliskajās struktūrās novēroto divu atšķirīgo eksperimentālo konformāciju vizuāls salīdzinājums – A zilā un B sarkanā krāsā, (b) dantrolēna potenciālās enerģijas virsma pie mainīgām diedrālā leņķa τ2 vērtībām un (c) eksperimentālajās struktūrās novērotie starpmolekulārie ūdeņraža saišu motīvi**

Salīdzinot molekulāro pakojumu dantrolēna bezūdens polimorfu un monohidrātu struktūrās, tos ir iespējams sakārtot trīs radniecīgu struktūru grupās (3.18. att.). 1. grupu veido I un III polimorfu kristāliskās struktūras, jo šajās struktūrās molekulām ir vienāda konformācija, ūdeņraža saišu motīvs un slāņi, kuros izvietotas molekulas gar a kristalogrāfisko asi, bet pakojums gar abām pārējām asīm ir atšķirīgs, kas rezultējas zemāka pakojuma līdzībā starp vienas un tās pašas grupas kristāliskajām formām. Lielākajā 2. grupā ietilpst polimorfi II, IV, V un monohidrāti MH-I, MH-II. Starp šīm formām ir novērojama vislielākā molekulu pakojuma līdzība, jo visās struktūrās ir novērojami vienādi 2D zig-zag slāņi. 3. grupu veido monohidrāts MH-III un šīs formas dehidratētā fāze – polimorfs VI. Galvenā pakojuma atšķirība starp šīm fāzēm ir saistīta ar nedaudz atšķirīgo VI formas molekulāro konformāciju (nitrobenzola grupa pagriezta par ~30°), ļaujot dantrolēna molekulām sapakoties ciešāk nekā MH-III struktūrā.

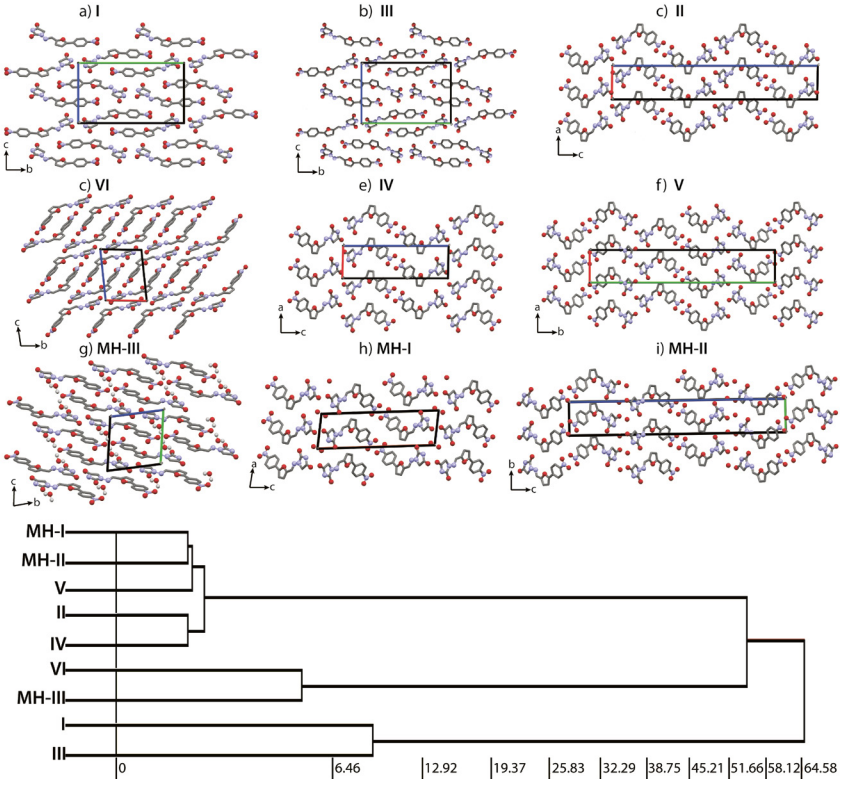

3.18. att. **Vizuāls un kvantitatīvs pakojuma līdzības attēlojums dantrolēna hidrātos un bezūdens polimorfos. Dendrogrammas horizontālā ass atbilst PSab vērtībai (līdzība)**

Lai apzinātu potenciāli enerģētiski izdevīgākās dantrolēna kristāliskās struktūras un lai pārbaudītu, vai starp eksperimentāli iegūtajiem polimorfiem ir atrodama struktūra ar viszemāko enerģiju, veikta *ab initio* kristālisko struktūru paredzēšana, izmantojot CrystalPredictor un CrystalOptimizer programmas. Pēc tam struktūras ar zemāko

enerģiju (138 struktūras, kam Z ≤ 4) vēlreiz optimizēja ar PBE-D2 metodi. Šī pati pieeja (CrystalOptimizer + PBE-D2) izmantota arī sešām eksperimentāli noteiktajām struktūrām. Iegūto kristālisko struktūru apkopojums redzams 3.19. attēlā. Šī skaitļošanas pieeja bija veiksmīga, lai identificētu piecas no sešām eksperimentālajām polimorfu kristāliskajām struktūrām pēc $RMSD_{15}$ vērtībām starp eksperimentālajām un paredzētajām struktūrām. Lai gan starp paredzētajām struktūrām ir struktūra (B1) ar vienādu konformāciju, telpisko grupu, līdzīgiem kristālrežģa parametriem un enerģiju kā III formai, tomēr tai ir atšķirīgs ūdeņraža saišu motīvs (B1 ir $R^2_2(8)$b, bet III formā $R^2_2(8)$a, skat. 3.17. c att.), kas rezultējas lielā $RMSD_{15}$ = 0,66 Å vērtībā. III formas trūkums, iespējams, ir saistīts ar plastisku zemtemperatūras pāreju starp B1 un III formu, kuras laikā mainās H saišu motīvs.

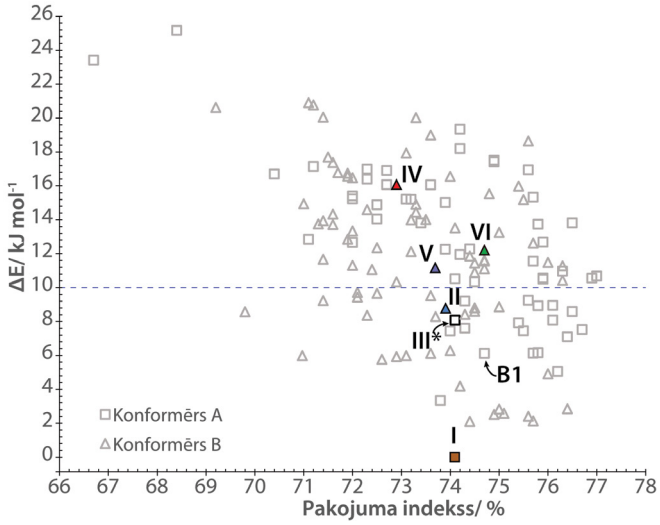

3.19. att. **Dantrolēna kristālisko struktūru apkopojums, kur katrs trijstūris un kvadrāts atspoguļo stabilu kristālrežģa enerģijas minimumu, kas iegūts kristālisko struktūru paredzēšanā un pēc tam veiktā ģeometrijas optimizācijā ar DFT-D. Identificētās eksperimentāli iegūtās struktūras ir iekrāsotas un marķētas. Apkopojums papildināts ar III formas eksperimentālo struktūru pēc identiska skaitļošanas protokola. Horizontālā punktētā līnija apzīmē tipisku polimorfo formu relatīvās enerģijas diapazonu 10 kJ·mol^{-1}**

Dantrolēna polimorfo formu termodinamiskā stabilitāte noteikta, izmantojot klasisko (DSK) un ultra ātro (FSK) skenējošās kalorimetrijas analīzi, politermiskās šķīdības eksperimentus, kas papildināti ar kristālrežga enerģijas aprēķiniem ar dažādām periodiskām DFT-D metodēm. Iegūtie rezultāti redzami 3.20. attēlā. No DSK rezultātiem iespējams noteikt, ka polimorfi IV, II, V, VI ir monotropi saistīti ar polimorfu I, par ko liecina eksotermiskās fāžu pārejas (3.20. a att.), bet endotermiska fāžu pāreja starp polimorfiem II un III liecina par pārejas punktu starp šīm formām. Tā kā dantrolēns kūstot arī sadalās, tad, lai atdalītu šos procesus un noteiktu savstarpējo stabilitāti atkarībā no

kušanas siltuma un temperatūras vērtībām, izmantota FSK metode ar karsēšanas ātrumu 2000 °C·s^{-1}. Iegūtie rezultāti liecina (3.20.b att.), ka starp I un II un starp I un III formu ir monotropa saistība un ka forma I ir termodinamiski visstabilākais polimorfs.

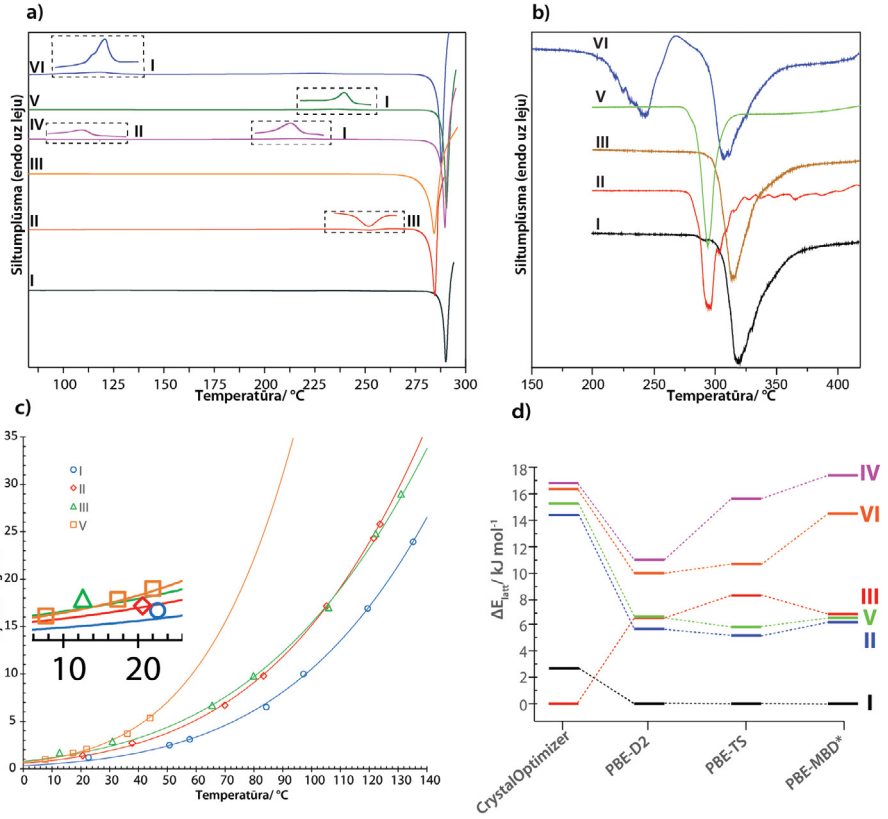

3.20. att. **a) dantrolēna polimorfu (I–VI) DSK termogrammas (10 °C·min^{-1}), b) dantrolēna polimorfu I, II, III, V un VI FSK termogrammas (2000 °C·s^{-1}), c) dantrolēna I, II, III un V formu politermiskā šķīdība (mg·ml^{-1}) cikloheksanonā, d) polimorfo formu relatīvās enerģijas, kas noteiktas, izmantojot dažādas periodiskas DFT-D metodes salīdzinājumā ar *CrystalOptimizer* iegūto enerģiju**

No šķīdības līknēm var spriest par aptuvenām fāžu pāreju temperatūrām starp polimorfiem II un III un starp V un III, skat. 3.20. c att.). Redzams, ka II un III formas šķīdības līknes krustojas aptuveni 110 °C temperatūrā, savukārt III un V formas līknes krustojas aptuveni 15 °C temperatūrā.

Tādējādi, apvienojot iegūtos rezultātus, kas iegūti no iepriekš minētajām metodēm kopā ar enerģijas aprēķiniem, var secināt, ka termodinamiskā stabilitāte laboratorijas (25 °C) apstākļos ir I > II > III > V > VI > IV. Bet, tā kā polimorfu pāri III/V un II/III ir enantiotropiski saistīti, tad zem 15 °C temperatūras šī stabilitātes rinda izmainās pret I > II > V > III > VI > IV, bet virs 110 °C temperatūras – I > III > II > V > VI > IV.

SECINĀJUMI

1. Visu trīs hifenadīna hidrogēnhlorīda polimorfo formu kristāliskajās struktūrās ir novērojams viens un tas pats ūdeņraža saišu motīvs (tetramērs, kas sastāv no diviem hifenadīna katjoniem un diviem hlorīda anjoniem). Dihidrāta struktūrā veidojas komplicēts ūdeņraža saišu tīkls, kas stabilizē šo struktūru. Ūdens molekulas atrodas struktūras kanālos un dehidratācijas rezultātā rodas strukturāli tuvs polimorfs B. Pāreja starp dihidrātu un B formu ir apgriezeniska un atkarīga no relatīvā gaisa mitruma.
2. Iegūti un strukturāli raksturoti seši sehifenadīna hidrogēnhlorīda polimorfi. Lai gan šo polimorfu struktūrās novēro trīs dažādas konformācijas, detalizēta struktūru analīze norāda, ka galvenās atšķirības starp šiem polimorfiem ir tieši pakojumā, ko nodrošina trīs dažādi ūdeņraža saišu motīvi. Visu iegūto sehifenadīna hidrogēnhlorīda hidrātu struktūras liecina, ka tie rodas, ūdenim iespiežoties specifisku polimorfu starpslāņu telpā.
3. Kopumā iegūti un strukturāli raksturoti desmit enceniklīna hidrogēnhlorīda polimorfi, kas ir jauns rekords gan pakojuma polimorfisma, gan arī organisku sāļu kategorijās. Visus termodinamiski nestabilos polimorfus var iegūt, desolvatējot specifiskus solvātus vai hidrātus, un šajā procesā saglabājas gan ūdeņraža saišu motīvi (izņemot hidrātus), gan arī pakojums. Visās struktūrās ir gandrīz identiska enceniklīna katjona konformācija, kas pieder pie viena enerģijas minimuma.
4. Dantrolēns ir spējīgs veidot vismaz sešus dažādus polimorfus, no kuriem trīs var iegūt kristalizācijā (I, II un III) un vēl trīs (IV, V un VI) dehidratācijas ceļā no trim dažādiem monohidrātiem. Galvenie šo formu rašanās iemesli ir vismaz divas enerģētiski izdevīgas konformācijas, iespēja veidot dažādas ūdeņraža saites, kā arī dehidratēto formu spēja saglabāt pamatstruktūru pēc ūdens molekulu aizvadīšanas no monohidrātu struktūrām.
5. Pulvera rentgendifrakcijas dati, globālās optimizēšanas metodes un periodisku dispersijas koriģēta blīvuma funkcionāļa teorijas aprēķinu izmantošana nodrošina neatkarīgu metodi kristāliskās struktūrās noteikšanai formām, kuras iegūtas sīkkristāliska pulvera veidā.
6. Desolvatējot farmaceitiski aktīvo vielu solvātus, iegūti vairāki polimorfi, kurus iespējams izmantot kā jaunas, stabilas, tai skaitā patentējamas, gatavo zāļu vielu formas.

LITERATŪRAS SARAKSTS

(1) Yu, L.; Stephenson, G. A.; Mitchell, C. A.; Bunnell, C. A.; Snorek, S. V; Bowyer, J. J.; Borchardt, T. B.; Stowell, J. G.; Byrn, S. R. Thermochemistry and Conformational Polymorphism of a Hexamorphic Crystal System. *J. Am. Chem. Soc.* **2000**, *122*, 585–591.

(2) Sun, C.; Grant, D. J. W. Influence of Crystal Structure on the Tableting Properties of Sulfamerazine Polymorphs. *Pharm. Res.* **2001**, *18*, 274–280.

(3) Pudipeddi, M.; Serajuddin, A. T. M. Trends in Solubility of Polymorphs. *J. Pharm. Sci.* **2005**, *94*, 929–939.

(4) Price, S. L. Control and Prediction of the Organic Solid State: A Challenge to Theory and Experiment. *Proc. R. Soc. A Math. Phys. Eng. Sci.* **2018**, *474* , 20180351.

(5) Bingham, A. L.; Hughes, D. S.; Hursthouse, M. B.; Lancaster, R. W.; Tavener, S.; Threlfall, T. L. Over One Hundred Solvates of Sulfathiazole. *Chem. Commun.* **2001**, *7,* 603–604.

(6) Chen, S.; Guzei, I. A.; Yu, L. New Polymorphs of ROY and New Record for Coexisting Polymorphs of Solved Structures. *J. Am. Chem. Soc.* **2005**, *127*, 9881–9885.

(7) Yu, L. Polymorphism in Molecular Solids: An Extraordinary System of Red, Orange, Yellow Crystals. *Acc. Chem. Res.* **2010**, *43*, 1257–1266.

(8) Tyler, A. R.; Ragbirsingh, R.; McMonagle, C. J.; Waddell, P. G.; Heaps, S. E.; Steed, J. W.; Thaw, P.; Hall, M. J.; Probert, M. R. Encapsulated Nanodroplet Crystallization of Organic-Soluble Small Molecules. *Chem.* **2020**, *6*, 1755–1765.

(9) Lévesque, A.; Maris, T.; Wuest, J. D. ROY Reclaims Its Crown: New Ways To Increase Polymorphic Diversity. *J. Am. Chem. Soc.* **2020**, *142*, 11873–11883.

(10) Li, X.; Ou, X.; Rong, H.; Huang, S.; Nyman, J.; Yu, L.; Lu, M. The Twelfth Solved Structure of ROY: Single Crystals of Y04 Grown from Melt Microdroplets. *Cryst. Growth Des.* **2020**, *20* , 7093–7097.

(11) Bobrovs, R.; Kons, A.; Bērziņš, A.; Rekis, T.; Actiņš, A. Formation and Transformations of Organic Salt Hydrates: Four Encenicline Hydrochloride Monohydrates and Respective Isostructural Desolvates. *Cryst. Growth Des.* **2018**, *18*, 2100–2111.

(12) Kons, A.; Bērziņš, A.; Actiņš, A.; Rekis, T.; van Smaalen, S.; Mishnev, A. Polymorphism of R-Encenicline Hydrochloride: Access to the Highest Number of Structurally Characterized Polymorphs Using Desolvation of Various Solvates. *Cryst. Growth Des.* **2019**, *19*, 4765–4773.

(13) Bhardwaj, R. M.; McMahon, J. A.; Nyman, J.; Price, L. S.; Konar, S.; Oswald, I. D. H.; Pulham, C. R.; Price, S. L.; Reutzel-Edens, S. M. A Prolific Solvate Former, Galunisertib, under the Pressure of Crystal Structure Prediction, Produces Ten Diverse Polymorphs. *J. Am. Chem. Soc.* **2019**, *141*, 13887–13897.

(14) Zeidan, T. A.; Trotta, J. T.; Tilak, P. A.; Oliveira, M. A.; Chiarella, R. A.; Foxman, B. M.; Almarsson, Ö.; Hickey, M. B. An Unprecedented Case of Dodecamorphism: The Twelfth Polymorph of Aripiprazole Formed by Seeding with Its Active Metabolite. *CrystEngComm* **2016**, *18*, 1486–1488.

(15) Li, X.; Ou, X.; Wang, B.; Rong, H.; Wang, B.; Chang, C.; Shi, B.; Yu, L.; Lu, M. Rich Polymorphism in Nicotinamide Revealed by Melt Crystallization and Crystal Structure Prediction. *Commun. Chem.* **2020**, *3*, 152.

(16) López-Mejías, V.; Kampf, J. W.; Matzger, A. J. Nonamorphism in Flufenamic Acid and a New Record for a Polymorphic Compound with Solved Structures. *J. Am. Chem. Soc.* **2012**, *134*, 9872–9875.

(17) López-Mejías, V.; Kampf, J. W.; Matzger, A. J. Polymer-Induced Heteronucleation of Tolfenamic Acid: Structural Investigation of a Pentamorph. *J. Am. Chem. Soc.* **2009**, *131*, 4554–4555.

(18) Case, D. H.; Srirambhatla, V. K.; Guo, R.; Watson, R. E.; Price, L. S.; Polyzois, H.; Cockcroft, J. K.; Florence, A. J.; Tocher, D. A.; Price, S. L. Successful Computationally Directed Templating of Metastable Pharmaceutical Polymorphs. *Cryst. Growth Des.* **2018**, *18*, 5322–5331.

(19) Braun, D. E.; Gelbrich, T.; Kahlenberg, V.; Tessadri, R.; Wieser, J.; Griesser, U. J. Stability of Solvates and Packing Systematics of Nine Crystal Forms of the Antipsychotic Drug Aripiprazole. *Cryst. Growth Des.* **2009**, *9*, 1054–1065.

(20) Lohani, S.; Grant, D. J. W. Thermodynamic of Polymorphs. In *Polymorphism: In the pharmaceutical industry*; 2006; 21–42.

(21) Grothe, E.; Meekes, H.; Vlieg, E.; ter Horst, J. H.; de Gelder, R. Solvates, Salts, and Cocrystals: A Proposal for a Feasible Classification System. *Cryst. Growth Des.* **2016**, *16*, 3237–3243.

(22) Yu, L.; Reutzel, S. M.; Stephenson, G. a. Physical Characterization of Polymorphic Drugs: An Integrated Characterization Strategy. *Pharm. Sci. Technolo. Today* **1998**, *1*, 118–127.

(23) Stahly, G. P. Diversity in Single- and Multiple-Component Crystals. The Search for and Prevalence of Polymorphs and Cocrystals. *Cryst. Growth Des.* **2007**, *7*, 1007–1026.

(24) Karpinski, P. H. Polymorphism of Active Pharmaceutical Ingredients. *Chem. Eng. Technol.* **2006**, *29*, 233–237.

(25) Chieng, N.; Rades, T.; Aaltonen, J. An Overview of Recent Studies on the Analysis of Pharmaceutical Polymorphs. *J. Pharm. Biomed. Anal.* **2011**, *55*, 618–644.

(26) Braga, D.; Grepioni, F.; Maini, L.; Polito, M. Crystal Polymorphism and Multiple Crystal Forms; 2009; 25–50.

(27) Näther, C.; Jess, I.; Jones, P. G.; Taouss, C.; Teschmit, N. Structural, Thermodynamic, and Kinetic Aspects of the Polymorphism of Trimethylthiourea: The Influence of Kinetics on the Transformations between Polymorphs. *Cryst. Growth Des.* **2013**, *13*, 1676–1684.

(28) Gavezzotti, A. A Solid-State Chemist's View of the Crystal Polymorphism of Organic Compounds. *Journal of Pharmaceutical Sciences*. 2007, 2232–2241.

(29) Sarma, B.; Chen, J.; Hsi, H.; Myerson, A. S. Solid Forms of Pharmaceuticals: Polymorphs, Salts and Cocrystals. *Korean J. Chem. Eng.* **2011**, *28*, 315–322.

(30) Day, G. M.; S Motherwell, W. D.; Jones, W. A Strategy for Predicting the Crystal Structures of Flexible Molecules: The Polymorphism of Phenobarbital. *Phys. Chem. Chem. Phys.* **2007**, *9*, 1693–1704.

(31) Seton, L.; Khamar, D.; Bradshaw, I. J.; Hutcheon, G. a. Solid State Forms of Theophylline: Presenting a New Anhydrous Polymorph. *Cryst. Growth Des.* **2010**, *10*, 3879–3886.

(32) Burger, A.; Ramberger, R. On the Polymorphism of Pharmaceuticals and Other Molecular Crystals. I. *Mikrochim. Acta*. **1979**, *72*, 259–271.

(33) Pindelska, E.; Sokal, A.; Kolodziejski, W. Pharmaceutical Cocrystals, Salts and Polymorphs: Advanced Characterization Techniques. *Adv. Drug Deliv. Rev.* **2017**, *117*, 111–146.

(34) Harris, K. D. M. Powder Diffraction Crystallography of Molecular Solids. *Top. Curr. Chem.* **2012**, *315*, 133–178.

(35) Brüning, J.; Schmidt, M. U. The Determination of Crystal Structures of Active Pharmaceutical Ingredients from X-Ray Powder Diffraction Data: A Brief, Practical Introduction, with Fexofenadine Hydrochloride as Example. *J. Pharm. Pharmacol.* **2015**, *67*, 773–781.

(36) J. Bernstein; S. M. Reutzel-Edensc. International Tables for Crystallography. In *International Tables for Crystallography*; Gilmore, C. J., Kaduk, J. A., Schenk, H., Eds.; International Union of Crystallography: Chester, England, 2019; Vol. H, 2019.

(37) Pawley, G. S. Unit-Cell Refinement from Powder Diffraction Scans. *J. Appl. Crystallogr.* **1981**, *14*, 357–361.

(38) Le Bail, A.; Duroy, H.; Fourquet, J. L. Ab-Initio Structure Determination of LiSbWO6 by X-Ray Powder Diffraction. *Mater. Res. Bull.* **1988**, *23*, 447–452.

(39) Boultif, A.; Louër, D. Powder Pattern Indexing with the Dichotomy Method. *J. Appl. Crystallogr.* **2004**, *37*, 724–731.

(40) Altomare, A.; Campi, G.; Cuocci, C.; Eriksson, L.; Giacovazzo, C.; Moliterni, A.; Rizzi, R.; Werner, P.-E. Advances in Powder Diffraction Pattern Indexing: N-TREOR09. *J. Appl. Crystallogr.* **2009**, *42*, 768–775.

(41) Oishi-Tomiyasu, R. Distribution Rules of Systematic Absences on the Conway Topograph and Their Application to Powder Auto-Indexing. *Acta Crystallogr. Sect. A Found. Crystallogr.* **2013**, *69*, 603–610.

(42) Van de Streek, J.; Neumann, M. A. Validation of Molecular Crystal Structures from Powder Diffraction Data with Dispersion-Corrected Density Functional Theory (DFT-D). *Acta Crystallogr. Sect. B Struct. Sci. Cryst. Eng. Mater.* **2014**, *70*, 1020–1032.

(43) Makarov, L.; Balykova, L.; Soldatova, O.; Komolyatova, V.; Serebruany, V. The Antiarrhythmic Properties of Quifenadine, H1-Histamine Receptor Blocker in Children with Premature Beats: A Randomized Controlled Pilot Trial. *Am. J. Ther.* **2012**, *17*, 396–401.

(44) Gankina, E. M.; Porodenko, N. V.; Kondratenko, R. Y.; Severin, E. S.; Kaminka, M. E.; Mashkovskii, M. D. Effect of Some Antihistamine Preparations on Binding Of3H-Mepyramine And3H-Cimetidine to Histamine Receptors in Rat Brain. *Pharm. Chem. J.* **1992**, *26*, 373–376.

(45) Prickaerts, J.; Van Goethem, N. P.; Chesworth, R.; Shapiro, G.; Boess, F. G.; Methfessel, C.; Reneerkens, O. A. H.; Flood, D. G.; Hilt, D.; Gawryl, M. EVP-6124, a Novel and Selective A7 Nicotinic Acetylcholine Receptor Partial Agonist, Improves Memory Performance by Potentiating the Acetylcholine Response of A7 Nicotinic Acetylcholine Receptors. *Neuropharmacology*. **2012**, *62*, 1099–1110.

(46) Oliver-Shaffer, P.; Shapiro, G.; Chesworth, R.; Kishida, M.; Ishige, T. Crystalline Form of (R)-7-Chloro-N-(Quinuclidin-3-Yl) Benzo [B] Thiophene-2-Carboxamide Hydrochloride Monohydrate. US 2014/0249179, 2014.

(47) Krause, T.; Gerbershagen, M. U.; Fiege, M.; Weißhorn, R.; Wappler, F. Dantrolene? A 1

Review of Its Pharmacology, Therapeutic Use and New Developments. *Anaesthesia*. **2004**, *59*, 364–373.

(48) Tanaka, R.; Akimoto, T.; Haramura, M.; Tanaka, A.; Hirayama, N. Structure of Dantrolene. *X-ray Struct. Anal. Online*. **2004**, *20*, 97.

(49) Wang, C.; Sun, C. C. Identifying Slip Planes in Organic Polymorphs by Combined Energy Framework Calculations and Topology Analysis. *Cryst. Growth Des.* **2018**, *18*, 1909–1916.

UNIVERSITY OF LATVIA

FACULTY OF CHEMISTRY

Artis Kons

USE OF POWDER X-RAY DIFFRACTION AND COMPUTATIONAL METHODS FOR STRUCTURAL CHARACTERIZATION OF SELECTED HIGHLY POLYMORPHIC ACTIVE PHARMACEUTICAL SOLIDS

Doctoral Thesis

Submitted for the Degree of Doctor of Chemistry

Subfield of Physical Chemistry

Scientific supervisor:

Asoc. prof., Dr. chem. **Agris Bērziņš**

RIGA, 2021

The Doctoral Thesis was carried out at the Chair of Physical Chemistry, Faculty of Chemistry, University of Latvia, Riga, Latvia from 2014 to 2020.

LATVIJAS
UNIVERSITĀTE

The Thesis contains the Summary in Latvian and English, 5 scientific articles. Form of the Thesis: collection of scientific articles in chemistry, Physical Chemistry.

Scientific supervisor:
Asoc. prof., *Dr. chem.* **Agris Bērziņš**

Reviewers:
1) Prof., *Dr. chem.* **Donāts Erts** (University of Latvia)
2) *Dr. chem.* **Mihails Arhangelskis** (University of Warsaw)
3) Prof., Dr. **Fabrizia Grepioni** (University of Bologna)

The Thesis will be defended in a public session of the Promotional Committee of Chemistry, University of Latvia at 14.00 on August 23, 2021 at the University of Latvia, Academic Center for Natural Sciences, Jelgavas 1, Riga.

The summary of the Thesis is available at the Library of the University of Latvia, Raiņa bulv. 19.

ISBN 978-9934-18-693-6
ISBN 978-9934-18-694-3 (PDF)

ABSTRACT

Several active pharmaceutical solids with abundant microcrystalline polymorphism have been studied. Screening of polymorphs and solvates/hydrates was carried out using crystallization from various solvents and by solid state transformation at different temperatures and relative humidity conditions. Stability and phase transformations among the obtained crystalline forms were investigated by X-ray powder diffraction (PXRD), differential scanning calorimetry (DSC), thermogravimetry analysis (TGA), and dynamic vapor sorption analysis. Slurry-bridging experiments at ambient temperature were carried out to ascertain the relative thermodynamic stability of the polymorphs. Crystal structures of 33 microcrystalline polymorphs have been determined from powder diffraction data. Crystal structure optimization and validation was carried out using dispersion corrected density functional theory (DFT-D) calculations. Crystal structure information is used to explain and rationalize the formation, phase transition and relative stability of polymorphs.

Keywords: *polymorphism, thermodynamic stability, microcrystalline powder, X-ray powder diffraction, structure determination, dispersion corrected density functional theory*

INTRODUCTION

Many organic molecules, including active pharmaceutical solids, are able to form polymorphs (i.e., compounds of identical chemical composition but different crystalline structure). Although this phenomenon has been known for at least 180 years, only in the last two decades there has been a significant increase in activity in this field, driven by both fundamental scientific curiosity and industrial need.

Different polymorphs can have significantly different solid-state properties like stability[1], mechanical properties[2] and bioavailabilitiy[3]. Thus, important aspects of research of polymorphism are discovery, structural characterization, and physicochemical understanding of the full range of polymorphic forms that are accessible to a given molecule, as well as development of reliable and reproducible procedures for the formation of each specific polymorph.

In order to understand the phenomenon of polymorphism, it is essential to have access to systems that exhibit abundant polymorphism comprising several well characterized polymorphs of a given molecule. Thus, while most published polymorph systems have only two known polymorphs, substances existing in large number of polymorphic forms provide more profound opportunities for exploring the fundamentals of polymorphism. Thus, the discovery and characterization of new systems that exhibit large number of polymorphic forms can make a significant contribution to improving our understanding of polymorphism.

The diversity of solid form landscape can be very different, as there are compounds that form only monomorphs[4], whereas for other substances 10 or more polymorphic forms are known. If we take into account the formation of solvates (i.e., phases that have solvent molecules in the crystalline lattice), the number of solid forms formed by a compound can grow to 100 or even more[5]. Currently the most abundant polymorphic systems is 5-methyl-2-[(2-nitrophenyl)amino]-3-thiophenecarbonitrile (ROY)[1,6–10] with 13 structurally characterized polymorphs, followed by R-encenicline hydrochloride[11,12] and galunisertib[13], both having 10 reported polymorphs with determined crystal structures, aripiprazole[14] and nicotinamide[15] with 9 polymorphs and flufenamic acid[16] and tolfenamic acid[17,18] with 8 polymorphs. Moreover, according to the Cambridge Structural Database, molecular solids with three or more polymorphs with determined crystal structures are very rare.

A high tendency of a substance to form solvates may limit the routes for crystallization of unsolvated phases, but at the same time it opens the possibility for using the desolvation to obtain such new polymorphs that might have been previously inaccessible via conventional crystallization techniques[19]. Although preparation of new polymorphs via desolvation is quite common, crystal structures of these phases often remain unknown, as single crystals of such phases cannot be prepared However, the determination of crystal structure is an important part of understanding the physicochemical properties of crystalline materials. To overcome this problem, structure determination from powder X-ray diffraction data can be used as the closest alternative to the general method of choice, single crystal X-ray diffraction, particularly in cases when single crystals of suitable size and quality are impossible to grow or solids can

be obtained only as microcrystalline powders, including those prepared by solid-state desolvation processes.

The **aim** of this research was to investigate highly polymorphic active pharmaceutical ingredients by using experimental and computational methods in order to rationalize structural and thermodynamic aspects of formation of such abundant polymorphic systems.

Accordingly, the **tasks** set to address this issue were:

1) to perform comprehensive polymorph and solvate screening of quifenadine hydrochloride, sequifenadine hydrochloride, encenicline hydrochloride and dantrolene, including different crystallization and solid-state transition experiments;
2) to characterize the obtained solid forms by using powder X-ray diffraction and thermal analysis methods;
3) to determinate crystal structures of nonsolvated polymorphs and their respective solvated phase (if any) by using powder or single crystal X-ray diffraction;
4) to perform crystal structure prediction of polymorphs of molecular compound – dantrolene;
5) to perform crystal structure analysis and quantum chemical calculations to rationalize the polymorph formation, their relative stability and phase transformations.

Scientific Novelty

1. The ability of Encenicline hydrochloride to form multiple different interactions providing efficient packing for several different arrangement of ions in the solid state allows this compound to form a record-breaking number (10) of packing polymorphs, in contrast to the other most polymorphic molecules where the main driving force for formation of the high number of polymorphic forms is the conformation variability.
2. For stability analysis of polymorphs an approach in which limited results from experimental methods are combined with computational studies has been used. Such approach reduces the amount of necessary experimental work and can provide more reliable conclusions about the stability over a broad temperature range for systems for which, because of various reasons, this cannot be determined by experimental methods alone.
3. In this work formation, stability, and phase transitions of polymorphs are rationalized using crystal structures of microcrystalline polymorphs determined from powder X-ray diffraction data, which would be impossible to achieve with traditional structure determination methods.

Practical Significance

1. Experimental and computational methodology for obtaining polymorphs of several pharmaceuticals by desolvation of solvates and hydrates has been developed. Thus, it can be used to obtain novel stable polymorphs, including patentable polymorphs,

allowing more pharmaceutical companies to produce highly polymorphic drugs, thus expanding the market access and reducing the final cost for the consumer.
2. The obtained general understanding of the formation of polymorphs can lead to fast and reliable prediction of the polymorph formation and stability in particular conditions.
3. The detailed characterization of highly polymorphic systems, including stability studies, allows a more reliable choice of commercial form with longer overall shelf life.

RESULTS PUBLISHED

Publications

1. Kons, A.; Mishnev, A.; Mukhametzyanov, T.; Buzyurov, A.; Semen, L.; Bērziņš, A. Hexamorphism of Dantrolene: Insight into the Crystal Structures, Stability, and Phase Transformations. *Cryst. Growth Des*. **2021**, 21, 1190–1201. (IF = 4.17)

   A. Kons carried out 90 % of the experimental work, developed the concept and wrote the article, prepared the experimental results according to the journal guidelines, as well as prepared the answers to the questions and remarks given by the reviewers.
2. Kons, A.; Bērziņš, A.; Actiņš, A.; Rekis, T.; van Smaalen, S.; Mishnev, A. Polymorphism of R-Encenicline Hydrochloride: Access to the Highest Number of Structurally Characterized Polymorphs Using Desolvation of Various Solvates. *Cryst. Growth Des.* **2019**, 19, 4765–4773. (IF = **4.17**)

   A. Kons carried out 90 % of the experimental work, developed the concept and wrote the article, prepared the experimental results according to the journal guidelines, as well as prepared the answers to the questions and remarks given by the reviewers.
3. Bobrovs, R.; Kons, A.; Bērziņš, A.; Rekis, T.; Actiņš, A. Formation and Transformations of Organic Salt Hydrates: Four Encenicline Hydrochloride Monohydrates and Respective Isostructural Desolvates. *Cryst. Growth Des.* **2018**, 18, 2100–2111. (IF = **4.21**)

   A. Kons carried out 90 % of the experimental work, contributed to writing the article (50 %), prepared the experimental results according to the journal guidelines, as well as contributed to answering the questions and remarks given by the reviewers.
4. Kons, A.; Bērziņš, A.; Actiņš, A. Polymorphs and Hydrates of Sequifenadine Hydrochloride: Crystallographic Explanation of Observed Phase Transitions and Thermodynamic Stability. *Cryst. Growth Des.* **2017**, 17, 1146–1158. (IF = **4.17**)

   A. Kons carried out 90 % of the experimental work, developed the concept and wrote the article, prepared the experimental results according to the journal guidelines, as well as prepared the answers to the questions and remarks given by the reviewers.
5. Kons, A.; Rutkovska, L.; Bērziņš, A.; Bobrovs, R.; Actiņš, A. Three anhydrous forms and a dihydrate form of quifenadine hydrochloride: a structural study of the thermodynamic stability and dehydration mechanism. *CrystEngComm.* **2015**, 17, 3627–3635. (IF = **3.97**)

   A. Kons carried out 90 % of the experimental work, developed the concept and wrote the article, prepared the experimental results according to the journal guidelines, as well as prepared the answers to the questions and remarks given by the reviewers.

Conferences

1. A. Kons, A. Mishnev, T. A. Mukhametzyanov, A. V. Buzyurov, S. E. Lapuk, A. Bērziņš, Hexamorphism of Dantrolene Insight into the Crystal Structures Stability and Phase Transformations. *University of Latvia 79th conference*, Rīga, Latvija, **2021.**

2. A. Kons, A. Bērziņš, Decamorphism of R-Encenicline hydrochloride. *University of Latvia 78th conference*, Rīga, Latvija, **2020.**
3. A. Kons, A. Bērziņš, T. Rekis, Polimorphism of R-Encenicline hydrochloride: Access to the highest number of structurally characterized polymorphs using desolvation of various solvates. *The 32nd European Crystallographic Meeting*, Vienna, Austria, **2019**.
4. A. Kons, A. Actiņš, Access to several crystalline forms of R-Encenicline hydrochloride using desolvation of various solvates. *The 31st European Crystallographic Meeting*, Oviedo, Spain, **2018**.
5. A. Kons, A. Actiņš, Polymorphs and Solvates of Encenicline Hydrochloride. *24th Congress and General Assembly of the International Union of Crystallography*, Hyderabad, India, **2017**.
6. A. Kons, A. Actiņš, Sekvifenadīna hidrogēnhlorīda 6 polimorfās formas: termodinamiskās stabilitātes un struktūru salīdzinājums. *University of Latvia 74th conference*, Riga, Latvia, **2016**.
7. A. Kons, A. Actiņš, Anhydrous and hydrated crystalline forms of sequifenadine hydrochloride: comparison of thermodynamic stability and crystal structures. *14th European Powder Diffraction Conference* (*EPDIC 2016*), Bari, Italia, **2016**.
8. A. Kons, L. Rutkovska, A. Bērziņš, R. Bobrovs, A. Actiņš, Three anhydrous forms and a dihydrate form of quifenadine hydrochloride: a structural study of the thermodynamic stability and dehydration mechanism. *8th Crystal Forms @ Bologna*, Bolona, Italia, **2015**.

Other publications (not included in the work)

1. Bērziņš, A.; Kons, A.; Saršūns, K.; Belyakov, S.; Actiņš, A. On the Rationalization of Formation of Solvates: Experimental and Computational Study of Solid Forms of Several Nitrobenzoic Acid Derivatives. *Cryst. Growth Des.* **2020**, 20, 5767–5784.
2. Rekis, T.; Bērziņš, A.; Sarceviča I.; Kons, A.; Balodis, M.; Orola, L.; Lorenz, H., Actiņš, A. A Maze of Solid Solutions of Pimobendan Enantiomers: An Extraordinary Case of Polymorph and Solvate Diversity. *Cryst. Growth Des.* **2018**, 18, 264–273.
3. Bērziņš, A.; Trimdale, A.; Kons, A.; Zvaniņa, D. On the formation and desolvation mechanism of organic molecule solvates: A structural study of methyl cholate solvates. *Cryst. Growth Des.* **2017**, 17, 5712–5724.
4. Bērziņš, K.; Kons, A.; Grante, I.; Dzabijeva, D.; Nakurte, I.; Actiņš, A. Multitechnique approach for qualitative and quantitative characterization of furazidin degradation kinetics under alkaline conditions. *J. Pharm. Biomed. Anal.* **2016,** 129, 433–440.
5. Sarceviča, I.; Kons, A.; Orola, L. Isoniazid cocrystallisation with dicarboxylic acids: vapochemical, mechanochemical and thermal methods. *CrystEngComm,* **2016**, 18, 1625–1635.
6. Orola, L.; Sarceviča, I.; Kons, A.; Actiņš, A.; Veidis, M.V. Conformation of the umifenovir cation in the molecular and crystal structures of four carboxylic acid salts. *J. Mol. Struct.* **2014**, 1056, 63–69.
7. Kons, A.; Bērziņš, A.; Krūkle-Bērziņa, K.; Actiņš A. Characterization and physicochemical evaluation of molecular complexes formed between umifenovir and dicarboxylic acids. *Latvian Journal of Chemistry,* **2014**, 52, 28–40.

1. RESEARCH BACKGROUND

1.1. Polymorphism of active pharmaceutical molecules and techniques for characterizing polymorphs

The drug molecules can exist in various solid-state forms which can be divided into crystalline and amorphous. In the crystalline forms there is a long-range molecular order, but the amorphous phases have no distinct molecular arrangement in a long-range scale, although can exhibit short-range order over few molecular spacing[20]. Crystalline solids can be further divided into the single component or multi component compounds. Multi component compounds includes solvates/hydrates (crystalline adducts containing solvent/water molecules within the crystal structure, in either stoichiometric or non-stoichiometric proportions), salts (solids formed between suitable counterions) and cocrystals (crystalline solid formed by two neutral molecules) polymorphs (compounds with same chemical composition, but with different molecular arrangement and/or conformation in the crystal lattice). Whereas **polymorphs** (compounds with same chemical composition, but with different molecular arrangement and/or conformation in the crystal lattice) can be both, single and multicomponent crystalline solids (Figure 1.1.). Moreover, combinations of two or more of these classes are also possible, like polymorphs and solvates of salts or cocrystals, and even solvates of salt cocrystals have been reported[21].

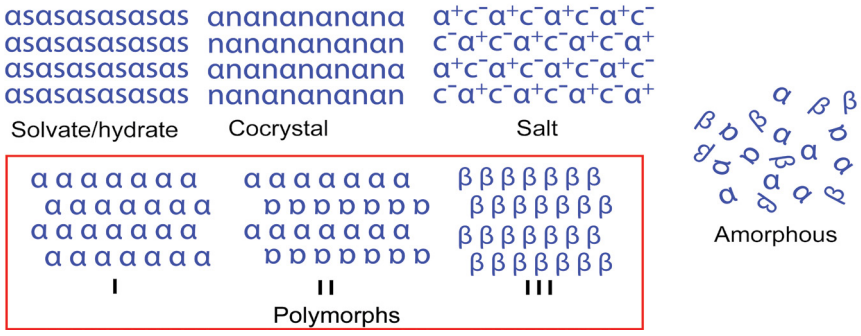

Figure 1.1. **Schematic classification of solid state materials (α and β are different conformers of a molecule, s = solvent molecules, n = molecules of a neutral solid, α^+ is a cation and c^- is an anion[22])**

It is estimated that over 80 % of organic compounds[23] and over 50 % of active pharmaceutical ingredient molecules[24] have more than one polymorphic form. Under certain conditions (temperature and pressure) there is only one thermodynamically stable polymorph that is recommended for use in the final drug dosage form, however, metastable polymorphs are often also used, due to better solubility or intellectual property issues[25,26].

Polymorphs can be categorized into two types: conformational and packing polymorphism. In packing polymorphism, the molecules (typically rigid) share the same molecular conformations but are packed differently in crystal lattice. Conformational polymorphs occur when conformationally different molecules exist in the crystalline state. Generally pharmaceutical molecules are conformationally flexibles due to the ability to rotate around C–C, C–N un C–O bonds[27–29], there are numerous examples of conformational polymorphs with ten or even more forms[1,8,9,12]. The packing and conformation of the molecules in crystals dependent on the intramolecular and intermolecular interactions, such as hydrogen bonds, halogen bonds, van der Waals or π-π interactions etc.[30,31]

Polymorphs can also be classified based on differences in the thermodynamic properties as either enantiotropes or monotropes, depending on whether one form can transform reversibly into another or not. In an enantiotropic system, a reversible transition between polymorphs is possible at a definite transition temperature below the melting point. In a monotropic system, no reversible transition is observed between the polymorphs below the melting point[22]. Four empirical rules have been developed to determine qualitatively where the two polymorphs are either enantiotropically or monotropically related. These rules are the Heat of Transition Rule, the Heat of Fusion Rule, the Infrared Rule and the Density Rule[32].

Table 1.1.

Summary of potential applications of various physicochemical methods to characterize pharmaceutical polymorphs[33]

	SC-XRD	PXRD	IR/ Raman	ssNMR	DSC	TG	DVS	HSM
Identification of crystalline phase	✓	✓	✓	✓	✓	✓	✓	✓
Crystal structure	✓	✓[a]		✓[a]				
Molecular structure				✓				
Geometric information on molecules	✓	✓[a]		✓				
Hydrogen bonding interactions	✓	✓[a]		✓[a]				
Weak interactions	✓	✓[a]						
Dynamics in the solids				✓				
Thermal stability		✓	✓	✓	✓	✓		✓
Mechanical stability	✓	✓	✓					
Phase transformation		✓	✓	✓	✓	✓	✓	✓
Melting point					✓			✓
Dehydration/hydration		✓	✓	✓	✓	✓	✓	✓
Hygroscopicity		✓	✓			✓	✓	
Habit/morphology								✓
Heterogeneous solids		✓	✓[a]	✓	✓	✓	✓	✓
Ionization state	✓	✓	✓	✓				
In situ monitoring processes		✓	✓	✓				

[a] Advanced methodology required

Many analytical methods can be used for identification, quantification and characterization of pharmaceutical polymorphs of which X-ray diffraction (PXRD and SC–XRD), thermal methods (DSC, TG), thermomicroscopy (HSM), vibrational spectroscopy (IR/ RAMAN), solid state NMR spectroscopy (ssNMR) and moisture sorption/desorption (DVS) are the most commonly used. To provide complete and detailed structural, thermodynamic and kinetic information about polymorphs a combination of various analytical methods and techniques must be used. Summary of potential applications of various physicochemical methods to characterize pharmaceutical polymorphs is presented in Table 1.1.

1.2. Structure determination from powder X-ray diffraction data

Crystal structure is a prerequisite for fully understanding phase stability, transformations, and physicochemical properties of given molecule. Although single crystal X-ray diffraction is the ultimate technique for determining the crystal structure, the main limitation of this method is the requirement of a single crystals of suitable size, quality, and stability, which is not always feasible, as many solids can be obtained only as microcrystalline powders, for example, phases prepared by quench cooling, solid-state desolvation processes and by solid state grinding, all common to the pharmaceutical industry. In such circumstances, powder X-ray diffraction becomes the method of choice for structural analysis. Nowadays more and more crystal structures are determined from laboratory PXRD data through the development of the direct-space approach.

Single crystal and powder diffraction patterns essentially contain the same structural information, but this information is distributed in 3D space in the single crystal XRD pattern, whereas it is compressed into 1D in the powder XRD pattern, see Figure 1.2. Consequently, there is usually considerable overlap of peaks in the powder XRD pattern, with information on the individual diffraction position and intensities obscured. The problem of peak overlap is often particularly severe for molecular solids, which typically have large unit cells and low symmetry[34]. Thus, the task of structure determination from powder XRD data is more challenging. Measures taken to ensure that the structure model is as accurate and precise as possible include carefully preparing highly crystalline, preferably phase-pure powders in thin-walled capillaries, and collecting data in transmission mode, while spinning the sample to minimize preferred particle orientation effects. For the high accuracy needed for structure solution, the experimental diffraction pattern is typically measured over a wide 2θ range, usually up to 70 or 80°[35,36].

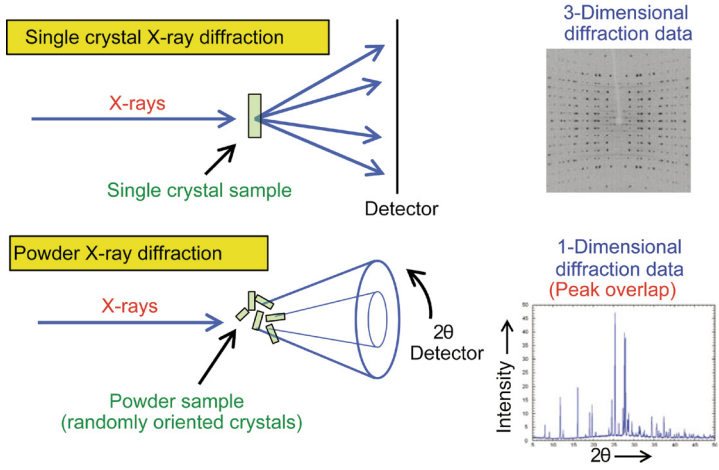

Figure 1.2. **Comparison of single-crystal and powder XRD measurements[34]**

The usual procedure of structure determination from X-ray powder data consists of five overall steps: (1) indexing, that is, determination of the lattice parameters from the reflection positions, followed by the determination of the space group and asymmetric unit; (2) fitting the determined lattice parameters and space group to experimental powder XRD pattern by refinement of different profile variables using Pawley[37] or Le Bail[38] methods; (3) inserting correct trial molecular model in the crystal lattice (4) structure solution in direct space by global optimization procedure; (5) Rietveld refinement, that is, fit of the structural model to the full powder pattern, resulting in the final crystal structure. Of all the steps in the powder structure solution process, the initial determination of the lattice parameters tends to be the most problematic. Clearly, the structure determination process cannot progress to the structure solution and structure refinement stages if the correct unit cell is not found at the indexing stage. Therefore, it is useful to employ different set of peaks and indexing algorithms (Dicvol[39], N-Treor[40], Conograph[41] et al.) to confirm that the same result is obtained. Further, the correct trial molecular model (crystallographically independent molecules, counter ions, water, or solvent molecules) must be given as an input in unit cell. Then the molecules are translated and rotated inside the unit cell; selected intramolecular degrees of freedom (torsion angles) are varied as well. In each step, the X-ray powder pattern is calculated and compared with the experimental pattern until a suitable agreement is obtained. For the real-space methods, algorithms, such as simulated annealing or parallel tempering, have been developed. The structure solution results in a structural model that is generally close to the final crystal structure. The final structural model is refined to the full powder pattern using the Rietveld method. This includes refinement of the lattice parameters, the atomic positions, a scale factor, an overall temperature factor, preferred orientation, occupancies of atoms or atomic groups (for example, in the case of partially occupied solvent positions) and selected peak profile and background parameters. Unreasonable distortions of the molecules are avoided by using restraints or constraints for bond lengths, bond angles and planar groups. Alternatively, molecular fragments can be described by rigid bodies.

The powder structure solution is assessed at the final Rietveld refinement stage by comparing its calculated powder pattern with the experimental pattern, the fit being qualitatively visualized by the difference curve (the black curve at the bottom of Fig. 1.3 a) and quantified by either a weighted powder profile R factor (R*wp*), full profile χ^2 etc.

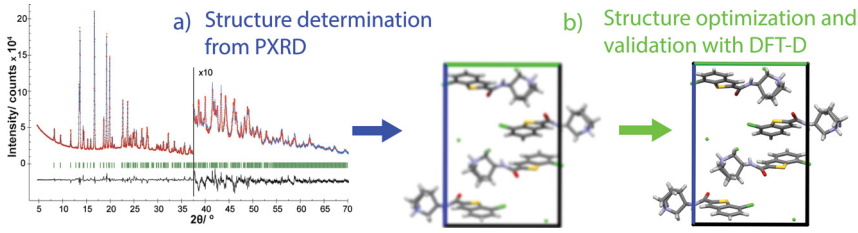

Figure 1.3. **Visual workflow of structure determination from powder X-ray data**

As a final proof, all crystal structures determined by PXRD should be energy minimized using dispersion corrected density functional theory (DFT-D) methods (Fig. 1.3.b.). If the optimization results in a mean Cartesian displacement of the nonhydrogen atoms of less than 0.35 Å, the structure can be regarded as correct[42]. Apart from structure validation, full DFT-D energies (lattice + conformational) can be used for polymorph thermodynamic stability ranking at 0 K.

1.3. Objects of Investigation

In total five compounds, obtained from JSC "Olainfarm" (Olaine, Latvia), were studied. Chemical structures with labeling of flexible dihedral angles are given in Figure 1.4.

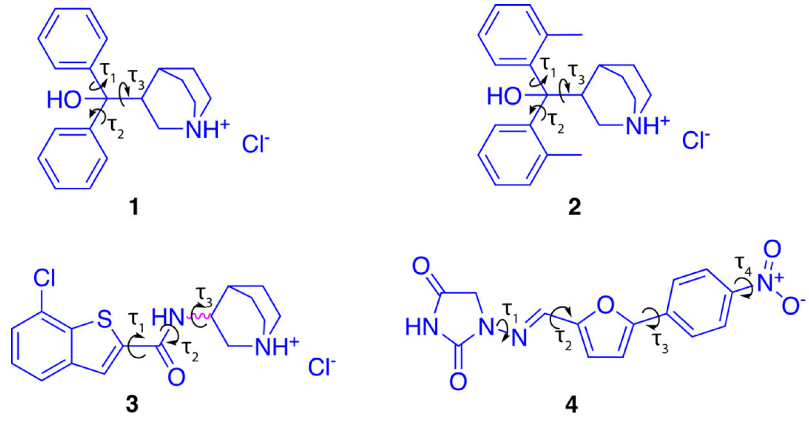

Figure 1.4. **Molecular structures of the compounds studied**
(1 – quifenadine HCl; 2 – sequifenadine HCl; 3 – encenicline HCl; 4 – dantrolene)

Quifenadine (1-azabicyclo[2.2.2]octan-3-yl(diphenyl)methanol) **hydrochloride** (**1**) tradename Fencarol and **sequifenadine** (1-azoniabicyclo[2.2.2]octan-3-yl-bis(2-methylphenyl)methanol) **hydrochloride** (**2**) tradename Bicarphen are active pharmaceutical ingredients used as antihistaminic agents that decrease the impact of histamine by blocking histamine H1-receptors[43,44]. There are no reports on the existence of polymorphs or solvates of quifenadine HCl or sequifenadine HCl prior to this work.

Encenicline (N-[(3R)-1- azabicyclo[2.2.2]oct-3-yl]-7-chloro-1-benzothiophene-2-carbox-amide) **hydrochloride** (**3**) is a partial, selective agonist of the α-7 nicotinic acetylcholine receptor which was developed for the treatment of cognitive deficits in schizophrenia and Alzheimer's disease[45]. Prior to this work three monohydrate phases (I, II, and X) of Encenicline HCl have been reported in a patent[46].

Dantrolene (**4**) (1-[(E)-[5-(4-nitrophenyl)furan-2-yl]methy lideneamino]imidazolidine-2,4-dione) is a hydantoin derivative and direct-acting skeletal muscle relaxant. It is used in treatment for malignant hyperthermia, management of neuroleptic malignant syndrome, muscle spasticity and ecstasy intoxication[47]. Prior to this work a crystal structure of methanol solvate determined from SCXRD data has been reported[48].

2. EXPERIMENTAL SECTION

1. Routine PXRD measurements were performed with a Bruker D8 Advance diffractometer using an X-ray tube with Cu radiation with Bragg–Brentano geometry and a LynxEye (1D) detector. The patterns were recorded from 3° to 30° on the 2θ scale, using a scan speed of 0.2 s/ 0.02° (University of Latvia, Latvia).
2. PXRD data for crystal structure determination were recorded on a Bruker D8 Discover diffractometer using an X-ray tube with Cu radiation and a LynxEye (1D) detector in transmission mode. The diffraction patterns were recorded on the 2θ scale from 3° or 4.5° to 70° at a 0.01° step size using a scan speed of 36 s per step (University of Latvia, Latvia).
3. SC-XRD data were collected on a Rigaku XtaLAB Synergy-S dualflex diffractometer equipped with a HyPix6000 detector and an X-ray tube with Mo or Cu radiation (Latvian Institute of Organic Synthesis, Latvia) and a MAR345 diffractometer equipped with an image plate detector and an X-ray tube with Ag radiation (University of Bayreuth, Germany).
3. DSC/TGA analyses of solvates were performed with a Mettler Toledo TGA/DSC2 instrument. Heating of samples from 25 to 320 °C was performed at a heating rate of 10 °C·min^{-1} under a N_2 flow (University of Latvia, Latvia).
4. DSC analyses of polymorphs were performed with a TA DSC 25 instrument. Heating of samples from 25 to 320 °C was performed at a heating rate of 5–20 °C·min^{-1} under a N_2 flow (University of Latvia, Latvia).
5. FSC analyses of dantrolene polymorphs were performed with a Mettler Toledo Flash DSC1instrument. Heating of samples from 25 to 350 °C was performed at a heating rate of 2000 °C·s^{-1} under a N_2 flow (Kazan Federal University, Russia).
6. Dynamic vapor sorption–desorption experiments were performed on the Surface Measurement Systems DVS Advantage apparatus. Samples were studied over a selected humidity range from 0 to 90 % RH with a step of 5 % at 25 °C (University of Latvia, Latvia).
7. Polythermal solubilities were determined by turbidity measurements using a Technobis Crystal16 instrument (University of Latvia, Latvia).
8. For thermo-microscopic investigations, a Leitz Laborlux 12 PolS polarized light microscope equipped with a heating stage and a DFC450 Leica camera was used (Riga Technical University, Latvia)
9. Structure solution from powder data and Rietveld refinement were performed using softwares *Expo2014* and *Topas5*, for periodical calculations using softwares *Quantum Espresso* un *Castep* and *Gaussian09* for molecular gas phase calculations.

3. RESULTS AND DISCUSSION

3.1. Trimorphism of quifenadine hydrochloride (1)

Through the screening process, quifenadine hydrochloride was found to crystallize in three crystalline modifications: two polymorphs (A and C) and dihydrate (DH). Additional polymorph B was obtained by dehydration of DH. In contrast to other polymorphic compounds described here, quifenadine hydrochloride has only three polymorphs. It can be partly explained by the fact that quifenadine HCl is not a prolific solvate former (like sequifenadine HCl, encenicline HCl and dantrolene) which prevents the possibility of obtaining new polymorphs by desolvation. Dihydrate can be prepared by recrystallizing quifenadine hydrochloride from water, polymorph C by recrystallizing from *n*-butanol or isobutanol and polymorph A can be obtained from any other solvent. Overlay of powder X-ray diffraction (PXRD) patterns of quifenadine hydrochloride polymorphs and dihydrate is depicted in Fig. 3.1.

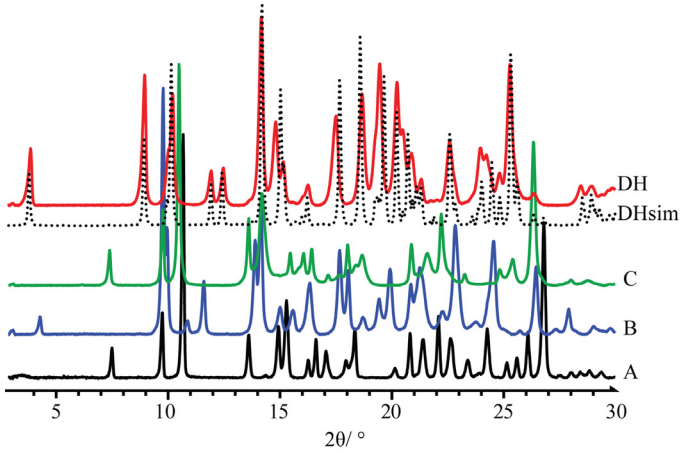

Figure 3.1. **PXRD patterns of quifenadine HCl forms A, B, C and DH**

Structures of polymorphs A, B, and C were determined using powder X-ray diffraction data, but the structure of DH by single-crystal X-ray diffraction. Crystallographic data for all forms are shown in Table 3.1. All these crystalline modifications crystallize in the $P\bar{1}$ space group. The crystal structure of each polymorph contains one quifenadine cation and one chloride anion in the asymmetric unit, whereas dihydrate contains additional two water molecules in the asymmetric unit.

Table 3.1.

Crystal structure data for quifenadine hydrochloride forms

	A	B	C	DH
Formula		$C_{20}H_{24}NOCl$		$C_{20}H_{24}NOCl{\cdot}2H_2O$
Weight, g·mol^{-1}		329.86		365.88
Sample type		Powder		Single crystal
Temperature, K		293(2)		173(2)
Crystal system			Triclinic	
Space group			$P\bar{1}$	
a, Å	6.372(2)	6.408(5)	6.449(2)	6.339(1)
b, Å	12.699(5)	9.281(6)	12.951(3)	8.601(2)
c, Å	10.759(4)	18.356(2)	11.222(2)	18.404(5)
α,°	96.03(2)	113.09(3)	97.60(1)	100.02(2)
β,°	98.88(2)	83.62(3)	106.61(2)	92.32(3)
γ,°	80.68(2)	116.50(3)	75.25(2)	103.45(2)
V, Å^3	845.9(1)	895.8(1)	862.9(1)	957.5(3)
ρ_{calc}, g·cm^3	1.295	1.223	1.270	1.269
Z (Z')	2 (1)	2 (1)	2 (1)	2 (1)
R_{wp} (R_p)/R_1 (wR_2), %	2.81 (1.89)	1.41 (0.99)	3.12 (2.32)	4.8 (14.8)
Packing index, %	73.1	71.7	69.1	68.4
[a]Energy, kJ·mol^{-1}	0	21.2	11.3	N/A

[a] relat. to A

A quifenadine molecule consists of two terminal phenyl groups, one quinuclidine moiety and one hydroxyl group linked together by a quaternary carbon. Although quinuclidine cation has three flexible dihedral angles (Fig 1.4.), conformation of the quifenadine cation in all crystal structures shows only small differences and corresponds to the same energy minimum. In quifenadine hydrochloride, the only easily accessible strong hydrogen bond acceptor is the Cl^- anion, and the possible donors allowing the formation of strong hydrogen bonds are the NH^+ group and the hydroxyl group. As shown in Figure 3.2., all three polymorphs have the same hydrogen bonding pattern where two chloride anions interact with two quifenadine cations through N–H···Cl and O–H···Cl bonds and form a tetramer with the graph set $R^2_4(16)$. The hydrogen bonding pattern in the quifenadine hydrochloride dihydrate structure is more complex due to the presence of two water molecules increasing the number of possible hydrogen bond acceptor and donor sites (Fig. 3.2.).

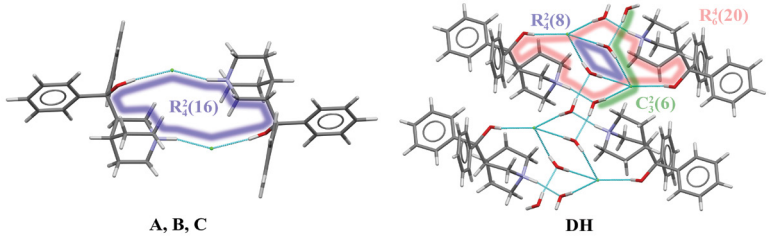

Figure 3.2. **The hydrogen bonding patterns in forms A, B, C and DH**

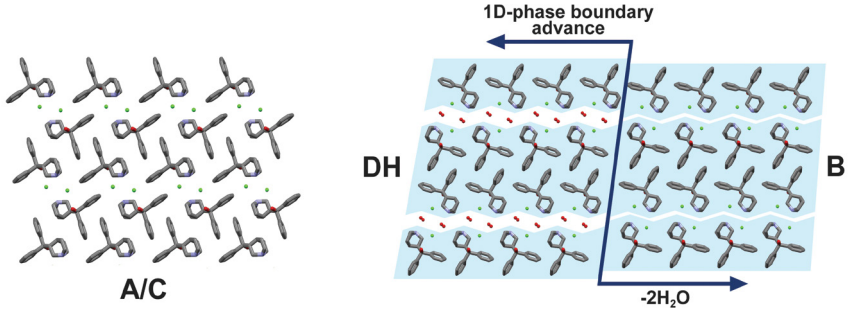

Figure 3.3. **The molecular packing in quifenadine HCl forms A, B, C and DH**

As shown in Fig. 3.3., forms A and C have the same monolayered molecular packing pattern where all neighboring molecules are in antiparallel orientation. The 2D pattern is defined by the same type of layers. However, there are marked differences between the packing of forms A/C and form B. The molecular packing of form B has a bilayered pattern where neighboring molecules are in the same direction and molecules in each layer are in opposite orientation to those in the adjacent layer. The molecular packing of form B has more distinguishable hydrophobic and hydrophilic layers than in forms A and C where the tetramers are packed more efficiently. The molecular packing of form DH shares common features with that of form B. The 2D structural pattern of DH is defined by the same molecular orientation and the same arrangement of the layers with respect to each other. The only difference is the inclusion of water molecules, which are located in structural channels between hydrophilic quinuclidine groups and chloride anions. Therefore, DH is a stoichiometric channel hydrate, which is confirmed by hot stage microscopy observations (Fig. 3.4.), as the dehydration occurs in direction of the water containing channels.

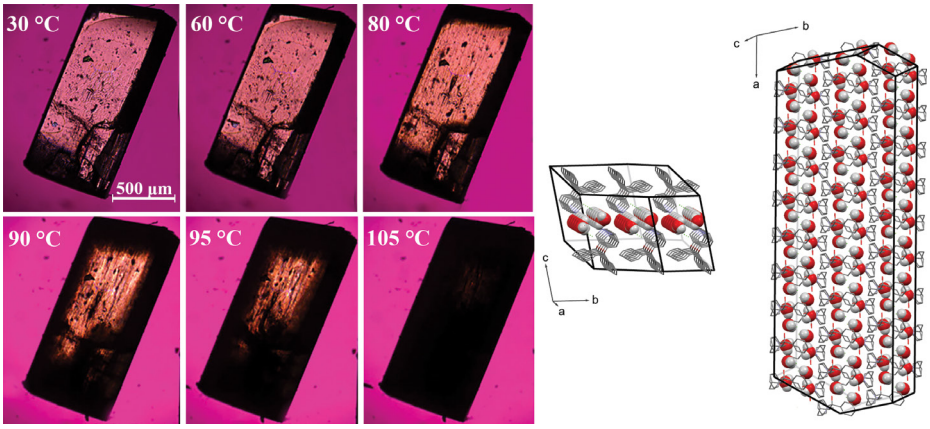

Figure 3.4. **Thermo photomicrographs and crystal morphology data showing water channels of DH**

Due to the high structural packing similarity, it is clear why the dehydration of DH leads to form B instead of A or C. This transition does not change the parallel orientation of quifenadine cations in the crystal structure, and it only decreases the distance between the quifenadine moieties. Calculation of the packing index yielded 73.1, 71.7, 69.1 and 68.4 % for forms A, C, B and DH, respectively, which are in agreement with the thermodynamic stability results for these polymorphic forms. The lowest packing index of form DH, however, suggests that the presence of water molecule channels does not lead to very efficient packing, but the stability of this crystal structure is provided by an energetically efficient hydrogen bonding network provided by the insertion of water molecules.

In order to better explore the differences between the very similar forms A and C, full geometry optimization of these two crystal structures was performed. The obtained results indicated that between forms A and C there is only a small energy barrier because after geometry optimization of both experimental structures an almost identical structure was obtained. Therefore, the only explanation why form C was obtained from *n*-butanol or isobutanol instead of very similar form A can be based on the presence and strength of some specific interactions between the solvent molecules and the quifenadine and chloride moieties during the crystallization, resulting in slightly different molecular packing, which, interestingly, was not able to rearrange to the very similar but thermodynamically more stable structure A.

3.2. Polymorphism of sequifenadine hydrochloride (2)

The crystal form screening experiments of sequifenadine HCl revealed the existence of at least six polymorphs (A, B, B', C, D, E), two dihydrates (DH and DH-II), a monohydrate (MH), a nonstoichiometric hydrate (NSH), and over 10 solvated phases. Figure 3.5. shows a flowchart illustrating the different polymorphs and hydrates discovered, their preparation, and observed phase transitions. It can be seen that polymorphs A and B are crystallized from different solvents, polymorph D is obtained by slurring anhydrous sequifenadine HCl in *n*-propanol, two other polymorphs C and E are obtained by desolvation of *n*-propanol (S_{PrOH}) and methanol solvates (S_{MeOH}) whereas polymorph B' is obtained by exposing other polymorphs (except for the D) to an elevated temperature. All the hydrates are obtained by exposing particular polymorphs or lower stoichiometry hydrates to a specific relative humidity.

The crystal structures of all nonsolvated polymorphs have been determined from PXRD data because numerous attempts to grow single crystals were unsuccessful, with only microcrystalline powders being obtained. Crystal structures of forms A, B and B' were solved in the triclinic system with $P\bar{1}$ space group and contain one sequifenadine cation and one chloride anion in the asymmetric unit. Polymorphs C, D, and E crystallize in the monoclinic system with $P2_1/c$, $P2_1/n$, and $C2/c$ space groups, respectively, and contain two sequifenadine cations and two chloride anions in the asymmetric unit.

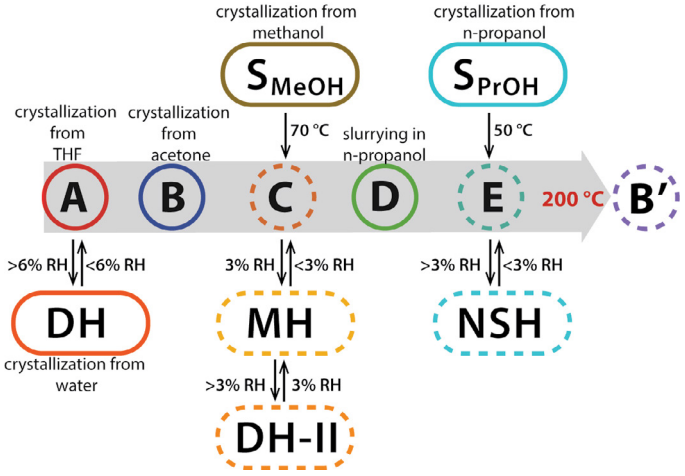

Figure 3.5. **Preparation and phase transformations of sequifenadine HCl forms. Solid boxes show forms which were crystallized from solution; dashed boxes show forms obtained by solid state transition**

In sequifenadine cation conformational difference arises due to rotation of the methylphenyl groups around C–C bonds. There are three conformations observed in the experimental crystal structures: conformer LM1 in form D, conformer LM2 in polymorph C and conformer GM in all other forms, see Figure 3.6. Moreover, in conformer LM1 the only major conformation difference is that one methylphenyl group is rotated by ~180°, while in the conformer LM2 both methylphenyl groups are rotated by 95–110°. It was found that the energies of the conformers LM1 and LM2 are similar, while the GM conformer observed in all other crystal structures is lower in energy by 8–10 kJ·mol^{-1}. Potential energy surface (PES) scans with respect to the flexible torsion angles confirmed that conformer observed in most cases (GM) is the most stable while conformers LM1 and LM2 correspond to one of the local energy minima.

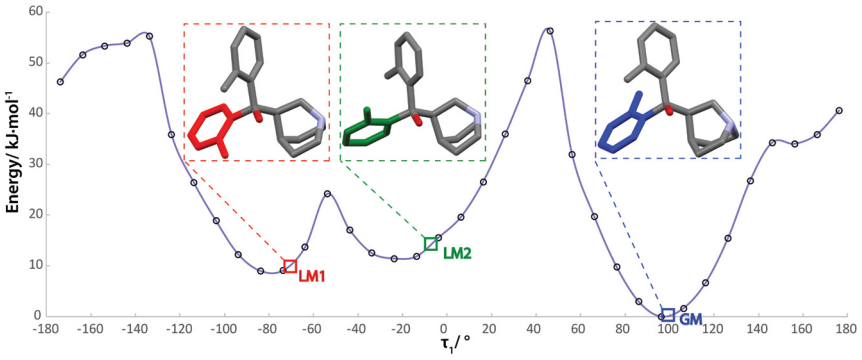

Figure 3.6. **Potential energy surface (PES) scan with respect to torsion angle 1 in sequifenadine cation. Conformations observed in the experimental crystal structures are represented with blue, green and red squares**

Based on the characteristic hydrogen bonding motifs three building blocks can be identified in all five polymorphs: $R^2_4(16)$ tetramer, which was already seen in quifenadine HCl structures; $R^2_4(10)$ tetramer, where sequifenadine cation and Cl^- anion pair forms tetramer by additionally employing weak hydrogen bonds, and $C^2_4(16)$ chain, all shown in Figure 3.7. Both tetramers are 0D building blocks, but $C^2_4(16)$ chains forms a 1D building block. 3D packing of these building blocks results in formation of structures of polymorphs E, C, and D, while $R^24(16)$ tetramers can additionally form 2D layers, by stacking of 1D chains of such tetramers (see layer 1 in Figure 3.7). Parallel stacking of such layers above each other results in the structure of polymorph A (stacking mode 1–1–1 in Figure 3.7.), whereas stacking of such layers so that the adjacent layers are shifted by 1, results the structures of B and B' (stacking mode 1–1'–1 in Figure 3.7.). As expected, forms B and B' have very similar crystal packing due to similarity in the 3D arrangement of the ions, with the most important difference being shift in the location of chloride anion. Hydrate structures appear as derived from those of particular polymorphs, by incorporation of water molecules between layers or in structure voids. As can be seen in Figure 3.7., layer 2 is observed in both structures of A and of DH, while layer 3 is common for structures of C and MH (although here half of the molecules have different molecular conformation). The water molecules are incorporated between these layers by thus introducing no other significant change in the molecule packing except for the increase of the space between the layers.

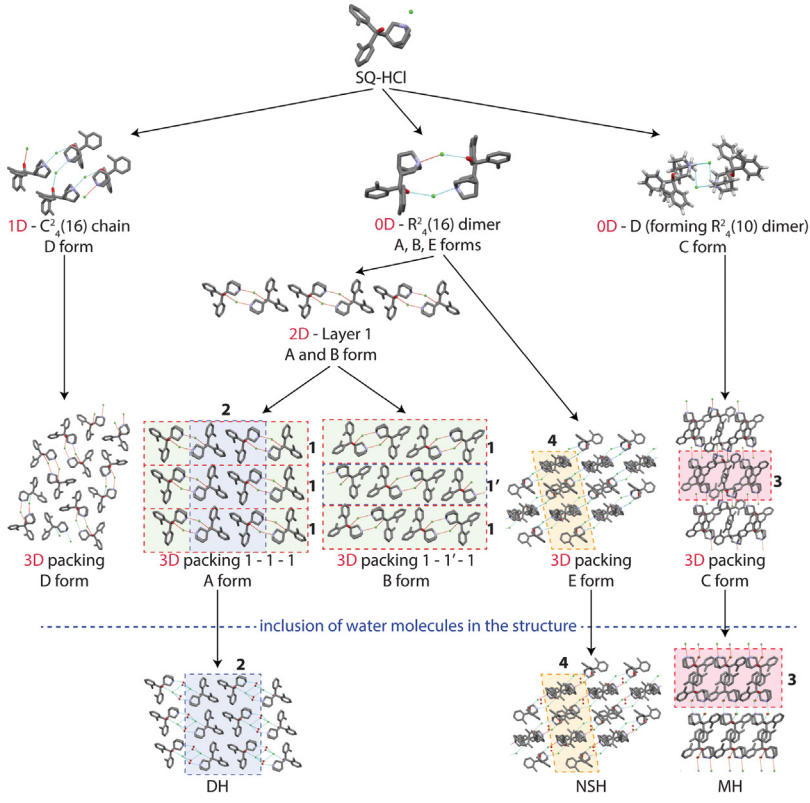

Figure 3.7. **Building blocks and packing similarities in polymorphs and hydrates**

This packing similarity explains the observation that the dehydration of DH leads to form A and dehydration of MH leads to form C. NSH and its isostructural dehydrate E share an identical 3D packing, as water molecules are situated in the voids of structure of polymorph E.

The thermodynamic stability order of polymorphs was established by comparing computed total cell energies, using periodic DFT-D calculations in and phase transitions occurring in slurry-bridging experiments. Total cell energies of forms A, B, B', C, D, and E indicate, that the form D is the most stable form, whereas the form C is the least stable form, having the highest total cell energy of 20.0 kJ·mol^{-1} (relative to form D). Total cell energies of forms A, B, B', and E (7.9, 10.2, 8.0, and 8.3 kJ·mol^{-1}, respectively) are too close to infer the stability relationships. Slurry-bridging experiments were carried out at ambient temperature. Because of the solvate formation with numerous different solvents, mixtures of polymorphs were slurred only in acetone and ethyl acetate to avoid the solvate formation. A summary of the results from the slurry-bridging experiments is given in Table 3.2. These observations demonstrate that the form D is the most thermodynamically stable form at ambient temperature, followed by forms B and A having progressively lower stability. However, relative stability between the forms C, and E is unclear, but by a combination of results from experimental and computational studies it is reasonable to conclude that thermodynamic stability at ambient temperature follows the order of D > B > A > E > C.

Table 3.2.

Results of the Slurry-Bridging Experiments

Mixture	Resulting phase
A/D	D
B/D	D
C/D	D
D/E	D
A/B	B
B/C	B
B/E	B
C/E	B
A/C	A
A/E	A

3.3. Decamorphism of encenicline hydrochloride (3)

In comparison to other compounds described here, encenicline HCl is the most prolific solvate former. In a crystal form screening of encenicline HCl, over 30 new solvates were obtained, with half of the solvates crystallizing as isomorphous solvates (based on the results from indexing of the respective PXRD patterns). The only polymorph which can be obtained in crystallization is IV_D and only from one solvent – dimethylformamide, whereas all the other known polymorphs can be obtained only

through desolvation of a specific solvate (see Figure 3.8.), including four monohydrates that produce four different polymorphs (I_D, II_D, III_D, X_D). Moreover, polymorphs VI_D, $VIII_D$, XI_D, and XII_D can be obtained only by desolvation of acetonitrile monosolvate 1 (S_{ACN-I}), acetic acid disolvate (DS_{AA}), formic acid monosolvate (S_{FA}) and acetonitrile monosolvate 2 (S_{ACN-II}) in a desiccator over P_2O_5, respectively. Desolvation in elevated temperature, however, produced different polymorphs. Overall, 12 polymorphs can be accessed via desolvation of various solvates.

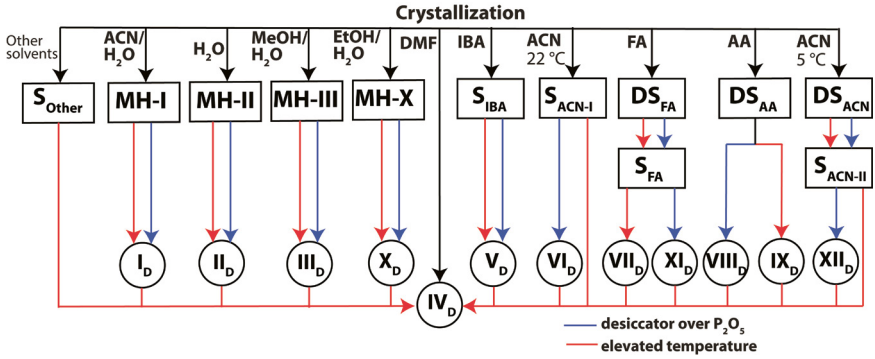

Figure 3.8. **Encenicline HCl phase transitions upon desolvation/heating**

The comparison of the PXRD patterns of the polymorphs and their respective precursor solvate/hydrate is illustrated in Figure 3.9. PXRD patterns of polymorphs I_D, II_D, III_D and X_D and their respective precursor hydrates (MH-I, MH-II, MH-III and MH-X) show high similarity indicating isostructurality between them. Each of the remaining crystalline phases have a unique and distinguishable PXRD pattern showing no similarity between precursor solvates and their respective desolvated phases.

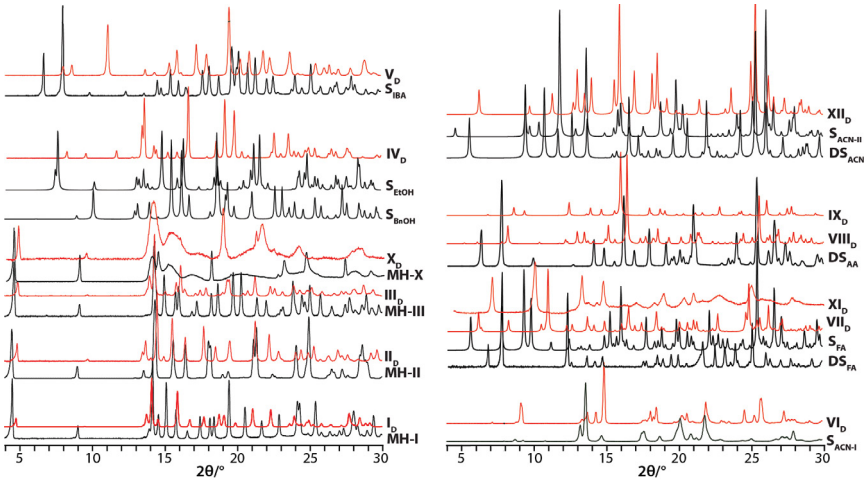

Figure 3.9. **PXRD patterns of encenicline HCl solvated (black) and neat (red) polymorphs**

In the PXRD patterns of MH-X, XI_D and XI_D, part of the peaks is narrow while the other part is wide. It seems that in the crystal structures of these phases, only two directions are well-determined, as all the narrow peaks can be indexed with only two axes, with the structure in the third direction largely undetermined. Although such behavior is unusual for pharmaceuticals, it can be attributed to stacking faults, which are common in materials that have a strongly layered character[49].

As already mentioned, 11 of 12 encenicline HCl polymorphs can be produced only by desolvation as microcrystalline powders of which 9 crystal structures were successfully determined from powder diffraction data. Unfortunately, no acceptable indexing solutions were found for the polymorphs X_D un XI_D due to their stacking fault disorder. Most of the polymorphs crystallize in two most frequent Sohncke space groups: $P2_1$ (VI_D, $VIII_D$ and IX_D) and $P2_12_12_1$ (IV_D, V_D, VII_D un XII_D). Polymorph I_D crystallizes in the $P3_221$ space group, whereas polymorphs II_D and III_D in the $C2$ space group. The space groups of the polymorphs are the same as those of the corresponding precursor solvates, and even the lattice parameters in most of the solvate–desolvate pairs are similar.

Encenicline has three flexible dihedral angles (Fig. 3.4). Analysis of the crystal structures revealed that the conformation of the encenicline cation in all crystal structures is highly similar. The largest conformation difference (up to 30°) arises due to the rotation of the chloro-benzothiophene group around the C–C bond (τ1) and quinuclidine group around the N–C bond (τ3). After geometry optimization and a calculation of 1D PES scan with respect to the corresponding torsion angles, it was concluded that the conformation in all crystal structures is the same (corresponds to the same energy minimum). Thus, we can point out that in contrast to the other most polymorphic molecules, galunisertib, aripiprazole, ROY, and flufenamic acid, conformation variability is not the main driving force for formation of the high number of polymorphic forms by Enc-HCl.

Analysis of intermolecular interactions and packing revealed that different crystal structures can form as a result of different packing possibilities. This is partly associated with the possibility to form different characteristic hydrogen bonding motifs, as five different hydrogen-bonded building blocks can be identified in all polymorph structures (Figure 3.10.): tetramer $R^2_4(14)$ in polymorph I_D; catamer 1 C^1_2 (7) in polymorph III_D, IV_D, VI_D, and XII_D; catamer 2 C^1_2 (7) in polymorph II_D, catamer 3 C^1_2 (7) in polymorph VII_D, $VIII_D$ and IX_D and catamer 4 C^1_1 (7) in polymorh V_D. All building blocks (except for catamer 4) are formed by N–H···Cl interactions, but catamer 4 is formed by N–H···O interaction. When solvent forms hydrogen bonds, it is just bonded to the Cl^- anion, and the hydrogen bonded chain existing in the respective structurally similar polymorph or any other hydrogen bond formation characteristic is not affected by the solvate formation. The exception from this is hydrates, where water compensates for the unsatisfied hydrogen bond acceptors present in the dehydrates and forms more complex hydrogen bonding networks, Hexamer 1 $R^4_6(18)$ in MH-I, Hexamer 2 $R^4_6(22)$ in MH-II and Hexamer 3 $R^4_6(20)$ in MH-III structure.

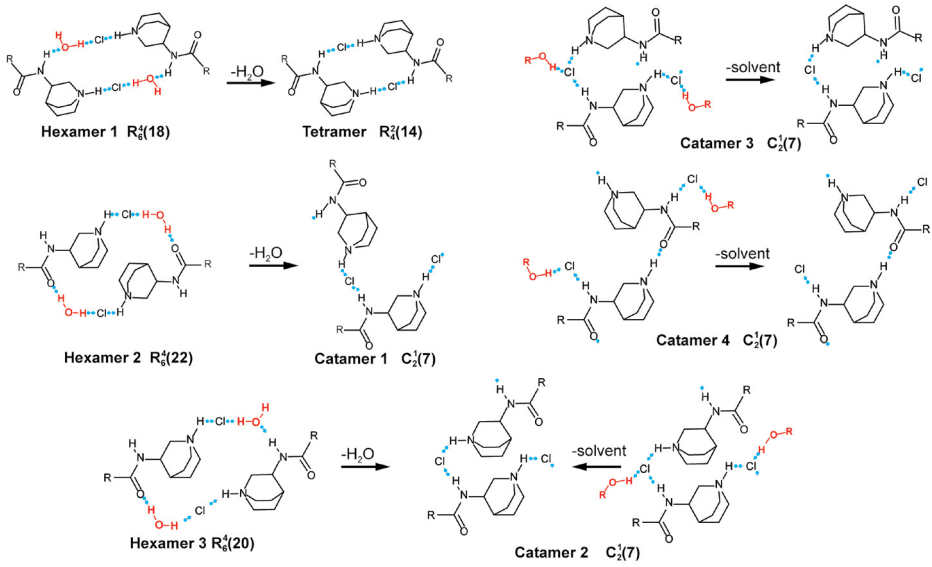

Figure 3.10. **Characteristic hydrogen bonding patterns in encenicline HCl crystalline structures**

The packing similarity of the encenicline HCl polymorphs with their respective parent solvate/hydrate is shown in Figure 3.11. It can be clearly seen that the packing of Enc-HCl moieties in solvates and in polymorphs obtained in their desolvation is similar: a comparison of structures confirmed that in all cases the characteristic packing features and hydrogen-bonding linkage are maintained after the desolvation even in those cases when larger structure rearrangement is observed. This observation is also confirmed by the packing similarity tree diagram generated in Figure 3.12. From the packing similarity dendrogram it can be identified that in most of the cases the closest packing characteristics are between precursor solvates/hydrate and their respective desolvated phases. The exceptions are MH-I/MH-III and I_D/III_D pairs having closer packing similarity than the respective hydrate-dehydrate pairs. The desolvation of most of the other discovered solvates produced polymorph IV_D. This can be associated both by the packing similarity of IV_D with the solvates, which is confirmed for S_{EtOH} (see Figures 3.11. and 3.12.), and also by the fact that IV_D is thermodynamically the most stable polymorph under the desolvation conditions.

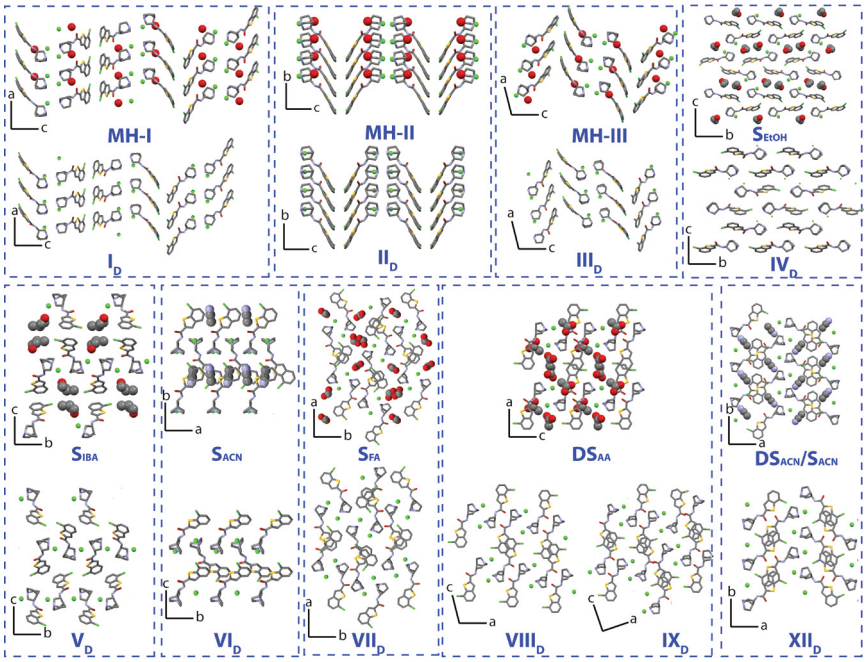

Figure 3.11. **Packing similarity of encenicline HCl polymorphs with their respective parent solvate/hydrate**

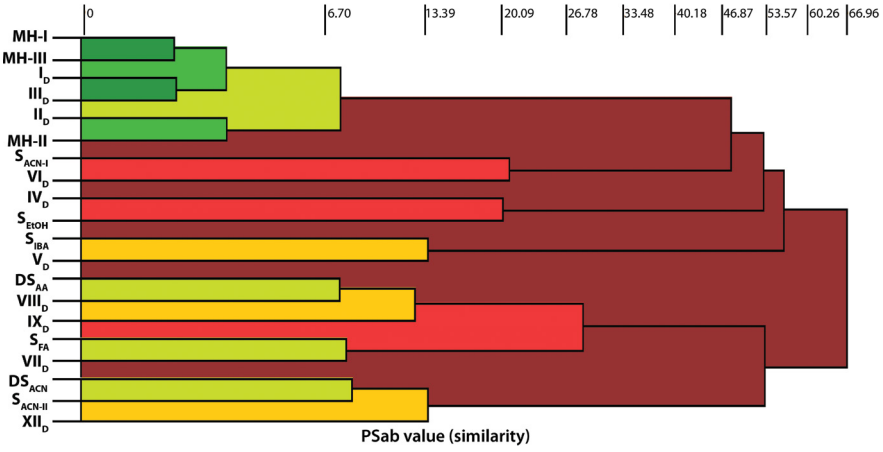

Figure 3.12. **Dendrogram showing packing similarity of forms of encenicline HCl**

Differential scanning calorimetry data (Figure 3.13 left) confirmed that form IV_D exhibits the highest melting point (286 ± 1 °C), while all the other polymorphs convert to form IV_D during the heating (Figure 4i) in one of three different ways: (1) via

endothermic phase transition (V_D), (2) via exothermic phase transition (VI_D and XI_D), or (3) in exothermic recrystallization from an unconventional melt/amorphous state (I_D, II_D, III_D, VII_D, $VIII_D$, IX_D, and XII_D). It is worth to mention that the endothermic process (140–190 °C) that leads to an amorphous state, as confirmed by PXRD, has too small enthalpy (2–7 kJ·mol^{-1}) to be used for establishment of the thermodynamic relationship according to the heat of fusion rule. Therefore, DSC data allowed the establishment of the thermodynamic relationship between only three polymorphic pairs: according to the heat of transition rule polymorphs V_D and IV_D have an enantiotropic thermodynamic relationship, but polymorphic pairs IV_D/VI_D and IV_D/XI_D are monotropically related. In slurry bridging experiments under ambient conditions in *n*-heptane, all polymorphs converted to form IV_D. Thus, at room and elevated temperatures, form IV_D is the most stable polymorph.

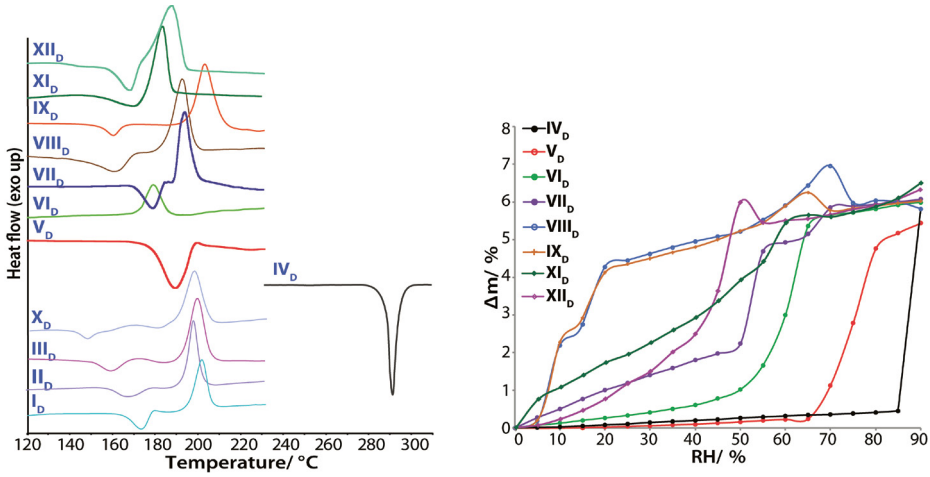

Figure 3.13. **Overlay of DSC curves (left) and water vapor sorption isotherms (right) of polymorphs**

The effect of relative humidity on the stability was also investigated, see Figure 3.13. right. It was found that the most stable polymorph with respect to moisture is IV_D, showing no significant mass change in the range from 0 to 85 % RH. At higher RH formation of monohydrate form MH-I was observed. Polymorphs V_D and VI_D are the second and the third most stable against the humidity, by starting to take up a significant amount of water at 70 % RH and 50 % RH, respectively. The least stable polymorphs against moisture are I_D, II_D, III_D, $VIII_D$ and IX_D already starting to take up a significant amount of water at > 5 % RH, meaning that these polymorphs are stable only at RH ≤ 5 %.

Although DSC measurements and slurry bridging experiments do not reveal information about the thermodynamic stability order of all polymorphs, this information can help to validate the relative DFD-D energies using different pseudopotentials and/or dispersion corrections methods. According to the experimental results polymorph V_D must be the lowest energy in 0 K, followed by IV_D, and energy of all ten polymorphs

have to be located within the range of ~15 kJ·mol^{-1} (melting enthalpy of polymorph IV_D). Taking in the account these restraints, the PBE-D3 computational approach yields the most reliable energy ranking (Figure 3.14.) where stability fallows order V_D > IV_D (+1.5 kJ·mol^{-1}) > VII_D (+3.3 kJ·mol^{-1}) >VI_D (+5.2 kJ·mol^{-1}) > I_D ≈ II_D (+7.1 kJ·mol^{-1}) > III_D ≈ IX_D (+8.5 kJ·mol^{-1}) > $VIII_D$ (+9.8 kJ·mol^{-1}) > XII_D (+12.2 kJ·mol^{-1}).

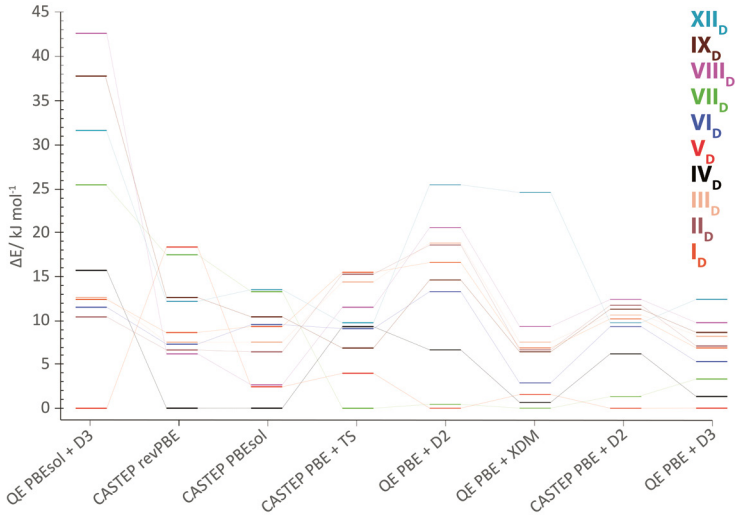

Figure 3.14. **Energy ranking for fully optimized structures using different pseudopotentials and/ or dispersion corrections**

3.4. Hexamorphism of dantrolene (4)

In comparison to other here described compounds dantrolene is a neutral molecule. However, dantrolene is also highly polymorphic compound polymorphs of which crystallize as microcrystalline powder. An initial polymorph screening of dantrolene was performed by using solvent evaporation, cooling crystallization and antisolvent addition experiments. The solvent-based screening resulted in a total of 22 crystal forms: three neat polymorphs (forms I, II and III), three monohydrates (MH-I, MH-II, MH-III) and sixteen monosolvates. Furthermore, three additional neat polymorphs (forms IV, V and VI) were obtained by dehydration of monohydrates MH-I, MH-II and MH-III, respectively. The experimental solid form landscape, showing the neat polymorphs and hydrated/solvated forms as well as the most convenient pathways to their preparation and interconversion is depicted in Figure 3.15.

Figure 3.16. shows the PXRD patterns of the dantrolene polymorphs and the precursor monohydrates. All the crystal forms, including hydrates and their respective dehydrates, give characteristic PXRD patterns, and therefore are easily distinguishable.

Crystal structures of form III and monohydrate MH-II were determined by SCXRD, whereas that of monohydrate MH-I and the rest of the neat polymorphs were successfully solved from PXRD data.

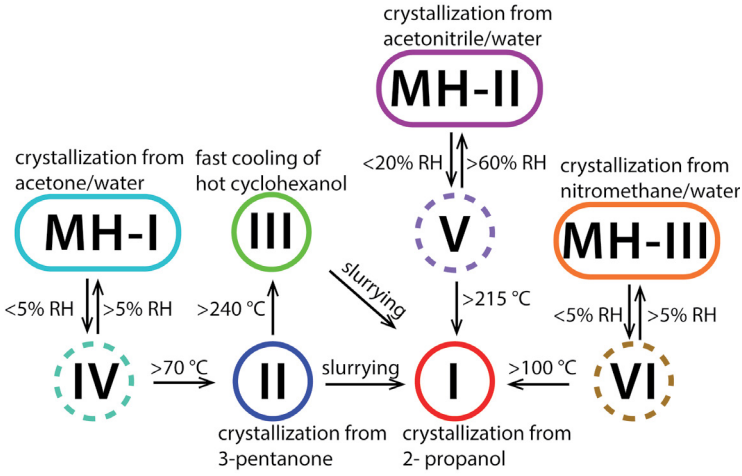

Figure 3.15. **Preparation and transition pathways of the dantrolene solid forms. Solid boxes show forms which were crystallized from solution; dashed boxes show forms obtained by solid state transition**

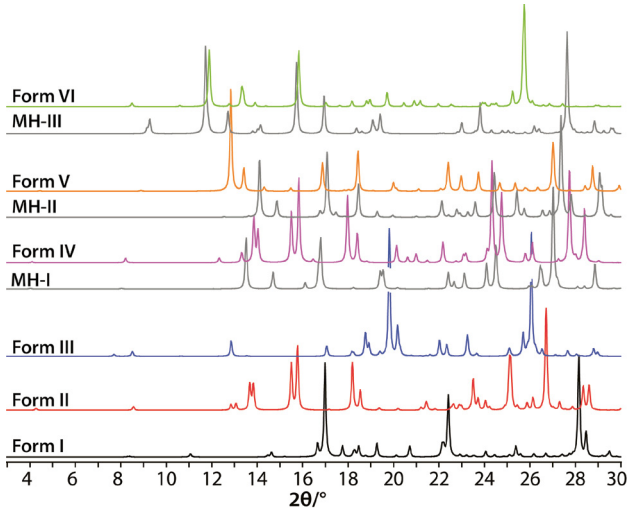

Figure 3.16. **PXRD patterns of dantrolene neat and hydrated (grey) crystalline forms**

Form I and form III crystallize in the centrosymmetric space group $P2_1/n$, forms II and VI crystallize in the centrosymmetric space groups $P2_1/c$ and $P\bar{1}$, respectively, but forms IV and V crystallize in the noncentrosymmetric space groups $P2_1$ and $P2_12_12_1$, respectively. In all determined crystal structures Z' = 1. Two distinct molecular conformations are found in the experimental crystal structures. Dantrolene molecules

in polymorphs I and III adopt global energy minimum conformation (conformation A), while molecules in crystal structures of other polymorphs adopt local energy minimum conformation (conformation B), with intramolecular energy (calculated in *Gaussian 09* and *CASTEP*) in experimental structures differing by ~ 3 kJ mol^{-1} (Figure 3.17.a). The main difference between both conformations is a rotation of the central furyl group by 180° around the torsion angle τ_2.

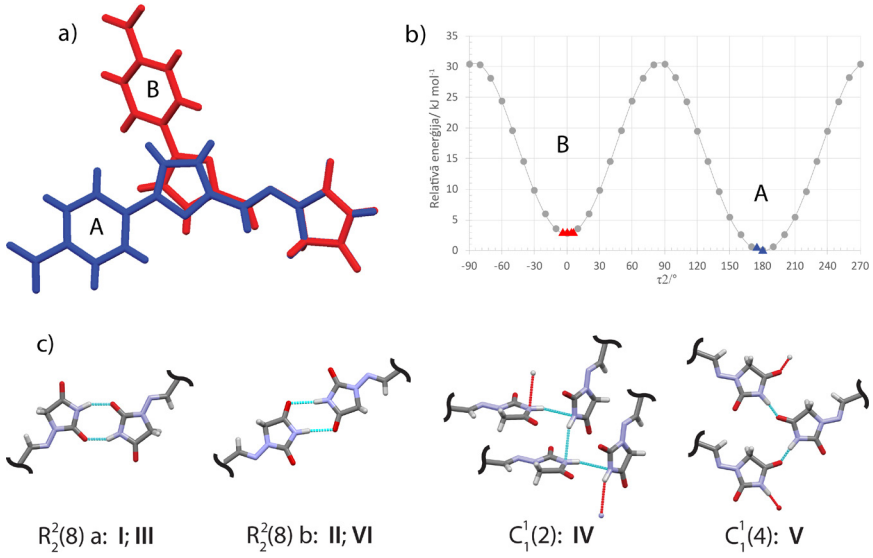

Figure 3.17. **(a) Overlay of the two distinct experimental conformations observed in dantrolene crystal structures – A in blue and B in red, (b) PES scan of dantrolene with respect to torsion angle τ_2 and (c) intermolecular hydrogen bonding motifs observed in the experimental structures of polymorphs**

The dantrolene molecule contains only one hydrogen bond donor site (N–H group) and several sites that can act as potential H-bond acceptors. Nevertheless, in the experimental structures of polymorphs three distinct hydrogen-bonding motifs formed by both strongest potential H-bond acceptors can be observed (Figure 3.17. c): $R^2_2(8)$ *a* in forms I and III formed by N2–H10···O1 interactions, $R^2_2(8)$ *b* in forms II and VI formed by N2–H10···O2 interactions and $C^1_1(4)$ in form V formed by N2–H10···O2 interactions. Meanwhile, form IV does not contain any conventional hydrogen bond, although motif $C^1_1(2)$ formed by weak N2–H10···N2 interaction can be observed. Comparison of the molecular packing of dantrolene neat polymorphs and monohydrates reveals that three distinct groups of related structures are present (Figure 3.18.).

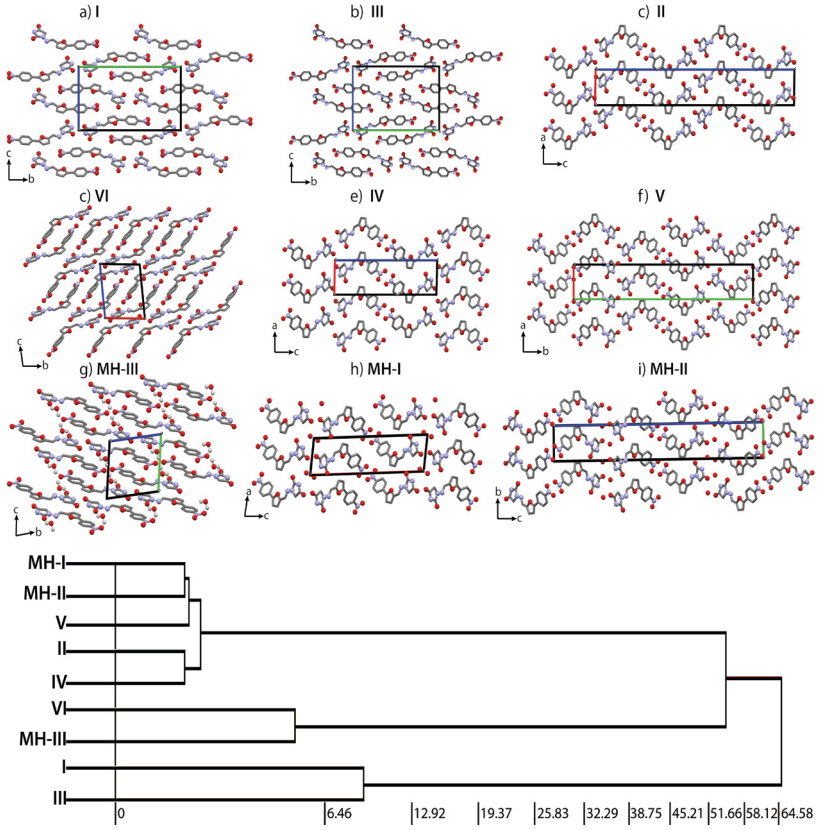

Figure 3.18. **Visual and quantitative representation of packing similarity in dantrolene hydrates and neat polymorphs. Hydrogen atoms are omitted for clarity. The horizontal axis of dendrogram corresponds to the PSab value (similarity)**

In the 1st group there are structurally related form I and form III, both sharing the same conformation, hydrogen bonding pattern and layers arranged along the *a* crystallographic axis. Meanwhile, the crystal packing along the other two axes is much more diverse resulting in the lowest crystal packing similarity among the forms belonging to the same group. The largest 2nd group includes forms II, IV, V and monohydrates MH-I, MH-II and have the highest crystal packing similarity. All these structures contain the same 2D zig zag layers. In the 3rd group containing MH-III and its respective dehydrate form VI the main packing difference is due to the slightly different molecular conformation in form VI (nitrobenzene group rotated by ~30°) allowing dantrolene molecules to pack more closely than in MH-III and also allowing more efficient π···π interactions.

The dantrolene anhydrate crystal energy landscape for Z' = 1 structures with two different conformations was calculated in CrystalPredictor and CrystalOptimizer followed by reoptimization of the most of the low energy structures (138 $Z \leq 4$ structures) with PBE-D2 computational approach. The same procedure (CrystalOptimizer + PBE-D2) was applied also for the six experimental structures of dantrolene polymorphs.

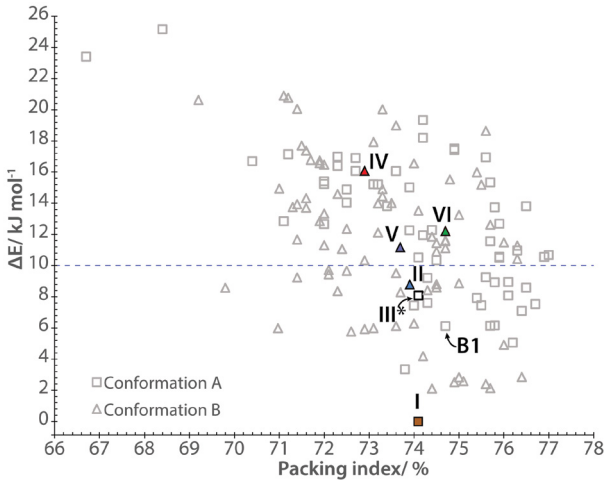

Figure 3.19. **Crystal structure landscape of the dantrolene, where each triangle and square represent a stable lattice energy minimum, generated in the CSP study after DFT-D geometry optimization. The identified experimental structures of polymorphs are colored and labelled. The landscape is complemented with the experimental structure of form III after identical computational protocol. The horizontal dashed line designates typical polymorph range of 10 kJ·mol^{-1}**

The obtained crystal structure landscape is given in Figure 3.19. This computational approach was successful in identifying five of the six experimental crystal structures of anhydrates by comparing $RMSD_{15}$ values between the experimental and the predicted structures. Although in the computationally generated crystal energy landscape there is a crystal structure (B1) with the same conformation, space group, similar lattice parameters and energy, it has different hydrogen bonding pattern (B1 has $R^2_2(8)$ *b* whereas form III has $R^2_2(8)$ *a* hydrogen bonding pattern, see Figure 3.17. c.) resulting in a quite high $RMSD_{15}$ of 0.66 Å. The absence of Form III among the predicted structures could possibly be because of a low temperature phase transformation between the predicted structure B1 and Form III, as rearrangement of molecule layers would result in change of the hydrogen bonding motif.

The thermodynamic properties of dantrolene polymorphs were examined by conventional (DSC) and fast scanning calorimetry analysis (FSC), polythermal solubility determination experiments and complemented with calculations of lattice energy values using different periodic DFT-D methods (Figure 3.20.). The conventional DSC traces of forms II, IV, V and VI shows exothermic phase transition to polymorph I (Figure 3.20. a). This substantiates the enantiotropic relationship between these polymorphs on the basis of the heat of transition rule, but endothermic phase transition between polymorphs II and III indicates a transition point between these forms. In order to avoid the degradation upon melting and to overcome the phase transitions before the melting, FSC at a high scanning rate (2000 °C·s^{-1}) was used (Figure 3.20. b). The obtained values of melting temperature and heat of fusion is sufficient to conclude that polymorphic pairs II/I and III/I are monotropically related on the basis of the heat of fusion rule and that Form I is the most thermodynamically stable polymorph. To determine

the thermodynamic transition temperature of polymorphs II and III, polythermal solubility determination experiments were performed (Figure 3.20. b). The intersection of solubility curves of forms II and III confirmed the enantiotropic relationship between these polymorphs with the transition point of these polymorphs lying between 105 and 110 °C. An additional intersection of solubility curves was observed at about 15–20 °C as the solubility of form V became lower than the solubility of polymorph III, indicating that polymorph V is more stable at lower temperature than polymorph III.

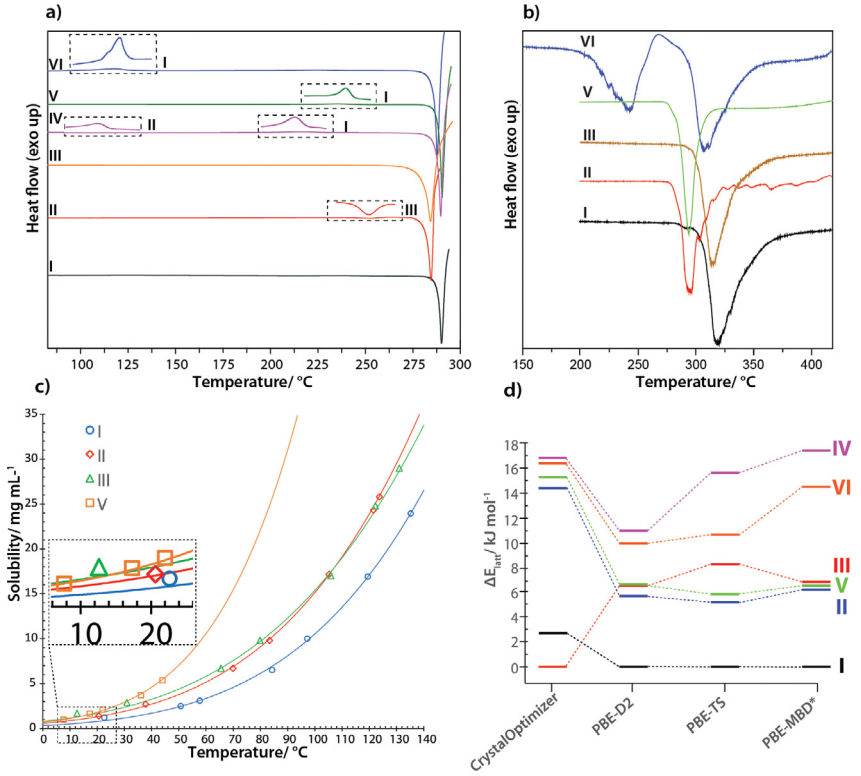

Figure 3.20. **a) DSC curves of dantrolene neat polymorphs (I–VI) recorded at a heating rate of 10 °C·min^{-1}, b) FSC curves of dantrolene neat polymorphs I, II, III, V and VI recorded at a heating rate of 2 000 °C·s^{-1}, c) Solubility (mg·mL^{-1}) of dantrolene forms I, II, III and V in cyclohexanone as a function of temperature and d) relative energy ranking of the dantrolene polymorphs using different periodic DFT+D methods compared to the ranking obtained using CrystalOptimizer**

By summarizing the results from DSC, FDC, solubility measurements and lattice energy calculations it is reasonable to conclude that the thermodynamic stability of dantrolene polymorphs at ambient temperature follows the order I > II > III > V > VI > IV, while because of the enantiotropic polymorph pairs of III and V as well as II and III this order is different below 15 °C (I > II > V > III > VI > IV) and above 110 °C (I > III > III > V > VI > IV).

CONCLUSIONS

1. Identical hydrogen bonded tetramer consisting of two quifenadine cations and two chloride anions was observed in the crystal structures of all three polymorphs of quifenadine HCl. In dihydrate structure, hydrogen bonds form a complex network, with water molecules playing a stabilizing role. Water molecules are located in structure channels and dehydration produces structurally similar polymorph B. Therefore, the solid-state hydration/dehydration transformation DH ⟷ B is reversible under ambient conditions and depends on the relative humidity.
2. Six structurally characterized polymorphs of sequifenadine HCl can be obtained. Although three different conformations of sequifenadine cation are observed in sequifenadine HCl polymorph structures, structural analysis showed that the major difference between all polymorphs is the mode of packing of the sequifenadine and chloride ions in the crystal structures, with three different hydrogen bonding patterns being one of the building elements resulting in different molecular packing. All hydrate structures appear as derived from those of particular polymorphs by incorporation of water molecules between layers or in structure voids.
3. Overall, ten structurally characterized polymorphs of encenicline HCl can be obtained. All thermodynamically metastable polymorphs can be accessed only through desolvation of various solvates or hydrates, and in this process the characteristic hydrogen bond network (except for hydrates) as well as packing present in the solvates are always maintained. Meanwhile, the conformation in all structures is nearly identical and corresponds to the same energy minimum.
4. Dantrolene represents another example of abundant molecular crystal polymorphism existing in at least six different neat polymorphs of which three can be obtained via crystallization (I, II and III) and additional three (IV, V and VI) via solid state dehydration from three different monohydrates. The main reasons appear to be at least two energetically favorable conformations, possibility to form different hydrogen bonds as well as stability of the remaining host framework after withdrawal of water molecules from the monohydrate structures.
5. The use of laboratory powder diffraction data, global optimization methods and periodic DFT-D calculations provide independent procedure for structure determination of a microcrystalline powder.
6. Several polymorphic forms of different pharmaceuticals have been obtained by desolvation of solvates. These polymorphs can be used as new stable and potentially patentable final dosage forms.

REFERENCES

(1) Yu, L.; Stephenson, G. A.; Mitchell, C. A.; Bunnell, C. A.; Snorek, S. V; Bowyer, J. J.; Borchardt, T. B.; Stowell, J. G.; Byrn, S. R. Thermochemistry and Conformational Polymorphism of a Hexamorphic Crystal System. *J. Am. Chem. Soc.* **2000**, *122*, 585–591.

(2) Sun, C.; Grant, D. J. W. Influence of Crystal Structure on the Tableting Properties of Sulfamerazine Polymorphs. *Pharm. Res.* **2001**, *18*, 274–280.

(3) Pudipeddi, M.; Serajuddin, A. T. M. Trends in Solubility of Polymorphs. *J. Pharm. Sci.* **2005**, *94*, 929–939.

(4) Price, S. L. Control and Prediction of the Organic Solid State: A Challenge to Theory and Experiment. *Proc. R. Soc. A Math. Phys. Eng. Sci.* **2018**, *474* , 20180351.

(5) Bingham, A. L.; Hughes, D. S.; Hursthouse, M. B.; Lancaster, R. W.; Tavener, S.; Threlfall, T. L. Over One Hundred Solvates of Sulfathiazole. *Chem. Commun.* **2001**, *7,* 603–604.

(6) Chen, S.; Guzei, I. A.; Yu, L. New Polymorphs of ROY and New Record for Coexisting Polymorphs of Solved Structures. *J. Am. Chem. Soc.* **2005**, *127*, 9881–9885.

(7) Yu, L. Polymorphism in Molecular Solids: An Extraordinary System of Red, Orange, Yellow Crystals. *Acc. Chem. Res.* **2010**, *43*, 1257–1266.

(8) Tyler, A. R.; Ragbirsingh, R.; McMonagle, C. J.; Waddell, P. G.; Heaps, S. E.; Steed, J. W.; Thaw, P.; Hall, M. J.; Probert, M. R. Encapsulated Nanodroplet Crystallization of Organic-Soluble Small Molecules. *Chem.* **2020**, *6*, 1755–1765.

(9) Lévesque, A.; Maris, T.; Wuest, J. D. ROY Reclaims Its Crown: New Ways To Increase Polymorphic Diversity. *J. Am. Chem. Soc.* **2020**, *142*, 11873–11883.

(10) Li, X.; Ou, X.; Rong, H.; Huang, S.; Nyman, J.; Yu, L.; Lu, M. The Twelfth Solved Structure of ROY: Single Crystals of Y04 Grown from Melt Microdroplets. *Cryst. Growth Des.* **2020**, *20* , 7093–7097.

(11) Bobrovs, R.; Kons, A.; Bērziņš, A.; Rekis, T.; Actiņš, A. Formation and Transformations of Organic Salt Hydrates: Four Encenicline Hydrochloride Monohydrates and Respective Isostructural Desolvates. *Cryst. Growth Des.* **2018**, *18*, 2100–2111.

(12) Kons, A.; Bērziņš, A.; Actiņš, A.; Rekis, T.; van Smaalen, S.; Mishnev, A. Polymorphism of R-Encenicline Hydrochloride: Access to the Highest Number of Structurally Characterized Polymorphs Using Desolvation of Various Solvates. *Cryst. Growth Des.* **2019**, *19*, 4765–4773.

(13) Bhardwaj, R. M.; McMahon, J. A.; Nyman, J.; Price, L. S.; Konar, S.; Oswald, I. D. H.; Pulham, C. R.; Price, S. L.; Reutzel-Edens, S. M. A Prolific Solvate Former, Galunisertib, under the Pressure of Crystal Structure Prediction, Produces Ten Diverse Polymorphs. *J. Am. Chem. Soc.* **2019**, *141*, 13887–13897.

(14) Zeidan, T. A.; Trotta, J. T.; Tilak, P. A.; Oliveira, M. A.; Chiarella, R. A.; Foxman, B. M.; Almarsson, Ö.; Hickey, M. B. An Unprecedented Case of Dodecamorphism: The Twelfth Polymorph of Aripiprazole Formed by Seeding with Its Active Metabolite. *CrystEngComm* **2016**, *18*, 1486–1488.

(15) Li, X.; Ou, X.; Wang, B.; Rong, H.; Wang, B.; Chang, C.; Shi, B.; Yu, L.; Lu, M. Rich Polymorphism in Nicotinamide Revealed by Melt Crystallization and Crystal Structure Prediction. *Commun. Chem.* **2020**, *3*, 152.

(16) López-Mejías, V.; Kampf, J. W.; Matzger, A. J. Nonamorphism in Flufenamic Acid and a New Record for a Polymorphic Compound with Solved Structures. *J. Am. Chem. Soc.* **2012**, *134*, 9872–9875.

(17) López-Mejías, V.; Kampf, J. W.; Matzger, A. J. Polymer-Induced Heteronucleation of Tolfenamic Acid: Structural Investigation of a Pentamorph. *J. Am. Chem. Soc.* **2009**, *131*, 4554–4555.

(18) Case, D. H.; Srirambhatla, V. K.; Guo, R.; Watson, R. E.; Price, L. S.; Polyzois, H.; Cockcroft, J. K.; Florence, A. J.; Tocher, D. A.; Price, S. L. Successful Computationally Directed Templating of Metastable Pharmaceutical Polymorphs. *Cryst. Growth Des.* **2018**, *18*, 5322–5331.

(19) Braun, D. E.; Gelbrich, T.; Kahlenberg, V.; Tessadri, R.; Wieser, J.; Griesser, U. J. Stability of Solvates and Packing Systematics of Nine Crystal Forms of the Antipsychotic Drug Aripiprazole. *Cryst. Growth Des.* **2009**, *9*, 1054–1065.

(20) Lohani, S.; Grant, D. J. W. Thermodynamic of Polymorphs. In *Polymorphism: In the pharmaceutical industry*; 2006; pp 21–42.

(21) Grothe, E.; Meekes, H.; Vlieg, E.; ter Horst, J. H.; de Gelder, R. Solvates, Salts, and Cocrystals: A Proposal for a Feasible Classification System. *Cryst. Growth Des.* **2016**, *16*, 3237–3243.

(22) Yu, L.; Reutzel, S. M.; Stephenson, G. a. Physical Characterization of Polymorphic Drugs: An Integrated Characterization Strategy. *Pharm. Sci. Technolo. Today* **1998**, *1*, 118–127.

(23) Stahly, G. P. Diversity in Single- and Multiple-Component Crystals. The Search for and Prevalence of Polymorphs and Cocrystals. *Cryst. Growth Des.* **2007**, *7*, 1007–1026.

(24) Karpinski, P. H. Polymorphism of Active Pharmaceutical Ingredients. *Chem. Eng. Technol.* **2006**, *29*, 233–237.

(25) Chieng, N.; Rades, T.; Aaltonen, J. An Overview of Recent Studies on the Analysis of Pharmaceutical Polymorphs. *J. Pharm. Biomed. Anal.* **2011**, *55*, 618–644.

(26) Braga, D.; Grepioni, F.; Maini, L.; Polito, M. Crystal Polymorphism and Multiple Crystal Forms; 2009; pp 25–50.

(27) Näther, C.; Jess, I.; Jones, P. G.; Taouss, C.; Teschmit, N. Structural, Thermodynamic, and Kinetic Aspects of the Polymorphism of Trimethylthiourea: The Influence of Kinetics on the Transformations between Polymorphs. *Cryst. Growth Des.* **2013**, *13*, 1676–1684.

(28) Gavezzotti, A. A Solid-State Chemist's View of the Crystal Polymorphism of Organic Compounds. *Journal of Pharmaceutical Sciences*. 2007, pp 2232–2241.

(29) Sarma, B.; Chen, J.; Hsi, H.; Myerson, A. S. Solid Forms of Pharmaceuticals: Polymorphs, Salts and Cocrystals. *Korean J. Chem. Eng.* **2011**, *28*, 315–322.

(30) Day, G. M.; S Motherwell, W. D.; Jones, W. A Strategy for Predicting the Crystal Structures of Flexible Molecules: The Polymorphism of Phenobarbital. *Phys. Chem. Chem. Phys.* **2007**, *9*, 1693–1704.

(31) Seton, L.; Khamar, D.; Bradshaw, I. J.; Hutcheon, G. a. Solid State Forms of Theophylline: Presenting a New Anhydrous Polymorph. *Cryst. Growth Des.* **2010**, *10*, 3879–3886.

(32) Burger, A.; Ramberger, R. On the Polymorphism of Pharmaceuticals and Other Molecular Crystals. I. *Mikrochim. Acta* **1979**, *72*, 259–271.

(33) Pindelska, E.; Sokal, A.; Kolodziejski, W. Pharmaceutical Cocrystals, Salts and Polymorphs: Advanced Characterization Techniques. *Adv. Drug Deliv. Rev.* **2017**, *117*, 111–146.

(34) Harris, K. D. M. Powder Diffraction Crystallography of Molecular Solids. *Top. Curr. Chem.* **2012**, *315*, 133–178.

(35) Brüning, J.; Schmidt, M. U. The Determination of Crystal Structures of Active Pharmaceutical Ingredients from X-Ray Powder Diffraction Data: A Brief, Practical Introduction, with Fexofenadine Hydrochloride as Example. *J. Pharm. Pharmacol.* **2015**, *67*, 773–781.

(36) J. Bernstein; S. M. Reutzel-Edensc. International Tables for Crystallography. In *International Tables for Crystallography*; Gilmore, C. J., Kaduk, J. A., Schenk, H., Eds.; International Union of Crystallography: Chester, England, 2019; Vol. H, p 2019.

(37) Pawley, G. S. Unit-Cell Refinement from Powder Diffraction Scans. *J. Appl. Crystallogr.* **1981**, *14*, 357–361.

(38) Le Bail, A.; Duroy, H.; Fourquet, J. L. Ab-Initio Structure Determination of LiSbWO6 by X-Ray Powder Diffraction. *Mater. Res. Bull.* **1988**, *23*, 447–452.

(39) Boultif, A.; Louër, D. Powder Pattern Indexing with the Dichotomy Method. *J. Appl. Crystallogr.* **2004**, *37*, 724–731.

(40) Altomare, A.; Campi, G.; Cuocci, C.; Eriksson, L.; Giacovazzo, C.; Moliterni, A.; Rizzi, R.; Werner, P.-E. Advances in Powder Diffraction Pattern Indexing: N-TREOR09. *J. Appl. Crystallogr.* **2009**, *42*, 768–775.

(41) Oishi-Tomiyasu, R. Distribution Rules of Systematic Absences on the Conway Topograph and Their Application to Powder Auto-Indexing. *Acta Crystallogr. Sect. A Found. Crystallogr.* **2013**, *69*, 603–610.

(42) van de Streek, J.; Neumann, M. A. Validation of Molecular Crystal Structures from Powder Diffraction Data with Dispersion-Corrected Density Functional Theory (DFT-D). *Acta Crystallogr. Sect. B Struct. Sci. Cryst. Eng. Mater.* **2014**, *70*, 1020–1032.

(43) Makarov, L.; Balykova, L.; Soldatova, O.; Komolyatova, V.; Serebruany, V. The Antiarrhythmic Properties of Quifenadine, H1-Histamine Receptor Blocker in Children with Premature Beats: A Randomized Controlled Pilot Trial. *Am. J. Ther.* **2012**, *17*, 396–401.

(44) Gankina, E. M.; Porodenko, N. V.; Kondratenko, R. Y.; Severin, E. S.; Kaminka, M. E.; Mashkovskii, M. D. Effect of Some Antihistamine Preparations on Binding Of3H-Mepyramine And3H-Cimetidine to Histamine Receptors in Rat Brain. *Pharm. Chem. J.* **1992**, *26*, 373–376.

(45) Prickaerts, J.; Van Goethem, N. P.; Chesworth, R.; Shapiro, G.; Boess, F. G.; Methfessel, C.; Reneerkens, O. A. H.; Flood, D. G.; Hilt, D.; Gawryl, M. EVP-6124, a Novel and Selective A7 Nicotinic Acetylcholine Receptor Partial Agonist, Improves Memory Performance by Potentiating the Acetylcholine Response of A7 Nicotinic Acetylcholine Receptors. *Neuropharmacology*. **2012**, *62*, 1099–1110.

(46) Oliver-Shaffer, P.; Shapiro, G.; Chesworth, R.; Kishida, M.; Ishige, T. Crystalline Form of (R)-7-Chloro-N-(Quinuclidin-3-Yl) Benzo [B] Thiophene-2-Carboxamide Hydrochloride Monohydrate. US 2014/0249179, 2014.

(47) Krause, T.; Gerbershagen, M. U.; Fiege, M.; Weißhorn, R.; Wappler, F. Dantrolene? A Review of Its Pharmacology, Therapeutic Use and New Developments. *Anaesthesia*. **2004**, *59*, 364–373.

(48) Tanaka, R.; Akimoto, T.; Haramura, M.; Tanaka, A.; Hirayama, N. Structure of Dantrolene. *X-ray Struct. Anal. Online* **2004**, *20*, 97.

(49) Wang, C.; Sun, C. C. Identifying Slip Planes in Organic Polymorphs by Combined Energy Framework Calculations and Topology Analysis. *Cryst. Growth Des.* **2018**, *18*, 1909–1916.

PUBLIKĀCIJAS / PUBLICATIONS

I

Kons, A., Mishnev, A., Mukhametzyanov, T., Buzyurov, A.,

Semen, L., Bērziņš, A.

HEXAMORPHISM OF DANTROLENE: INSIGHT INTO THE CRYSTAL STRUCTURES, STABILITY, AND PHASE TRANSFORMATIONS

Cryst. Growth Des. **2021**, 21, 1190–1201

CRYSTAL GROWTH & DESIGN

pubs.acs.org/crystal Article

Hexamorphism of Dantrolene: Insight into the Crystal Structures, Stability, and Phase Transformations

Artis Kons,* Anatoly Mishnev, Timur A. Mukhametzyanov, Alexey V. Buzyurov, Semen E. Lapuk, and Agris Bērziņš

Cite This: https://dx.doi.org/10.1021/acs.cgd.0c01508 Read Online

ACCESS | Metrics & More | Article Recommendations | Supporting Information

ABSTRACT: Dantrolene represents yet another interesting example of abundant molecular crystal polymorphism existing in at least six different neat polymorphs, three of which can be obtained via crystallization (I−III) and an additional three (IV− VI) via solid-state dehydration from three different monohydrates (MH-I−MH-III). The reasons for polymorph formation were rationalized by analyzing the crystal structures of the polymorphs and hydrates used in their preparation. The thermodynamic relations among the polymorphs were established from calorimetric data, solubility measurements, and lattice energy calculations.

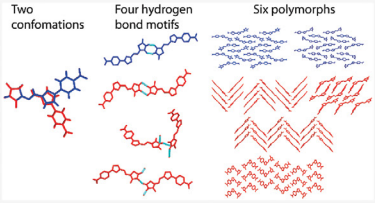

INTRODUCTION

Polymorphism is the ability of a compound to exist in a number of crystalline forms. This phenomenon is highly important in the manufacturing of pharmaceuticals, since properties such as solubility, dissolution rate, melting point, density, tabletability, etc. of different polymorphs may differ. The number of polymorphs formed by a compound as well as what tools can be used to predict this are still among the unresolved questions in organic crystal polymorphism.[1] The solid-phase landscapes of different compounds can differ significantly, and there are compounds that are able to form more than 10 polymorphs and notably a larger number of solvates[2,3] (with the largest reported number of solvates formed exceeding 100[4]). The most prolific polymorphic systems today are ROY[5−10] with 13 structurally characterized polymorphs, followed by encenicline hydrochloride[11,12] and galunisertib,[13] both having 10 reported polymorphs with determined crystal structures, aripiprazole[14−16] and nicotinamide[17] with 9 polymorphs, and flufenamic acid[18] and tolfenamic acid[19,20] with 8 polymorphs. Yet a survey of crystal structures deposited in the Cambridge Structural Database[21] showed that for molecular solids rarely more than 4 polymorphs have been reported.

On the one hand, a high tendency to form solvates will limit the possibilities to prepare the unsolvated phase(s) of a compound. On the other hand, desolvation of solvates often produces new polymorphs which cannot be obtained using conventional crystallization techniques.[22−25] Despite the fact that new polymorphs obtained using desolvation are reported rather often,[26] it is common that their crystal structures remain undetermined, as usually the polymorphs are obtained in the form of a powder. Nevertheless, the advancement of crystal structure determination from powder diffraction by using direct-space methods complemented by DFT-D calculations[11,27,28] or from electron diffraction measurements[29,30] is being successfully used more and more often for crystal structure determination.

Recently it has been shown that an additional understanding of the experimental solid form landscape can be provided by crystal structure prediction (CSP) methods, a tool for prediction of the lowest energy hypothetical crystal structures.[13,31] This approach is often used to ensure that the most stable forms have been found or justify expanding the experimental search. However, CSP frequently overpredicts the possibility of polymorphism and does not yet identify experimentally achievable structures[32,33] which may form following rare nucleation events that have not been accessed during limited variations of the experimental crystallization procedures.[34,35]

In this work, we present a structural and experimental study of polymorphs of dantrolene (1-[[5-(4-nitrophenyl)furan-2-yl]methylideneamino]imidazolidine-2,4-dione) (Figure 1). Dantrolene is a skeletal muscle relaxant that depresses the intrinsic mechanisms of excitation−contraction coupling. It reduces the spasms, cramping, and muscle stiffness caused by certain medical problems, such as disseminated sclerosis, a

Received: November 6, 2020
Revised: December 28, 2020

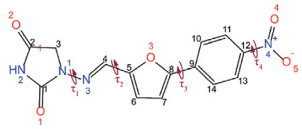

Figure 1. Molecular diagram of dantrolene with the numbering of non-hydrogen atoms and labeling of flexible dihedral angles.

stroke, or an injured spine.[36] The only previously reported crystal structure of dantrolene is a methanol solvate.[37]

In the performed solid form screening of six neat polymorphs, three obtained in crystallization and three in desolvation, three monohydrates and numerous solvates have been obtained and characterized. With the crystal structures of six polymorphs having been characterized, dantrolene is among the most polymorphic molecules reported. A structural and physicochemical characterization of solid forms of such polymorphic and diverse molecules contribute toward our understanding of polymorphic behavior and factors regulating the formation and stability of different polymorphs. To obtain complete information on the polymorphic forms and to establish a better comprehension of the thermodynamic and kinetic phase relationships, different experimental techniques, including powder X-ray diffraction (PXRD) and single crystal X-ray diffraction (SC-XRD), differential scanning calorimetry (DSC) and fast scanning calorimetry (FDC), dynamic vapor sorption (DVS)/desorption, and solubility measurements complemented with crystal structure prediction (CSP) and lattice energy calculations were used.

■ EXPERIMENTAL SECTION

Materials. Dantrolene (purity >99%) was obtained from JSC Olainfarm (Olaine, Latvia). The sample consisted of a mixture of anhydrous forms I–III. Analytical grade organic solvents were purchased from commercial sources and used without further purification.

Sample Preparation. A standard solvate screening was performed by cooling a hot solution of dantrolene in a selected solvent to room temperature or by evaporation of a saturated solution at ambient temperature. Both methods overall produced 18 solvates with methanol, ethanol, trifluoroethanol, acetone/water, methyl ethyl ketone/water, tetrahydrofuran/water, acetonitrile, nitromethane, dimethyl sulfoxide, dimethylformamide, dimethylacetamide, dimethyl carbonate, 1,4-dioxane, 1,3-dioxalene, formic acid, and acetic acid. The monohydrate MH-I was prepared by adding water as an antisolvent to a saturated hot solution of dantrolene in acetone. The monohydrate MH-II was prepared by slow evaporation of an acetonitrile/water mixture (95/5 v/v). Monohydrate MH-III was obtained by slow evaporation of an nitromethane/water mixture (95/5 v/v). Form I was obtained by crystallization from 2-propanol or by slurrying any other crystalline form in 2-propanol or cyclohexanone. Form II was prepared by crystallization from 3-pentanone. Form III was obtained by fast cooling of a hot cyclohexanol solution. Polymorphs IV–VI were obtained by dehydrating monohydrates MH-I–MH-III in a desiccator over P_2O_5, respectively.

Powder X-ray Diffraction. Routine PXRD measurements were performed with a Bruker D8 Advance diffractometer using copper radiation (Cu Kα, λ = 1.54180 Å) with Bragg–Brentano geometry and a LynxEye (1D) detector. The tube voltage and current were set to 40 kV and 40 mA, respectively. The divergence and antiscattering slits were set at 0.6 and 8 mm, respectively. The patterns were recorded from 3° to 30° on the 2θ scale, using a scan speed of 0.2 s/0.02°. When necessary, to prevent the atmospheric humidity effect, samples were covered with a 10 μm polyethylene film.

PXRD data for crystal structure determination were recorded on a Bruker D8 Discover diffractometer using copper radiation (Cu Kα, λ = 1.54180 Å) and a LynxEye (1D) detector in transmission mode. The tube was employed with voltage and current settings of 40 kV and 40 mA, respectively. The sample was loaded into a special glass No. 10 capillary (0.5 mm diameter). A capillary spinner (60 rpm) and upper and lower knife edges were used. The diffractometer incident beam path was equipped with a Göbel mirror, Soller slit, and a 0.6 mm divergence slit, while the diffracted beam path was equipped only with a Soller slit. The diffraction patterns were recorded on the 2θ scale from 3° or 4.5° to 70° at a 0.01° step size using a scan speed of 36 s per step.

Structure Determination from PXRD Data. Indexing, space group determination, and structure solution were performed using EXPO2014.[38] The unit cell dimensions were determined by applying the N-TREOR09[39] and Dicvol06[40] indexing procedures with a set of 20–25 reflections found in 4.5–30° 2θ range. Space group determination was carried out using a statistical assessment of systematic absences, and Z′ was determined on the basis of density considerations. The cell and diffraction pattern profile parameters were refined according to the Le Bail algorithm.[41,42] The background was modeled by a 20th-order polynomial function of the Chebyshev type; peak profiles were described by the Pearson VII function.

The initial geometry of dantrolene was taken from the crystal structure of methanol solvate.[37] Simulating Annealing algorithm was used to optimize the dantrolene model against the experimental powder diffraction pattern set in direct space by adjusting the conformation, position, and orientation of the trial model in the unit cell.

The best structure solution was then used for Rietveld refinement using TOPAS5.[43] The background was modeled with Chebyshev polynomials, and the modified Thompson–Cox–Hastings pseudo-Voigt function was used for peak shape fitting. The geometry of each molecule was defined by a rigid body. Rotation and translation parameters were refined simultaneously with the dihedrals of each independent molecule in the asymmetric unit. A global isotropic atomic displacement parameter (B_{iso}) was refined for non-hydrogen atoms, and for hydrogen atoms it was set to 1.2B_{iso}.

Single-Crystal X-ray Diffraction. SC-XRD data of forms III and MH-II were collected on a XtaLAB Synergy-S dualflex diffractometer (RIGAKU Oxford Diffraction) equipped with a HyPix6000 detector and a microfocus sealed X-ray tube with Mo Kα radiation (λ = 0.7107 Å). A single crystal with approximate dimensions of 0.08 × 0.08 × 0.06 mm^3 was fixed with oil in a nylon loop of a magnetic CryoCap and set on a goniometer head. The sample was cooled to 150 K, and ω scans were performed with a step size of 0.5°. Data collection and reduction were performed with the CrysAlisPro 1.171.40.35a software. Structure solution and refinement were performed with AutoChem3.0 and SHELXL[44] software that are parts of the CrysAlisPro suite. Non-hydrogen atoms were refined anisotropically. Hydrogen atoms were added geometrically and refined using a "riding" model.

Differential Scanning Calorimetry. Conventional DSC analyses of neat polymorphs were performed with a TA DSC 25 instrument. Closed 70 μL aluminum pans were used. Heating of samples from 25 to 300 °C was performed at a heating rate of 10 °C min^{-1} under a 50 mL min^{-1} nitrogen flow. The sample mass was approximately 5 mg.

FSC analyses of neat polymorphs were performed with a Mettler Toledo Flash DSC1 instrument. A sample of crystalline dantrolene (ca. 10 ng) was placed in the center of the measuring area of an UFS1 sensor (circular area of 500 μm diameter) with the help of a thin copper wire (ϕ = 0.03 mm). In preliminary experiments, the empty sensor was conditioned according to the manufacturer's procedure to establish the correct relation between the measured signal and the temperature of the sample. The FSC scans were performed under an inert atmosphere of nitrogen with a flow rate of about 50 mL min^{-1} at a heating rate of 2000 °C s^{-1}. Optical images of the samples under study were taken with an Olympus BXFM microscope with 10× lens in reflection mode and a DCM 510 camera before and after each thermal scanning.

https://dx.doi.org/10.1021/acs.cgd.0c01508
Cryst. Growth Des. XXXX, XXX, XXX–XXX

Dynamic Water Vapor Sorption and Desorption Studies. Dynamic vapor sorption−desorption experiments were performed on the Surface Measurement Systems DVS Advantage apparatus. All samples (5−12 mg) were initially dried under a 200 mL stream of N_2 to establish the equilibrium dry mass under 25 °C. Samples were studied over a selected humidity range from 0 to 90% RH with a step of 5% at 25 °C. Each humidity step was taken with equilibration set to dm/dt 0.002%/min on a 5 min time frame (with a minimum hold time of 10 min and a maximum of 300 min).

Solubility Determination. The solubilities of forms I−III and V in cyclohexanone and forms I−III in *n*-pentanol were determined by turbidity measurements using a Technobis Crystal16 instrument at 0.2 °C min^{-1}.

Crystal Structure Prediction and Theoretical Calculations. CSP was performed with CrystalPredictor 2.2[45] for the two most likely conformers held rigid. Conformer **A** was used with τ_2 being 180° and **B** with τ_2 being 0 (see Figure 1), while other torsion angles were as in all determined experimental crystal structures. The conformational energy difference, ΔE_{intra}, was calculated with Gaussian 09[46] at the M06-2X/6-31G(d,p) level of theory and combined with the dominant intermolecular energy U_{inter} calculated as a sum of an electrostatic component derived from point charges and a repulsion−dispersion component derived from the empirically fitted FIT potential.[47] Crystal structures were generated in the 61 most common space groups in the CSD (see the Supporting Information) with $Z' = 1$ by generating a total of 1000000 structures for each conformer.

After structure prediction the obtained structures were analyzed using the Analysis tool, and those having reasonable lattice energy and no obvious errors were optimized in DMACRYS[48] using the FIT potential and multipoles generated with GDMA[49] after M06-2X/6-21G(d,p) calculation in Gaussian 09.

The structures were then clustered, and 3350 unique structures were refined using CrystalOptimizer 2.4.7.[50] The intermolecular lattice energy was calculated using DMACRYS modeling electrostatic interactions with distributed multipoles calculated by GDMA on charge densities of isolated molecules calculated in Gaussian 09. Other intermolecular forces were calculated with an atom−atom *exp*-6 repulsion−dispersion potential using the empirically fitted FIT parameters. The conformational energies and distributed multipoles used were calculated at the M06-2X/6-31G(d,p) level. During the CrystalOptimizer optimizations torsion angles τ_1−τ_4 and the bond angle H−N2−C1 were optimized. After CrystalOptimizer, structures which showed a negative eigenvalue (corresponding to a high-symmetry saddle point) were reminimized in a lower symmetry space group. The optimized structures were then clustered to obtain the final set of unique predicted crystal structures.

The geometry optimization and the resulting calculation of total energy of the most stable predicted anhydrates (138 structures, $Z \leq 4$, covering an energy range of 20 kJ mol^{-1} with respect to the global minimum) was performed in the CASTEP[51] plane wave code by relaxing lattice parameters and atomic positions using the PBE[52] exchange-correlation density functional and on-the-fly generated ultrasoft pseudopotentials,[53] with the addition of a semiempirical Grimme D2[54] dispersion correction. *K* points were chosen to provide a maximum spacing of 0.07 $Å^{-1}$, and the basis set cutoff was 570 eV.

The lattice energies of dantrolene neat polymorphs were calculated using the same settings and also using TS[55] and MBD*[56] dispersion correction methods. Isolated molecule minimizations to compute the energy of isolated dantrolene were performed by placing a single molecule in a fixed cubic 30 × 30 × 30 $Å^3$ unit cell and performing geometry optimization with the same settings as those used for calculation of the periodic crystal structures. For polymorph III, an ordered version of the nitro group was used for the calculations.

1D relaxed potential energy surfaces (PES) and conformation energy were calculated in Gaussian09 at the M06-2X/6-31++G(d,p) level by scanning the τ_2 flexible torsion angle (see Figure 1) with a step size of 10°.

Crystal Structure Comparison and Analysis. Mercury 2020.2.0 software[57,58] was used for crystal structure analysis and simulation of PXRD patterns on the basis of the crystal structure data. Detailed analyses of the molecular packing similarities were performed using CrystalCMP.[59] Crystal structures for a quantitative molecular packing comparison in CrystalCMP and calculations of packing coefficients were used after geometry optimization with the periodic boundary DFT code for more reliable and consistent results. For form III, an ordered structure model was used. ConQuest 2020.2.0 was used to search the CSD (v5.41 November 2019 Updates).

RESULTS AND DISCUSSION

Solid Form Screening. Solid forms of dantrolene were screened using solvent evaporation, cooling crystallization, and antisolvent addition experiments. These experiments resulted in a total of 27 crystal forms: 3 neat polymorphs (I−III), 3 monohydrates (MH-I−MH-III) and 16 monosolvates (acetonitrile, nitromethane, methanol, ethanol, trifluoroethanol, acetone, methyl ethyl ketone, tetrahydrofuran, 1,4-dioxane, 1,3-dioxalene, formic acid, acetic acid, dimethyl carbonate, dimethylformamide, dimethylacetamide, dimethyl sulfoxide). Furthermore, three additional neat polymorphs (forms IV−VI) were obtained by dehydration of monohydrates MH-I−MH-III, respectively (see the Experimental Section for more details). All of the obtained solvates were characterized by PXRD and DSC/TGA methods to confirm the solvate stoichiometry and desolvation products (see Table S1 and Figure S1 in the Supporting Information), but no further characterization was performed. Upon desolvation by heating, all solvates transform to forms I−III, mixtures of these polymorphs, or a low crystallinity/amorphous phase.

Figure 2 shows the PXRD patterns of the dantrolene polymorphs and the precursor monohydrates. All of the crystal forms, including hydrates and their respective dehydrates, give characteristic PXRD patterns and therefore are easily distinguishable. The experimental solid-phase landscape,

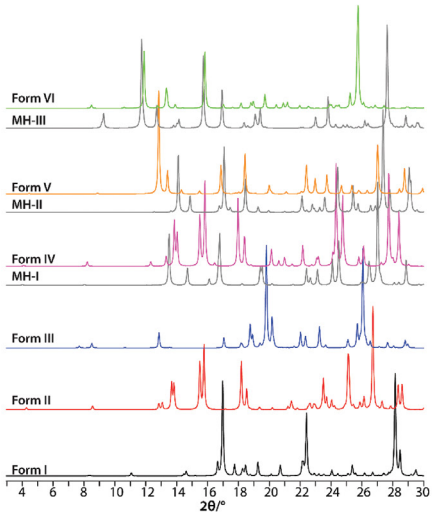

Figure 2. PXRD patterns of dantrolene neat and hydrated (gray) crystalline forms.

https://dx.doi.org/10.1021/acs.cgd.0c01508
Cryst. Growth Des. XXXX, XXX, XXX−XXX

showing the neat polymorphs and hydrates, and the most convenient pathways to their preparation and interconversion are depicted in Figure 3.

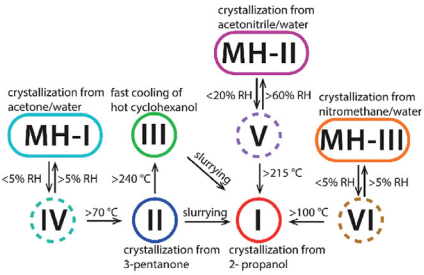

Figure 3. Preparation and transition pathways of the dantrolene solid forms. Solid ovals show forms that were obtained from solution; dashed ovals show forms accessed by solid-state transitions.

Water Sorption/Desorption Analysis. The water sorption/desorption behavior of the neat and hydrated forms of dantrolene was determined using dynamic vapor sorption/desorption analysis at 25 °C. Forms I−III show no significant moisture sorption (<0.6%) up to 95% RH (Figure 4a). No transitions to the hydrated phases were observed, and on the basis of the obtained sorption isotherms, form I can be classified as nonhygroscopic, while forms II and III are slightly hygroscopic.[60] In contrast, forms IV and VI have very low stability against humidity and very rapidly transform to the structurally related hydrated phases MH-I and MH-III, respectively, at ≥5% RH (Figure 4b,d), confirming that these two anhydrates are not stable under ambient conditions and can transform back to the anhydrous phase only at 0% RH or/and at elevated temperature. Form V absorbs a significant amount of water (>0.5%) above 60% RH, transforming to the hydrate MH-II, with water sorption being reversible, as the anhydrous phase V is obtained when the RH is reduced below 30% (Figure 4c). The presence of large hysteresis (~30% RH) between the sorption and desorption isotherms indicates that water molecules in the crystal structure are not located in an easily exchangeable way, as in open channels, but are rather located in isolated pockets, resulting in a kinetically hindered water egress/ingress process, opposite to that observed for the IV/MH-I and VI/MH-III systems. The water content in all three of these hydrates remains sufficiently constant over their relative humidity existence ranges so that the hydrate stoichiometry can be determined as monohydrates.

Characterization of Crystal Structures of Dantrolene Neat and Hydrated Forms. Crystal structures of the neat

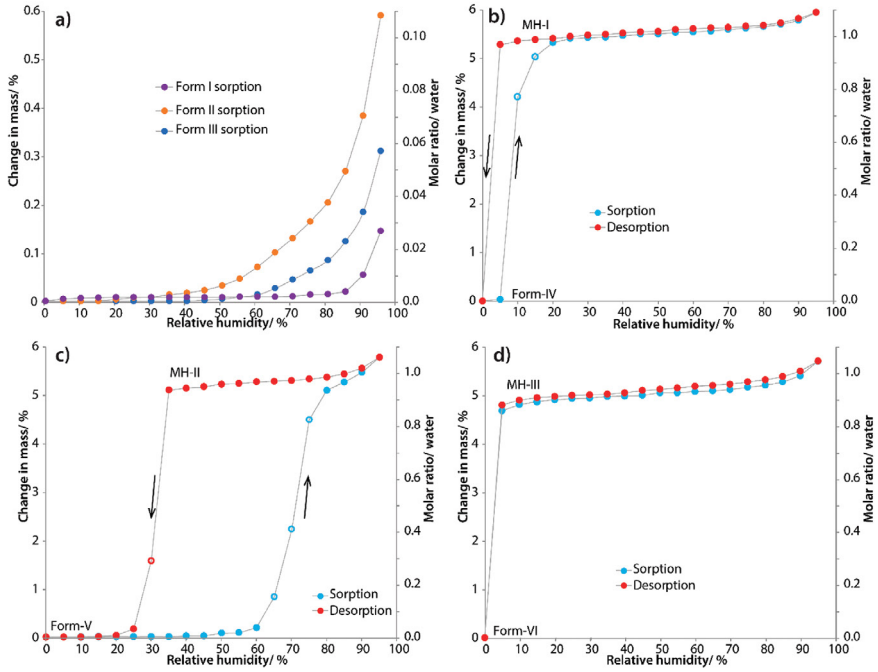

Figure 4. Water vapor sorption−desorption isotherms of dantrolene forms at 25 °C.

https://dx.doi.org/10.1021/acs.cgd.0c01508
Cryst. Growth Des. XXXX, XXX, XXX−XXX

Table 1. Crystallographic Data Structure Refinement Parameters for Neat Polymorphs of Dantrolene

	I	II	III	IV	V	VI
formula				$C_{14}H_{10}N_4O_5$		
formula wt, g mol^{-1}				314.25		
sample type	powder	powder	single crystal	powder	powder	powder
cryst syst	monoclinic	monoclinic	monoclinic	monoclinic	orthorhombic	triclinic
space group	$P2_1/n$	$P2_1/c$	$P2_1/n$	$P2_1$	$P2_12_12_1$	$P\bar{1}$
a, Å	5.383(5)	6.884(2)	4.8677(4)	6.64(2)	6.990(3)	7.989(6)
b, Å	21.26(2)	4.933(4)	20.7390(14)	4.828(16)	39.749(18)	8.8790(10)
c, Å	12.109(12)	42.037(7)	13.8153(9)	21.52(7)	4.957(2)	10.762(6)
α, deg	90	90	90	90	90	79.33(6)
β, deg	92.3042(16)	91.040(10)	94.553(7)	91.3380(18)	90	76.75(4)
γ, deg	90	90	90	90	90	70.99(8)
V, Å^3	1385(3)	1427.3(13)	1390.27(17)	690(4)	1377.3(10)	698(2)
ρ_{calc}, g cm^{-3}	1.507	1.462	1.501	1.513	1.516	1.507
Z/Z'	4/1	4/1	4/1	2/1	4/1	2/1
temp, K	293(2)	293(2)	293(2)	293(2)	293(2)	293(2)
$2\theta_{min}$–$2\theta_{max}$ /increment, deg	4.0–70.0/0.01			3.0–70.0/0.01	4.0–70.0/0.01	4.0–70.0/0.01
R_{wp} (R_p), %	5.71 (4.08)	5.60 (4.18)		4.98 (3.46)	7.64 (5.84)	3.71(2.81)
R_{exp}, %	0.52	0.81		0.68	0.72	0.58
R1 (wR_2), %			5.56 (17.88)			
CCDC no.	2036322	2036317	2036318	2036321	2036319	2036320

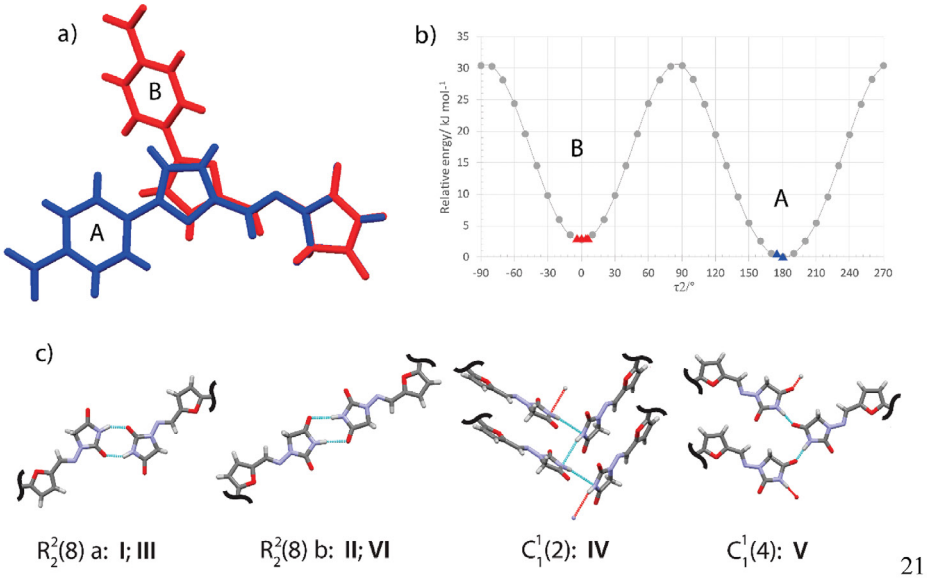

Figure 5. (a) Overlay of the two conformations in experimental dantrolene crystal structures, with **A** in blue and **B** in red. (b) PES scan of dantrolene with respect to torsion angle τ_2 with marked values observed in the experimental crystal structures of neat polymorphs. (c) Intermolecular H-bonded motifs observed in the experimental crystal structures of neat polymorphs.

polymorph III and the monohydrate MH-II were determined by SCXRD, whereas that of monohydrate MH-I and the rest of the neat polymorphs were successfully solved from PXRD data. Crystallographic data for neat polymorphs are given in Table 1 and for the hydrated phases in Table S2 in the Supporting Information, and Rietveld fits for all crystal structures solved from PXRD data are shown in Figures S3–S9, in the Supporting Information. The correctness of the structures calculated from the PXRD data was validated by the DFT-D geometry optimization of crystal structures, after which the RMSD with the experimental structures was always acceptable[61] (see Figures S10–S16 in the Supporting Information).

https://dx.doi.org/10.1021/acs.cgd.0c01508
Cryst. Growth Des. XXXX, XXX, XXX–XXX

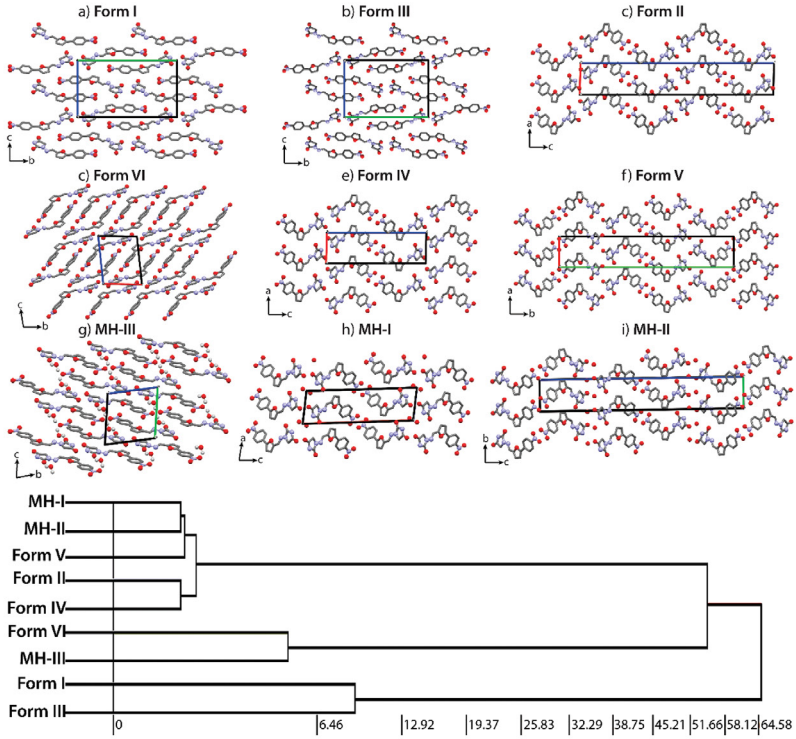

Figure 6. Visual and quantitative representation of packing similarities in dantrolene hydrates and neat polymorphs. The horizontal axis of the dendrogram corresponds to the PSab value (similarity).

Forms I and III crystallize in the centrosymmetric space group $P2_1/n$, and forms II and VI crystallize in the centrosymmetric space groups $P2_1/c$ and $P\bar{1}$, respectively, but forms IV and V crystallize in the noncentrosymmetric space groups $P2_1$ and $P2_12_12_1$, respectively. In all determined crystal structures $Z' = 1$. Two distinct molecular conformations are found in the experimental crystal structures. Dantrolene molecules in polymorphs I and III adopt global energy minimum conformations (conformation **A**), while molecules in crystal structures of the other polymorphs adopt local energy minimum conformations (conformation **B**), with the intramolecular energy (calculated in Gaussian and CASTEP) in experimental structures differing by ~3 kJ mol^{-1} (Figure 5a). The main difference between both conformations is a rotation of the central furyl group by 180° around the torsion angle τ_2.

The dantrolene molecule contains only one hydrogen bond donor site (N2−H group) and several sites that can act as potential hydrogen-bond acceptors (Figure 1). Nevertheless, in the experimental structures of the polymorphs three distinct hydrogen-bonding motifs formed by both strongest potential H-bond acceptors can be observed (Figure 5c): $R^2_2(8)$ *a* in forms I and III formed by N2−H10···O1 interactions, $R^2_2(8)$ *b* in forms II and VI formed by N2−H10···O2 interactions, and $C^1_1(4)$ in form V formed by N2−H10···O2 interactions. Meanwhile, form IV does not contain any conventional hydrogen bond, although motif $C^1_1(2)$ formed by weak a N2−H10···N2 interaction can be observed.

A comparison of the molecular packing of dantrolene neat polymorphs and monohydrates reveals that three distinct groups of related structures are present (Figure 6). In the first group there are the structurally related forms I and III, both sharing the same conformation, hydrogen-bonding pattern, and layers arranged along the *a* crystallographic axis. Meanwhile, the molecular packing along the other two axes is much more diverse, resulting in the lowest crystal packing similarity among the forms belonging to the same group. The second and largest group includes forms II, IV, and V and monohydrates MH-I and MH-II and has the highest crystal packing similarity. All of these structures contain the same 2D zigzag layers. In the third group containing MH-III and its respective dehydrate form VI, the main packing difference is due to the slightly different molecular conformation in form VI (nitrobenzene group rotated by ~30°), allowing dantrolene molecules to pack more closely than in MH-III and also allowing more efficient $\pi\cdots\pi$ interactions.

https://dx.doi.org/10.1021/acs.cgd.0c01508
Cryst. Growth Des. XXXX, XXX, XXX−XXX

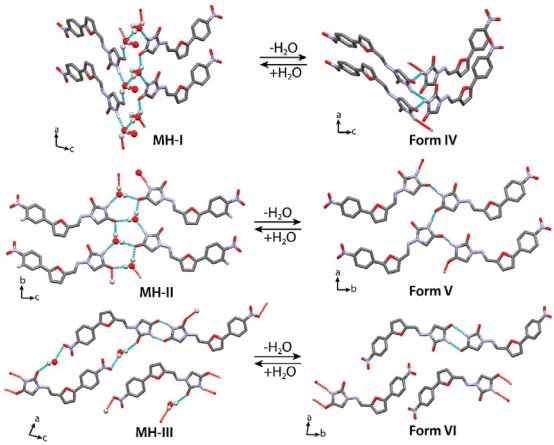

Figure 7. Visual comparation of the hydrogen bonding motifs of the experimental dantrolene monohydrates (MH-I–MH-III) and their respective dehydrates (forms IV–VI).

The water molecules in each of the monohydrates are incorporated differently (see Figure 7 and Figure S17 in the Supporting Information). In the structure of MH-I one water molecule is connected to two dantrolenes and two more neighboring water molecules via H bonds, creating a channel of water along the *b* axis. Although the presence of water channels often is characteristic of nonstoichiometric hydrates, MH-I is a stable stochiometric monohydrate (see Figure 4b) and it this most likely due to the strong interactions between dantrolene and water molecules (water is involved in the formation of three strong H bonds, see Figure 7 and Table S3). After the departure of water molecules from the structure the hydrogen bond network collapses and the unstable isomorphic dehydrate (form IV) without any conventional hydrogen bonds is obtained.

In the structure of MH-II water molecules are located in isolated pockets and are bonded only to dantrolene molecules via three hydrogen bonds (see Figure 7 and Table S3). During the dehydration molecules of dantrolene move closer together without any notable rearrangement in molecular packing by forming new, effective hydrogen bonds between dantrolene molecules, thus forming the relatively stable anhydrous form V. In the structure of MH-III water molecules are also located in isolated pockets but, in contrast to the other two monohydrates, water molecules are not a part of the main strong hydrogen-bond network in this structure but rather work as space fillers and provide a secondary hydrogen-bonding network by forming two hydrogen bonds (but note that these are rather weak hydrogen bonds; see Table S3). As a result, in the dehydration of this structure form VI with no significant differences in packing and hydrogen bonding is obtained. Nevertheless, the role of the water in MH-III is significant enough for this hydrate to be a very stable monohydrate (see Figure 4d), which could be explained by the relatively low stability of the respective anhydrate form VI (see below).

Crystal Structure Prediction. The predicted crystal energy landscape for dantrolene ($Z' = 1$) structures with two different conformations was calculated in CrystalPredictor and CrystalOptimizer (see in the Supporting Information) followed by reoptimization of most of the low-energy structures (138 $Z \leq 4$ structures) with the PBE-D2 computational approach. The same procedure (CrystalOptimizer + PBE-D2) was applied also for the six experimental structures of dantrolene polymorphs. The obtained crystal structure landscape is given in Figure 8 (the crystal structure

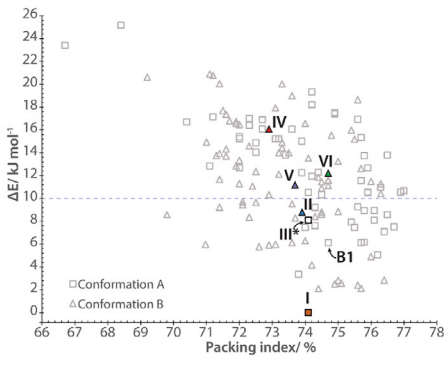

Figure 8. Crystal structure landscape of dantrolene, where each triangle and square represents a stable lattice energy minimum, generated in the CSP study after DFT-D geometry optimization. The identified experimental structures of polymorphs are colored and labeled. The landscape is complemented with the experimental structure of form III after an identical computational protocol. The horizontal dashed line designates the typical polymorph range of 10 kJ mol^{-1}.

https://dx.doi.org/10.1021/acs.cgd.0c01508
Cryst. Growth Des. XXXX, XXX, XXX–XXX

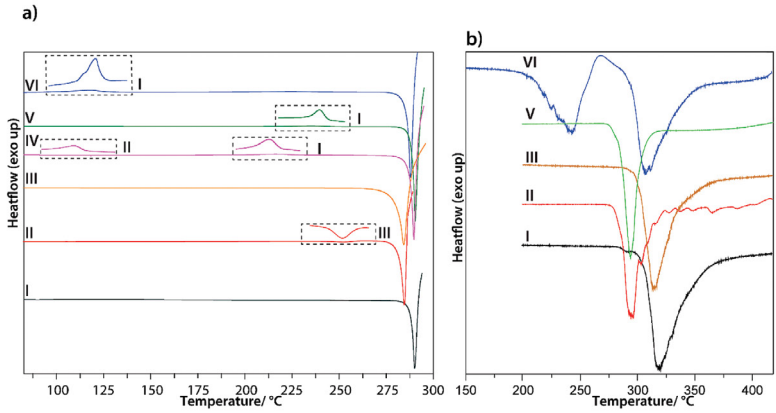

Figure 9. (a) DSC curves of dantrolene neat polymorphs (I–VI) recorded at a heating rate of 10 °C min^{-1}. (b) FSC curves of dantrolene neat polymorphs I–III, V, and VI recorded at a heating rate of 000 °C s^{-1}.

landscape including all structures after optimization in CrystalOptimizer is given in Figure S18 in the Supporting Information). This computational approach was successful in identifying five of the six experimental crystal structures of anhydrates by comparing $RMSD_{15}$ values between the experimental and the predicted structures. The geometry of the corresponding predicted structures of forms I, II, and IV–VI are in reasonably good agreement with the experimental structures ($RMSD_{15}$ < 0.35 Å), while form III is not present among the generated structures. Although in the crystal energy landscape there is a crystal structure (B1) with the same conformation and space group and similar lattice parameters and energy, it has a different hydrogen bonding pattern (B1 has $R^2_2(8)$ *b*, whereas form III has an $R^2_2(8)$ *a* hydrogen-bonding pattern, see Figure 5c), resulting in a quite high $RMSD_{15}$ value of 0.66 Å. The absence of form III among the predicted structures could possibly be because of a low-temperature phase transformation between the predicted structure B1 and form III, as a rearrangement of molecule layers would result in a different hydrogen-bonding motif. An existence of a plastic phase and reorganization of sufficiently weak hydrogen bonding for a molecule also containing the C(=O)NHC=O moiety have been reported previously.[62] Form I was determined to be the global minimum structure, and polymorphs II and III fall within the typical polymorph range[63] of 10 kJ mol^{-1}, while the structures that correspond to the dehydrate forms VI, V, and particularly form IV (note that no conventional hydrogen bond is present in form IV) had even higher energy.

The already mentioned $R^2_2(8)$ *b* is the most common (36%) H-bonding pattern in the top 47 computationally generated crystal structures (fitting in the typical polymorph range of 10 kJ mol^{-1}), while the second most common (30%) hydrogen-bonding pattern is $C^1_1(15)$ formed by a N2–H10···O5 interaction (see Figure S19 in the Supporting Information). Despite the common appearance of this hydrogen-bonding motif in the lowest energy predicted structures, it was not observed in any of the experimental structures. This could be a result of the overprediction of polymorphs or be caused by a potential scenario that structures containing such a hydrogen-bonding motif could be inaccessible because of notably slower nucleation in comparison to other structures.[34] It can also be added that in this study only crystallizations from solvent and desolvation in ambient pressure were covered, while notably different techniques likely to allow the preparation of structures containing notably different intermolecular interactions, e.g., crystallization from melt or in the presence of additives, were not explored. The hydrogen-bonding pattern $R^2_2(8)$ *a* as in polymorphs I and III is present only in 9% of the top 47 computationally generated crystal structures. An additional analysis of the difference between patterns $R^2_2(8)$ *a* and $R^2_2(8)$ *b* did not give a solid explanation for the preferential appearance of the second pattern in the computationally generated crystal structures, as the pairwise interaction energy between hydrogen-bonded dantrolene molecules (calculated using Crystal Explorer 17.5 at the B3LYP-D2/6-31G(d,p) level[64]) in forms I and III containing $R^2_2(8)$ *a* is in fact more negative (∼−59 kJ mol^{-1}) than that in II and B1 containing $R^2_2(8)$ *b* (∼−51 kJ mol^{-1}) (see Table S4). An analysis of the crystal structures of molecules containing a 2,4-imidazolidinedione ring (including all N1- and C3-substituted derivatives) deposited in the CSD revealed that both of these hydrogen-bonding patterns are observed with similar probability (42 hits for structures with $R^2_2(8)$ *a* and 45 hits for structures with $R^2_2(8)$ *b*).

Thermal and Thermodynamic Stability. Thermal properties of dantrolene polymorphs were examined by conventional and FDSC analysis. The conventional DSC traces of forms I and III show no thermal events (Figure 9a) prior to the melting/decomposition endotherm. Polymorph II displays an endothermic peak at about 250 °C attributed to a transition to form III as confirmed by a PXRD analysis. This substantiates the enantiotropic relationship between these polymorphs on the basis of the heat of transition rule. Polymorph IV shows an exothermic phase transition to form II at temperatures above 105 °C, which substantiates the monotropic relationship between these polymorphs on the basis of the heat of transition rule. Interestingly, if polymorph

https://dx.doi.org/10.1021/acs.cgd.0c01508
Cryst. Growth Des. XXXX, XXX, XXX–XXX

II is obtained from polymorph IV in the solid-state transition, then an exothermic phase transition to form I is observed in the DSC traces, not the endothermic phase transition to form III as observed for form II obtained in the crystallization. This may be related to the fact that more crystalline form II is obtained in the crystallization, as confirmed by the PXRD analysis (see Figure S20 in the Supporting Information). Also, polymorphs V and VI show an exothermic phase transition prior to the melting/decomposition event, with both forms transforming to polymorph I at about 235 and 115 °C, respectively, and thus being monotropically related to form I.

As demonstrated in Figures S21 and S22 in the Supporting Information, melting of polymorphs I and III is accompanied by degradation and there is a shift of the onset by using different heating rates, implying that part of the endothermic peak corresponds to decomposition. In order to avoid the degradation upon melting and to overcome the phase transitions before the melting, FSC at a high scanning rate (2000 °C s^{-1}) was used for polymorphs I–III, V, and VI (see Figure 9b). In an FSC experiment, the sample is usually premelted to ensure uniform thermal contact between the sample and the chip. However, premelting is impossible when the properties of the polymorphs are researched, as the fusion process is irreversible for all but the most stable polymorph. The FSC data for polymorphs thus were gathered by averaging results from different (at least four) individual samples of each polymorph. A melting point of 294 ± 1 °C was recoded for form I, 281 ± 3 °C for form II, 292 ± 2 °C for form III, 279 ± 3 °C for form V, and 196 ± 6 °C for form VI. As can be seen, form VI is the only polymorph with a significantly lower melting point (80–100 °C) and a recrystallization, most likely to form I, after the melting. Unfortunately, FSC does not allow a straightforward quantitative determination of the melting enthalpy, since it is not possible to determine the sample mass. However, the sample mass can be calculated by the ratio of the absolute heat capacity of the sample on the chip obtained from the reference scans and the specific heat capacity of crystalline dantrolene independently determined by conventional DSC.[65,66] Using this approach, the melting enthalpy of form I has been estimated as 79 ± 2 kJ mol^{-1}, 71 ± 2 kJ mol^{-1} for form II, 73 ± 6 kJ mol^{-1} for form III, and 84 ± 4 kJ mol^{-1} for polymorph V. Unfortunately, the calculated heat of fusion values have too large an uncertainty for complete characterization of the thermodynamic relationships among all polymorphs and the largest enthalpy of fusion for polymorph V contradicts the results from conventional DSC. The fusion enthalpy of form V, however, might be overestimated due to the notably different shapes of the melting peaks. Also, the exothermic transition from form V to from I is a reflection of the relative enthalpies of both forms at the temperature of the transition. Thus, the difference between fusion enthalpies may change due to a temperature variation of the respective enthalpies.[67] Nevertheless, this information is sufficient to conclude that polymorphic pairs II/I and III/I are monotropically related on the basis of the heat of fusion rule, which also means that form IV has a monotropic relation to form I.

To verify the results from DSC and FSC measurements and to determine the thermodynamic transition temperature of polymorphs II and III, polythermal solubility determination experiments in cyclohexanone and pentanol-1 using a Crystal16 parallel reactor system were performed. Polymorphs IV and VI were too unstable for solubility measurements, as solvent-mediated phase transformations were faster than the dissolution. Form IV transformed to polymorph II and form VI transformed to polymorph I during the solubility measurements. Also, above 45 °C the solvent-mediated phase transition of polymorph V to polymorph II occurred before the complete dissolution. As shown in Figure 10 and Figure S23, in the Supporting Information, the solubility of form I is lower than those of forms II and III in the investigated temperature range (10–140 °C for cyclohexanone and 90–130 °C for *n*-pentanol), additionally confirming that form I is the most thermodynamically stable polymorph. The intersection of solubility curves of forms II and III confirmed the enantiotropic relationship between these polymorphs with the transition point of these polymorphs lying between 105 and 110 °C. Unfortunately, solvent-mediated phase transformation experiments to more precisely determine the thermodynamic transition temperatures of this polymorph pair failed, as a transition to form I was preferred over the transformation between both polymorphs in the corresponding temperature range. An additional intersection of solubility curves was observed at about 15–20 °C as the solubility of form V became lower than the solubility of polymorph III, indicating that polymorph V is more stable at lower temperature than polymorph III. This transition point also explains the lower (more negative) lattice energy of form V.

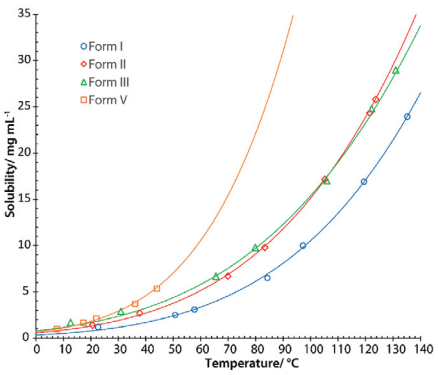

Figure 10. Temperature dependent solubility curves (mg mL^{-1}) of dantrolene polymorphs I–III and V in cyclohexanone.

The experimental thermodynamic stability order was complemented by calculations of lattice energy values using different periodic DFT-D methods. Figure 11 shows that the energy ranking with various dispersion correction methods is consistent, while the intermolecular potential method used in the CrystalOptimizer misranks polymorph III as the most stable (lowest energy) polymorph instead of polymorph I, as determined by other approaches.

The results from DSC, FDC, solubility measurements, and lattice energy calculations can be summarized by concluding that the order of the thermodynamic stability of dantrolene polymorphs at ambient temperature is I > II > III > V > VI > IV, while because of the enantiotropic polymorph pairs of III and V as well as II and III this order is different below 15 °C and above 110 °C.

https://dx.doi.org/10.1021/acs.cgd.0c01508
Cryst. Growth Des. XXXX, XXX, XXX–XXX

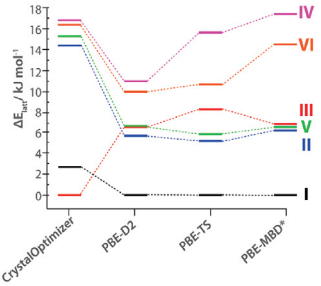

Figure 11. Relative energy ranking of the dantronele polymorphs using different periodic DFT+D methods in comparison to the ranking obtained using CrystalOptimizer.

CONCLUSIONS

Dantrolene represents yet another interesting example of abundant molecular crystal polymorphism existing in at least six different neat polymorphs, three of which can be obtained via crystallization (I–III) and an additional three (IV–VI) via solid-state dehydration from three different monohydrates (MH-I–MH-III). Thermodynamic stabilities and interrelationships among all neat polymorphs have been successfully clarified by combining various experimental and computational techniques. The results confirmed that form I is the most thermodynamically stable polymorph, while polymorphic pairs II/III and V/III are enantiotropically related. Structural aspects of the formation of the highly polymorphic system have been rationalized by analyzing experimental crystal structures as well as computationally generated structures of neat polymorphs. The main reasons appear to be at least two energetically favorable conformations and the possibility to form different hydrogen bonds as well as the stability of the remaining host framework after withdrawal of water molecules from the monohydrate structures.

ASSOCIATED CONTENT

Supporting Information

The Supporting Information is available free of charge at https://pubs.acs.org/doi/10.1021/acs.cgd.0c01508.

Results of solvate screening, PXRD patterns of solvates and desolvates, crystallographic information on monohydrates, Rietveld fit for structures calculated from PXRD, overlay of crystal structures calculated from PXRD data, and crystal structures after DFT optimization, comparisons of packing and hydrogen bonds between monohydrates and dehydrated phases, crystal structure landscape generated in the CSP study, PXRD patterns of dantrolene form II, DSC curves of forms I and III, and solubility curves of I–III in *n*-pentanol (PDF)

Accession Codes

CCDC 2036317–2036325 contain the supplementary crystallographic data for this paper. These data can be obtained free of charge via www.ccdc.cam.ac.uk/data_request/cif, or by emailing data_request@ccdc.cam.ac.uk, or by contacting The Cambridge Crystallographic Data Centre, 12 Union Road, Cambridge CB2 1EZ, UK; fax: +44 1223 336033.

AUTHOR INFORMATION

Corresponding Author

Artis Kons – *Faculty of Chemistry, University of Latvia, Riga LV-1004, Latvia;* orcid.org/0000-0002-4055-8442; Phone: +(371)-67033903; Email: artis.kons@lu.lv

Authors

Anatoly Mishnev – *Latvian Institute of Organic Synthesis, Riga LV-1006, Latvia*

Timur A. Mukhametzyanov – *Department of Physical Chemistry, Kazan Federal University, 420008 Kazan, Russia*

Alexey V. Buzyurov – *Department of Physical Chemistry, Kazan Federal University, 420008 Kazan, Russia*

Semen E. Lapuk – *Department of Physical Chemistry, Kazan Federal University, 420008 Kazan, Russia*

Agris Bērziņš – *Faculty of Chemistry, University of Latvia, Riga LV-1004, Latvia;* orcid.org/0000-0002-4149-8971

Complete contact information is available at: https://pubs.acs.org/10.1021/acs.cgd.0c01508

Funding

This work has been funded by the Latvian Council of Science, project "Crystal engineering of pharmaceutical multicomponent phases for more efficient crystalline phase design", project No. lzp-2018/1–0312 (A.K., A.B.), the University of Latvia Foundation through the SIA "Mikrotikls" supported project "Development of integrated experimental and computer modeling research methodology for prediction of the properties and diversity of phases of active pharmaceutical solids" (A.K.), and the Ministry of Education and Science of the Russian Federation, grant 14.726.31.0019 (T.A.M., A.V.B., S.E.L.)

Notes

The authors declare no competing financial interest.

ACKNOWLEDGMENTS

The crystal structure prediction work was carried out at UCL in the laboratory of Prof. Sally Price using the CSP computational infrastructure developed under EPSRC EP/K039229/1. We thank Professors Adjiman and Pantelides (Imperial College) for the use of CrystalPredictor and CrystalOptimizer and Prof. Sally Price and Dr. Louise Price for an introduction with the background and practical aspects of crystal structure prediction and helpful comments on the manuscript.

REFERENCES

(1) Cruz-Cabeza, A. J.; Feeder, N.; Davey, R. J. Open Questions in Organic Crystal Polymorphism. *Commun. Chem.* **2020**, *3*, 10–13.

(2) Campeta, A. M.; Chekal, B. P.; Abramov, Y. A.; Meenan, P. A.; Henson, M. J.; Shi, B.; Singer, R. A.; Horspool, K. R. Development of a Targeted Polymorph Screening Approach for a Complex Polymorphic and Highly Solvating API. *J. Pharm. Sci.* **2010**, *99*, 3874–3886.

(3) Bhardwaj, R. M.; Price, L. S.; Price, S. L.; Reutzel-Edens, S. M.; Miller, G. J.; Oswald, I. D. H.; Johnston, B. F.; Florence, A. J. Exploring the Experimental and Computed Crystal Energy Landscape of Olanzapine. *Cryst. Growth Des.* **2013**, *13*, 1602–1617.

(4) Bingham, A. L.; Hughes, D. S.; Hursthouse, M. B.; Lancaster, R. W.; Tavener, S.; Threlfall, T. L. Over One Hundred Solvates of Sulfathiazole. *Chem. Commun.* **2001**, *7*, 603–604.

(5) Yu, L.; Stephenson, G. A.; Mitchell, C. A.; Bunnell, C. A.; Snorek, S. V.; Bowyer, J. J.; Borchardt, T. B.; Stowell, J. G.; Byrn, S. R.

Thermochemistry and Conformational Polymorphism of a Hexamorphic Crystal System. *J. Am. Chem. Soc.* **2000**, *122*, 585−591.
(6) Chen, S.; Guzei, I. A.; Yu, L. New Polymorphs of ROY and New Record for Coexisting Polymorphs of Solved Structures. *J. Am. Chem. Soc.* **2005**, *127*, 9881−9885.
(7) Yu, L. Polymorphism in Molecular Solids: An Extraordinary System of Red, Orange, and Yellow Crystals. *Acc. Chem. Res.* **2010**, *43*, 1257−1266.
(8) Tyler, A. R.; Ragbirsingh, R.; McMonagle, C. J.; Waddell, P. G.; Heaps, S. E.; Steed, J. W.; Thaw, P.; Hall, M. J.; Probert, M. R. Encapsulated Nanodroplet Crystallization of Organic-Soluble Small Molecules. *Chem.* **2020**, *6*, 1755−1765.
(9) Lévesque, A.; Maris, T.; Wuest, J. D. ROY Reclaims Its Crown: New Ways To Increase Polymorphic Diversity. *J. Am. Chem. Soc.* **2020**, *142*, 11873−11883.
(10) Li, X.; Ou, X.; Rong, H.; Huang, S.; Nyman, J.; Yu, L.; Lu, M. The Twelfth Solved Structure of ROY: Single Crystals of Y04 Grown from Melt Microdroplets. *Cryst. Growth Des.* **2020**, *20*, 7093−7097.
(11) Bobrovs, R.; Kons, A.; Bērziņš, A.; Rekis, T.; Actiņš, A. Formation and Transformations of Organic Salt Hydrates: Four Encenicline Hydrochloride Monohydrates and Respective Isostructural Desolvates. *Cryst. Growth Des.* **2018**, *18*, 2100−2111.
(12) Kons, A.; Bērziņš, A.; Actiņš, A.; Rekis, T.; van Smaalen, S.; Mishnev, A. Polymorphism of R-Encenicline Hydrochloride: Access to the Highest Number of Structurally Characterized Polymorphs Using Desolvation of Various Solvates. *Cryst. Growth Des.* **2019**, *19*, 4765−4773.
(13) Bhardwaj, R. M.; McMahon, J. A.; Nyman, J.; Price, L. S.; Konar, S.; Oswald, I. D. H.; Pulham, C. R.; Price, S. L.; Reutzel-Edens, S. M. A Prolific Solvate Former, Galunisertib, under the Pressure of Crystal Structure Prediction, Produces Ten Diverse Polymorphs. *J. Am. Chem. Soc.* **2019**, *141*, 13887−13897.
(14) Zeidan, T. A.; Trotta, J. T.; Tilak, P. A.; Oliveira, M. A.; Chiarella, R. A.; Foxman, B. M.; Almarsson, Ö; Hickey, M. B. An Unprecedented Case of Dodecamorphism: The Twelfth Polymorph of Aripiprazole Formed by Seeding with Its Active Metabolite. *CrystEngComm* **2016**, *18*, 1486−1488.
(15) Nanubolu, J. B.; Sridhar, B.; Babu, V. S. P.; Jagadeesh, B.; Ravikumar, K. Sixth Polymorph of Aripiprazole - an Antipsychotic Drug. *CrystEngComm* **2012**, *14*, 4677.
(16) Tessler, L.; Goldberg, I. Crystal Structures of Aripiprazole, a New Anti-Psychotic Drug, and of Its Inclusion Compounds with Methanol, Ethanol and Water. *J. Inclusion Phenom. Mol. Recognit. Chem.* **2006**, *55*, 255−261.
(17) Li, X.; Ou, X.; Wang, B.; Rong, H.; Wang, B.; Chang, C.; Shi, B.; Yu, L.; Lu, M. Rich Polymorphism in Nicotinamide Revealed by Melt Crystallization and Crystal Structure Prediction. *Commun. Chem.* **2020**, *3*, 152.
(18) López-Mejías, V.; Kampf, J. W.; Matzger, A. J. Nonamorphism in Flufenamic Acid and a New Record for a Polymorphic Compound with Solved Structures. *J. Am. Chem. Soc.* **2012**, *134*, 9872−9875.
(19) López-Mejías, V.; Kampf, J. W.; Matzger, A. J. Polymer-Induced Heteronucleation of Tolfenamic Acid: Structural Investigation of a Pentamorph. *J. Am. Chem. Soc.* **2009**, *131*, 4554−4555.
(20) Case, D. H.; Srirambhatla, V. K.; Guo, R.; Watson, R. E.; Price, L. S.; Polyzois, H.; Cockcroft, J. K.; Florence, A. J.; Tocher, D. A.; Price, S. L. Successful Computationally Directed Templating of Metastable Pharmaceutical Polymorphs. *Cryst. Growth Des.* **2018**, *18*, 5322−5331.
(21) Williams, P. A.; Hughes, C. E.; Lim, G. K.; Kariuki, B. M.; Harris, K. D. M. Discovery of a New System Exhibiting Abundant Polymorphism: M -Aminobenzoic Acid. *Cryst. Growth Des.* **2012**, *12*, 3104−3113.
(22) Braun, D. E.; Gelbrich, T.; Kahlenberg, V.; Tessadri, R.; Wieser, J.; Griesser, U. J. Stability of Solvates and Packing Systematics of Nine Crystal Forms of the Antipsychotic Drug Aripiprazole. *Cryst. Growth Des.* **2009**, *9*, 1054−1065.
(23) Bērziņš, A.; Skarbulis, E.; Actiņš, A. Structural Characterization and Rationalization of Formation, Stability, and Transformations of Benperidol Solvates. *Cryst. Growth Des.* **2015**, *15*, 2337−2351.
(24) Kons, A.; Bērziņš, A.; Actiņš, A. Polymorphs and Hydrates of Sequifenadine Hydrochloride: Crystallographic Explanation of Observed Phase Transitions and Thermodynamic Stability. *Cryst. Growth Des.* **2017**, *17*, 1146−1158.
(25) Kons, A.; Rutkovska, L.; Bērziņš, A.; Bobrovs, R.; Actiņš, A. Three Anhydrous Forms and a Dihydrate Form of Quifenadine Hydrochloride: A Structural Study of the Thermodynamic Stability and Dehydration Mechanism. *CrystEngComm* **2015**, *17*, 3627−3635.
(26) Minkov, V. S.; Beloborodova, A. A.; Drebushchak, V. A.; Boldyreva, E. V. Furosemide Solvates: Can They Serve As Precursors to Different Polymorphs of Furosemide? *Cryst. Growth Des.* **2014**, *14*, 513−522.
(27) Watts, A. E.; Maruyoshi, K.; Hughes, C. E.; Brown, S. P.; Harris, K. D. M. Combining the Advantages of Powder X-Ray Diffraction and NMR Crystallography in Structure Determination of the Pharmaceutical Material Cimetidine Hydrochloride. *Cryst. Growth Des.* **2016**, *16*, 1798−1804.
(28) Hughes, C. E.; Boughdiri, I.; Bouakkaz, C.; Williams, P. A.; Harris, K. D. M. Elucidating the Crystal Structure of Dl-Arginine by Combined Powder X-Ray Diffraction Data Analysis and Periodic DFT-D Calculations. *Cryst. Growth Des.* **2018**, *18*, 42−46.
(29) Eddleston, M. D.; Hejczyk, K. E.; Bithell, E. G.; Day, G. M.; Jones, W. Determination of the Crystal Structure of a New Polymorph of Theophylline. *Chem. - Eur. J.* **2013**, *19*, 7883−7888.
(30) Van Genderen, E.; Clabbers, M. T. B.; Das, P. P.; Stewart, A.; Nederlof, I.; Barentsen, K. C.; Portillo, Q.; Pannu, N. S.; Nicolopoulos, S.; Gruene, T.; et al. Ab Initio Structure Determination of Nanocrystals of Organic Pharmaceutical Compounds by Electron Diffraction at Room Temperature Using a Timepix Quantum Area Direct Electron Detector. *Acta Crystallogr., Sect. A: Found. Adv.* **2016**, *72*, 236−242.
(31) Braun, D. E.; Vickers, M.; Griesser, U. J. Dapsone Form V: A Late Appearing Thermodynamic Polymorph of a Pharmaceutical. *Mol. Pharmaceutics* **2019**, *16*, 3221−3236.
(32) Price, S. L.; Reutzel-Edens, S. M. The Potential of Computed Crystal Energy Landscapes to Aid Solid-Form Development. *Drug Discovery Today* **2016**, *21*, 912−923.
(33) Braun, D. E.; Lingireddy, S. R.; Beidelschies, M. D.; Guo, R.; Müller, P.; Price, S. L.; Reutzel-Edens, S. M. Unraveling Complexity in the Solid Form Screening of a Pharmaceutical Salt: Why so Many Forms? Why so Few? *Cryst. Growth Des.* **2017**, *17*, 5349−5365.
(34) Price, S. L. Why Don't We Find More Polymorphs? *Acta Crystallogr., Sect. B: Struct. Sci., Cryst. Eng. Mater.* **2013**, *69*, 313−328.
(35) Price, S. L. Is Zeroth Order Crystal Structure Prediction (CSP_0) Coming to Maturity? What Should We Aim for in an Ideal Crystal Structure Prediction Code? *Faraday Discuss.* **2018**, *211*, 9−30.
(36) Krause, T.; Gerbershagen, M. U.; Fiege, M.; Weißhorn, R.; Wappler, F. Dantrolene ? A Review of Its Pharmacology, Therapeutic Use and New Developments. *Anaesthesia* **2004**, *59*, 364−373.
(37) Tanaka, R.; Akimoto, T.; Haramura, M.; Tanaka, A.; Hirayama, N. Structure of Dantrolene. *Anal. Sci.: X-Ray Struct. Anal. Online* **2004**, *20*, x97−x98.
(38) Altomare, A.; Cuocci, C.; Giacovazzo, C.; Moliterni, A.; Rizzi, R.; Corriero, N.; Falcicchio, A. EXPO2013: A Kit of Tools for Phasing Crystal Structures from Powder Data. *J. Appl. Crystallogr.* **2013**, *46*, 1231−1235.
(39) Altomare, A.; Campi, G.; Cuocci, C.; Eriksson, L.; Giacovazzo, C.; Moliterni, A.; Rizzi, R.; Werner, P.-E. Advances in Powder Diffraction Pattern Indexing: N-TREOR09. *J. Appl. Crystallogr.* **2009**, *42*, 768−775.
(40) Boultif, A.; Louër, D. Powder Pattern Indexing with the Dichotomy Method. *J. Appl. Crystallogr.* **2004**, *37*, 724−731.
(41) Wahl, H.; Haynes, D. a; le Roex, T. Porous Salts Based on the Pamoate Ion. *Chem. Commun. (Cambridge, U. K.)* **2012**, *48*, 1775−1777.

https://dx.doi.org/10.1021/acs.cgd.0c01508
Cryst. Growth Des. XXXX, XXX, XXX−XXX

(42) Le Bail, A.; Duroy, H.; Fourquet, J. L. Ab-Initio Structure Determination of LiSbWO6 by X-Ray Powder Diffraction. *Mater. Res. Bull.* **1988**, *23*, 447−452.
(43) Coelho, A. A.; Kern, A. Indexing of Powder Diffraction Patterns by Iterative Use of Singular Value Decomposition. *Acta Crystallogr., Sect. A: Found. Crystallogr.* **2002**, *58*, c227.
(44) Sheldrick, G. M. Crystal Structure Refinement with SHELXL. *Acta Crystallogr., Sect. C: Struct. Chem.* **2015**, *71*, 3−8.
(45) Van Eijck, B. P.; et al. Ab Initio Crystal Structure Predictions for Flexible Hydrogen-Bonded Molecules. Part II. Accurate Energy Minimization. *J. Comput. Chem.* **2001**, *22*, 805−815.
(46) Frisch, M. J.; Trucks, G. W.; Schlegel, H. B.; Scuseria, G. E.; Robb, M. A.; Cheeseman, J. R.; Scalmani, G.; Barone, V.; Mennucci, B.; Petersson, G. A.; Nakatsuji, H.; Caricato, M.; Li, X.; Hratchian, H. P.; Izmaylov, A. F.; Bloino, J.; Zheng, G.; Sonnenberg, J. L.; Hada, M.; Ehara, M.; Toyota, K.; Fukuda, R.; Hasegawa, J.; Ishida, M.; Nakajima, T.; Honda, Y.; Kitao, O.; Nakai, H.; Vreven, T.; Montgomery, J. A., Jr.; Peralta, J. E.; Ogliaro, F.; Bearpark, M.; Heyd, J. J.; Brothers, E.; Kudin, K. N.; Staroverov, V. N.; Kobayashi, R.; Normand, J.; Raghavachari, K.; Rendell, A.; Burant, J. C.; Iyengar, S. S.; Tomasi, J.; Cossi, M.; Rega, N.; Millam, J. M.; Klene, M.; Knox, J. E.; Cross, J. B.; Bakken, V.; Adamo, C.; Jaramillo, J.; Gomperts, R.; Stratmann, R. E.; Yazyev, O.; Austin, A. J.; Cammi, R.; Pomelli, C.; Ochterski, J. W.; Martin, R. L.; Morokuma, K.; Zakrzewski, V. G.; Voth, G. A.; Salvador, P.; Dannenberg, J. J.; Dapprich, S.; Daniels, A. D.; Farkas, O.; Foresman, J. B.; Ortiz, J. V.; Cioslowski, J.; Fox, D. J. *Gaussian 09, Revision D.01*; Gaussian Inc.: Wallingford, CT, 2009.
(47) Coombes, D. S.; Price, S. L.; Willock, D. J.; Leslie, M. Role of Electrostatic Interactions in Determining the Crystal Structures of Polar Organic Molecules. A Distributed Multipole Study. *J. Phys. Chem.* **1996**, *100*, 7352−7360.
(48) Price, S. L.; Leslie, M.; Welch, G. W. A.; Habgood, M.; Price, L. S.; Karamertzanis, P. G.; Day, G. M. Modelling Organic Crystal Structures Using Distributed Multipole and Polarizability-Based Model Intermolecular Potentials. *Phys. Chem. Chem. Phys.* **2010**, *12*, 8478−8490.
(49) Stone, A. J. Distributed Multipole Analysis: Stability for Large Basis Sets. *J. Chem. Theory Comput.* **2005**, *1*, 1128−1132.
(50) Kazantsev, A. V.; Karamertzanis, P. G.; Adjiman, C. S.; Pantelides, C. C. Efficient Handling of Molecular Flexibility in Lattice Energy Minimization of Organic Crystals. *J. Chem. Theory Comput.* **2011**, *7*, 1998−2016.
(51) Clark, S. J.; Segall, M. D.; Pickard, C. J.; Hasnip, P. J.; Probert, M. I. J.; Refson, K.; Payne, M. C. First Principles Methods Using CASTEP. *Z. Kristallogr. - Cryst. Mater.* **2005**, *220*, 567−570.
(52) Perdew, J. P.; Burke, K.; Ernzerhof, M. Generalized Gradient Approximation Made Simple. *Phys. Rev. Lett.* **1996**, *77*, 3865−3868.
(53) Vanderbilt, D. Soft Self-Consistent Pseudopotentials in a Generalized Eigenvalue Formalism. *Phys. Rev. B: Condens. Matter Mater. Phys.* **1990**, *41*, 7892−7895.
(54) Grimme, S. Semiempirical GGA-Type Density Functional Constructed with a Long-Range Dispersion Correction. *J. Comput. Chem.* **2006**, *27*, 1787−1799.
(55) Tkatchenko, A.; Scheffler, M. Accurate Molecular van Der Waals Interactions from Ground-State Electron Density and Free-Atom Reference Data. *Phys. Rev. Lett.* **2009**, *102*, 6−9.
(56) Tkatchenko, A.; DiStasio, R. A.; Car, R.; Scheffler, M. Accurate and Efficient Method for Many-Body van Der Waals Interactions. *Phys. Rev. Lett.* **2012**, *108*, 236402.
(57) Macrae, C. F.; Bruno, I. J.; Chisholm, J. A.; Edgington, P. R.; McCabe, P.; Pidcock, E.; Rodriguez-Monge, L.; Taylor, R.; van de Streek, J.; Wood, P. A.; et al. Mercury CSD 2.0 − New Features for the Visualization and Investigation of Crystal Structures. *J. Appl. Crystallogr.* **2008**, *41*, 466−470.
(58) Macrae, C. F.; Sovago, I.; Cottrell, S. J.; Galek, P. T. A.; McCabe, P.; Pidcock, E.; Platings, M.; Shields, G. P.; Stevens, J. S.; Towler, M.; et al. Mercury 4.0: From Visualization to Analysis, Design and Prediction. *J. Appl. Crystallogr.* **2020**, *53*, 226−235.
(59) Rohlíček, J.; Skořepová, E.; Babor, M.; Čejka, J. CrystalCMP: An Easy-to-Use Tool for Fast Comparison of Molecular Packing. *J. Appl. Crystallogr.* **2016**, *49*, 2172−2183.
(60) Spek, A. L. Structure Validation in Chemical Crystallography. *Acta Crystallogr., Sect. D: Biol. Crystallogr.* **2009**, *65*, 148−155.
(61) Reutzel-Edens, S. M.; Braun, D. E.; Newman, A. W. Hygroscopicity and Hydrates in Pharmaceutical Solids. In *Polymorphism in the Pharmaceutical Industry: Solid Form and Drug Development*; Hilfiker, R., Von Raumer, M., Eds.; Wiley-VCH: 2018; Vol. 2.
(62) van de Streek, J.; Neumann, M. A. Validation of Molecular Crystal Structures from Powder Diffraction Data with Dispersion-Corrected Density Functional Theory (DFT-D). *Acta Crystallogr., Sect. B: Struct. Sci., Cryst. Eng. Mater.* **2014**, *70*, 1020−1032.
(63) Hulme, A. T.; Johnston, A.; Florence, A. J.; Fernandes, P.; Shankland, K.; Bedford, C. T.; Welch, G. W. A.; Sadiq, G.; Haynes, D. A.; Motherwell, W. D. S.; et al. Search for a Predicted Hydrogen Bonding Motif − A Multidisciplinary Investigation into the Polymorphism of 3-Azabicyclo[3.3.1]Nonane-2,4-Dione. *J. Am. Chem. Soc.* **2007**, *129*, 3649−3657.
(64) Cruz-Cabeza, A. J.; Reutzel-Edens, S. M.; Bernstein, J. Facts and Fictions about Polymorphism. *Chem. Soc. Rev.* **2015**, *44*, 8619−8635.
(65) Cebe, P.; Thomas, D.; Merfeld, J.; Partlow, B. P.; Kaplan, D. L.; Alamo, R. G.; Wurm, A.; Zhuravlev, E.; Schick, C. Heat of Fusion of Polymer Crystals by Fast Scanning Calorimetry. *Polymer* **2017**, *126*, 240−247.
(66) Abdelaziz, A.; Zaitsau, D. H.; Mukhametzyanov, T. A.; Solomonov, B. N.; Cebe, P.; Verevkin, S. P.; Schick, C. Melting Temperature and Heat of Fusion of Cytosine Revealed from Fast Scanning Calorimetry. *Thermochim. Acta* **2017**, *657*, 47−55.
(67) Yagofarov, M. I.; Nagrimanov, R. N.; Solomonov, B. N. New Aspects in the Thermochemistry of Solid-Liquid Phase Transitions of Organic Non-Electrolytes. *J. Mol. Liq.* **2018**, *256*, 58−66.

https://dx.doi.org/10.1021/acs.cgd.0c01508
Cryst. Growth Des. XXXX, XXX, XXX−XXX

II

Kons, A., Bērziņš, A., Actiņš, A., Rekis, T., van Smaalen, S., Mishnev, A.

POLYMORPHISM OF R-ENCENICLINE HYDROCHLORIDE: ACCESS TO THE HIGHEST NUMBER OF STRUCTURALLY CHARACTERIZED POLYMORPHS USING DESOLVATION OF VARIOUS SOLVATES

Cryst. Growth Des. **2019**, 19, 4765–4773

CRYSTAL GROWTH & DESIGN

Article

Cite This: Cryst. Growth Des. 2019, 19, 4765−4773

pubs.acs.org/crystal

Polymorphism of R-Encenicline Hydrochloride: Access to the Highest Number of Structurally Characterized Polymorphs Using Desolvation of Various Solvates

Artis Kons,*[,†] Agris Bērziņš,[†] Andris Actiņš,[†] Toms Rekis,[‡] Sander van Smaalen,[‡] and Anatoly Mishnev[§]

[†]Faculty of Chemistry, University of Latvia, Jelgavas iela 1, Riga, LV-1004, Latvia

[‡]Laboratory of Crystallography, University of Bayreuth, 95440 Bayreuth, Germany

[§]Latvian Institute of Organic Synthesis, 21 Aizkraukles Street, Riga, LV-1006, Latvia

Supporting Information

ABSTRACT: In a study of the solid form landscape of R-encenicline hydrochloride (Enc-HCl), it was found that this compound is dodecamorphic and presents the first published example of polymorphism with a record-breaking 10 solved crystal structures. In addition to the four known polymorphs, eighth new polymorphs and their precursor solvates as well as several new hydrates have been characterized. The polymorph formation behavior is investigated by analyzing crystal structures of polymorphs and solvates used in their preparation. Molecular packing in crystal structures of the polymorphs is highly similar to that in the precursor solvates, whereas conformations in all structures are nearly identical and correspond to the same energy minimum.

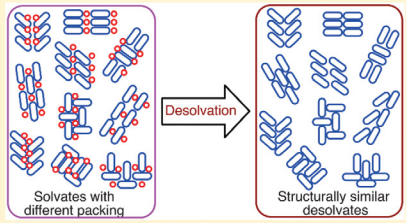

INTRODUCTION

Exploring the solid-state landscape of pharmaceuticals has become an essential part of drug development as different crystal forms have different stabilities,[1] mechanical properties,[2,3] and bioavailabilities.[4] Moreover, the relationships between these solid phases also must be established to ensure the correct choice of a given phase including polymorphs[5] and solvates/hydrates.[6]

The complexity of the solid form landscape can be very different, as 10 or more polymorphs and, moreover, dozens[7,8] or even more than 100 solvates[9] can be formed by a particular compound. Currently the most abundant polymorphic systems are aripiprazole and ROY, both having 12 reported polymorphs, nine of which are structurally characterized.[1,10−13] The closest follower, flufenamic acid, has seven polymorphs with determined structures.[14] The formation of such a large number of different structures for these compounds is achieved by different possible packings of several notably different conformers. Meanwhile, to the best of our knowledge, the highest number of structurally characterized polymorphs among organic salts belongs to 1,4-diazabicyclo[2.2.2]octane hydroiodide (dabcoHI), which has six ambient pressure polymorphs, with four additional polymorphs obtained under pressure,[15] differing mainly with the arrangement of the chains of cations and iodide anions. Moreover, according to the Cambridge Structural Database,[16] molecular solids with four or more polymorphs with determined structures are very rare.

A high tendency to form solvates can limit the possible routes for preparation of unsolvated phase(s). However, particularly stable solvates, typically but not exclusively hydrates, can be used as the marketed form. Meanwhile the desolvation processes can be applied to discover and prepare new polymorphic forms that might have been previously inaccessible via conventional crystallization techniques.[17−19] Although preparation of new polymorphs via desolvation is quite common,[20] crystal structures of these phases often remain unknown, as single crystals of such phases cannot be prepared. However, the determination of crystal structure is an important part of understanding the physicochemical properties of crystalline materials. Recently, structure determination from powder diffraction has been successfully employed as the closest alternative to the general method of choice, single crystal X-ray diffraction, particularly in cases when single crystals of suitable size and quality are impossible to grow or solids can be obtained only as microcrystalline powders, including those prepared by solid-state desolvation processes.[21−23]

Here, we report a structural and experimental study of polymorphs of encenicline hydrochloride (Figure 1), a partial, selective agonist of the α-7 nicotinic acetylcholine receptor

Received: May 20, 2019
Revised: July 3, 2019
Published: July 9, 2019

DOI: 10.1021/acs.cgd.9b00648
Cryst. Growth Des. 2019, 19, 4765−4773

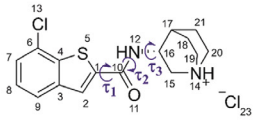

Figure 1. Chemical structure of encenicline hydrochloride.

which was developed for the treatment of cognitive deficits in schizophrenia and Alzheimer's disease. In solid form screening, numerous solvates have been obtained, and their desolvation produced eight polymorphs of R-encenicline hydrochloride (Enc-HCl). For seven of them, crystal structures were determined. Together with the previously discovered and described four polymorphs of Enc-HCl, this increases the number of neat polymorphs of this compound to 12, with 10 of these forms having the crystal structure solved, which allows this compound to break a record for the highest number of structurally characterized polymorphs.

■ EXPERIMENTAL SECTION

Materials. R-Encenicline hydrochloride (purity >99%) was obtained from JSC Olainfarm (Olaine, Latvia). The sample consisted of monohydrate (**MH-II**) phase. Inorganic compounds and organic solvents of analytical grade were purchased from commercial sources and used without further purification.

Sample Preparation. Standard solvate screening was performed by cooling a hot solution of Enc-HCl in a selected solvent to room temperature or by evaporation of saturated solution at ambient temperature with relative humidity <5%. Acetonitrile monosolvate 1 ($\mathbf{S}_{\mathbf{ACN\text{-}I}}$) was prepared by evaporation of a hot concentrated solution of Enc-HCl in acetonitrile at ambient temperature with relative humidity <5%. Acetonitrile disolvate ($\mathbf{DS}_{\mathbf{ACN}}$) was prepared by cooling of a hot concentrated solution of Enc-HCl in acetonitrile to 5 °C. Acetonitrile monosolvate 2 ($\mathbf{S}_{\mathbf{ACN\text{-}II}}$) was obtained by storing $\mathbf{DS}_{\mathbf{ACN}}$ in a desiccator with P_2O_5. Formic acid disolvate ($\mathbf{DS}_{\mathbf{FA}}$), acetic acid disolvate ($\mathbf{DS}_{\mathbf{AA}}$), *i*-butanol monosolvate ($\mathbf{S}_{\mathbf{IBA}}$), ethanol monosolvate ($\mathbf{S}_{\mathbf{EtOH}}$), and benzyl alcohol monosolvate ($\mathbf{S}_{\mathbf{BnOH}}$) were obtained by cooling a hot saturated solution of Enc-HCl in the respective solvent to room temperature. Formic acid monosolvate ($\mathbf{S}_{\mathbf{FA}}$) was obtained by desolvation of $\mathbf{DS}_{\mathbf{FA}}$ in air at ambient temperature. Polymorphs $\mathbf{V}_{\mathbf{D}}$, $\mathbf{VII}_{\mathbf{D}}$, and $\mathbf{IX}_{\mathbf{D}}$ were prepared by desolvation of $\mathbf{S}_{\mathbf{IBA}}$, $\mathbf{S}_{\mathbf{FA}}$, and $\mathbf{DS}_{\mathbf{AA}}$ at 80 °C, respectively. Polymorphs $\mathbf{VI}_{\mathbf{D}}$, $\mathbf{VIII}_{\mathbf{D}}$, $\mathbf{XI}_{\mathbf{D}}$, and $\mathbf{XII}_{\mathbf{D}}$ were obtained by storing $\mathbf{S}_{\mathbf{ACN\text{-}I}}$, $\mathbf{DS}_{\mathbf{AA}}$, $\mathbf{S}_{\mathbf{FA}}$, and $\mathbf{S}_{\mathbf{ACN\text{-}II}}$ in a desiccator with P_2O_5, respectively. Polymorph $\mathbf{IV}_{\mathbf{D}}$ was obtained by crystallization from dimethylformamide or by heating any form at 200 °C. All anhydrous polymorphs were stored in a desiccator over P_2O_5 to prevent the absorption of water. Single crystals of $\mathbf{IV}_{\mathbf{D}}$ were prepared by cooling a hot solution of Enc-HCl in DMF to −5 °C and storing it in mother liquor. Single crystals of $\mathbf{S}_{\mathbf{EtOH}}$ and $\mathbf{DS}_{\mathbf{ACN}}$ were prepared by cooling a hot solution of Enc-HCl in the respective solvent to −5 °C and storing it in mother liquor. Similarly, single crystals of $\mathbf{DS}_{\mathbf{AA}}$ were obtained by cooling a hot solution of Enc-HCl in acetic acid to ambient temperature and stored in mother liquor.

Powder X-ray Diffraction (PXRD). Routine PXRD measurements were performed on a Bruker D8 Advance diffractometer using copper radiation (Cu Kα = 1.54180 Å) with Bragg−Brentano geometry and a LynxEye (1D) detector. The tube voltage and current were set to 40 kV and 40 mA, respectively. The divergence and antiscattering slits were set at 0.6 mm and 8 mm, respectively. The patterns were recorded from 3° to 30° on the 2θ scale, using a scan speed of 0.2 s/0.02°. When necessary, to prevent the atmospheric humidity effect, samples were covered with a 10 μm polyethylene film.

Variable temperature (VT) PXRD experiments were performed on a Bruker D8 Discover diffractometer equipped with an MRI temperature chamber and controller. Copper radiation (Cu Kα = 1.54180 Å) with Bragg−Brentano geometry and a LynxEye (1D) detector was used. The diffractometer incident beam path was equipped with a Göbel mirror, Soller slit, and a 0.6 mm divergence slit, while the diffracted beam path was equipped only with a Soller slit. The patterns were recorded from 4.5° to 30° on the 2θ scale, using a scan speed of 0.4 s/0.02°.

For structure determination, PXRD patterns were recorded on a Bruker D8 Discover diffractometer using copper radiation (Cu Kα = 1.54180 Å) in transmission mode and a LynxEye (1D) detector. The tube was employed with voltage and current settings of 40 kV and 40 mA. The sample was loaded into a special glass number 10 capillary (0.5 mm diameter). A capillary spinner (60 rpm) and upper and lower knife edges were used. The diffractometer incident beam path was equipped with a Göbel mirror, Soller slit, and a 0.6 mm divergence slit, while the diffracted beam path was equipped only with a Soller slit. The diffraction patterns were recorded on the 2θ scale from 3 or 4.5 to 70° at a 0.01° step size using a scan speed of 36 s per step.

Single Crystal X-ray Diffraction (SC-XRD). Single-crystal intensities of Enc-HCl $\mathbf{IV}_{\mathbf{D}}$, $\mathbf{DS}_{\mathbf{AA}}$, and $\mathbf{S}_{\mathbf{EtOH}}$ were collected on a MAR345 diffractometer equipped with an image plate detector (sample-to-detector distance of 100 mm was chosen). A rotating anode X-ray generator was used with a wavelength of 0.56089 Å (silver anode). The samples were cooled down to 171 K in an open-flow nitrogen cryostat. Crystals of sizes around 0.20 × 0.15 × 0.10 mm^3 were glued on a glass fiber and mounted on the goniometer head. Data indexation and integration was performed with the *CrysAlisPro 39.46* software.

Structure solution and refinements were performed with the *JANA2006* software suite.[24,25] Non-hydrogen atoms were refined anisotropically. Hydrogens were added geometrically or located from the difference Fourier maps; riding ADPs were applied. A rigid body approach for the quinuclidine moiety was used in the structure of encenicline polymorph $\mathbf{IV}_{\mathbf{D}}$, where it was found to be disordered over two orientations.

Single-crystal intensities of Enc-HCl $\mathbf{S}_{\mathbf{ACN}}$ were collected on an XtaLAB Synergy-S dualflex diffractometer (RIGAKU Oxford Diffraction) equipped with a HyPix6000 detector and microfocus sealed X-ray tube with Cu Kα radiation (λ = 1.54184 Å). A single crystal with approximate dimensions of 0.08 × 0.08 × 0.06 mm^3 was fixed with oil in a nylon loop of a magnetic CryoCap and set on a goniometer head. The sample was cooled down to 150 K, and ω-scans were performed with a step size of 0.5°. Data collection and reduction were performed with the CrysAlisPro 1.171.40.35a software. Structure solution and refinement were performed with AutoChem3.0 and SHELXL[26] software that are parts of the CrysAlisPro suite. Non-hydrogen atoms were refined anisotropically. Hydrogen atoms were added geometrically and refined using a "riding" model.

Structure Determination from PXRD Data. Indexing, space group determination, and structure solution were performed using EXPO2014.[27] The unit cell dimensions were determined by applying the N-TREOR09[28] and Dicvol06[29] indexing procedures with a set of 20−25 reflections found in 4.5−30° 2θ range. Space group determination was carried out using a statistical assessment of systematic absences, and Z' was determined based on density considerations. The cell and diffraction pattern profile parameters were refined according to the LeBail algorithm.[30,31] The background was modeled by a 20th-order polynomial function of the Chebyshev type; peak profiles were described by the Pearson VII function.

The initial geometry of the encenicline cation was taken from the crystal structure of monohydrate **MH-II**.[21] The Monte Carlo/Simulating Annealing technique was used to constantly adjust the conformation, position, and orientation of the trial model in the unit cell to maximize the agreement between calculated and measured diffraction data.

The final Rietveld refinement was performed using EXPO2014 or TopasS[32] software. In EXPO2014, soft constraints on bond distances and angles were used. The planar phenyl ring was treated as a rigid body, and restraints on bond distances and angles were used. For the Rietveld refinement in TopasS, the encenicline cation and solvent molecules were treated as rigid bodies.

DOI: 10.1021/acs.cgd.9b00648
Cryst. Growth Des. 2019, 19, 4765−4773

Differential Scanning Calorimetry/Thermogravimetric Analysis (DSC/TGA). DSC/TGA analyses of Enc-HCl solvates were performed with a Mettler Toledo TGA/DSC2 instrument. Open or closed 100 μL aluminum pans were used. Heating of samples from 25 to 310 °C was performed at a heating rate of 10 °C·min^{-1} under a 100 mL·min^{-1} nitrogen flow. The sample mass was approximately 7–15 mg.

DSC analyses of EnC-HCl polymorphs were performed with a TA DSC 25 instrument. Closed 70 μL aluminum pans were used. Heating of samples from 25 to 320 °C was performed at the heating rate of 5 °C·min^{-1} under a 50 mL·min^{-1} nitrogen flow. The sample mass was approximately 5–8 mg.

Dynamic Water Vapor Sorption and Desorption Studies. Dynamic vapor sorption–desorption experiments were performed on the Surface Measurement Systems DVS Advantage. All samples (5–12 mg) were initially dried under a 200 mL stream of N_2 to establish the equilibrium dry mass under 25 °C. Samples were studied over a selected humidity range from 0–90% RH with step of 5% at 25 °C. Each humidity step was taken with equilibration set to dm/dt 0.002%/min on a 5 min time frame (with a minimum hold time of 10 min and maximum of 300 min).

Theoretical Calculations. The geometry optimization and the resulting calculation of total energy of Enc-HCl polymorphs and solvates was performed in CASTEP plane wave code by relaxing positions of all atoms. Calculations were performed with the PBE exchange correlation density functional and on-the-fly generated ultrasoft pseudopotentials, with the addition of a semiempirical Grimme D2 dispersion correction. K-points were chosen to provide a maximum spacing of 0.07 Å^{-1}, and the basis set cutoff was 570 eV.

The 1D relaxed potential energy surfaces (PES) were calculated in Gaussian 09[33] at the M06-2X/6-31++G(d,p) level by scanning all three flexible torsion angles (see Figure 1) of the encenicline cation with a step size of 10°.

Crystal Structure Comparison and Analysis. Mercury 3.9 software[34] was used for crystal structure analysis and simulation of PXRD patterns based on crystal structure data. Detailed analysis of the molecular packing was performed using CrystalCMP.[35] The packing coefficients in crystal structures were calculated by PLATON.[36] Crystal structures for quantitative molecular packing comparison in CrystalCMP and calculation of packing coefficients were used after geometry optimized with periodic boundary DFT code for more reliable results.

■ RESULTS AND DISCUSSION

Solid Form Screening. Previous studies of solid Enc-HCl forms have reported four monohydrates designated here as **MH-I**, **MH-II**, **MH-III**, and **MH-X**, and in our previous article we described that dehydration of each of the four monohydrates produces a different polymorph ($\mathbf{I_D}$, $\mathbf{II_D}$, $\mathbf{III_D}$, $\mathbf{X_D}$), each being structurally related to the respective monohydrate by keeping the main packing features.[21,37] In a crystal form screening of Enc-HCl, over 30 new solvates were obtained. All the obtained solvates were characterized using PXRD patterns and DSC/TGA analysis; phase transformations upon desolvation were studied by identifying the desolvation routes and products. On the basis of the results from indexing of the respective PXRD patterns, most of the Enc-HCl solvates can be classified into three solvate types, see Table S1, Supporting Information, with half of the solvates crystallizing as type 2 solvates. In the present work, only selected solvates that are precursors to the new polymorphs and/or represent each solvate type are characterized in detail: isobutanol monosolvate ($\mathbf{S_{IBA}}$), formic acid disolvate ($\mathbf{DS_{FA}}$), formic acid monosolvate ($\mathbf{S_{FA}}$), acetic acid disolvate ($\mathbf{DS_{AA}}$), acetonitrile disolvate ($\mathbf{DS_{ACN}}$), acetonitrile monosolvate 1 ($\mathbf{S_{ACN\text{-}I}}$) and monosolvate 2 ($\mathbf{S_{ACN\text{-}II}}$), ethanol monosolvate ($\mathbf{S_{EtOH}}$), and benzyl alcohol monosolvate ($\mathbf{S_{BnOH}}$). The desolvation of these solvates produced eight new polymorphs ($\mathbf{IV_D}$, $\mathbf{V_D}$, $\mathbf{VI_D}$, $\mathbf{VII_D}$, $\mathbf{VIII_D}$, $\mathbf{IX_D}$, $\mathbf{XI_D}$, and $\mathbf{XII_D}$) named in consecutive order of appearance. In Figure 2, there is a flowchart illustrating the different polymorphs and the path for their preparation—the respective solvate and desolvation conditions. The only polymorph which can be obtained in crystallization is $\mathbf{IV_D}$ and only from one solvent–dimethylformamide, whereas all the other known polymorphs can be obtained only through desolvation of a specific solvate (or solvate type for $\mathbf{V_D}$). Moreover, polymorphs $\mathbf{VIII_D}$, $\mathbf{XI_D}$, and $\mathbf{XII_D}$ can be obtained only by desolvation in a desiccator over P_2O_5. Upon heating, all polymorphs transform to form $\mathbf{IV_D}$.

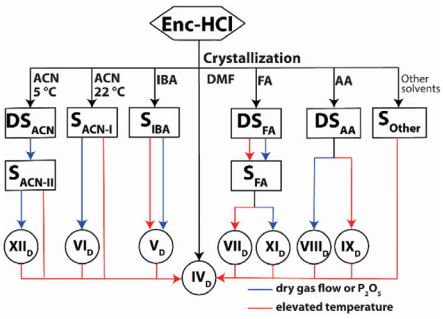

Figure 2. Enc-HCl phase transitions upon desolvation/heating.

Powder X-ray Diffraction. Each crystalline form has a unique and distinguishable PXRD pattern (Figure 3) showing no similarity between precursor solvates and their respective desolvated phases. In the PXRD pattern of $\mathbf{XI_D}$, part of the peaks are narrow while other parts are wide. Such a characteristic was also observed in the PXRD patterns of **MH-X** and $\mathbf{X_D}$.[21] It seems that in the crystal structures of these phases, only two directions are well-determined, as all the narrow peaks can be indexed with only two axes, with the structure in the third direction largely undetermined. Although such behavior is unusual for pharmaceuticals, it can be attributed to stacking faults, which are common in materials that have a strongly layered character, and such behavior has been observed in structures of Enc-HCl **MH-I**, **MH-II**, **MH-III**, $\mathbf{I_D}$, $\mathbf{II_D}$ and $\mathbf{III_D}$.

Thermal and Thermodynamic Stability. The results of the TGA and DSC investigations of the eight Enc-HCl solvates as well as DSC plots of polymorphs are shown in Figure 4. Guest loss temperature and observed weight loss confirmed the stoichiometry of each solvate; data are given in Table S2, SI, together with the desolvation products. According to the mass loss, $\mathbf{DS_{FA}}$ (24.0%), $\mathbf{DS_{AA}}$ (21.6%), and $\mathbf{DS_{ACN}}$ (18.5%) are disolvates, whereas $\mathbf{S_{IBA}}$ (16.5%), $\mathbf{S_{ACN\text{-}I}}$ (9.8%), $\mathbf{S_{ACN\text{-}II}}$ (10.6%), $\mathbf{S_{FA}}$ (11.6%), $\mathbf{S_{BnOH}}$ (24.9%), and $\mathbf{S_{EtOH}}$ (11.2%) are monosolvates. The TGA and DSC curves show that for all solvates, except for the $\mathbf{DS_{FA}}$, desolvation is a single step process. Despite two acetonitrile monosolvates having been obtained ($\mathbf{S_{ACN\text{-}I}}$, $\mathbf{S_{ACN\text{-}II}}$), DSC/TGA traces of $\mathbf{DS_{ACN}}$ did not contain any evidence of two step desolvation, although partial desolvation to $\mathbf{S_{ACN\text{-}II}}$ is visible in the VT-PXRD experiment (see Figure S1, SI). The measured DSC peak temperature of the desolvation process was 60 and 120 °C for $\mathbf{DS_{FA}}$ and $\mathbf{S_{FA}}$

DOI: 10.1021/acs.cgd.9b00648
Cryst. Growth Des. 2019, 19, 4765–4773

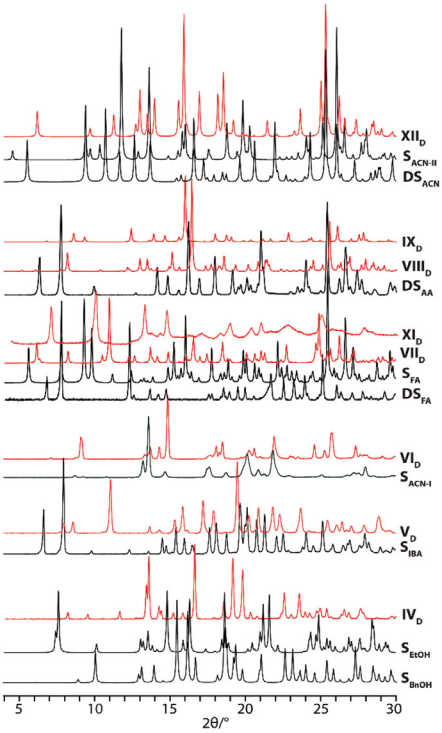

Figure 3. PXRD patterns of presented Enc-HCl solvated (black) and neat (red) crystalline forms.

(Figure 4a), 120 °C for $\mathbf{DS_{AA}}$ (Figure 4b), 79 °C for $\mathbf{DS_{ACN}}$ (Figure 4c), 138 °C for $\mathbf{S_{IBA}}$ (Figure 4d), 84 °C for $\mathbf{S_{ACN\text{-}I}}$ (Figure 4e), 72 °C for $\mathbf{S_{ACN\text{-}II}}$ (Figure 4f open pan), 123 °C for $\mathbf{S_{BnOH}}$ (Figure 4g), and 99 °C for $\mathbf{S_{EtOH}}$ (Figure 4h). The thermal desolvation product of all three acetonitrile solvates, $\mathbf{S_{BnOH}}$, and $\mathbf{S_{EtOH}}$ are polymorph $\mathbf{IV_D}$, while desolvation of $\mathbf{S_{IBA}}$, $\mathbf{S_{FA}}$, and $\mathbf{DS_{AA}}$ gives polymorphs $\mathbf{V_D}$, $\mathbf{VII_D}$, and $\mathbf{VIII_D}$, respectively. When heating $\mathbf{S_{ACN\text{-}II}}$ in a closed pan in the DSC/TGA experiment, before the desolvation, an endothermic effect at 70 °C without mass loss was observed (Figure 4f, closed pan). This endothermic peak is attributed to a solid-state phase transition from $\mathbf{S_{ACN\text{-}II}}$ to $\mathbf{S_{ACN\text{-}I}}$, as confirmed by the PXRD analysis. This endothermic solid-state phase transition indicates that solvates $\mathbf{S_{ACN\text{-}I}}$ and $\mathbf{S_{ACN\text{-}II}}$ are enantiotropically related, where $\mathbf{S_{ACN\text{-}I}}$ is thermodynamically more stable at higher temperatures. This statement is supported by total energy calculation using CASTEP, as the energy of $\mathbf{S_{ACN\text{-}I}}$ is higher than that of $\mathbf{S_{ACN\text{-}II}}$ (+6 kJ·mol^{-1}).

DSC data confirmed that form $\mathbf{IV_D}$ exhibits the highest melting point (286 ± 1 °C), while all the other polymorphs convert to form $\mathbf{IV_D}$ during the heating (Figure 4i) in three different ways: (1) via endothermic phase transition ($\mathbf{V_D}$), (2) via exothermic phase transition ($\mathbf{VI_D}$ and $\mathbf{XI_D}$), or (3) in exothermic recrystallization from an amorphous state ($\mathbf{VII_D}$, $\mathbf{VIII_D}$, $\mathbf{IX_D}$, and $\mathbf{XII_D}$).

It is worth it to mention that the endothermic process that leads to an amorphous state, as confirmed by PXRD, has very small enthalpy (2−7 kJ·mol^{-1}), and the onset temperature tends to shift with different heating rates. So, it is reasonable to conclude that this process is not attributed to the melting of the respective phase. As the melting process of form $\mathbf{IV_D}$ is accompanied by mass loss (see Figure 4a−h), it is certain that there is a degradation upon melting, and the integration of the apparent melting peaks provides erroneous melting enthalpy. Nevertheless, this allowed the establishment of the thermodynamic relationship between only three polymorphic pairs: according to the heat of transition rule polymorphs $\mathbf{V_D}$ and $\mathbf{IV_D}$ have an enantiotropic thermodynamic relationship, but polymorphic pairs $\mathbf{IV_D}$ /$\mathbf{VI_D}$ and $\mathbf{IV_D}$ /$\mathbf{XI_D}$ are monotropically related.

In slurry bridging experiments under ambient conditions in *n*-heptane, all polymorphs converted to form $\mathbf{IV_D}$. Thus, at room and elevated temperatures, form $\mathbf{IV_D}$ is the most stable polymorph of Enc-HCl. Stability of the polymorphs was also investigated by comparing the computed total energies of structures after geometry optimization either by relaxing only positions of all atoms or by relaxing positions and unit cell parameters using periodic DFT calculations, representing low-temperature (approaching 0 K) stability. Total energies after relaxing only atomic positions (Table 1) indicate that form $\mathbf{V_D}$ is the most stable form, followed by $\mathbf{VII_D}$ (+4.9 kJ·mol^{-1}), $\mathbf{IV_D}$ (+6.3 kJ·mol^{-1}), $\mathbf{IX_D}$ (+9.6 kJ·mol^{-1}), $\mathbf{VI_D}$ (+11.3 kJ·mol^{-1}), and $\mathbf{VIII_D}$ (+12.4 kJ·mol^{-1}), whereas form $\mathbf{XII_D}$ is the least stable polymorph with +14.1 kJ·mol^{-1}. After full geometry optimization (positions + unit cell), the energy range is narrower but energy ranking between polymorphs is similar (Table 1).

The effect of relative humidity on the stability was also investigated. Figure 5 illustrates a comparison of representative sorption isotherms of Enc-HCl polymorphs recorded from 0 to 90% RH with a step of 5%.

It was found that the most stable polymorph against moisture is $\mathbf{IV_D}$, showing no significant mass change in the range from 0 to 85% RH. A further, steep increase of the slope with a mass change of 5.8% can be observed at 90% RH, attributed to the hydration by forming monohydrate form **MH-I**, as confirmed by PXRD. Polymorphs $\mathbf{V_D}$ and $\mathbf{VI_D}$ start to take up a significant amount of water at 70% RH and 50% RH, respectively, also transforming to the monohydrate **MH-I**. The two least stable polymorphs against moisture—$\mathbf{VIII_D}$ and $\mathbf{IX_D}$ already start to take up a significant amount of water (2.2%) at 10% RH, transforming to a new hydrated phase with hemihydrate stoichiometry (**HH**), which further at 20% RH transforms to a new monohydrate (**MH-V**), meaning that polymorphs $\mathbf{VIII_D}$ and $\mathbf{IX_D}$ are stable only at ≤5% RH. At 65−70% RH, recrystallization from **MH-V** to **MH-I** is observed. Moreover, polymorph $\mathbf{VII_D}$ at 55% RH produces yet another new monohydrate (**MH-VI**), but in contrast to relatively stable **MH-V** (stable at 20−60% RH), **MH-VI** is stable in a very small RH range (55−60%). At higher RH, **MH-VI** transforms to **MH-I**. Polymorphs $\mathbf{XI_D}$ and $\mathbf{XII_D}$ are hygroscopic and, until 50−60% RH, gradually absorb up to 6% water by further recrystallizing to **MH-I** at higher RH. PXRD patterns, cyclic DVS isotherms, DSC, and TGA data of **MH-V** and **MH-VI** are given in Figuers S6−S9, SI. The crystal structure of **MH-V** was determined from PXRD data. It is worth it to mention that

DOI: 10.1021/acs.cgd.9b00648
Cryst. Growth Des. 2019, 19, 4765−4773

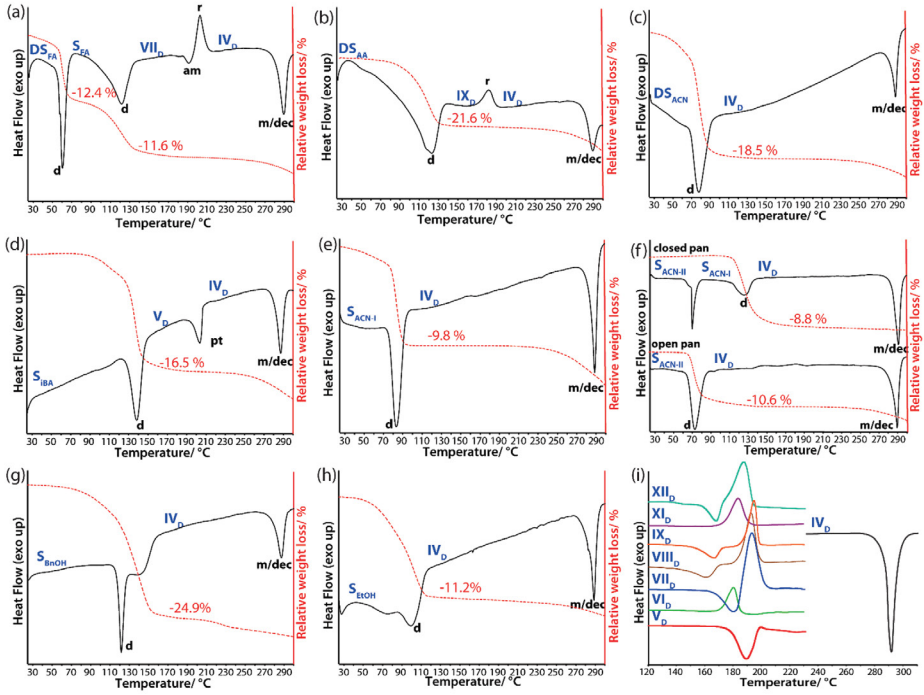

Figure 4. (a–h) DSC/TGA traces of Enc-HCl solvates. d, desolvation; pt, phase transition; am, amorphization; r, recrystallization; m/dec, melting with decomposition (10 °C/min heating rate). (i) Overlay of DSC curves of Enc-HCl polymorphs at 5 °C/min heating rate.

when DSC measurements of **MH-V** and **MV-VI** were performed using sealed crucibles, exothermic phase transition was observed for both monohydrates prior the melting (see Figure S9c). As confirmed by PXRD measurements of stopped DSC/TGA experiments and the onset temperature of the following incongruent or congruent melting event, **MH-V** transforms to monohydrate **MH-X**, but **MH-VI** transforms to **MH-I**, indicating that **MH-V** and **MH-VI** are less stable than the previously reported monohydrates.[21] This statement is also supported by the total energy calculation in CASTEP, as **MH-V** has the highest energy among the Enc-HCl monohydrates (+12 kJ·mol^{-1}).

Characterization of Enc-HCl Crystal Structures. Crystal structures of $\mathbf{IV}_D$, $\mathbf{DS}_{ACN}$, $\mathbf{DS}_{AA}$, and $\mathbf{S}_{EtOH}$ were determined by SCXRD, whereas those of all other solvated and unsolvated phases are from the PXRD data. Crystallographic data for neat polymorphs is given in Table 1 and for solvated phases in Table S3, SI. The correctness of the structures calculated from the PXRD data was confirmed by the good agreement between the experimental and calculated diffraction patterns (Rietveld fit for polymorph $\mathbf{V}_D$ is shown in Figure 6 and for the rest of the structures in Figures S10–S19, SI), as well as by the DFT geometry optimization, after which the RMSD with the experimental structures was always acceptable[38] (see Figures S20–S30, SI).

In this study, all the determined crystal forms of Enc-HCl crystallize in two most frequent Sohncke space groups: $P2_1$ and $P2_12_12_1$. The space groups of the polymorphs are the same as those of the corresponding precursor solvates, and even the lattice parameters in most of the solvate–desolvate pairs are similar. Although encenicline has three flexible dihedral angles, analysis of the crystal structures revealed that the conformation of the encenicline cation in all crystal structures is highly similar and also similar to that in the previously published monohydrates and their dehydrates (see Table S4). The largest conformation difference (up to 30°) arises due to the rotation of the chloro-benzothiophene group around the C1–C10 bond (τ1) and quinuclidine group around the N12–C16 bond (τ3). To ascertain that the conformation in all crystal structures corresponds to the same energy minimum, geometry optimization and a 1D PES scan with respect to the corresponding torsion angles were performed (Figure S31, SI). Results showed that, in all structures, τ1 corresponds to the second lowest local energy minimum ($\Delta E \sim 5$ kJ mol^{-1}); τ2 corresponds to the global energy minimum and τ3 to the third local energy minimum (ΔE up to 25 kJ mol^{-1}). The occupation of a conformation different from the global minimum appears to be associated with the possibility of forming more efficient intermolecular interactions. Also, the energy-minimized *in vacuo* geometry was highly similar to the

DOI: 10.1021/acs.cgd.9b00648
Cryst. Growth Des. 2019, 19, 4765–4773

Table 1. Crystallographic Data for Enc-HCl Polymorphs

	IV_D	V_D	VI_D	VII_D	$VIII_D$	IX_D	XII_D
formula				$C_{16}H_{18}Cl_2N_2OS$			
formula weight, g·mol^{-1}				357.3			
sample type	crystal	powder	powder	powder	powder	powder	powder
crystal system	orthorhombic	orthorhombic	monoclinic	orthorhombic	monoclinic	monoclinic	orthorhombic
space group	$P2_12_12_1$	$P2_12_12_1$	$P2_1$	$P2_12_12_1$	$P2_1$	$P2_1$	$P2_12_12_1$
a, Å	7.4165(3)	6.6885(7)	9.8043(17)	28.0018(18)	13.533(4)	17.049(2)	26.523(2)
b, Å	13.0667(7)	11.4163(12)	8.8566(16)	16.8624(12)	6.8230(16)	6.9599(8)	9.2661(6)
c, Å	18.2772(10)	21.6990(2)	10.4080(17)	7.1411(4)	10.703(4)	14.5383(18)	6.9971(3)
α, deg	90	90	90	90	90	90	90
β, deg	90	90	106.496(3)	90	106.554(9)	92.914(4)	90
γ, deg	90	90	90	90	90	90	90
V, Å^3	1771.23(15)	1656.9(2)	866.6(3)	3371.9(4)	947.3(5)	1722.9(4)	1719.65(18)
ρ_{calcd}, g·cm^{-3}	1.34	1.43	1.37	1.41	1.25	1.38	1.38
Z/Z'	4/1	4/1	2/1	8/2	2/1	4/2	4/1
temperature, K	174	293(2)	293(2)	293(2)	293(2)	293(2)	293(2)
$2\theta_{min}-2\theta_{max}$ /increment, °		4.5−70/0.01	4.5−70/0.01	5.0−70/0.01	5.0−70/0.01	5.0−70/0.01	5.0−70/0.01
Rwp		0.05122	0.04661	0.02740	0.03188	0.02498	0.03426
Rp		0.03945	0.03458	0.02013	0.00558	0.01760	0.02428
R_{exp}		0.01098	0.00916	0.00935	0.01879	0.00900	0.00754
R_1 (wR_2)	0.0464 (0.0620)						
energy, kJ·mol^{-1}[a]	6.3	0	11.3	4.9	12.4	9.6	14.1
energy, kJ·mol^{-1}[b]	6.3	0	8.8	1.5	8.9	9.3	12.4
packing index, %[c]	66.7	72.6	70.8	73.7	64.9	70.4	71.4
CCDC no.	1895196	1895197	1895199	1895194	1895188	1895193	1918036

[a]Relative energy by relaxing positions of all atoms (relative to $\mathbf{V_D}$). [b]Relative energy by relaxing positions of all atoms and unit cell parameters (relative to $\mathbf{V_D}$). [c]After geometry optimization by relaxing positions of all atoms and unit cell parameters.

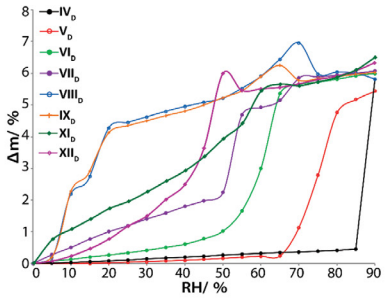

Figure 5. Water vapor sorption isotherms of Enc-HCl polymorphs at 25 °C.

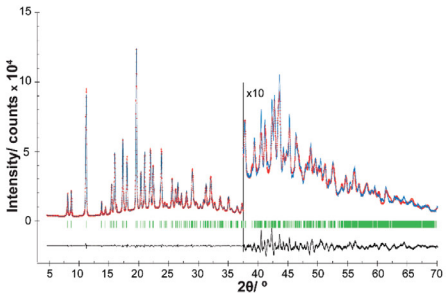

Figure 6. Final Rietveld fit for Enc-HCl polymorph $\mathbf{V_D}$: red crosses, measured data points; blue line, calculated profile; black line, difference curve; green tick marks, calculated peak positions.

initial geometry observed in the crystal structures and identical for all of the crystal structures. Therefore, it is reasonable to conclude that the conformation in all crystal structures is the same. Thus, we can point out that in contrast to the other most polymorphic molecules, aripiprazole, ROY, and flufenamic acid, conformation variability is not the main driving force for formation of the high number of polymorphic forms by Enc-HCl.

Analysis of intermolecular interactions and packing revealed that different crystal structures can form as a result of different packing possibilities. This is partly associated with the possibility of forming different characteristic hydrogen bonding motifs, as three different hydrogen-bonded building blocks can be identified in all structures (Figure 7): Chain 1 $C_2^1(7)$ in forms $\mathbf{DS_{ACN}}$, $\mathbf{S_{ACN}}$, $\mathbf{S_{ACN\text{-}II}}$, $\mathbf{S_{BnOH}}$, $\mathbf{S_{EtOH}}$, $\mathbf{IV_D}$, $\mathbf{VI_D}$, and $\mathbf{XII_D}$; Chain 2 $C_2^1(7)$ in forms $\mathbf{DS_{AA}}$, $\mathbf{S_{FA}}$, $\mathbf{VII_D}$, $\mathbf{VIII_D}$, and $\mathbf{IX_D}$ formed by N12−H12···Cl23 and N14−H···Cl23 interactions; and Chain 3 $C_1^1(7)$ in forms $\mathbf{S_{IBA}}$ and $\mathbf{V_D}$ formed by N14−H···O11. Interestingly, the relative arrangement of encenicline cation and chloride anion in all of the structures is very similar, and hydrogen bonds N12−H···Cl23 with similar geometry are always present. Moreover, interaction N14−H···Cl23 is also always present, although in polymorph $\mathbf{V_D}$ its length is relatively large and angle significantly deviated from 180°.

The packing similarity of the Enc-HCl polymorphs with their respective parent solvate are shown in Figure 7 and in Figures S32−S37, SI. It can be clearly seen that the packing of Enc-HCl moieties in solvates and in polymorphs obtained in their desolvation is similar: a comparison of structures

DOI: 10.1021/acs.cgd.9b00648
Cryst. Growth Des. 2019, 19, 4765−4773

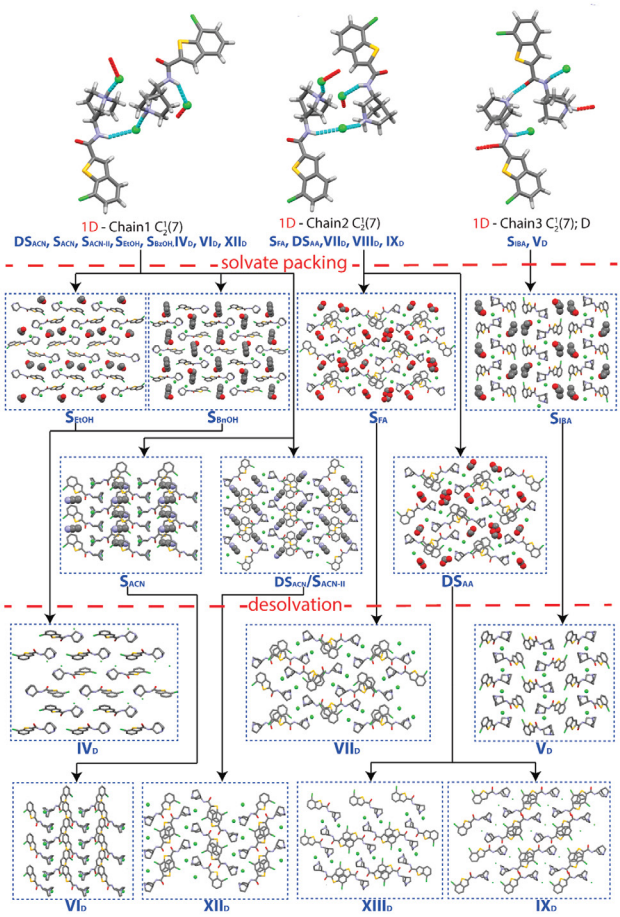

Figure 7. Hydrogen bonding and packing similarity of Enc-HCl solvates and respective neat polymorphs. Hydrogen atoms are omitted for clarity.

confirmed that in all cases the characteristic packing features and hydrogen-bonding linkage are maintained after the desolvation even in those cases when larger structure rearrangement is observed. This observation is also confirmed by the packing similarity tree diagram generated in CrystalCMP software (Figure 8). From the packing similarity dendrogram, it can be identified that in all cases the closest packing characteristics are between precursor solvates and their respective desolvated phases.

The desolvation of most of the other discovered solvates produced polymorph $\mathbf{IV_D}$. This can be associated both by the packing similarity of $\mathbf{IV_D}$ with the solvates (which is confirmed for $\mathbf{S_{BzOH}}$ and $\mathbf{S_{EtOH}}$) and also by the fact that $\mathbf{IV_D}$ is thermodynamically the most stable polymorph under the desolvation conditions.

The driving force for the formation of the analyzed solvates mainly seems to be the incorporation of solvent molecules to reduce the void space.[39,40] Even in cases when solvent forms hydrogen bonds, it is just bonded to the Cl^- anion, and the hydrogen bonded chain existing in the respective structurally similar polymorph or any other hydrogen bond formation characteristic is not affected by the solvate formation. The exception from this is hydrates, particularly **MH-V** (see Figure S38, SI), where water compensates for the unsatisfied hydrogen bond acceptors present in the dehydrates and forms more complex hydrogen bonding networks. Although on numerous occasions, this results in formation of similar structures (see Table S1, SI), the inclusion of some particular solvents results in the possibility for different packing, which is maintained when the solvent molecules are removed from the

DOI: 10.1021/acs.cgd.9b00648
Cryst. Growth Des. 2019, 19, 4765−4773

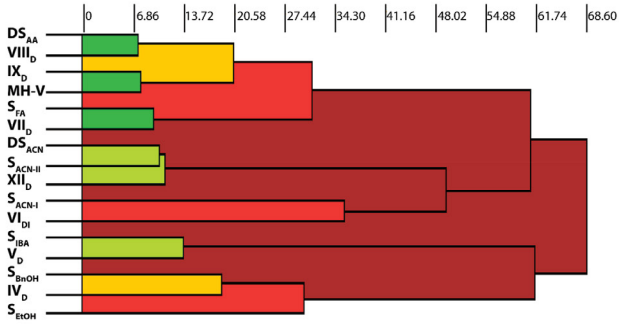

Figure 8. Dendrogram showing packing similarity of solid forms of Enc-HCl. The horizontal axis corresponds to the PSab value (similarity).

structure by producing an exceptionally high number of polymorphs. In this light, particularly interesting is water, as apparently because of its different hydrogen bonding possibilities with Enc-HCl, it is able to form several different monohydrates, four of which now are structurally characterized. Moreover, as the packing features are kept during the desolvation, each hydrate produces a differently packed polymorph.[21]

■ CONCLUSIONS

Overall, 10 structurally characterized polymorphs of Enc-HCl can be accessed, six of which here are described for the first time. This allows Enc-HCl to set a record for having the highest number of published structurally characterized polymorphs as well as, to the best of our knowledge, the most published polymorphs among organic salts under ambient pressure. All thermodynamically metastable polymorphs can be accessed only through desolvation of various solvates, and in this process the characteristic hydrogen bond network and packing present in the solvates are always maintained. Meanwhile, the conformation in all structures is nearly identical and corresponds to the same energy minimum.

■ ASSOCIATED CONTENT

Supporting Information

The Supporting Information is available free of charge on the ACS Publications website at DOI: 10.1021/acs.cgd.9b00648.

Results of solvate screening; thermal characterization and variable temperature PXRD patterns of selected solvates; cyclic DVS isotherms, PXRD patterns, DSC and TG thermograms of monohydrates **MH-V** and **MH-VI**; crystallographic information on solvated phases, Rietveld fit for structures calculated from PXRD, overlay of crystal structures calculated from PXRD data and crystal structures after DFT optimization; PES scans and torsion angles; packing similarity between solvated and respective desolvated phases; hydrogen bonding network in **MH-V** structure (PDF)

Accession Codes

CCDC 1895188−1895191, 1895193−1895199, 1916266−1916269, and 1918036 contain the supplementary crystallographic data for this paper. These data can be obtained free of charge via www.ccdc.cam.ac.uk/data_request/cif, or by emailing data_request@ccdc.cam.ac.uk, or by contacting The Cambridge Crystallographic Data Centre, 12 Union Road, Cambridge CB2 1EZ, UK; fax: + 44 1223 336033.

■ AUTHOR INFORMATION

Corresponding Author

*Telephone: +(371)-67033903. E-mail: artis.kons@lu.lv.

ORCID

Artis Kons: 0000-0002-4055-8442

Agris Bērziņš: 0000-0002-4149-8971

Toms Rekis: 0000-0001-5128-4611

Sander van Smaalen: 0000-0001-9645-8240

Funding

This work has been funded by the Latvian Council of Science, project "Crystal Engineering of Pharmaceutical Multicomponent Phases for More Efficient Crystalline Phase Design," project No. lzp-2018/1-0312 and University of Latvia Foundation trough SIA "Mikrotikls" supported project "Development of Integrated Experimental and Computer Modeling Research Methodology for Prediction of the Properties and Diversity of Phases of Active Pharmaceutical Solids."

Notes

The authors declare no competing financial interest.

■ REFERENCES

(1) Yu, L.; Stephenson, G. A.; Mitchell, C. A.; Bunnell, C. A.; Snorek, S. V.; Bowyer, J. J.; Borchardt, T. B.; Stowell, J. G.; Byrn, S. R. Thermochemistry and Conformational Polymorphism of a Hexamorphic Crystal System. *J. Am. Chem. Soc.* **2000**, *122*, 585−591.

(2) Sun, C.; Grant, D. J. W. Influence of Crystal Structure on the Tableting Properties of Sulfamerazine Polymorphs. *Pharm. Res.* **2001**, *18*, 274−280.

(3) Khomane, K. S.; More, P. K.; Bansal, A. K. Counterintuitive Compaction Behavior of Clopidogrel Bisulfate Polymorphs. *J. Pharm. Sci.* **2012**, *101*, 2408−2416.

(4) Pudipeddi, M.; Serajuddin, A. T. M. Trends in Solubility of Polymorphs. *J. Pharm. Sci.* **2005**, *94*, 929−939.

(5) Llinàs, A.; Goodman, J. M. Polymorph Control: Past, Present and Future. *Drug Discovery Today* **2008**, *13*, 198−210.

(6) Censi, R.; Di Martino, P. Polymorph Impact on the Bioavailability and Stability of Poorly Soluble Drugs. *Molecules* **2015**, *20*, 18759−18776.

(7) Campeta, A. M.; Chekal, B. P.; Abramov, Y. A.; Meenan, P. A.; Henson, M. J.; Shi, B.; Singer, R. A.; Horspool, K. R. Development of

a Targeted Polymorph Screening Approach for a Complex Polymorphic and Highly Solvating API. *J. Pharm. Sci.* **2010**, *99*, 3874−3886.
(8) Bhardwaj, R. M.; Price, L. S.; Price, S. L.; Reutzel-Edens, S. M.; Miller, G. J.; Oswald, I. D. H.; Johnston, B. F.; Florence, A. J. Exploring the Experimental and Computed Crystal Energy Landscape of Olanzapine. *Cryst. Growth Des.* **2013**, *13*, 1602−1617.
(9) Bingham, A. L.; Hughes, D. S.; Hursthouse, M. B.; Lancaster, R. W.; Tavener, S.; Threlfall, T. L. Over One Hundred Solvates of Sulfathiazole. *Chem. Commun.* **2001**, *7*, 603−604.
(10) Zeidan, T. A.; Trotta, J. T.; Tilak, P. A.; Oliveira, M. A.; Chiarella, R. A.; Foxman, B. M.; Almarsson, Ö.; Hickey, M. B. An Unprecedented Case of Dodecamorphism: The Twelfth Polymorph of Aripiprazole Formed by Seeding with Its Active Metabolite. *CrystEngComm* **2016**, *18*, 1486−1488.
(11) Chen, S.; Guzei, I. A.; Yu, L. New Polymorphs of ROY and New Record for Coexisting Polymorphs of Solved Structures. *J. Am. Chem. Soc.* **2005**, *127*, 9881−9885.
(12) Yu, L. Polymorphism in Molecular Solids: An Extraordinary System of Red, Orange, and Yellow Crystals. *Acc. Chem. Res.* **2010**, *43*, 1257−1266.
(13) Gushurst, K. S.; Nyman, J.; Boerrigter, S. X. M. The PO13 Crystal Structure of ROY. *CrystEngComm* **2019**, *21*, 1363−1368.
(14) López-Mejías, V.; Kampf, J. W.; Matzger, A. J. Nonamorphism in Flufenamic Acid and a New Record for a Polymorphic Compound with Solved Structures. *J. Am. Chem. Soc.* **2012**, *134*, 9872−9875.
(15) Olejniczak, A.; Katrusiak, A.; Szafrański, M. Ten Polymorphs of NH+···N Hydrogen-Bonded 1,4-Diazabicyclo[2.2.2]Octane Complexes: Supramolecular Origin of Giant Anisotropic Dielectric Response in Polymorph V. *Cryst. Growth Des.* **2010**, *10*, 3537−3546.
(16) Williams, P. A.; Hughes, C. E.; Lim, G. K.; Kariuki, B. M.; Harris, K. D. M. Discovery of a New System Exhibiting Abundant Polymorphism: M -Aminobenzoic Acid. *Cryst. Growth Des.* **2012**, *12*, 3104−3113.
(17) Braun, D. E.; Gelbrich, T.; Kahlenberg, V.; Tessadri, R.; Wieser, J.; Griesser, U. J. Stability of Solvates and Packing Systematics of Nine Crystal Forms of the Antipsychotic Drug Aripiprazole. *Cryst. Growth Des.* **2009**, *9*, 1054−1065.
(18) Bērziņš, A.; Skarbulis, E.; Actiņš, A. Structural Characterization and Rationalization of Formation, Stability, and Transformations of Benperidol Solvates. *Cryst. Growth Des.* **2015**, *15*, 2337−2351.
(19) Kons, A.; Bērziņš, A.; Actiņš, A. Polymorphs and Hydrates of Sequifenadine Hydrochloride: Crystallographic Explanation of Observed Phase Transitions and Thermodynamic Stability. *Cryst. Growth Des.* **2017**, *17*, 1146−1158.
(20) Minkov, V. S.; Beloborodova, A. A.; Drebushchak, V. A.; Boldyreva, E. V. Furosemide Solvates: Can They Serve As Precursors to Different Polymorphs of Furosemide? *Cryst. Growth Des.* **2014**, *14*, 513−522.
(21) Bobrovs, R.; Kons, A.; Bērziņš, A.; Rekis, T.; Actiņš, A. Formation and Transformations of Organic Salt Hydrates: Four Encenicline Hydrochloride Monohydrates and Respective Isostructural Desolvates. *Cryst. Growth Des.* **2018**, *18*, 2100−2111.
(22) Watts, A. E.; Maruyoshi, K.; Hughes, C. E.; Brown, S. P.; Harris, K. D. M. Combining the Advantages of Powder X-Ray Diffraction and NMR Crystallography in Structure Determination of the Pharmaceutical Material Cimetidine Hydrochloride. *Cryst. Growth Des.* **2016**, *16*, 1798−1804.
(23) Hughes, C. E.; Boughdiri, I.; Bouakkaz, C.; Williams, P. A.; Harris, K. D. M. Elucidating the Crystal Structure of Dl-Arginine by Combined Powder X-Ray Diffraction Data Analysis and Periodic DFT-D Calculations. *Cryst. Growth Des.* **2018**, *18*, 42−46.
(24) Palatinus, L.; Chapuis, G. SUPERFLIP − a Computer Program for the Solution of Crystal Structures by Charge Flipping in Arbitrary Dimensions. *J. Appl. Crystallogr.* **2007**, *40*, 786−790.
(25) Petříček, V.; Dušek, M.; Palatinus, L. Crystallographic Computing System JANA2006: General Features. *Z. Kristallogr. - Cryst. Mater.* **2014**, *229*, 345−352.
(26) Sheldrick, G. M. Crystal Structure Refinement with SHELXL. *Acta Crystallogr., Sect. C: Struct. Chem.* **2015**, *71*, 3−8.
(27) Altomare, A.; Cuocci, C.; Giacovazzo, C.; Moliterni, A.; Rizzi, R.; Corriero, N.; Falcicchio, A. EXPO2013: A Kit of Tools for Phasing Crystal Structures from Powder Data. *J. Appl. Crystallogr.* **2013**, *46*, 1231−1235.
(28) Altomare, A.; Campi, G.; Cuocci, C.; Eriksson, L.; Giacovazzo, C.; Moliterni, A.; Rizzi, R.; Werner, P. E. Advances in Powder Diffraction Pattern Indexing: N-TREOR09. *J. Appl. Crystallogr.* **2009**, *42*, 768−775.
(29) Boultif, A.; Louër, D. Powder Pattern Indexing with the Dichotomy Method. *J. Appl. Crystallogr.* **2004**, *37*, 724−731.
(30) Wahl, H.; Haynes, D. A.; le Roex, T. Porous Salts Based on the Pamoate Ion. *Chem. Commun. (Cambridge, U. K.)* **2012**, *48*, 1775−1777.
(31) Le Bail, A.; Duroy, H.; Fourquet, J. L. Ab-Initio Structure Determination of LiSbWO6 by X-Ray Powder Diffraction. *Mater. Res. Bull.* **1988**, *23*, 447−452.
(32) Coelho, A. A.; Kern, A. Indexing of Powder Diffraction Patterns by Iterative Use of Singular Value Decomposition. *J. Appl. Crystallogr.* **2003**, *36*, 86−95.
(33) Frisch, M. J.; Trucks, G. W.; Schlegel, H. B.; Scuseria, G. E.; Robb, M. A.; Cheeseman, J. R.; Scalmani, G.; Barone, V.; Mennucci, B.; Petersson, G. A.; Nakatsuji, H.; Caricato, M.; Li, X.; Hratchian, H. P.; Izmaylov, A. F.; Bloino, J.; Zheng, G.; Sonnenberg, J. L.; Hada, M.; Ehara, M.; Toyota, K.; Fukuda, R.; Hasegawa, J.; Ishida, M.; Nakajima, T.; Honda, Y.; Kitao, O.; Nakai, H.; Vreven, T.; Montgomery, J. A., Jr.; Peralta, J. E.; Ogliaro, F.; Bearpark, M.; Heyd, J. J.; Brothers, E.; Kudin, K. N.; Staroverov, V. N.; Kobayashi, R.; Normand, J.; Raghavachari, K.; Rendell, A.; Burant, J. C.; Iyengar, S. S.; Tomasi, J.; Cossi, M.; Rega, N.; Millam, J. M.; Klene, M.; Knox, J. E.; Cross, J. B.; Bakken, V.; Adamo, C.; Jaramillo, J.; Gomperts, R.; Stratmann, R. E.; Yazyev, O.; Austin, A. J.; Cammi, R.; Pomelli, C.; Ochterski, J. W.; Martin, R. L.; Morokuma, K.; Zakrzewski, V. G.; Voth, G. A.; Salvador, P.; Dannenberg, J. J.; Dapprich, S.; Daniels, A. D.; Farkas, O.; Foresman, J. B.; Ortiz, J. V; Cioslowski, J.; Fox, D. J. *Gaussian 09*, Revision D.01; Gaussian Inc.: Wallingford, CT, 2009.
(34) Macrae, C. F.; Bruno, I. J.; Chisholm, J. A.; Edgington, P. R.; McCabe, P.; Pidcock, E.; Rodriguez-Monge, L.; Taylor, R.; van de Streek, J.; Wood, P. A.; et al. Mercury CSD 2.0 − New Features for the Visualization and Investigation of Crystal Structures. *J. Appl. Crystallogr.* **2008**, *41*, 466−470.
(35) Rohlíček, J.; Skořepová, E.; Babor, M.; Čejka, J. CrystalCMP: An Easy-to-Use Tool for Fast Comparison of Molecular Packing. *J. Appl. Crystallogr.* **2016**, *49*, 2172−2183.
(36) Spek, A. L. Structure Validation in Chemical Crystallography. *Acta Crystallogr., Sect. D: Biol. Crystallogr.* **2009**, *65*, 148−155.
(37) Oliver-Shaffer, P.; Shapiro, G.; Chesworth, R.; Kishida, M.; Ishige, T. Crystalline Form of (R)-7-Chloro-N-(Quinuclidin-3-Yl) Benzo [B] Thiophene-2-Carboxamide Hydrochloride Monohydrate. U.S. Patent US2014/0249179, 2014.
(38) van de Streek, J.; Neumann, M. A. Validation of Molecular Crystal Structures from Powder Diffraction Data with Dispersion-Corrected Density Functional Theory (DFT-D). *Acta Crystallogr., Sect. B: Struct. Sci., Cryst. Eng. Mater.* **2014**, *70*, 1020−1032.
(39) Price, C. P.; Glick, G. D.; Matzger, A. J. Dissecting the Behavior of a Promiscuous Solvate Former. *Angew. Chem., Int. Ed.* **2006**, *45*, 2062−2066.
(40) Berziņš, A.; Zvaniņa, D.; Trimdale, A. Detailed Analysis of Packing Efficiency Allows Rationalization of Solvate Formation Propensity for Selected Structurally Similar Organic Molecules. *Cryst. Growth Des.* **2018**, *18*, 2040−2045.

DOI: 10.1021/acs.cgd.9b00648
Cryst. Growth Des. 2019, 19, 4765−4773

III

Bobrovs, R., Kons, A., Bērziņš, A., Rekis, T., Actiņš, A.

FORMATION AND TRANSFORMATIONS OF ORGANIC SALT HYDRATES: FOUR ENCENICLINE HYDROCHLORIDE MONOHYDRATES AND RESPECTIVE ISOSTRUCTURAL DESOLVATES

Cryst. Growth Des. **2018**, 18, 2100–2111

CRYSTAL GROWTH & DESIGN

Article

Cite This: *Cryst. Growth Des.* 2018, 18, 2100−2111

pubs.acs.org/crystal

Formation and Transformations of Organic Salt Hydrates: Four Encenicline Hydrochloride Monohydrates and Respective Isostructural Desolvates

Raitis Bobrovs, Artis Kons,* Agris Bērziņš, Toms Rekis, and Andris Actiņš

Faculty of Chemistry, University of Latvia, Jelgavas iela 1, Riga, LV1004, Latvia

Supporting Information

ABSTRACT: Encenicline hydrochloride (Enc-HCl) crystallizes in four different monohydrate phases, but at the same time crystallization in a nonsolvated phase is not observed, indicating that water plays a crucial role in guiding the crystallization process and ensuring structure stability. All monohydrate phases show exceptionally high stability, and the main structural motif stays intact even after dehydration, leading to isostructural (for I and II) or isomorphic (for III) desolvates. Three monohydrate phases with determined crystal structure information consists of Enc-HCl-water hexamers that are stacked into similar slabs, that are further packed identically in monohydrates I, II, and III. The features of these hexamer slabs determine the properties of the Enc-HCl monohydrates and dehydrates, the dehydration mechanism, and stability of each phase. It was justified that in the Enc-HCl system efficient intermolecular interactions provided by the incorporation of water in the crystal structure play a crucial role in stabilization of the structures.

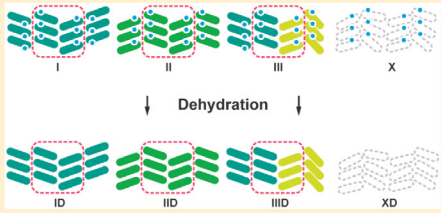

1. INTRODUCTION

Polymorphism—the ability of a compound to crystallize in more than one crystalline phase—is a well-known phenomenon.[1−3] Additionally, it is common that in the crystallization solvent molecules are incorporated into the crystal lattice in a stoichiometric or unstoichiometric ratio.[4−6] The largest number of solvates contain water (thus are hydrates), and it is reported that at least one-third of pharmaceutical compounds are capable of forming hydrates.[2,7] The identity of the solid form obtained in the manufacturing process has particular importance for pharmaceutical molecules as different polymorphs, and, particularly, solvates have different stability,[8] mechanical properties,[9−11] and bioavailability (linked to the different solubility[12]).

The main structural driving forces of solvate formation are the ability of the solvent to compensate for unsatisfied potential intermolecular interactions, particularly hydrogen bonds, between the host molecules,[13,14] and the ability to decrease the void space and/or lead to more efficient packing,[15−18] with most solvates including contributions from both of these driving forces.[15,19] Thus, the ability of water to form multiple hydrogen bonds along with its small size leads to the observed high prevalence of hydrates, both if there is an imbalance in the number of acceptors and donors in the host molecule,[20] and also if the incorporation of water molecules just leads to more efficient intermolecular interactions.[21,22] Meanwhile, the frequent presence of water in the crystallization process and in the environment provides the widespread discovery of hydrates.

Primarily based on the moisture sorption/desorption behavior, hydrates are divided in stoichiometric and nonstoichiometric hydrates, where stoichiometric hydrates show step-shaped sorption/desorption isotherms characterized by a fixed water content over a specific relative humidity (RH) range, whereas nonstoichiometric hydrates have a continuously variable composition over a certain RH range not associated with any significant change in the crystal lattice, except for some anisotropic expansion of the network to accommodate the water.[23−25] As water molecules are essential for the preservation of the crystal structure, dehydration of stoichiometric hydrates leads to different crystal structures or amorphous phases, and commonly involves significant molecule rearrangement.[26−28] Dehydration of nonstoichiometric hydrates, however, mostly produces isomorphic dehydrate—a one-component phase that exhibits the main structural features of its parent phase,[29,30] although often such dehydration leads to loss of crystallinity, and the obtained phase is partially amorphous.[26]

While about two-thirds of all the organic compounds are shown to exist in more than one crystalline phase,[2,3] polymorphism of multicomponent systems (solvates and cocrystals) is reported and studied less often than that in single component systems.[31,32] The most studied polymorphic multicomponent system is gallic acid monohydrate because of

Received: November 8, 2017
Revised: February 21, 2018
Published: March 1, 2018

DOI: 10.1021/acs.cgd.7b01561
Cryst. Growth Des. 2018, 18, 2100−2111

its fivepolymorphic forms: I, II, III, IV, and V.[33,34] Olanzapine has three polymorphs of its dihydrate with reported crystal structures (forms B, D, and E).[35] Here we are presenting a study of another multicomponent system crystallizing in multiple polymorphic forms. Encenicline (*N*-[(3*R*)-1-azabicyclo[2.2.2]oct-3-yl]-7-chloro-1-benzothiophene-2-carboxamide) hydrochloride (Enc-HCl, Figure 1) is a partial, selective

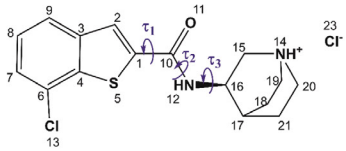

Figure 1. Molecular structure of encenicline hydrochloride (Enc-HCl) with the numbering of non-hydrogen atoms.

agonist of the α-7 nicotinic acetylcholine receptor. It is being developed for the treatment of cognitive deficits in schizophrenia and Alzheimer's disease. Enc-HCl is reported to exist in three monohydrate phases (I, II, and X)[36] with phases I and II being related enantiotropically, and phases I and X being related monotropically. However, no information on their crystal structures or phase transformations upon dehydration is available.

In this study we now report a fourth polymorph of Enc-HCl monohydrate (form III) and present crystal structures for three Enc-HCl monohydrate polymorphs and the respective dehydrated phases. The aim of this study was to use the obtained crystal structure information to explain and rationalize the relative stability of the Enc-HCl monohydrate polymorphs, try to understand the structural features leading to formation of the four obtained structurally similar hydrates, and study the dehydration mechanism of Enc-HCl monohydrates.

2. RESULTS AND DISCUSSION

2.1. Crystallographic Characterization of Enc-HCl Monohydrates and Their Dehydrates. Our research revealed that besides the three reported monohydrate phases (I, II, and X), Enc-HCl monohydrate also exists in form III. The desolvation (over P_2O_5 at 30 °C or at elevated temperature) of each polymorph of monohydrate results in a different phase with a powder X-ray diffraction (PXRD) pattern similar to that of the respective hydrate. The desolvates are designated as I_D, II_D, III_D, and X_D, respectively. In high relative humidity, a nonstoichiometric hydrate II′ with a PXRD pattern similar to that of monohydrate II is obtained. Crystal structures for three of these Enc-HCl monohydrate polymorphs, their respective dehydrates, and nonstoichiometric hydrate were determined from the PXRD data (form I, I_D, II_D, and III_D) or from single crystal X-ray diffraction (SCXRD) data (forms II, III, and II′). Crystallographic data for all forms are shown in Table 1. The correctness of the structures calculated from the PXRD patterns was confirmed by the good agreement between experimental and calculated diffraction patterns (Rietveld fit for form I is shown in Figure 2, and for the dehydrated phases in Figure S3), as well as by the geometry optimization in Quantum ESPRESSO[37] introducing only small changes (RMSD < 0.13 Å)[38] in the crystal structures (comparison of solved and optimized crystal structures are given in Figure S4). Structural information on the fourth monohydrate polymorph and its dehydrate was not determined due to its disordered nature (as suggested by the wide peaks in PXRD patterns, see Figure S1). However, the highly similar solid-state NMR spectra for all four Enc-HCl monohydrates (Figure S2) suggest that building blocks in the crystal structure of the X form is highly similar to those in the remaining monohydrates.

Enc-HCl monohydrate form I crystallizes in the $P3_221$ space group, whereas forms II and III crystallize in the *C*2 space group, with identical space groups maintained for the corresponding dehydrate forms I_D, II_D, and III_D. Also II′ crystallizes in the *C*2 space group, with the crystal structure nearly identical to that of II. Thus, II can be considered a limiting structure of nonstoichiometric II′ with water content corresponding to monohydrate stoichiometry (see Section 2.3.3).

Although encenicline cation has three flexible dihedral angles, conformation of the encenicline cation in all crystal structures shows only small differences (Figure 3, see more details in the Supporting Information), with the same conformation also maintained in the Enc-HCl dehydrates. Therefore, all three Enc-HCl monohydrates can be considered as packing polymorphs.

2.1.1. Intermolecular Interactions and Packing in Enc-HCl Monohydrates. The main building blocks in all monohydrate crystal structures are hexamers. Form I consists of Enc-HCl hexamers 1 (Figure 4), where two encenicline cations (through quinuclidine groups) interact with two chloride anions and two water molecules through N12−H···O22, O22−H···Cl23, and N14−H···Cl23 hydrogen bonds (graph set $R_6^4(18)$), thus employing water as hydrogen bond acceptor and donor. Form II consists of hexamers 2 (Figure 4), where the water forms hydrogen bond with carbonyl group (O11), instead of the amide group (N12−H) as in hexamer 1; thus hexamer 2 is connected through N14−H···Cl23, O22−H···Cl23, and O22−H···O11 hydrogen bonds ($R_6^4(22)$), with water employing both hydrogen bond donors.

Unlike form I and II, form III crystallizes with two cations and anions in the asymmetric unit. One of the encenicline cations forms the previously mentioned hexamer 1 (an overlay of hexamers 1 in form I and form III is given in Figure S6). The second encenicline cation of the asymmetric unit forms hydrogen bonded hexamer 3, where two encenicline cations are connected through N35−H···O46−H···Cl45···H−N37 and N37−H···Cl45···H−O46−H···O34 hydrogen bonds ($R_6^4(20)$). Unlike hexamers 1 and 2 that have symmetrical graph sets, hexamer 3 is not bonded in a symmetrical graph set ring, and each of the two water molecules employ different hydrogen bonding functions. Both hexamers formed from the symmetrically different encenicline cations in form III are not hydrogen bonded with each other.

Additional to connecting Enc-HCl moieties within the hexamers, the water molecules also interconnect these hexamers through hydrogen bonds O22−H···O11 or N12−H···O22 forming chains $C_2^2(6)$ along the *b* axis in form I, and along the *a* axis in form II. Such a hydrogen bonding pattern results in individual hexamer slabs that are stacked in the (001) direction (along the *ab* plane) in all monohydrates (see Figure 5). Thus, Enc-HCl monohydrate I is constructed from hexamer 1 molecular slabs (further identified as slab 1), monohydrate II − slabs formed from hexamers 2 (slab 2), whereas form III − from alternating slabs 1 and slabs 3 (constructed from hexamers 3). In Figure 5 the identical slabs 1 in forms I and III are marked with a light blue rectangle. By considering the

DOI: 10.1021/acs.cgd.7b01561
Cryst. Growth Des. 2018, 18, 2100−2111

Table 1. Crystal Data for Polymorphs of Enc-HCl Monohydrate, Their Dehydrates, and Nonstoichiometric Hydrate II′

	I	II	II′	III	I_D	II_D	III_D
empirical formula	$C_{16}H_{20}Cl_2N_2O_2S$	$C_{16}H_{20}Cl_2N_2O_2S$	$C_{16}H_{19.08}Cl_2N_2O_{2.53}S$	$C_{16}H_{20}Cl_2N_2O_2S$	$C_{16}H_{18}Cl_2N_2OS$	$C_{16}H_{18}Cl_2N_2OS$	$C_{16}H_{18}Cl_2N_2OS$
sample type	powder	single crystal	single crystal	single crystal	powder	powder	powder
crystal system	trigonal	monoclinic	monoclinic	monoclinic	trigonal	monoclinic	monoclinic
space group	$P3_221$	$C2$	$C2$	$C2$	$P3_221$	$C2$	$C2$
a, Å	7.3310(3)	12.9266(4)	12.9556(16)	12.4528(3)	7.4020(3)	12.5729(6)	12.9587(8)
b, Å	7.3310(3)	7.0801(2)	7.1006(11)	7.4435(2)	7.4020(3)	7.7428(4)	7.3161(5)
c, Å	58.3338(19)	20.3955(8)	20.393(3)	39.4052(9)	55.501(2)	18.7170(8)	37.069(2)
α, °	90	90	90	90	90	90	90
β, °	90	106.8611(13)	106.523(6)	98.7689(11)	90	104.652(11)	97.239(19)
γ, °	120	90	90	90	120	90	90
V, Å^3	2715.1(3)	1786.38(10)	1798.5(4)	3609.87(15)	2633.5(3)	1762.84(17)	3486.4(4)
ρ_{calc} g·cm^{-3}	1.377	1.395	1.417	1.381	1.352	1.346	1.361
Z/Z'	6/1	4/1	4/1	8/2	6/1	4/1	8/2
temperature, K	293(2)	193(2)	193(2)	193(2)	293(2)	293(2)	293(2)
$2\theta_{min} - 2\theta_{max}$/increment, °	3.0−70.0/0.01				3.0−70.0/0.01	3.0−70.0/0.01	3.0−70.0/0.01
R_{wp}, %	2.97				3.93	3.96	2.60
R_p, %	2.12				2.75	2.78	3.54
R_{exp}, %	0.71				1.40	1.06	1.29
R_1 (wR_2), %		4.71(8.97)	8.23(18.35)	7.16(19.46)			
rel. energy, kJ·mol^{-1}[a]	7	0	*b*	15			
rel. energy, kJ·mol^{-1}[c]					0	8	0

[a]Total monohydrate energy, kJ·mol^{-1} (relatively to II). [b]Cannot be compared due to the different chemical composition. [c]Total anhydrate energy, kJ·mol^{-1} (relatively to II_D).

DOI: 10.1021/acs.cgd.7b01561
Cryst. Growth Des. 2018, 18, 2100−2111

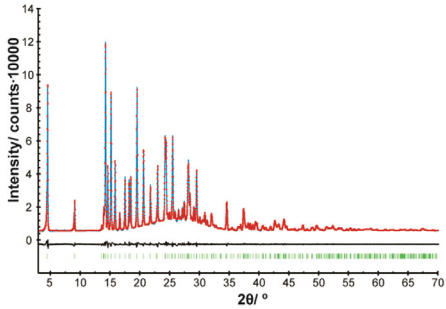

Figure 2. Final Rietveld fit for encenicline hydrochloride form I: red crosses - measured data points; blue line - calculated profile; black line - difference curve; green tick marks - calculated peak positions.

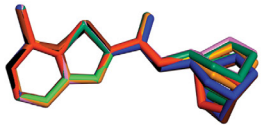

Figure 3. Overlay of the encenicline hydrochloride cation in I (blue), II (black); III molecule A (brown); III molecule B (green); I_D (orange); II_D (pink); III_D molecule A (red); III_D molecule B (yellow).

arrangement of water molecules and their involvement in the hydrogen bonding pattern, all these Enc-HCl monohydrates are classified as isolated site hydrates.

There are no hydrogen bonds between the described hydrogen bonded slabs, and the adjacent slabs interact with dispersion interactions (CH···π) and halogen bonds C−Cl···Cl formed by the benzothiophene groups (indicated with red rectangle in Figure 5). Analysis of packing similarity in XPac[39] identified that this two-dimensional (2D) layer of interacting benzothiophene moieties is identical in all Enc-HCl monohydrates and, in fact, appears also in all structures of the dehydrated phases. This suggest that this stacked motif plays a crucial role in formation and stabilization of Enc-HCl crystal structures, or is by far the best way to effectively pack these differently stacked layers of hexamers.

The observed molecule stacking pattern partly could be attributed to the fact that the best proton donor and acceptor groups are located in one side of the molecule, and while these groups are involved in intermolecular hydrogen bonds, thus forming the previously mentioned hexamers, the other side of the molecule is electrostatically rather neutral and have an ability to form only weaker intermolecular interactions, like the observed dispersion interactions and halogen bonds.

2.1.2. Intermolecular Interactions and Packing in Enc-HCl Dehydrated Phases. Although usually isostructural/isomorphic desolvates arise from desolvation of nonstoichiometric solvates,[2] the dehydrates of Enc-HCl monohydrates are structurally very similar and shares the main structural characteristics with the respective hydrates (see Figure 6), even though the Enc-HCl monohydrates are all stoichiometric (see Section 2.3.3). Analysis of packing similarity in XPac confirmed that Enc-HCl monohydrates I and II dehydrates into respective isostructural dehydrated phases (3D structural similarity is maintained), while differences of III and III_D are slightly higher with 2D structural similarity between these forms, which therefore can be considered isomorphic.

Upon the dehydration the hexamer 1 motif in both forms I and III loses the water molecule "bridge" and changes to tetramer ($R_4^2(14)$) where two proton donor groups of two encenicline cations are connected through two chloride anions (Figure 4). The dehydration leads to a drop of packing efficiency (calculated using Platon[40]) from 68.0% in form I to 66.8% in form I_D. The drop of the packing efficiency is also present for the dehydration of form II (from 69.4% to 66.6%), whereas a slight increase is observed during the dehydration of form III (68.2 to 69.0%).

During the dehydration hexamer 2 and hexamer 3 motifs undergo more significant changes of hydrogen bonding pattern: the bonding between amide group of encenicline cation and carbonyl group of another encenicline cation through chloride anion and water molecule changes into bonding between two amide groups of encenicline cations connected through a chloride anion (Figure 4). These new hydrogen bonding patterns do not form any cyclic motifs, but chains $C_2^1(7)$ along the *b* axis in both forms II_D and III_D (Figure 4) are formed instead. These chains are cross-linked to each other along the *a* axis by a weak hydrogen bond C9═O1···H−C8 (with O1···H distance 2.28 Å in II_D and 2.27 Å in III_D).

While the hydrogen bonding pattern in all dehydrated phases changes if compared to that in the monohydrates, the dispersion interactions between the benzothiophene groups (indicated with red rectangle in Figure 5) remain the same (see structure overlay in Figure 6), thus being one of the factors proving the high structural similarity between the monohydrates and the respective dehydrates.

The higher difference between III and III_D is caused by more significant changes of the encenicline cation position during the loss of the water from hexamer 3 present in form III (as seen in Figure S6) compared to only minor changes of encenicline cation position in the rest of the hexamers.

This in fact is consistent with the observed increase of the packing efficiency upon the dehydration of form III, in contrast to Enc-HCl monohydrates I and II. Since slab 1 in forms I and III rearranges identically, the observed packing efficiency increase must have been at the expense of a more significant rearrangement of Enc-HCl moiety within the slab 3. This assumption is additionally supported by volume of solvent accessible voids located between two encenicline cations; see the Supporting Information.

2.2. Dehydration Mechanism. Analysis of dehydration kinetics in isothermal mode (at 50, 60, 70, 80, and 90 °C) indicated that all four Enc-HCl monohydrates lose the water according to 2D phase boundary model R2 (dehydration kinetic curves are given in Figure S12).[41] More on dehydration kinetic models and their identification can be found elsewhere.[42,43] The observed dehydration behavior can easily be rationalized if we take a look at the crystal structures of Enc-HCl monohydrates. In crystal structures of all monohydrates water molecules and voids are situated in the *ab* plane between two encenicline cations forming the hexamers, and transport of water molecule in and out from the structure along the *c* axis direction is very unlikely. This means that water molecules most likely will escape in the *a* or *b* direction, and move through the available void space (see Figure 7).

DOI: 10.1021/acs.cgd.7b01561
Cryst. Growth Des. 2018, 18, 2100−2111

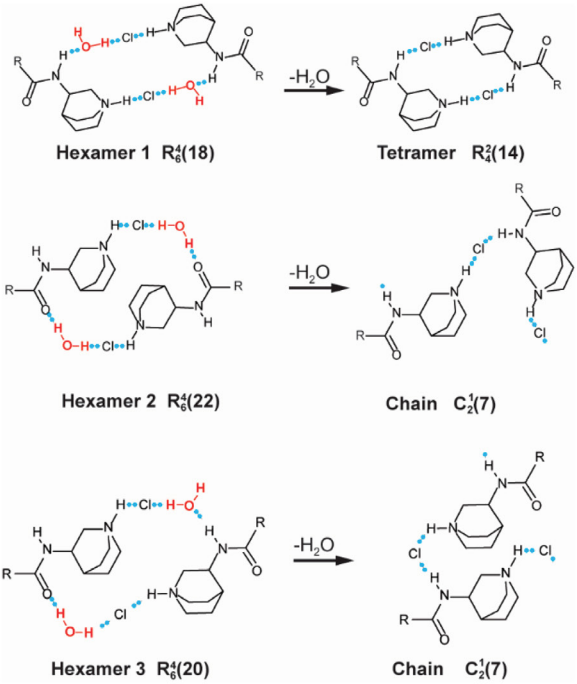

Figure 4. Characteristic hydrogen bonding patterns in Enc-HCl monohydrates and the respective dehydrates.

Such dehydration behavior results in crystal structures of dehydrates that are similar to the respective monohydrates. This is rather unusual (but have been observed previously[44,45]) for isolated site hydrates where water molecules are segregated in the pockets of the crystal structure. Typically, in isolated site hydrates, removal of the water molecules requires an appreciable driving force to ensure a disruption of the hydrate crystal structure and ensure the escape of the water molecules. While the thermal stability of all Enc-HCl monohydrates is indeed high (see Section 2.3.1), the dehydration activation energy is not particularly high (55−81 kJ·mol^{-1}, see Table S4), as the energy barrier for phase transformation between such structurally similar phases is expected to be relatively low.

While water molecules are removed from the structure through void filled plane in-between hydrogen bonded encenicline cations, the slab of stacked benzothiophene group stays intact, and, in fact, might be the reason why the main crystal structure carcass is retained. That is, the stacked benzothiophene group slab might act as a backbone that keeps Enc-HCl moieties arranged during escape of the water molecule and changes of hydrogen bonding pattern occurring at the other end of Enc-HCl moieties.

2.3. Thermodynamic and Thermal Stability of Enc-HCl Crystal Forms. *2.3.1. Thermal Stability of Enc-HCl hydrates.* First, thermal analysis (differential scanning calorimetry (DSC) and thermogravimetric (TG)) were used to evaluate the relative stability of monohydrate phases. The DSC curves of Enc-HCl monohydrates I, II, III, and X are given in Figure 8, and the corresponding thermal data are compared in Table 2. Each DSC curve has an endothermic effect between 70 °C and ∼145 °C associated with a weight loss of ∼5.0% in the TGA and thus corresponding to the dehydration of Enc-HCl monohydrates. The observed slightly increased weight loss (5.0% compared to the theoretical 4.8%) most likely is due to water adsorbed on the sample surface. Dehydration results in the respective dehydrate forms I_D, II_D, III_D, and X_D. Further, the obtained dehydrates partially melt (small endothermic effect at ∼140−160 °C) and recrystallize (exothermic effect at ∼185 °C) to another anhydrous form. The newly acquired high temperature anhydrous form IV melts at ∼285 °C. The partial melting of polymorphs I_D, II_D, III_D, and X_D is confirmed by visual inspection of the DSC pan and by thermo-microscopy measurements (see Section 6 in Supporting Information).

Additionally, a comparison of the thermal stability and phase transitions of Enc-HCl monohydrates at elevated temperature was performed by variable-temperature PXRD (VT-PXRD, see S16−S19 in SI). VT-PXRD patterns show that upon heating form I is stable up to 80 °C, forms II and III are stable up to 70 °C, and form X is stable up to 90 °C. The dehydration initiation observed in the VT-PXRD data is consistent with dehydration peak temperatures in DSC and indicates that the thermal stability decreases in a row X > I > II ≈ III. After the

DOI: 10.1021/acs.cgd.7b01561
Cryst. Growth Des. 2018, 18, 2100−2111

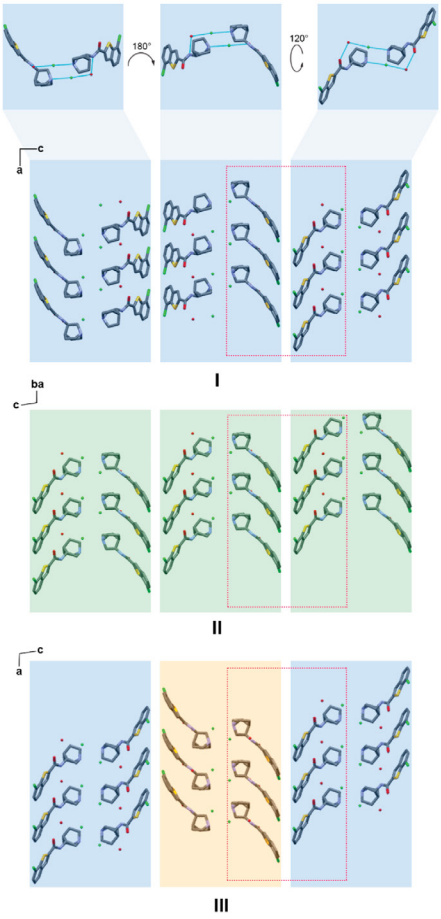

Figure 5. Comparison of crystal structure fragments from Enc-HCl monohydrate forms I, II, and III. The blue rectangle indicates slab 1 constructed by hexamers 1; green - slab 2 constructed by hexamers 2; and light orange - slab 3 constructed by hexamers 3. Top section of the figure schematically illustrates how slabs are positioned relative to each other in form I. The identically stacked fragment present in all crystal structures is indicated with a red rectangle.

dehydration all monohydrates transform to their respective dehydrated phases which are stable up to the melting, observed as appearance of an amorphous pattern (150−170 °C for X_D and 170 °C for I_D, II_D, and III_D). Further heating of all samples at 180 °C led to the appearance of characteristic peaks of polymorph IV, with complete transformation to IV occurring at 190 °C. The PXRD pattern of the obtained form IV was unchanged until the end of the experiment at 250 °C.

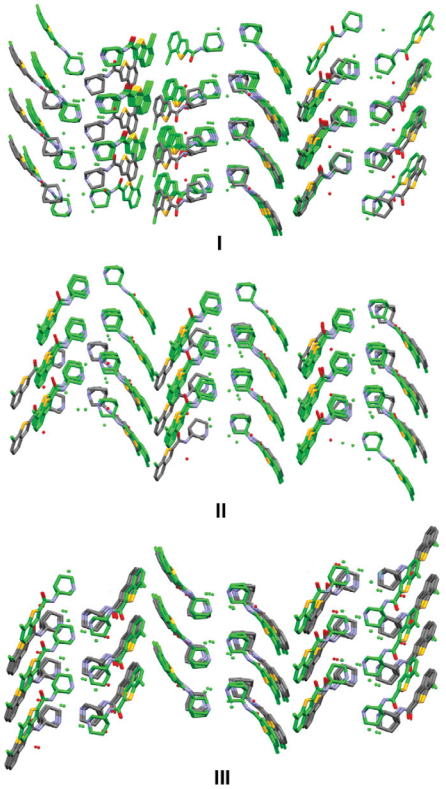

Figure 6. Overlay of structure fragments from Enc-HCl monohydrates and the respective dehydrates (dehydrate phases are green).

2.3.2. Thermodynamic Stability of Enc-HCl Forms. The relative thermodynamic stability of monohydrates was expected to be assessed on the basis of the enthalpy of fusion rule;[46] however, the lack of information on the melting behavior (incongruent or congruent) of the Enc-HCl monohydrates prevented use of the obtained melting points (see Table 2) and enthalpies (see Table S4 in Supporting Information) for this purpose. Therefore, the relative thermodynamic stability of Enc-HCl monohydrates was investigated using the computed total energy using periodic DFT calculation in Quantum ESPRESSO[47] and solubility experiments. The total energies (Table 1) of monohydrate forms I, II, and III indicate that the most stable is form II, and the least stable - form III, with the difference of the total energy of 15 kJ·mol^{-1}.

Solubility measurements were carried out at ambient temperature (Figure 9) and illustrate that form II has the lowest solubility while form III has the highest. The solubility data are consistent with the theoretical calculations and indicate that the stability of monohydrates follows the order of II > X > I > III. This is also consistent with the melting points of the

DOI: 10.1021/acs.cgd.7b01561
Cryst. Growth Des. 2018, 18, 2100−2111

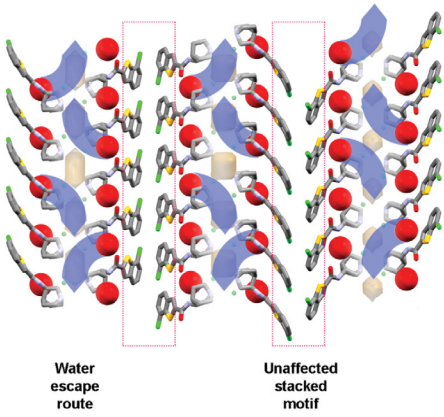

Figure 7. Schematic water escape route in crystal structure of Enc-HCl monohydrate I.

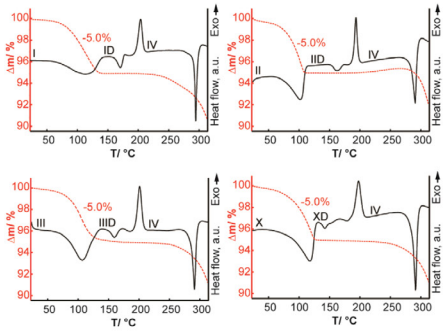

Figure 8. DSC/TG curves of Enc-HCl monohydrate forms I, II, III, and X in open cups under N_2 flow.

Table 2. Summary of Thermal Data for the Enc-HCl Crystalline Forms

	melting point (T_{on})/°C	water loss (T_{peak})/°C	weight loss/%	stoichiometry
I	151[a]	115[a]	5.0[a]	1:1
II	146	105	5.0	1:1
III	141	109	5.0	1:1
X	144	122	4.9	1:1
I_D	162			
II_D	151			
III_D	150			
X_D	139			

[a]For monohydrates, the melting point was determined in closed cups, while water loss was characterized in open cups under N_2 flow.

hydrates and the available information that I and II are related enantiotropically, while I and X – monotropically,[36] and the transition point between I and II is between the ambient temperature and melting point.

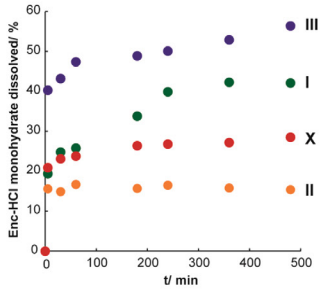

Figure 9. Dissolution profiles of Enc-HCl monohydrates in water at ambient temperature.

The theoretical calculations of Enc-HCl anhydrous form relative stability indicate that forms I_D and III_D are equally stable, whereas form II_D is less stable (total energy is higher by 8 kJ·mol^{-1}). This means that upon the dehydration the relative stability of form III noticeably increases, whereas that of form II decreases. This, alongside the increase of the packing efficiency and only 2D structural similarity between III and III_D, indicates that the highest structural rearrangement upon the dehydration results in the most significant improvement in stability of the structure.

Since dehydrated phases I_D and III_D have the same anhydrous slab 1 in their crystal structures, the noticeable stability improvement of form III_D in a pair I_D–III_D (if compared to that in pair I–III) must be at the expense of increase of packing efficiency in slab 3 upon the dehydration. Besides, the fact that form I_D and III_D have the same total energy indicates that dehydrated slabs 1 and 3 must have similar slab energy (as slab–slab interaction energies in the respective phases are nearly identical, see Section 3 in Supporting Information).

Form II, on the other hand, undergoes the smallest structure alterations among all Enc-HCl monohydrates (as confirmed by the XPac dissimilarity index). Such retaining of the structure upon the dehydration results in the most significant decrease of packing efficiency and relative stability compared to the other dehydrated phases.

2.3.3. Water Sorption/Desorption Study. The stability of the monohydrates was also evaluated by dynamic vapor sorption (DVS) of water at 30 °C. DVS experiments (Figure 10) revealed that all Enc-HCl monohydrates are very stable and lose structurally bound water only in relative humidity below 6%, by transforming into the respective dehydrates. In the relative humidity region from 10% to 50% the water content in all hydrates correspond to 1:1 stoichiometry, whereas, by increasing the relative humidity above 50%, water content in forms I, III, and X increases up to approximately 1:1.2. As no changes in the PXRD patterns are observed during the water sorption, it is safe to assume that these hydrates are stoichiometric, and the weight increase in these hydrates could be attributed to water sorption on the sample surface. When the relative humidity exceeds 90% for forms I and X, and 73% for form III, irreversible transformation to more stable form II/II′ (see below) occurs.

DOI: 10.1021/acs.cgd.7b01561
Cryst. Growth Des. 2018, 18, 2100–2111

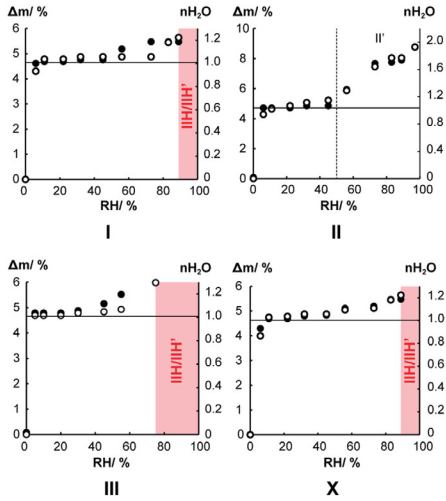

Figure 10. Water sorption/desorption isotherms of Enc-HCl at 30 °C. Solid points represent water sorption/desorption from monohydrate phase, empty points - water sorption by the dehydrate phase. Horizontal line shows water content corresponding to the monohydrate stoichiometry.

While forms I, III, and X were identified as stoichiometric in all RH range from 10% up to the observed transformation into form II/II′, the most stable Enc-HCl monohydrate form II exhibits stoichiometric behavior only up to relative humidity of 50%, while in higher relative humidity form II starts to incorporate additional water in a nonstoichiometric manner by reaching Enc-HCl/H_2O ratio of 1:1.9 at 95% RH. This water sorption in RH above 50% results in minor changes in the crystal structure, reflected as changes in the PXRD pattern (see Figure S1). The obtained phase is indicated as form II′, and the incorporated additional 0.9 mol of water is situated in the lattice in positions where there are voids in form II (Figure 11). The incorporation of the water results in increase of cell volume only by 0.7%, with increase of the *b*-axis length by 0.3% being the most significant. In form II′ no hydrogen bonds or other significant weak interactions were identified between the additionally incorporated water molecules and the other molecular moieties.

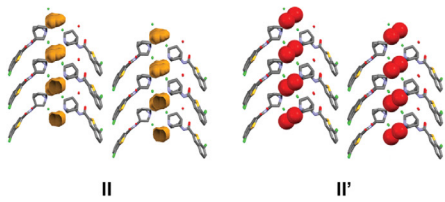

Figure 11. Structure fragments of form II and II′. Hydrogen atoms are omitted for clarity. The yellow translucent spheres in form II represent voids; red spheres in II′ represent the water molecules incorporated in nonstoichiometric manner.

The absence of hysteresis in all sorption/desorption isotherms can be related to the fact that the water molecules are situated in the crystal lattice in a way allowing fast water egress/ingress without significant distortion of the overall crystal structure (see Section 2.2, Figure 7).

As demonstrated, the water sorption/desorption behavior of all monohydrate phases is very similar (except for the II at high RH). This is due to highly similar crystal structures of the 3 monohydrate phases (and also X, as suggested by the recorded solid-state NMR spectra, see Figure S2). All crystal structures contain similar building blocks (similar slabs formed from hexamer building units, containing similar isolated voids just between the hexamers near the quinuclidine group) packed in similar way in both hydrated and dehydrated phases (see Figure S10). Meanwhile in high RH water molecules are incorporated in the crystal structure voids only in form II. It is believed that in case of forms I and III (and also X) water molecules are adsorbed on the surface, and start to penetrate the crystal structure only in relatively high RH, but apparently because of the different Enc-HCl building blocks this is possible only by causing changes of the crystal structure observed as transformation into II′.

While building blocks in form II do not allow noticeable structure contraction upon the dehydration (as described above), in high RH structure expansion of form II occurs (in *a* (+0.2%) and *b* (+0.3%) directions) allowing it to accommodate more water (up to 0.9 mol) than in the theoretically calculated void volume of the original structure of II (0.42 mol). Forms I and III, on the other hand, are prone to more noticeable void volume and structure contraction during the dehydration (the cell volume in pair I/I_D decreases by 3.1%, in III/III_D by 6.4%, while in pair II/II_D only by 1.3%), but does not allow structure expansion to accommodate additional water in the structure.

2.4. Role of the Water. It can easily be seen there is an imbalance of hydrogen bond donors and acceptors present in Enc-HCl (two donors and three acceptors, counting chloride anion as two acceptors). Thus, all dehydrated structures contain an unused hydrogen bond acceptor group (carbonyl group) in their crystal structures, and additionally appear to some extent frustrated with respect to their packing efficiency (except for form III_D).

It is not possible to obtain the described anhydrous phases in any other way than by dehydration of the respective monohydrates. Moreover, no nonsolvated Enc-HCl phase crystallized from solution has been reported so far. This leads us to think that the solvent, water in this case, may play a crucial role in enabling and guiding crystallization of Enc-HCl.

The introduction of the water molecules in the system brings additional proton donors and acceptor in the system by providing a possibility to diversify options for hydrogen bond formation and turn at least one of the proton acceptor sites into proton donor. Water molecules in all three Enc-HCl monohydrates act as a "bridge" that connects the carbonyl group, amide group, and chlorine anion. This is clearly visible if we take a look at hydrogen bonding of carbonyl group—while the carbonyl group of the encenicline cation is involved in hydrogen bonding with the amide group of the adjacent encenicline cation through water molecules in all monohydrate phases, in dehydrate phases a similar connection is not present. Thus, the main role of the water here is to form an efficient hydrogen bond network and compensate the mismatch

DOI: 10.1021/acs.cgd.7b01561
Cryst. Growth Des. 2018, 18, 2100−2111

between the hydrogen bond donor and acceptor groups in Enc-HCl, while only in II′ the nonstoichiometrically incorporated water can be considered as a space filler (see Section 2.3.3).

Despite the fact that water molecules provide better opportunities for the hydrogen bonding and ensure higher packing efficiency of Enc-HCl hydrates if compared to the respective dehydrated phases (except for III), monohydrates also have larger solvent accessible voids between the encenicline cations than the respective anhydrous phases (see Section 4 in Supporting Information). This apparently is because the hexamer motifs having water molecules in-between Enc-HCl moieties are bigger than the analogue dehydrated motifs, and particularly this part of the structure cannot pack as close, by compensating it with significantly more efficient intermolecular interactions.

3. CONCLUSIONS

Enc-HCl crystallizes in four different monohydrate phases, but at the same time crystallization in a nonsolvated phase is not observed, indicating that water plays a crucial role in guiding the crystallization process and ensuring structure stability. Interestingly, all the obtained hydrates show very high stability, and lose structural water in rather harsh conditions (both in the DVS experiments and thermal dehydration), leaving the main structural motifs intact by dehydrating into respective isostructural (I and II) or isomorphic (III) desolvates. To the best of our knowledge, this is rather unusual behavior for stoichiometric hydrates.

The available hydrogen bond donors and acceptors and the hydrogen bond forming capability of water results in several possibilities to form efficient hydrogen bond network, leading to the different polymorphs of Enc-HCl. Meanwhile, there appears to be only one efficient way for stacking the aromatic rings, leading to high similarity of the crystal structures for all Enc-HCl monohydrates.

Despite having some conformational freedom, the encenicline cation has the same conformation in all crystalline phases. All three monohydrate phases with determined crystal structure information consist of Enc-HCl-water hexamers that are stacked into similar slabs which in all forms are packed in an identical way. Crystal structures of Enc-HCl monohydrates I and II consist of different Enc-HCl-water hexamers (hexamer 1 and hexamer 2, respectively), while form III, having two different Enc-HCl moieties in asymmetric unit, consists of two different hexamer motifs: the hexamer 1 and hexamer 3.

The slabs formed from these hexamers determine properties of the Enc-HCl monohydrates and dehydrates, including the stability of each phase and dehydration mechanism. Hexamer 2 makes the most stable monohydrate structure, which expands in high relative humidity allowing incorporation of additional water in the structure leading to nonstoichiometric hydrate II′, whereas such an arrangement does not allow effective structure contraction upon the dehydration. Hexamer 1 and 3 motifs, on the other hand, allow better structure contraction during the dehydration leading to more stable dehydrated phases, but it does not allow crystal structure expansion and water molecule incorporation in their structures in high relative humidity. Therefore, in high relative humidity Enc-HCl form I and III transforms to form II′. The least stable is the hexamer 3 motif in form III, having the lowest packing efficiency and largest void space, making form III the least stable of the monohydrates, whereas during dehydration this motif undergoes the most significant structural changes by transforming in a motif that is as stable as the motif obtained by dehydrating hexamer 1, making anhydrous form III_D as stable as form I_D.

In general, higher packing efficiency is observed for the Enc-HCl hydrates. However, at the same time they also have larger solvent accessible voids between the encenicline cations. This, together with the fact that all Enc-HCl monohydrates are exceptionally stable, while the dehydrates are rather unstable, indicates that in the Enc-HCl system efficient intermolecular interactions provided by the incorporation of water in the crystal structure play a crucial role in structure stabilization.

All monohydrate phases dehydrate according to the 2D phase boundary model R2, meaning that escape of water molecule from the structure takes place in two directions—through the available void space in the 001 plane.

4. EXPERIMENTAL SECTION

4.1. Materials. *R*-Encenicline hydrochloride (purity >99%) was obtained from JSC Olainfarm (Olaine, Latvia). The sample consisted of monohydrate form II. Inorganic compounds and organic solvents of analytical grade were purchased from commercial sources and used without further purification.

4.2. Crystal Phase Preparation. Enc-HCl monohydrate I was obtained by crystallizing from mixture of acetonitrile/water (95/5 v/v), form III – from mixture of methanol/water (95/5 v/v), and form X – from mixture of ethanol/water (95/5 v/v). Form II was obtained by crystallizing form water or solvent mixtures, where water content was above 5%. Dehydration of forms I, II, III, and X at 80 °C for 30 min (or over P_2O_5 at 30 °C for 3 days) resulted in respective isostructural dehydrated phases I_D, II_D, III_D, and X_D.

4.3. Single Crystal X-ray Diffraction (SCXRD). The single-crystal X-ray diffraction data for II, II′, and III were collected at 173 K on a Nonius Kappa CCD diffractometer using Mo Kα radiation (λ = 0.71073 Å) and Oxford Cryostream open-flow nitrogen cryostat for sample temperature control. The structures were solved by direct methods in OLEX2[47] software and refined by full-matrix least-squares on F^2 using SHELXL.[48] All non-hydrogen atoms were refined anisotropically. Mercury 3.8[49] software was used for crystal structure analysis and simulation of powder X-ray diffraction patterns based on the crystal structure data.

4.4. Powder X-ray Diffraction. For routine measurements, the PXRD patterns were recorded on a Bruker D8 Advance diffractometer using copper radiation (CuK_α = 1.54180 Å) with Bregg-Brentano geometry and LynxEye (1D) detector. The tube voltage and current were set to 40 kV and 40 mA respectively. The divergence and antiscattering slits were set at 0.6 mm and 8 mm, respectively. The patterns were recorded from 3° to 30° on the 2θ scale, using a scan speed of 0.2 s/0.02°. When necessary, to prevent the atmospheric humidity effect, samples were covered with a 10 μm polyethylene film.

For structure determination, PXRD patterns were recorded on a Bruker D8 Discover diffractometer using copper radiation (CuK_α = 1.54180 Å) in transmission mode and LynxEye (1D) detector. The tube voltage and current were set to 40 kV and 40 mA. The sample was loaded into a special glass Nr. 10 capillary (0.5 mm diameter), mounted in-between upper and lower knife edge, and rotated at 60 rpm throughout the measurement. The diffractometer incident beam path was equipped with a Göbel mirror, Soller slit, and a 0.6 mm divergence slit, while the diffracted beam path was equipped with only a Soller slit. The diffraction patterns were recorded on the 2θ scale from 3 or 4.5 to 70° at scan speed of 36 s/0.01°.

VT-PXRD experiments were determined on a Bruker D8 Discover diffractometer equipped with MRI temperature chamber and Asyco controller. Copper radiation (CuK_α = 1.54180 Å) with Bregg-Brentano geometry and LynxEye (1D) detector was used. The divergence and antiscattering slits were set at 0.6 mm and 8 mm, respectively. The patterns were recorded from 3° to 30° on the 2θ scale, using a scan speed of 0.5 s/0.02°.

4.5. Thermal Analysis Methods. DSC/TGA analysis were performed with a Mettler Toledo TGA/DSC2 instrument. Open

DOI: 10.1021/acs.cgd.7b01561
Cryst. Growth Des. 2018, 18, 2100−2111

100 μL aluminum pans were used. Heating of samples from 25 to 310 °C was performed at the heating rate of 10 °C/min under a 100 mL/min nitrogen flow. The sample mass was approximately 7−15 mg.

Sealed cup experiments were performed on a Setaram DSC 111 instrument from 70 to 200 °C at the heating rate 5 °C/min.

Thermomicroscopy experiments were performed on a Leica Laborlux 12 POL S microscope, equipped with hot stage (temperature control unit Newtronic), and Leica DFC450 digital camera. Heating rate was 10 °C/min.

Isothermal dehydration studies were carried out at 50−90 °C using a Mettler Toledo TGA/DSC2 apparatus. The heater unit was preset to the required temperature allowing fast stabilization of the necessary temperature at the start of the experiment. The sample mass was 8.0 ± 1.0 mg, and the nitrogen flow rate was 100 ± 10 mL·min^{-1}.

4.6. Solid-State NMR Measurements. High-resolution solid-state NMR spectra were obtained using a Bruker Avance III HD spectrometer operating at 125.67 MHz for ^{13}C (499.72 MHz for ^{1}H) with a 4.0 mm (rotor o.d.) MAS probe. The spectra were recorded at ambient temperature under MAS conditions using cross-polarization with a sample spin rate of 10 kHz. Spectra were referenced with respect to external neat TMS by setting the high-frequency signal from a replacement sample of adamantane to 38.4 ppm.

4.7. Solubility Determination. The solubility studies for powder samples of Enc-HCl monohydrate were performed in aqueous media at 25 °C. Excess amounts (∼20 mg) of samples were suspended in 2.5 mL of water in a 10 mL vial, and the slurries were stirred at 70 rpm using a magnetic stirrer. The suspensions were withdrawn with a 1 mL syringe and passed through a nylon filter (0.2 μm). The filtered aliquots were sufficiently diluted, and the content of encenicline was assayed using HPLC (Waters 2690) equipped with an ACE C18 column (5 μm, 3.0 mm × 150 mm), temperature of the column was set at 35 °C. Separations were conducted using the mobile phases: A - pH 5.5 phosphate buffer and acetonitrile (4:1), B - acetonitrile, at isocratic elution of 0.8 mL·min^{-1} with eluent composition A:B = 88:12. An injected volume of 10 μL was used. Detection wavelength in the UV−visible was set at 307 nm. A linear calibration curve was constructed at a concentration range of approximately 5−100 μg·mL^{-1} and with an R^2 of 0.99. All measurements were made in triplicates.

4.8. Water Vapor Sorption/Desorption Studies. Water vapor sorption and desorption were studied in desiccators with controlled relative humidity. PXRD was used to analyze the phase transitions taking place. To provide a variety of RH values, saturated salt solutions and P_2O_5 were used. The salts used for this experiment and the corresponding RH values were LiBr (6%), LiCl (11%), CH_3CO_2K (23%), $MgCl_2$ (32%), NaBr (56%), KI (68%), NaCl (75%), KCl (84%), K_2SO_4 (97%), and also P_2O_5 (∼0%).[50]

4.9. Structure Determination from Powder X-ray Diffraction Data. Indexing, space group determination, structure solution, and Rietveld refinement were performed using EXPO2014.[51] The unit cell dimensions were determined by applying the N-TREOR09[52] and Dicvol06[53] indexing procedures with a set of 20−25 reflections found in the 4.5−30° 2θ range. Space group determination was carried out using a statistical assessment of systematic absences, and Z' was determined based on density considerations. The cell and diffraction pattern profile parameters were refined according to the LeBail algorithm.[54] The background was modeled by a 20th-order polynomial function of the Chebyshev type; peak profiles were described by the Pearson VII function.

The initial geometry of molecules was taken from the crystal structure of form II. The Monte Carlo/Simulated Annealing technique was used to constantly adjust the conformation, position, and orientation of the trial model in the unit cell in order to maximize the agreement between calculated and measured diffraction data.

The Rietveld refinement was carried out using soft constraints on bond distances and angles. In the Rietveld refinement, profile and cell parameters, isotropic thermal vibration, and preferred orientation parameters (using March-Dollase model[55,56]) were optimized to get an optimum crystal structure. The planar phenyl ring was treated as a rigid body. The final Rietveld refinement showed a good agreement between the observed and the calculated profiles (see Figure S3). Relevant crystal data and refinement details for I, I_D, II_D, and III_D are summarized in Table 1.

4.10. Theoretical Calculations. Crystal structures of forms I, II, II′, III, I_D, II_D, and III_D were optimized using the DFT PWscf package within Quantum ESPRESSO.[57] Calculations were performed with the PBE[57] exchange correlation functional with vdW interactions treated according to the D2 method of Grimme,[58] using ultrasoft pseudopotentials with a wave function cutoff of 44 Ry. Pseudopotentials as well as energy and force thresholds for structural relaxation were used as described in the literature.[59] A k-point grid of 2 × 2 × 2 was used.

Conformer energies were calculated in Gaussian09[60] at the B3LYP/6-311G(d,p) level for molecular geometries directly extracted from the crystal structures after the geometry optimization in Quantum ESPRESSO.

■ ASSOCIATED CONTENT

Supporting Information

The Supporting Information is available free of charge on the ACS Publications website at DOI: 10.1021/acs.cgd.7b01561.

Characterization of solid phases; conformation analysis; quantum chemical calculations of interactions between molecular slabs; dehydration of Enc-HCl monohydrate phases; thermal stability and phase transitions; determination of the relative thermodynamic stability of Enc-HCl monohydrates (PDF)

Accession Codes

CCDC 1584615−1584621 contain the supplementary crystallographic data for this paper. These data can be obtained free of charge via www.ccdc.cam.ac.uk/data_request/cif, or by emailing data_request@ccdc.cam.ac.uk, or by contacting The Cambridge Crystallographic Data Centre, 12 Union Road, Cambridge CB2 1EZ, UK; fax: +44 1223 336033.

■ AUTHOR INFORMATION

Corresponding Author

*Phone: +(371)-67033907. E-mail: artis.kons@lu.lv.

ORCID

Raitis Bobrovs: 0000-0002-0221-8658

Artis Kons: 0000-0002-4055-8442

Agris Bērziņš: 0000-0002-4149-8971

Toms Rekis: 0000-0001-5128-4611

Notes

The authors declare no competing financial interest.

■ ACKNOWLEDGMENTS

The authors gratefully acknowledge JSC Olainfarm for supplying encenicline hydrochloride, Sergey Belyakov and Inese Sarcevica (Latvian Institute of Organic Synthesis) for the help with single-crystal structure determination, and Ligita Rutkovska for performing some of the experiments as part of her Master's thesis. The authors also thank Professors Heike Lorenz and Andreas Seidel-Morgenstern (Max Planck Institute for Dynamics of Complex Technical Systems in Magdeburg) for the opportunity to perform fixed volume DSC and hot-stage microscopy measurements, Martins Balodis for solid-state NMR measurements (Department of Chemistry, Durham University), and Alla Petrenko and Igors Boikovs for Enc-HCl solubility determination (JSC Olainfarm).

■ REFERENCES

(1) Bernstein, J. *Polymorphism in Molecular Crystals*; Clarendon Press: Oxford, UK, 2002.

DOI: 10.1021/acs.cgd.7b01561
Cryst. Growth Des. 2018, 18, 2100−2111

(2) Hilfiker, R. *Polymorphism: In the Pharmaceutical Industry*; Wiley-VCH: Weinheim, 2006.
(3) Brittain, H. G. Polymorphism and Solvatomorphism 2010. *J. Pharm. Sci.* **2012**, *101*, 464−484.
(4) Cruz-Cabeza, A. J.; Reutzel-Edens, S. M.; Bernstein, J. Facts and Fictions about Polymorphism. *Chem. Soc. Rev.* **2015**, *44*, 8619−8635.
(5) Bhardwaj, R. M.; Price, S. L.; Reutzel-Edens, S. M.; Miller, G. J.; Oswald, I. D. H.; Johnston, B. F.; Florence, A. J. Exploring the Experimental and Computed Crystal Energy Landscape of Olanzapine. *Cryst. Growth Des.* **2013**, *13*, 1602−1617.
(6) Campeta, A. M.; Chekal, B. P.; Abramov, Y. A.; Meenan, P. A.; Henson, M. J.; Shi, B.; Singer, R. A.; Horspool, K. R. Development of a Targeted Polymorph Screening Approach for a Complex Polymorphic and Highly Solvating API. *J. Pharm. Sci.* **2010**, *99*, 3874−3886.
(7) Stahly, G. P. Diversity in Single- and Multiple-Component Crystals. The Search for and Prevalence of Polymorphs and Cocrystals. *Cryst. Growth Des.* **2007**, *7*, 1007−1026.
(8) Yu, L.; Stephenson, G. A.; Mitchell, C. A.; Bunnell, C. A.; Snorek, S. V.; Bowyer, J. J.; Borchardt, T. B.; Stowell, J. G.; Byrn, S. R. Thermochemistry and Conformational Polymorphism of a Hexamorphic Crystal System. *J. Am. Chem. Soc.* **2000**, *122*, 585−591.
(9) Sun, C.; Grant, D. J. W. Influence of Crystal Structure on the Tableting Properties of Sulfamerazine Polymorphs. *Pharm. Res.* **2001**, *18*, 274−280.
(10) Khomane, K. S.; More, P. K.; Bansal, A. K. Counterintuitive Compaction Behavior of Clopidogrel Bisulfate Polymorphs. *J. Pharm. Sci.* **2012**, *101*, 2408−2416.
(11) Picker -Freyer, K. M.; Liao, X.; Zhang, G.; Wiedmann, T. S. Evaluation of the Compaction of Sulfathiazole Polymorphs. *J. Pharm. Sci.* **2007**, *96*, 2111−2124.
(12) Pudipeddi, M.; Serajuddin, A. T. M. Trends in Solubility of Polymorphs. *J. Pharm. Sci.* **2005**, *94*, 929−939.
(13) Tieger, E.; Kiss, V.; Pokol, G.; Finta, Z.; Rohlíček, J.; Skořepová, E.; Dušek, M. Rationalization of the Formation and Stability of Bosutinib Solvated Forms. *CrystEngComm* **2016**, *18*, 9260−9274.
(14) Zhang, X.; Zhou, L.; Wang, C.; Li, Y.; Wu, Y.; Zhang, M.; Yin, Q. Insight into the Role of Hydrogen Bonding in the Molecular Self-Assembly Process of Sulfamethazine Solvates. *Cryst. Growth Des.* **2017**, *17*, 6151−6157.
(15) Price, C. P.; Glick, G. D.; Matzger, A. J. Dissecting the Behavior of a Promiscuous Solvate Former. *Angew. Chem., Int. Ed.* **2006**, *45*, 2062−2066.
(16) Bērziņš, A.; Trimdale, A.; Kons, A.; Zvaniņa, D. On the Formation and Desolvation Mechanism of Organic Molecule Solvates: A Structural Study of Methyl Cholate Solvates. *Cryst. Growth Des.* **2017**, *17*, 5712−5724.
(17) Bērziņš, A.; Skarbulis, E.; Actiņš, A. Structural Characterization and Rationalization of Formation, Stability, and Transformations of Benperidol Solvates. *Cryst. Growth Des.* **2015**, *15*, 2337−2351.
(18) Roy, S.; Quiñones, R.; Matzger, A. J. Structural and Physicochemical Aspects of Dasatinib Hydrate and Anhydrate Phases. *Cryst. Growth Des.* **2012**, *12*, 2122−2126.
(19) Vippagunta, S. R.; Brittain, H. G.; Grant, D. J. W. Crystalline Solids. *Adv. Drug Delivery Rev.* **2001**, *48*, 3−26.
(20) Infantes, L.; Fábián, L.; Motherwell, W. D. S. Organic Crystal Hydrates: What Are the Important Factors for Formation. *CrystEngComm* **2007**, *9*, 65−71.
(21) Tilbury, C. J.; Chen, J.; Mattei, A.; Chen, S.; Sheikh, A. Y. Combining Theoretical and Data-Driven Approaches To Predict Drug Substance Hydrate Formation. *Cryst. Growth Des.* **2018**, *18*, 57−67.
(22) Braun, D. E.; Kahlenberg, V.; Griesser, U. J. Experimental and Computational Hydrate Screening: Cytosine, 5-Flucytosine, and Their Solid Solution. *Cryst. Growth Des.* **2017**, *17*, 4347−4364.
(23) Brittain, H. G. *Polymorphism in Pharmaceutical Solids*; Informa Healthcare USA, Inc.: New York, NY, 2009.
(24) Braun, D. E.; Koztecki, L. H.; Mcmahon, J. A.; Price, S. L.; Reutzel-Edens, S. M. Navigating the Waters of Unconventional Crystalline Hydrates. *Mol. Pharmaceutics* **2015**, *12*, 3069−3088.
(25) Authelin, J. R. Thermodynamics of Non-Stoichiometric Pharmaceutical Hydrates. *Int. J. Pharm.* **2005**, *303*, 37−53.
(26) Mimura, H.; Kitamura, S.; Kitagawa, T.; Kohda, S. Characterization of the Non-Stoichiometric and Isomorphic Hydration and Solvation in FK041 Clathrate. *Colloids Surf., B* **2002**, *26*, 397−406.
(27) Braun, D. E.; Griesser, U. J. Stoichiometric and Non-stoichiometric Hydrates of Brucine. *Cryst. Growth Des.* **2016**, *16*, 6111−6121.
(28) Tieger, E.; Kiss, V.; Pokol, G.; Finta, Z.; Dušek, M.; Rohlíček, J.; Skořepová, E.; Brázda, P. Studies on the Crystal Structure and Arrangement of Water in Sitagliptin Tartrate Hydrates. *CrystEngComm* **2016**, *18*, 3819−3831.
(29) Khankari, R. K.; Grant, D. J. W. Pharmaceutical Hydrates. *Thermochim. Acta* **1995**, *248*, 61−79.
(30) Stephenson, G. A.; Groleau, E. G.; Kleemann, R. L.; Xu, W.; Rigsbee, D. R. Formation of Isomorphic Desolvates: Creating a Molecular Vacuum. *J. Pharm. Sci.* **1998**, *87*, 536−542.
(31) Aitipamula, S.; Chow, P. S.; Tan, R. B. H. Polymorphism in Cocrystals: A Review and Assessment of Its Significance. *CrystEngComm* **2014**, *16*, 3451.
(32) Healy, A. M.; Worku, Z. A.; Kumar, D.; Madi, A. M. Pharmaceutical Solvates, Hydrates and Amorphous Forms: A Special Emphasis on Cocrystals. *Adv. Drug Delivery Rev.* **2017**, *117*, 25−46.
(33) Clarke, H. D.; Arora, K. K.; Wojtas, Ł.; Zaworotko, M. J. Polymorphism in Multiple Component Crystals: Forms III and IV of Gallic Acid Monohydrate. *Cryst. Growth Des.* **2011**, *11*, 964−966.
(34) Braun, D. E.; Bhardwaj, R. M.; Florence, A. J.; Tocher, D. A.; Price, S. L. Complex Polymorphic System of Gallic Acid - Five Monohydrates, Three Anhydrates, and over 20 Solvates. *Cryst. Growth Des.* **2013**, *13*, 19−23.
(35) Reutzel-Edens, S. M.; Bush, J. K.; Magee, P. A.; Stephenson, G. A.; Byrn, S. R. Anhydrates and Hydrates of Olanzapine: Crystallization, Solid-State Characterization, and Structural Relationships. *Cryst. Growth Des.* **2003**, *3*, 897−907.
(36) Oliver-Shaffer, P.; Shapiro, G.; Chesworth, R.; Kishida, M.; Ishige, T. Crystalline Form of (R)-7-Chloro-N-(Quinuclidin-3-Yl) Benzo [B] Thiophene-2-Carboxamide Hydrochloride Monohydrate. U.S. Patent 2014/0249179, 2014.
(37) Giannozzi, P.; Baroni, S.; Bonini, N.; Calandra, M.; Car, R.; Cavazzoni, C.; Ceresoli, D.; Chiarotti, G. L.; Cococcioni, M.; Dabo, I.; Dal Corso, A.; de Gironcoli, S.; Fabris, S.; Fratesi, G.; Gebauer, R.; Gerstmann, U.; Gougoussis, C.; Kokalj, A.; Lazzeri, M.; Martin-Samos, L.; Marzari, N.; Mauri, F.; Mazzarello, R.; Paolini, S.; Pasquarello, A.; Paulatto, L.; Sbraccia, C.; Scandolo, S.; Sclauzero, G.; Seitsonen, A. P.; Smogunov, A.; Umari, P.; Wentzcovitch, R. M. QUANTUM ESPRESSO: A Modular and Open-Source Software Project for Quantum Simulations of Materials. *J. Phys.: Condens. Matter* **2009**, *21*, 395502.
(38) Van De Streek, J.; Neumann, M. A. Validation of Molecular Crystal Structures from Powder Diffraction Data with Dispersion-Corrected Density Functional Theory (DFT-D). *Acta Crystallogr., Sect. B: Struct. Sci., Cryst. Eng. Mater.* **2014**, *70*, 1020−1032.
(39) Gelbrich, T.; Hursthouse, M. B. A Versatile Procedure for the Identification, Description and Quantification of Structural Similarity in Molecular Crystals. *CrystEngComm* **2005**, *7*, 324−336.
(40) Spek, A. L. Structure Validation in Chemical Crystallography. *Acta Crystallogr., Sect. D: Biol. Crystallogr.* **2009**, *65*, 148−155.
(41) Vyazovkin, S.; Burnham, A. K.; Criado, J. M.; Pérez-Maqueda, L. a.; Popescu, C.; Sbirrazzuoli, N. ICTAC Kinetics Committee Recommendations for Performing Kinetic Computations on Thermal Analysis Data. *Thermochim. Acta* **2011**, *520*, 1−19.
(42) Khawam, A.; Flanagan, D. R. Solid-State Kinetic Models: Basics and Mathematical Fundamentals. *J. Phys. Chem. B* **2006**, *110*, 17315−17328.
(43) Khawam, A.; Flanagan, D. R. Basics and Applications of Solid-State Kinetics: A Pharmaceutical Perspective. *J. Pharm. Sci.* **2006**, *95*, 472−498.

DOI: 10.1021/acs.cgd.7b01561
Cryst. Growth Des. 2018, 18, 2100−2111

(44) Bērziņš, A.; Actiņš, A. Dehydration of Mildronate Dihydrate: A Study of Structural Transformations and Kinetics. *CrystEngComm* **2014**, *16*, 3926.
(45) Shankland, N.; David, W. I. F.; Shankland, K.; Kennedy, A. R.; Frampton, C. S.; Florence, A. J. Structural Transformations in Zopiclone. *Chem. Commun.* **2001**, *21*, 2204−2205.
(46) Burger, A.; Ramberger, R. On the Polymorphism of Pharmaceuticals and Other Molecular Crystals. I. *Microchim. Acta* **1979**, *72*, 259−271.
(47) Dolomanov, O. V.; Bourhis, L. J.; Gildea, R. J.; Howard, J. a. K.; Puschmann, H. OLEX2: A Complete Structure Solution, Refinement and Analysis Program. *J. Appl. Crystallogr.* **2009**, *42*, 339−341.
(48) Sheldrick, G. M. A Short History of SHELX. *Acta Crystallogr., Sect. A: Found. Crystallogr.* **2008**, *64*, 112−122.
(49) Macrae, C. F.; Bruno, I. J.; Chisholm, J. A.; Edgington, P. R.; McCabe, P.; Pidcock, E.; Rodriguez-Monge, L.; Taylor, R.; van de Streek, J.; Wood, P. A. Mercury CSD 2.0 - New Features for the Visualization and Investigation of Crystal Structures. *J. Appl. Crystallogr.* **2008**, *41*, 466−470.
(50) Greenspan, L. Humidity Fixed Points of Binary Saturated Aqueous Solutions. *J. Res. Natl. Bur. Stand., Sect. A* **1977**, *81A*, 89−96.
(51) Altomare, A.; Cuocci, C.; Giacovazzo, C.; Moliterni, A.; Rizzi, R.; Corriero, N.; Falcicchio, A. EXPO2013: A Kit of Tools for Phasing Crystal Structures from Powder Data. *J. Appl. Crystallogr.* **2013**, *46*, 1231−1235.
(52) Altomare, A.; Campi, G.; Cuocci, C.; Eriksson, L.; Giacovazzo, C.; Moliterni, A.; Rizzi, R.; Werner, P.-E. Advances in Powder Diffraction Pattern Indexing: N-TREOR09. *J. Appl. Crystallogr.* **2009**, *42*, 768−775.
(53) Boultif, A.; Louër, D. Powder Pattern Indexing with the Dichotomy Method. *J. Appl. Crystallogr.* **2004**, *37*, 724−731.
(54) Le Bail, A.; Duroy, H.; Fourquet, J. L. Ab-Initio Structure Determination of LiSbWO6 by X-Ray Powder Diffraction. *Mater. Res. Bull.* **1988**, *23*, 447−452.
(55) Dollase, W. A. Correction of Intensities for Preferred Orientation in Powder Diffractometry: Application of the March Model. *J. Appl. Crystallogr.* **1986**, *19*, 267−272.
(56) March, A. Mathematische Theorie der Regelung nach der Korngestalt bei affiner Deformation. *Z. Kristallogr. - Cryst. Mater.* **1932**, *81*, 285−297.
(57) Perdew, J. P.; Burke, K.; Ernzerhof, M. Generalized Gradient Approximation Made Simple. *Phys. Rev. Lett.* **1996**, *77*, 3865−3868.
(58) Grimme, S. Semiempirical GGA-Type Density Functional Constructed with a Long-Range Dispersion Correction. *J. Comput. Chem.* **2006**, *27*, 1787−1799.
(59) Lund, A. M.; Orendt, A. M.; Pagola, G. I.; Ferraro, M. B.; Facelli, J. C. Optimization of Crystal Structures of Archetypical Pharmaceutical Compounds: A Plane-Wave DFT-D Study Using Quantum Espresso. *Cryst. Growth Des.* **2013**, *13*, 2181−2189.
(60) Frisch, M. J.; Trucks, G. W.; Schlegel, H. B.; Scuseria, G. E.; Robb, M. A.; Cheeseman, J. R.; Scalmani, G.; Barone, V.; Mennucci, B.; Petersson, G. A.; Nakatsuji, H.; Caricato, M.; Li, X.; Hratchian, H. P.; Izmaylov, A. F.; Bloino, J.; Zheng, G.; Sonnenberg, J. L.; Hada, M.; Ehara, M.; Toyota, K.; Fukuda, R.; Hasegawa, J.; Ishida, M.; Nakajima, T.; Honda, Y.; Kitao, O.; Nakai, H.; Vreven, T.; Montgomery, J. A. J.; Peralta, J. E.; Ogliaro, F.; Bearpark, M.; Heyd, J. J.; Brothers, E.; Kudin, K. N.; Staroverov, V. N.; Kobayashi, R.; Normand, J.; Raghavachari, K.; Rendell, A.; Burant, J. C.; Iyengar, S. S.; Tomasi, J.; Cossi, M.; Rega, N.; Millam, J. M.; Klene, M.; Knox, J. E.; Cross, J. B.; Bakken, V.; Adamo, C.; Jaramillo, J.; Gomperts, R.; Stratmann, R. E.; Yazyev, O.; Austin, A. J.; Cammi, R.; Pomelli, C.; Ochterski, J. W.; Martin, R. L.; Morokuma, K.; Zakrzewski, V. G.; Voth, G. A.; Salvador, P.; Dannenberg, J. J.; Dapprich, S.; Daniels, A. D.; Farkas, Ö.; Foresman, J. B.; Ortiz, J. V; Cioslowski, J.; Fox, D. J. *Gaussian 09, Revision D.01*; Gaussian Inc.: Wallingford, CT, 2009.

DOI: 10.1021/acs.cgd.7b01561
Cryst. Growth Des. 2018, 18, 2100−2111

IV

Kons, A., Bērziņš, A., Actiņš, A.

POLYMORPHS AND HYDRATES OF SEQUIFENADINE HYDROCHLORIDE: CRYSTALLOGRAPHIC EXPLANATION OF OBSERVED PHASE TRANSITIONS AND THERMODYNAMIC STABILITY

Cryst. Growth Des. **2017**, 17, 1146–1158

CRYSTAL GROWTH & DESIGN

Article

pubs.acs.org/crystal

Polymorphs and Hydrates of Sequifenadine Hydrochloride: Crystallographic Explanation of Observed Phase Transitions and Thermodynamic Stability

Artis Kons,* Agris Bērziņš, and Andris Actiņš

Faculty of Chemistry, University of Latvia, Jelgavas iela 1, Riga, LV-1004, Latvia

Supporting Information

ABSTRACT: In this study, detailed analysis of crystal structures was used to rationalize the observed stability and phase transformations of sequifenadine hydrochloride polymorphs and hydrates, as well as to understand the observed structural diversity. The performed polymorph and hydrate screening revealed the existence of six polymorphs and four hydrates. Crystal structures of these phases were determined either from single crystal or from powder diffraction data. The different possibilities for packing of sequifenadine cations were found to be the main reason for the observed structural diversity of polymorphs. The hydrate structures were found to be structurally similar and related to those of particular polymorphs, which was consistent with the observed easy phase transitions among the related pairs.

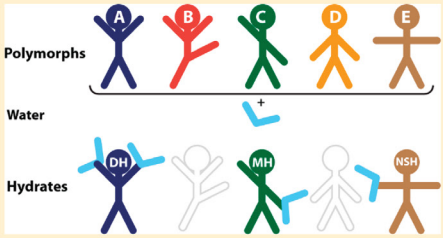

1. INTRODUCTION

Active pharmaceutical ingredients (APIs) can exist in different crystalline modifications, such as polymorphs and solvates/hydrates. Polymorphism is the ability of solids to crystallize in two or more distinct crystalline forms. Pseudopolymorphs or solvates (including hydrates) are crystalline solids that contain one or more solvent molecules in the crystal lattice in either stoichiometric or nonstoichiometric ratio.[1,2] In some cases,[3−5] solvates may be the only way to obtain certain polymorphs or hydrates. Screening for crystalline forms is important, because polymorphic and pseudopolymorphic transformations have been shown to affect the physicochemical properties of a compound, such as density,[6] stability,[7] solubility,[8] and dissolution rate,[9] due to the differences in crystal structures.

In general, knowledge of polymorph and pseudopolymorph crystal structures is a prerequisite for understanding phase stability, transformations, and physicochemical properties. Although single crystal X-ray diffraction is the ultimate technique for determining the crystal structure of APIs, the main limitation of this method is the requirement of a single crystals of suitable size, quality, and stability, which is not always feasible. Many crystalline solids can be obtained only as microcrystalline powders, for example, phases prepared by solid-state desolvation processes[10] and by solid state grinding.[11,12] In such circumstances, powder X-ray diffraction (PXRD) becomes the first choice method for structural analysis. Crystal structures can now be determined relatively easily from laboratory PXRD data through the development of the direct-space approach.[13,14]

Sequifenadine (1-azabicyclo[2.2.2]oct-3-yl[bis(2-methylphenyl)]-methanol) hydrochloride (Figure 1) is a H_1-receptor antagonist which also inhibits 5-HT_1 receptors of serotonin, thus decreasing the activity of allergy mediators histamine and serotonin.[15,16] Sequifenadine is a quinuclidine derivative, which is structurally related to quifenadine.[17] To the best of our

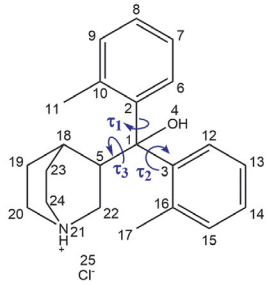

Figure 1. Molecular structure of sequifenadine hydrochloride with the numbering of non-hydrogen atoms and labeling of flexible dihedral angles.

Received: October 19, 2016
Revised: January 12, 2017
Published: January 23, 2017

DOI: 10.1021/acs.cgd.6b01534
Cryst. Growth Des. 2017, 17, 1146−1158

knowledge, there are no reports on the existence of polymorphs or solvates of sequifenadine hydrochloride.

The aims of this study were to (1) perform screening of the polymorphs and hydrates, determine their crystal structures, stability, and phase transformations between them; and (2) use the obtained crystallographic information and the experimental data to rationalize the phase transformations and stability as well as packing similarities. Screening of polymorphs and hydrates was carried out using the crystallization in various solvents and by solid state transformation at different temperatures and relative humidity conditions. Stability and phase transformations among the obtained crystalline forms were investigated by PXRD, differential scanning calorimetry (DSC), thermogravimetry analysis (TGA), variable temperature X-ray diffraction (VT-XRD), and dynamic vapor sorption analysis. Slurry-bridging experiments at room temperature were carried out in order to ascertain the relative thermodynamic stability of the polymorphs. Crystal structures of six polymorphs and three hydrates are presented. The phase transformations and stabilities were rationalized based on the obtained data.

2. EXPERIMENTAL SECTION

2.1. Materials. Racemic Sequifenadine hydrochloride (purity >99%) was obtained from JSC Olainfarm (Olaine, Latvia). The sample consisted of the commercial dihydrate (DH) phase. Inorganic compounds and organic solvents of analytical grade were purchased from commercial sources and used without further purification.

2.2. Sample Preparation. Polymorph A was obtained by recrystallization from THF or by dehydration of DH at 80 °C/0% relative humidity. Polymorph B was prepared by slow evaporation of the solution of sequifenadine hydrochloride in acetone at room temperature with relative humidity <5%. Polymorph C was obtained by desolvation of methanol solvate at 70 °C or by dehydration of DH-II at 80 °C/0% relative humidity. Polymorph D was prepared by slurring other anhydrous forms in *n*-propanol. Polymorph E was obtained by desolvation of *n*-propanol solvate at 50 °C. All anhydrous polymorphs were stored in desiccator with P_2O_5. Polymorph of dihydrate (DH-II) was obtained by hydration of the form C at 22% relative humidity. Storing forms C or DH-II in a desiccator with saturated CsF solution (RH = 3%) yielded monohydrate (MH), but nonstoichiometric hydrate (NSH) was obtained by hydration of the form E at 6−32% relative humidity. For structure determination of NSH with monohydrate stoichiometry, the sample was loaded and sealed in capillary at RH = 32%. Single crystals of DH were obtained by slow evaporation of a mixture of acetonitrile/water (95/5 v/v) and stored at ambient conditions. Methanol solvate (S_{MeOH}) was prepared by slow cooling of hot concentrated solution of sequifenadine hydrochloride in methanol and was stored in mother liquor at ambient conditions. Slow evaporation of *n*-propanol solution at room temperature with relative humidity <5% yielded *n*-propanol solvate (S_{PrOH}).

2.3. Slurry-Bridging Experiments. Slurries were prepared by adding equimolar amounts (0.28 mmol) of two polymorphs (A/B, B/C, etc.) to 5 mL of acetone or ethyl acetate. The slurries were shaken for 24 h at ambient temperature. Samples were withdrawn, filtered, dried over P_2O_5, and then examined by PXRD.

2.4. Powder X-ray Diffraction (PXRD). For routine measurements, PXRD patterns were determined on a Bruker D8 Advance diffractometer using copper radiation (CuK_α = 1.54180 Å) with Bragg−Brentano geometry and a LynxEye (1D) detector. The tube voltage and current were set to 40 kV and 40 mA, respectively. The divergence and antiscattering slits were set at 0.6 mm and 8 mm, respectively. The patterns were recorded from 3° to 30° on the 2θ scale, using a scan speed of 0.2 s/0.02. To prevent the atmospheric humidity effect, samples were covered with a 10 μm polyethylene film when necessary.

VT-PXRD experiments were determined on a Bruker D8 Discover diffractometer equipped with MRI temperature chamber and Asyco controller. Copper radiation (CuK_α = 1.54180 Å) with Bregg-Brentano geometry and a LynxEye (1D) detector was used. The divergence and antiscattering slits were set at 0.6 mm and 8 mm, respectively. The patterns were recorded from 3° to 30° on the 2θ scale, using a scan speed of 0.5 s/0.02.

For structure determination PXRD patterns were recorded on a Bruker D8 Discover diffractometer using copper radiation (CuK_α = 1.54180 Å) in transmission mode and a LynxEye (1D) detector. The tube was employed with voltage and current settings of 40 kV and 40 mA. The sample was loaded into a special glass nr. 10 capillary (0.5 mm diameter). To capillary spinner (60 rpm) was used to minimize instrumental and sample packing aberrations. An upper knife edge was used to reduce the background produced by air scattering, and a lower knife edge was used to block the primary beam. The diffractometer incident beam path was equipped with a Göbel mirror, Soller slit, and 0.6 mm divergence slit, while the diffracted beam path was equipped with only a Soller slit. The diffraction patterns were recorded on the 2θ scale from 3 or 5 to 70° with 0.01° increments, using a scan speed of 36 s per step.

2.5. Single Crystal X-ray Diffraction (SCXRD). The single-crystal X-ray diffraction data for sequifenadine hydrochloride DH was collected at 173 K on a Nonius Kappa CCD diffractometer using Mo Kα radiation (λ = 0.71073 Å) and Oxford Cryostream open-flow nitrogen cryostat for sample temperature control. The structures were solved by direct methods in OLEX2[18] software and refined by full-matrix least-squares on F^2 using SHELXL.[19] All non-hydrogen atoms were refined anisotropically. Mercury 3.7[20] software was used for crystal structure analysis and simulation of PXRD patterns, based on the crystal structure data.

2.6. Differential Scanning Calorimetry/Thermogravimetric Analysis (DSC/TGA). DSC/TGA analyses were performed with a Mettler Toledo TGA/DSC2 instrument. Open and closed 100 μL aluminum pans were used. Heating of samples from 25 to 350 °C was performed at a heating rate of 10 °C·min^{-1} under a 100 mL·min^{-1} nitrogen flow. The sample mass was approximately 7−15 mg. To identify the phase that is formed after the thermal event, the DSC/TG experiment was stopped just after this event, and PXRD analysis of the sample was performed.

2.7. Water Vapor Sorption and Desorption Studies. Dynamic vapor sorption experiments were performed on a Surface Measurement Systems DVS Advantage. All samples (5−12 mg) were initially dried under a 200 mL stream of N_2 to establish the equilibrium dry mass at 25 °C. The samples were studied over a selected humidity range (from 0−35% RH to 0−100% RH) at 25 °C. Each humidity step was taken with the equilibration set to dm/dt 0.002%/min on a 5 min time frame (with the minimum hold time of 10 min and the maximum of 300 min).

Additionally, water vapor sorption and desorption were studied in desiccators with controlled relative humidity (RH) by using PXRD to analyze the phase transitions taking place. To provide a variety of RH values, saturated salt solutions and P_2O_5 were used. The salts used in this experiment and the corresponding RH values were CsF (3%), LiBr (6%), LiCl (11%), CH_3CO_2K (23%), $MgCl_2$ (32%), NaBr (56%), KI (68%), NaCl (75%), KCl (84%), K_2SO_4 (97%), and also P_2O_5 (~0%).[21]

2.8. Structure Determination from Powder X-ray Diffraction Data. Indexing, space group determination, structure solution, and Rietveld refinement were performed using EXPO2014.[22] The unit cell dimensions were determined by applying the N-TREOR09[23] and Dicvol06[24] indexing procedures, with a set of 20−25 reflections found in 4.5−30° 2θ range. Space group determination was carried out using a statistical assessment of systematic absences, and Z' was determined based on density considerations. The cell and diffraction pattern profile parameters were refined according to the LeBail algorithm.[25] The background was modeled by a 20th order polynomial function of the Chebyshev type; peak profiles were described by the Pearson VII function.

DOI: 10.1021/acs.cgd.6b01534
Cryst. Growth Des. 2017, 17, 1146−1158

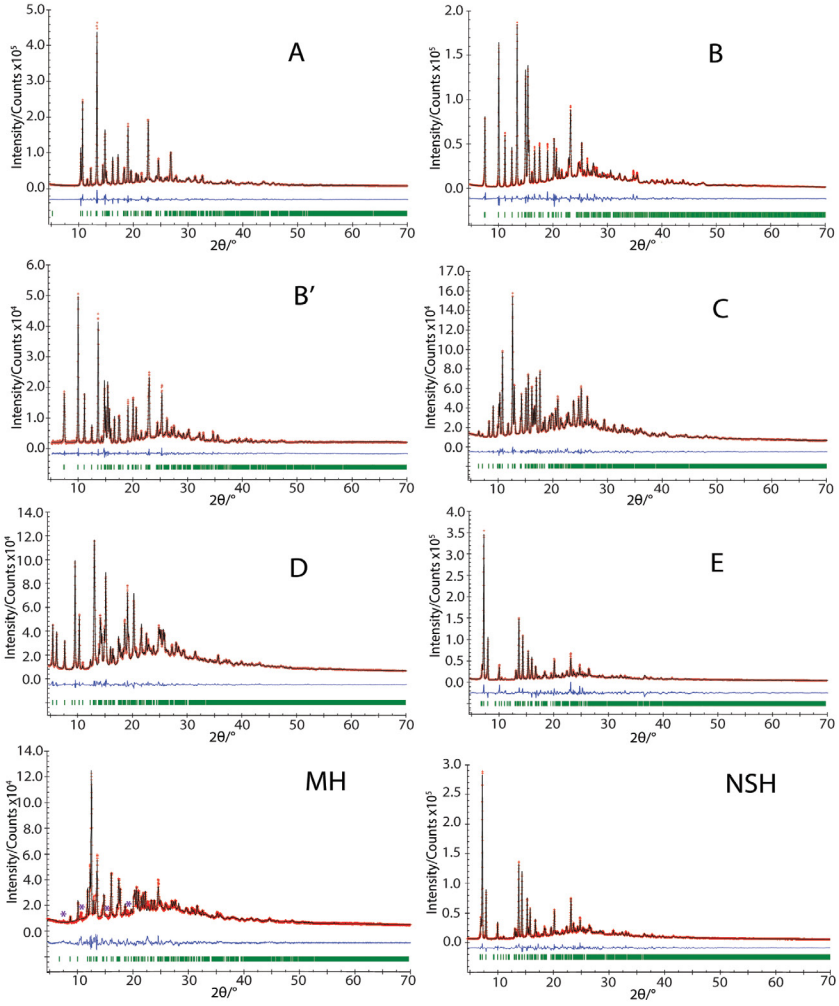

Figure 2. Final Rietveld fit for SQ-HCl forms A, B, B′ C, D, E, MH, and NSH: red crosses - measured data points; black line - calculated profile; blue line - difference curve; green tick marks - calculated peak positions. With asterisks impurities of unknown phase in MH sample are shown.

The initial geometry of molecules was taken from the crystal structure of DH. The Monte Carlo/Simulating Annealing technique was used to constantly adjust the conformation, position, and orientation of the trial model in the unit cell in order to maximize the agreement between calculated and measured diffraction data.

The Rietveld refinement was carried out using soft constraints on bond distances and angles. In the Rietveld refinement, profile and cell parameters, isotropic thermal vibration, and preferred orientation parameters (using March-Dollase model[26,27]) were optimized to get the optimal crystal structure. The planar phenyl ring was treated as a rigid body, and soft constraints on bond distances and angles were used. The final Rietveld refinement showed a good agreement between the observed and the calculated profiles (Figure 2). Relevant crystal data and refinement details for A, B, B′, C, D, E, NSH, MH, and DH are summarized in Table 1.

2.9. Theoretical Calculations. Geometries of the A, B, B′, C, D, and E crystal structures were optimized using the DFT PWscf package within Quantum ESPRESSO.[28] Calculations were performed with the PBE[29] exchange correlation functional with vdW interactions treated according to the D2 method of Grimme,[30] and ultrasoft

DOI: 10.1021/acs.cgd.6b01534
Cryst. Growth Des. 2017, 17, 1146−1158

Table 1. Crystal Data for SQ·HCl Forms

	A	B	B′	C	D	E	NSH (at RH = 32%)	MH	DH	DH-II
empirical formula	$C_{22}H_{28}NOCl$	$C_{22}H_{28}NOCl$	$C_{22}H_{28}NOCl$	$C_{22}H_{28}NOCl$	$C_{22}H_{28}NOCl$	$C_{22}H_{28}NOCl$	$C_{22}H_{30}NO_2Cl$	$C_{22}H_{30}NO_2Cl$	$C_{22}H_{32}NO_2Cl$	$C_{22}H_{32}NO_2Cl$
formula weight	357.90	357.90	357.90	357.90	357.90	357.90	375.92	375.92	377.81	377.81
sample type	powder	powder	powder	powder	powder	powder	powder	powder	single crystal	powder
crystal system	triclinic	triclinic	triclinic	monoclinic	monoclinic	monoclinic	monoclinic	monoclinic	triclinic	monoclinic
space group	$P\bar{1}$	$P\bar{1}$	$P\bar{1}$	$P21/c$	$P21/n$	$C2/c$	$C2/c$	$C2/c$	$P\bar{1}$	$C2/c$
a, Å	*7.0130(4)*	*7.2303(16)*	*7.1647(11)*	*13.7397(6)*	*7.0114(16)*	*31.182(5)*	*31.017(4)*	*28.689(17)*	*6.8261(2)*	*25.8323(8)*
b, Å	*8.5448(5*	*11.820(2)*	*11.949(2)*	*11.7290(5)*	*28.655(6)*	*14.653(2)*	*14.612(2)*	*11.009(5)*	*8.5259(2)*	*12.1918(4)*
c, Å	*17.3156(10)*	*12.041(4)*	*11.9707(17)*	*24.9421(11)*	*19.732(5)*	*22.617(4)*	*22.933(4)*	*14.505(7)*	*18.7897(5)*	*14.1149(50*
α, °	*91.524(3)*	*95.644(12)*	*95.976(9)*	90	90	90	90	90	*98.3460(10)*	90
β, °	*99.332(3)*	*99.357(10)*	*91.450(8)*	*96.229(3)*	*95.933(17)*	*123.624(8)*	*123.988(6)*	*114.33(3)*	*94.7400(10)*	*108.196(5)*
γ, °	*103.955(2)*	*92.580(12)*	*97.993(9)*	90	90	90	90	90	*101.9530(15)*	90
V, Å^3	*991.34(10)*	*1008.5(4)*	*1008.5(3)*	*3995.8(3)*	*3943.2(16)*	*8605(3)*	*8618(2)*	*4174(4)*	*1051.30(5)*	*4223.1(13)*
ρ_{calc} g·cm^{-3}	1.199	1.179	1.179	1.190	1.206	1.105	1.159	1.196	1.245	1.239
Z/Z'	2/1	2/1	2/1	8/2	8/2	*16/2*	*16/2*	8/1	2/1	8/1
temperature, K	293(2)	293(2)	293(2)	293(2)	293(2)	293(2)	293(2)	293(2)	173(2)	293(2)
$2\theta_{min}$−$2\theta_{max}$ /increment, °	4.5−70.0/0.01	4.5−70/0.01	5.0−70/0.01	4.5−70/0.01	4.5−70/0.01	4.5−70/0.01	4.5−70/0.01	4.5−70/0.01		4.5−70/0.01
R_{wp}	0.0501	0.0606	0.0387	0.0277	0.0547	0.0685	0.0551	0.0609		
R_p	0.0354	0.0416	0.0260	0.0203	0.0382	0.0494	0.0386	0.0418		
R_{exp}	0.0074	0.0083	0.0108	0.0079	0.0081	0.0095	0.0091	0.0093		
R_1 (wR_2), %									5.18 (11.93)	
total cell energy, kJ·mol^{-1} (relat. to form D)	7.9	8.0	10.2	20.0	0	8.3				

DOI: 10.1021/acs.cgd.6b01534
Cryst. Growth Des. 2017, 17, 1146−1158

pseudopotentials with a wave function cutoff of 44 Ry. Pseudopotential files C.pberrkjus.UPF, H.pbe-rrkjus.UPF, N.pbe-rrkjus.UPF, O.pberrkjus.UPF, and Cl.pbe-n-van.UDF were acquired from the Quantum ESPRESSO pseudopotential database.[31] Pseudopotentials, energy and force thresholds for structural relaxation were used as described in the literature.[32] A k-point grid of 2 × 2 × 2 was used.

Conformer and pairwise interaction energies were calculated in Gaussian09[33] using B3LYP/6-311G (d,p) level set to molecular geometries directly extracted from the crystal structures after the geometry optimization in Quantum ESPRESSO. The basis set superposition error was corrected using the counterpoise method. The interaction energy was calculated as the difference between the total energy of the dimer and the corresponding isolated moieties.

3. RESULTS AND DISCUSSION

3.1. Screening. The crystal form screening experiments reveal the existence of at least six SQ-HCl polymorphs (A, B, B′, C, D, E), two dihydrates (DH and DH-II), a monohydrate (MH), a nonstoichiometric hydrate (NSH), and numerous solvated forms which will be reported in a following paper. The polymorphs and the dihydrates were designated according to their chronological order of discovery. Figure 3 shows a

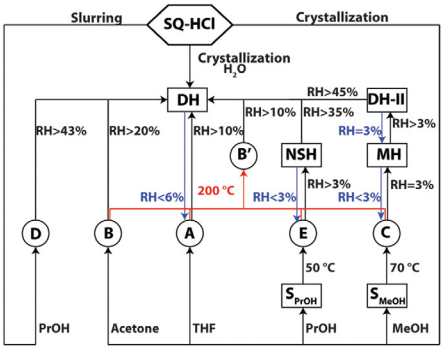

Figure 3. Preparation and phase transformations of SQ-HCl polymorphs and hydrates.

flowchart illustrating the different polymorphs and hydrates discovered, their preparation, and observed phase transitions (*n*-propanol and ethanol solvates S_{PrOH} and S_{MeOH} are also included, since polymorphs E and C are obtained by their desolvation).

It can be seen that polymorphs A and B are crystallized from different solvents, polymorph D is obtained by slurring anhydrous SQ-HCl in *n*-propanol, two other polymorphs E and C are obtained by desolvation of particular SQ-HCl solvates, whereas polymorph B′ is obtained by exposing other SQ-HCl polymorphs (except for the D) to an elevated temperature. All of the hydrates are obtained by exposing particular SQ-HCl polymorphs or lower stoichiometry hydrates to a specific relative humidity.

Overlay of the PXRD patterns of SQ-HCl crystalline forms is depicted in Figure 4. Each form has a unique and distinguishable PXRD pattern, except for pairs B/B′ and E/NSH, where the PXRD patterns are distinguishable only by small peak shifts to lower or higher 2θ values. Note that highly similar PXRD patterns suggested very high structural similarity between forms

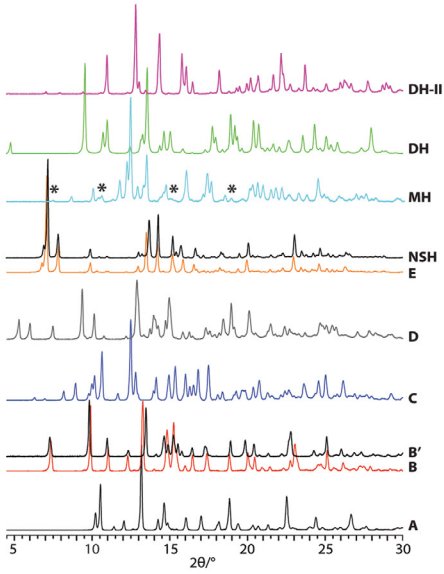

Figure 4. PXRD patterns of SQ-HCl crystalline forms A, B, B′, C, D, E, NSH, MH, DH, and DH-II. The signals of impurities of unknown phase are marked with black asterisks.

B/B′ and also between forms E/NSH. The sample of MH contains an impurity from an unknown phase (marked by black asterisks in Figure 4).

3.2. Thermal Characterization. Figure 5 shows the DSC curves for the polymorphs of SQ-HCl. All polymorphs (except B and C) display two overlapping endothermic effects associated with the melting process, immediately followed by decomposition. These results indicate that the melting temperatures (determined from the onset of the respective peaks) of polymorphs A, B, B′, D, and E range from 286 to 298 °C. Interestingly, the structurally closest polymorphs B and B′ (see section 3.53.5) have the most diverse melting temperatures. For the form C, an exothermic peak at 210 °C is observed prior to the melting/decomposition peaks. This exothermic peak corresponds to a phase transition from C to B′, as confirmed by PXRD analysis, which substantiates the monotropic relationship between these polymorphs on the basis of the heat of transition rule.[34] However, it was not possible to determine the thermodynamic relationships for other polymorphic pairs due to the coinciding melting and decomposition processes (making it impossible to directly measure the enthalpy of fusion).

Simultaneous DSC/TGA analyses of forms DH, DH-II, MH, and NSH were performed by using both open and closed pans, for more comprehensive characterization of the transformations taking place during the dehydration. The observed weight loss confirmed the given stoichiometry and are given in Table 2 together with the dehydration products.

A single dehydration endotherm of form DH was observed under both conditions with a peak temperature of 70 °C in the

DOI: 10.1021/acs.cgd.6b01534
Cryst. Growth Des. 2017, 17, 1146−1158

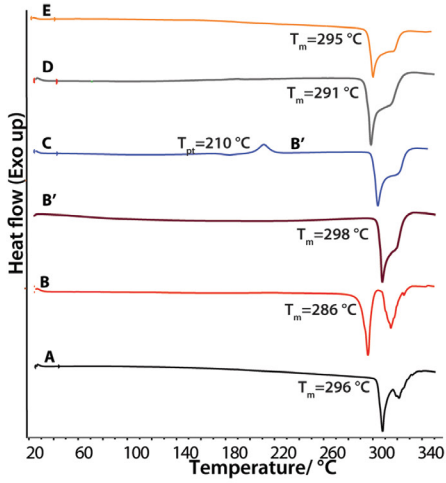

Figure 5. (A–E) DSC curves of the SQ-HCl polymorphs (heating rate 10 °C·min^{-1}).

Table 2. Observed and Calculated Weight Loss, and Dehydration Products of SQ-HCl Hydrates

hydrate	stoichiometry	observed, %	calculated, %	dehydration product
DH	1:2	8.9–9.0	9.1	A
DH-II	1:2	8.7–8.8	9.1	C
MH	1:1	4.6	4.8	C
NSH	1:1	3.7–3.9[a]	4.8	E

[a]When stored in ~25% RH at 25 °C.

open pan and 140 °C in the closed pan (Figure 6a). The observed weight loss confirmed the dihydrate stoichiometry. The dehydration product in the open pan was polymorph A, while in the closed pan it was form B′, as confirmed by the PXRD analysis.

When form DH-II was dehydrated using the open pan (Figure 6b), two-step dehydration was observed as two overlapping endothermic peaks, with peak temperatures of 79 and 96 °C. Despite the absence of distinct steps in TGA plot, the presence of two endothermic peaks is due to the formation of an intermediate monohydrate MH, with the final dehydration product being the polymorph C, as confirmed by the PXRD analysis. Following an exothermic event with a peak temperature of 200 °C a phase transition from the form C to B′ is already observed. When heating was performed using a closed pan, a different thermal plot was obtained. Before the dehydration an exothermic effect at 107 °C was observed. This exothermic peak is attributed to a solid-state phase transition from form DH-II to DH, as confirmed by the PXRD analysis. This observation substantiates that DH is thermodynamically more stable than DH-II. Following an endothermic peak at 140 °C (peak temperature) is attributed to the dehydration of DH. The dehydration product under these conditions is also the form B′. Therefore, in closed pans dehydration of DH always produced B′.

Simultaneous DSC/TGA curves of MH are shown in Figure 6c. In an open pan dehydration of MH was observed as a single broad endothermic peak in the DSC with a peak temperature of 97 °C and an associated weight loss of 4.6% in the TGA. However, in a closed pan a sharp endothermic signal immediately followed by an exothermic signal was observed just before the dehydration. We suggest that the sharp endothermic effect with a peak temperature of 123 °C is attributed to congruent melting or decomposition and the following exothermic effect with peak temperature of 128 °C is associated with crystallization of a mixture of forms DH and B′ as confirmed by the PXRD analysis. The final endothermic peak at 138 °C is attributed to the dehydration of DH by producing polymorph B′ as the dehydration product.

Simultaneous DSC/TGA curves of NSH are shown in Figure 6d. In an open pan a single broad dehydration endotherm between room temperature and 80 °C was observed. Within this interval, the associated weight loss for NSH with maximum water content was 3.7%. However, in a closed pan NSH showed an exothermic peak at around 100 °C and broader endothermic peak at around 140 °C. The exothermic peak is attributed to the decomposition of NSH to a mixture of forms DH and B′, as confirmed by the PXRD analysis. The endothermic peak, associated with a weight loss of 3.9%, was due to the dehydration of DH to B′.

3.3. Thermodynamic Stability of SQ-HCl Polymorphs.

The thermodynamic stability order of polymorphs was established by comparing computed total cell energies, using periodic DFT calculations in Quantum ESPRESSO and phase transitions occurring in slurry-bridging experiments. Total cell energies (Table 1) of forms A, B, B′, C, D, and E indicate, that the form D is the most stable form, whereas the form C is the least stable form, having the highest total cell energy of 20.0 kJ·mol^{-1} (relative to form D). Total cell energies of forms A, B, B′, and E (7.9, 10.2, 8.0, and 8.3 kJ·mol^{-1}, respectively) are too close to infer the stability relationships. Slurry-bridging experiments were carried out at ambient temperature. Because of the solvate formation with numerous different solvents, mixtures of polymorphs were slurred only in acetone and ethyl acetate to avoid the solvate formation. A summary of the results from the slurry-bridging experiments is given in Table 3. These observations demonstrate that the form D is the most thermodynamically stable form at ambient temperature, followed by forms B and A having progressively lower stability. However, relative stability between the forms B′, C, and E is unclear, but by a combination of results from experimental and computational studies it is reasonable to conclude that thermodynamic stability at ambient temperature follows the order of D > B > A > E > C.

Additionally, a comparison of the thermal stability of forms A, B, C, D, and E at an elevated temperature was performed by VT-PXRD (see S1–S5, Supporting Information). VT-PXRD patterns show that upon heating all polymorphs, except for the D, transformed to B′. The polymorph A is relatively stable between 30–220 °C; however, as the sample was heated at 220 °C for 2 h, characteristic peak of polymorph B′ appeared, and complete transformation to B′ was observed in 16 h. PXRD profile of the form C was relatively unchanged between 30–140 °C, after which the sample transformed to B′ at 150 °C. The polymorph E was relatively stable between 30–100 °C, after which the sample gradually transformed into B′, with complete transformation occurring at 190 °C.

DOI: 10.1021/acs.cgd.6b01534
Cryst. Growth Des. 2017, 17, 1146–1158

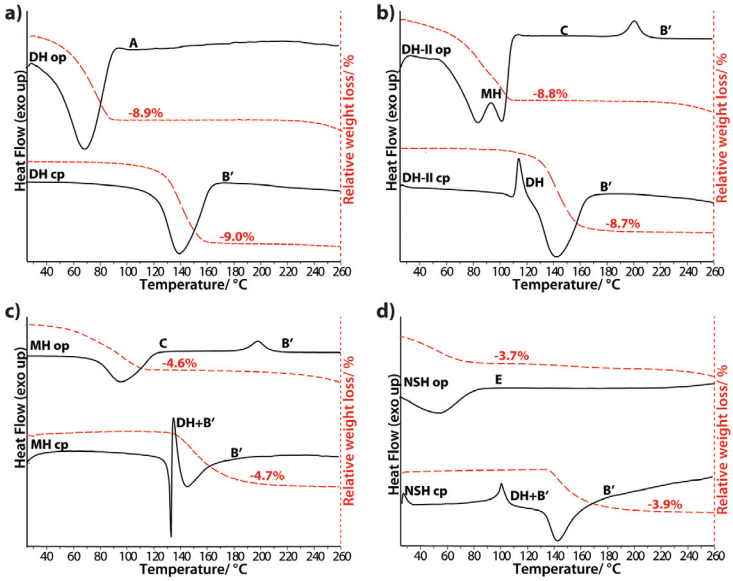

Figure 6. Simultaneous DSC and TGA curves (10 C·min^{-1}) of the SQ-HCl hydrates (a) DH, (b) DH-II, (c) MH, and (d) NSH in open pan (op) and closed pan (cp).

Table 3. Results of the Slurry-Bridging Experiments

mixture	resulting phase
A/D	D
B/D	D
B′/D	D
C/D	D
D/E	D
A/B	B
A/B′	B
B/B′	B
B/C	B
B/E	B
B′/C	B
B′/E	B
C/E	B
A/C	A
A/E	A

3.4. Dynamic Vapor Sorption (DVS) Experiments. The hydration and dehydration behavior of A/DH, C/MH/DH-II, and E/NSH was investigated by moisture sorption/desorption experiments by determining both the weight change (using DVS) and the phase composition (using PXRD) of the samples.

As shown in Figure 7a, form A undergoes full hydration to DH at 14% RH with a weight gain of 9.4%, consistent with the formation of dihydrate. No significant mass change was observed with a further increase of RH. The dehydration of DH occurs only at RH = 8%, indicating the high stability of DH. The single step hydration and dehydration, as well as the stoichiometric number of incorporated water molecules, are characteristic of stoichiometric hydrates. Small hysteresis (~6% RH) between the sorption and desorption isotherms shows that there is almost no kinetically controlled delay between the hydration and dehydration, and this reversible phase transition has a low energy barrier, suggesting that crystal structures of these two forms are likely to be similar.

The moisture sorption/desorption isotherms of forms C/MH/DH-II (Figure 7b) show one-step stoichiometric hydration and two-step dehydration. Anhydrous form C is stable in the 0−6% RH range. When RH is increased to 10%, the mass increases by 8.5%, consistent with the formation of dihydrate. A small mass increase up to 9.3% from the initial mass was observed with a further increase of RH. Form DH-II is stable only up to 45% RH, and at higher RH it irreversibly transforms to DH. The first dehydration step of DH-II occurs at RH = 3%, and lower hydrate is obtained in these conditions. The observed weight change of 4.1−4.9% is consistent with monohydrate stoichiometry, and using PXRD analysis the dehydration product was confirmed to be MH. MH is stable only in a narrow RH range (3−1%). When RH was decreased to 0% further dehydration process was observed and anhydrous form C was obtained. Similar to the A/DH system, there is only a small kinetically controlled delay between hydration and dehydration as observed by the small hysteresis (~7% RH) between the sorption and desorption isotherms.

Figure 7c shows sorption/desorption isotherms for forms E/NSH. During the sorption/desorption experiment the mass gradually changed depending on the RH, indicating that NSH is a nonstoichiometric hydrate. The maximum weight gain of

DOI: 10.1021/acs.cgd.6b01534
Cryst. Growth Des. 2017, 17, 1146−1158

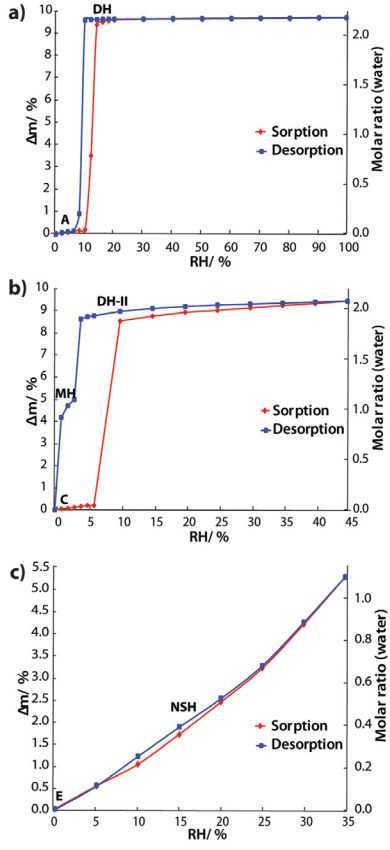

Figure 7. Moisture sorption and desorption isotherms of SQ-HCl forms A/DH (a), C/MH/DH-II (b), and E/NSH (c) at 25 °C.

5.4% was observed in 35% RH, which corresponds to ~1.2 mol of water per mol of SQ-HCl. Under higher RH, NSH irreversibly transforms to DH. PXRD analysis of the sample in variable humidity was performed to confirm that form NSH is a nonstoichiometric hydrate, and that the continuous change of mass in the sorption/desorption experiments is not caused by the adsorption of water in the sample. The results showed that peak positions and intensities changed by changing the relative humidity (Figure. 8). Such variation of the PXRD pattern is characteristic for nonstoichiometric hydrates, where water molecules can absorb and desorb from the crystal structure without introducing any significant changes, and confirms that form E is its isostructural dehydrate.

Moisture sorption analysis of forms B and D showed that these forms were stable up to 22% and 43% RH, respectively. Under higher RH, irreversible transformation to form DH was observed.

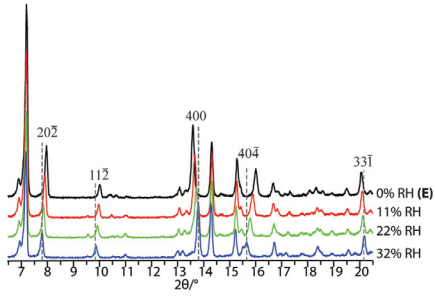

Figure 8. PXRD patterns of the SQ-HCl form NSH under different relative humidity conditions.

3.5. Crystal Structures. In this work, the crystal structures of A, B, B′, C, D, E, and MH have been determined from PXRD data because numerous attempts to grow single crystals were unsuccessful, with only microcrystalline powders being obtained, while the structure of DH was determined using SCXRD data. Unfortunately, no acceptable structure solution was found for the form DH-II, thus only the unit cell parameters determined after indexing are given. The crystallographic data for all forms are summarized in Table 1. In order to validate the crystal structures of SQ-HCl determined from the PXRD data and obtain the total cell energy, relaxation of the positions of all atoms with fixed unit cell parameters was carried out, using periodic DFT calculations in Quantum ESPRESSO software. The optimized and experimentally determined crystal structures were in good agreement (see Figures S6–S12), Supporting Information) indicating that the determined structures are close to the energy minima within the given space group and unit cell parameters. Crystal structures of forms A, B, B′, and DH were solved in the triclinic system with $P\bar{1}$ space group and contain one sequifenadine cation and one chloride anion in the asymmetric unit, except for DH, which has two additional water molecules in the asymmetric unit. Forms C, D, and E crystallize in the monoclinic system with $P2_1/c$, $P2_1/n$, and $C2/c$ space groups, respectively, and contain two sequifenadine cations and two chloride anions in the asymmetric unit. Hydrates MH and DH-II crystallize in the monoclinic system $C2/c$ space group with $Z' = 1$.

3.5.1. Conformation. The overlay of the all symmetry-independent sequifenadine cations from the crystal structures is shown in Figure 9, and the torsion angle values are summarized in Table 4. In sequifenadine cation conformational difference arises mainly due to rotation of the methylphenyl groups and quinuclidine moiety around bonds C(1)–C(2), C(1)–C(3), and C(1)–C(5). However, molecular conformations in most of the crystal structures were found to be nearly identical, except for the conformer 1 in form C (designated C1) and for the conformer 2 in form D (D2), colored light blue and red in Figure 9, respectively. Moreover, in conformer D2 the only major conformation difference is that one methylphenyl group is rotated by ~180°, while in the conformer C1 both methylphenyl groups are rotated by 95–110°. To determine which of the conformers (C1, D2 or the one observed in all other crystal structures) has lower energy (i.e., is more stable), full *in vacuo* geometry optimization for all the 11 starting

DOI: 10.1021/acs.cgd.6b01534
Cryst. Growth Des. 2017, 17, 1146–1158

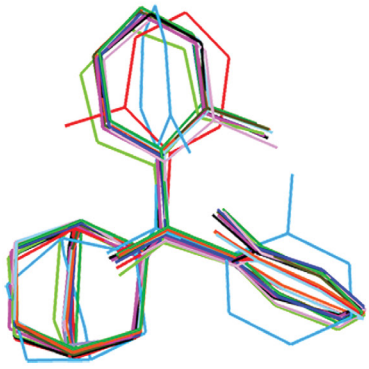

Figure 9. Superimposition of the sequifenadine cation geometries extracted from the crystal structures of A (black), B (green), B′ (yellow), C1 (light blue), C2 (violet), D1 (blue), D2 (red), E1 (brown), E2 (orange), MH (lime), and DH (pink).

geometries was performed. Energy-minimized geometry was highly similar to the starting geometry taken from the crystal structures and identical for all similar conformers (all except for C1 and D2). It was found that the energies of the conformers C1 and D2 are almost identical, while the conformer observed in all other crystal structures is lower in energy by 8.6 kJ·mol^{-1}.

Therefore, the observation that form D (containing less favorable conformer D2) is the most stable polymorph (according to both slurry bridging experiments and full energy calculation in Quantum ESPRESSO) means that intermolecular interactions in this form are significantly energetically more favorable than those in other polymorphs.

PES scans with respect to flexible torsion angles, performed in Gaussian 09, were complicated by the fact that other torsion angles changed significantly during these scans. Nevertheless, based on the obtained data it was confirmed that conformer observed in most cases is the most stable (designated GM), while confomers D2 and C1 correspond to one of the local energy minima (designated LM1 and LM2).

3.5.2. Intermolecular Interactions. The hydrogen bonding patterns in SQ·HCl forms A, B, B′, C, D, E, MH, and DH are shown in Figure 10, while the intermolecular hydrogen bond geometry is summarized in Table S1, Supporting Information. Forms A, B, and B′ are characterized by identical intermolecular hydrogen bonding pattern, where two chloride anions interact with two sequifenadine cations through N21−H···Cl25 and O4−H···Cl25 bonds, and forming a tetramer with the graph set $R_4^2(16)$. Formation of the same hydrogen bonding pattern was also observed in form E; however, as the tetramer was formed by two symmetrically different SQ cations and two different chloride anions, four different hydrogen bonds are present (N21−H···Cl50, O4−H···Cl25, N46−H···Cl25, and O29−H···Cl50). Although in forms A, B, B′ and E strong N−H···Cl, and O−H···Cl hydrogen bonds are very similar, there are differences in formation of the weak intermolecular C−H···Cl hydrogen bonds (for details see Table S1, Supporting Information). There are two weak intermolecular hydrogen bonds in B and B′ structures, whereas three in the structure of form A and five in the structure of form E. The main structural difference between polymorphs B and B′ is the location of the chloride anion with respect to the SQ cation, resulting different C−H···Cl interaction. In polymorphic form C, however, there is only one strong hydrogen bond between NH^+ group and Cl^- anion in each asymmetric moiety (graph set D), while the other potential hydrogen bond donor (OH group) does not form any conventional hydrogen bonds; however there are six weak intermolecular C−H···Cl bonds that compensate for a lack of the O−H···Cl hydrogen bonds. In form D sequifenadine cations and chloride anions do not form tetramers, but instead are connected by one-dimensional (1D) infinite chains of hydrogen bonds along the *a*-axis, characterized by graph set $C_4^2(16)$. Each chloride anion is connected to two symmetrically different sequifenadine cations through N21−H···Cl25, O4−H···Cl50, N46−H···Cl50, and O29−H···Cl25 bonds. In form MH there is a similar hydrogen bonding configuration as in forms A, B, B′ and E, although, due to the incorporation of water molecules, a hexamer is formed instead. Two sequifenadine cations, two chloride anions, and two water molecules form a hexamer with graph set $R_6^4(20)$ through N21−H···Cl25, O4−H···O26, and O26−H···Cl25 interactions. In DH structure, six different conventional hydrogen bonds are present. As in form MH, two sequifenadine cations, two

Table 4. Torsion Angles (°) for Conformers in Structures of A, B, B′, C, D, E, MH, and DH as well as for Optimized Conformers in Local Minima (LM1 and LM2) and Global Minimum (GM)

conformer	τ_1 (C5−C1−C2−C6)	τ_2 (C5−C1−C3−C12)	τ_3 (C3−C1−C5−C18)
A	108.3	5.1	−175.3
B	113.3	2.4	−170.2
B′	111.5	5.1	−175.2
C2	103.8	−0.5	−167.2
D1	110.9	4.7	−172.5
E1	105.4	6.3	−174.9
E2	106.6	15.0	−174.3
MH	100.6	−7.0	−171.9
DH	105.8	6.4	−171.4
optimized geometry GM	105.1	8.45	−172.0
C1	−0.4	100.6	−172.5
optimized geometry LM2	−2.2	104.6	−166.8
D2	−65.7	18.1	−178.6
optimized geometry LM1	−71.1	15.13	−174.5

DOI: 10.1021/acs.cgd.6b01534
Cryst. Growth Des. 2017, 17, 1146−1158

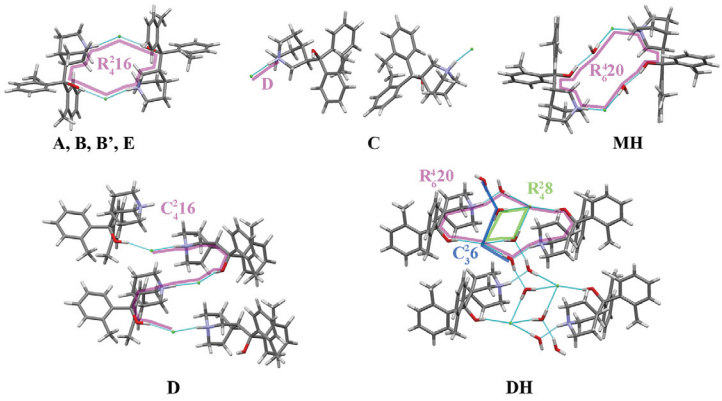

Figure 10. Hydrogen bonding patterns in SQ-HCl forms A, B, B′, C, D, E, MH, and DH.

chloride anions, and two water molecules form a hexamer with graph set $R_6^4(20)$, but the hydrogen bonds formed are different (O4−H···Cl25, N21−H···O27, and O27−H27A···Cl25). In fact, DH is the only SQ-HCl structure where the N−H···Cl hydrogen bonds are not present. Besides, the Cl^- is the acceptor for two additional hydrogen bonds with water molecules: O26−H26A···Cl25 and O26−H26B···Cl25, forming a hydrogen bonded ring, characterized by graph set $R_4^2(8)$. Additionally, water molecules and chloride anion form 1D infinite hydrogen bond chains $C_4^2(16)$ along the *a*-axis. It appears that this complex hydrogen bond network in DH structure is very efficient and therefore explains the observed stability of this form.

To investigate the energetics of the characteristic intermolecular interactions observed in SQ-HCl polymorphs, interaction energies corresponding to ions interacting via conventional hydrogen bonds were calculated. The obtained data are given in Table S2, Supporting Information. It shows that the most efficient interactions are in the structure of the form D which are 12−36 kJ/mol of SQ-HCl more efficient than in other SQ-HCl polymorphs, where sequifenadine cations form two hydrogen bonds. This is probably one of the main reasons leading to D as the most stable polymorph. Nevertheless, in this case it is not possible to distinguish whether this is due to stronger hydrogen bonds or more efficient electrostatic interactions resulting from different molecular packing. Besides, because of these electrostatic interactions, different molecular packing can strongly alter the intermolecular interaction energy between other SQ moieties as well.

Evidently, one of the main reasons for low thermodynamic stability of C is the formation of only one hydrogen bond by the sequifenadine cations.

3.5.3. Molecular Packing in SQ-HCl Polymorphs. Representation of molecular packing in SQ-HCl polymorphs and solvates is given in Figure S13, Supporting Information. The XPac[35] and Mercury software were used to establish the relationship between all crystalline forms with regard to their molecular packing similarities. On the basis of the characteristic hydrogen bonding motifs three building blocks for all five SQ-HCl polymorphs can be identified: already mentioned $R_4^2(16)$ tetramers, SQ cation, and Cl anion pair further forming tetramer $R_4^2(10)$ by additionally employing weak hydrogen bonds (both 0D building blocks), as well as already mentioned $C_4^2(16)$ chains (1D building block), all shown in Figure 11. 3D packing of these building blocks results in formation of structures of polymorphs E, C, and D, while $R_4^2(16)$ tetramers can additionally form 2D layers, by stacking of 1D chains of such tetramers (see layer 1 in Figure 11). Parallel stacking of such layers above each other results in the structure of polymorph A (stacking mode 1−1−1 in Figure 11), whereas stacking of such layers, so that adjacent layers are shifted by 1 SQ cation, results the structures of B and B′ (stacking mode 1−1′−1 in Figure 11). As expected, forms B and B′ have very similar crystal packing due to similarity in the 3D arrangement of the ions, with the most important difference being shift in the location of chloride anion. In a more detailed analysis of common building elements in SQ-HCl structures four 0D building blocks were identified: already mentioned $R_4^2(16)$ tetramers and $R_4^2(10)$ tetramers, as well as two SQ cation dimers interacting via dispersion or other weak intermolecular interactions; see Figure S14, Supporting Information.

3.5.4. Incorporation of Water Molecules in SQ-HCl Structures. Comparison of molecular packing in SQ-HCl polymorphs and hydrates reveals that all hydrate structures appear as derived from those of particular polymorphs, by incorporation of water molecules between layers or in structure voids. As can be seen in Figure 11, layer 2 is observed in both structures of A and of DH, while layer 3 is common for structures of C and MH (although here half of the molecules have different molecular conformation). The water molecules are incorporated between these layers by thus introducing no other significant change in the molecule packing except for the increase of the space between the layers. This packing similarity explains the observation that the dehydration of DH leads to form A and dehydration of MH leads to form C. Therefore, these reversible transformations require only minor molecular reorganization, which explains very easy and reversible transformation between the hydrates (DH and MH) and the respective anhydrous forms (A and C respectively).

DOI: 10.1021/acs.cgd.6b01534
Cryst. Growth Des. 2017, 17, 1146−1158

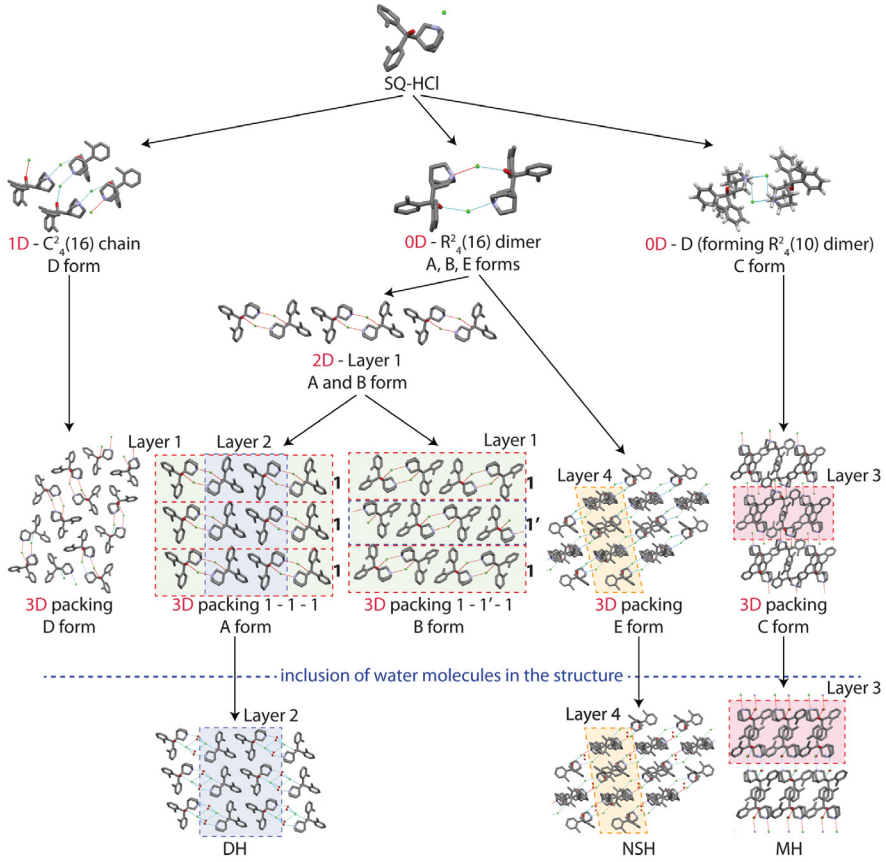

Figure 11. Building and packing similarities in SQ-HCl polymorphs and hydrates (layer 1 is colored green, layer 2 is colored blue, layer 3 is colored red, and layer 4 is colored orange).

As expected, NSH and its isostructural dehydrate E share an identical 3D packing, as water molecules are situated in the voids of structure of polymorph E; see Figure 12. Additionally, layer 4 is common for both structures of E and of NSH, and is the most invariable and characteristic part of these structures. Water molecules in NSH form hydrogen bond with the chloride anion, while only dispersion interactions are formed with SQ cation.

Typically, the unit cell of nonstoichiometric hydrates expands during sorption and contracts during desorption,[36−38] but in this case the volumes of fully dehydrated structure (form E) and NSH structure, containing the maximum detected amount of water (at RH = 32%), are almost the same (see Table 1). Figure 12 shows that form E contains 8 water accessible voids with a total volume of about 645 Å^3 (calculated in Mercury with default parameters using contact surface), which is about the same as the volume occupied by the 16 water molecules (2 per asymmetric unit) in the NSH structure with the monohydrate stoichiometry. As the positions of the voids in form E and the positions of the water molecules in NSH are identical, the voids are created due to the loss of the water molecules. Interestingly, after the dehydration the structure does not shrink, explaining almost identical volumes of both forms. However, there are still small voids in the NSH structure because only part of the voids in the E structure are filled by the water molecules. More detailed analysis, however, showed that insertion of water molecules increases the distance between layers 4 (increase of lattice parameter *c* by 1.4% and shift of peaks (202) and (404) to higher *d* values, see Figure 8), whereas the packing in other crystallographic directions becomes more compact (decrease of lattice parameters *a* and *b* by 0.5% and 0.3% and shift of peak (400) to lower *d* values; see Figure 8).

Similar incorporation of water molecules in structures of B and D is not possible since there are no structure voids nor

DOI: 10.1021/acs.cgd.6b01534
Cryst. Growth Des. 2017, 17, 1146−1158

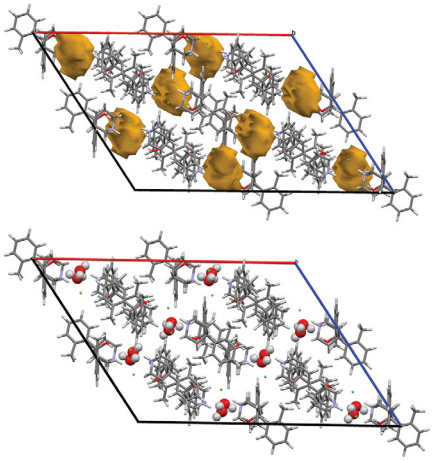

Figure 12. Crystal structure of form E with structure voids highlighted in brown and the crystal structure of NSH with water molecules enlarged for clarity.

layers, between which water molecules could squeeze in with retention of efficient packing. The obtained crystallographic data (see Table 1) and observed phase transformations suggest that the crystal structure of DH-II is similar to that of MH (and therefore also C), with additional water molecules in the crystal structure.

4. CONCLUSIONS

In the present work, six new anhydrous polymorphs (A, B, B′, C, D, and E), two dihydrates (DH and DH-II), a monohydrate (MH), and a nonstoichiometric hydrate (NSH) of SQ-HCl are reported. Polymorph A is obtained by dehydration of the dihydrate DH or by recrystallization from tetrahydrofuran. Polymorph B is obtained by recrystallization from acetone, and polymorph D is obtained by slurring anhydrous SQ-HCl in *n*-propanol. The methanol and *n*-propanol solvates are used as precursors to obtain C and E polymorphs through the thermal desolvation, whereas polymorph B′ is obtained by exposing other SQ-HCl polymorphs (except for the D) to elevated temperature. All of the hydrates are obtained by exposing particular SQ-HCl polymorphs or lower stoichiometry hydrates to a particular relative humidity.

Thermodynamic stability of polymorphs has been established from thermal analysis, slurry-bridging experiments, and DFT calculations, confirming that stability at ambient temperature follows the order of D > B > A > E > C, while form B′ is stable at elevated temperature. DVS and DSC analysis confirms that DH is the most stable hydrate.

Although three different conformations of sequifenadine cation are observed in SQ-HCl polymorph structures, structural analysis showed that the major difference between all polymorphs is the mode of packing of the SQ and chloride ions in the crystal structures, with three different hydrogen bonding patterns being one of the building elements resulting in different molecular packing. All hydrate structures appear as derived from those of particular polymorphs by incorporation of water molecules between layers or in structure voids. The products of phase transformations during the hydration and dehydration confirm the observed structural similarities, while the ease of these transformations shows the limited structural change involved in this process, as suggested by the structure analysis.

■ ASSOCIATED CONTENT

Supporting Information

The Supporting Information is available free of charge on the ACS Publications website at DOI: 10.1021/acs.cgd.6b01534.

Additional data from the variable temperature PXRD measurements, comparison of experimental and optimized crystal structures, analysis of molecular packing, as well as intermolecular interactions and their energy (PDF)

Accession Codes

CCDC 1510409−1510417 contain the supplementary crystallographic data for this paper. These data can be obtained free of charge via www.ccdc.cam.ac.uk/data_request/cif, or by emailing data_request@ccdc.cam.ac.uk, or by contacting The Cambridge Crystallographic Data Centre, 12 Union Road, Cambridge CB2 1EZ, UK; fax: +44 1223 336033.

■ AUTHOR INFORMATION

Corresponding Author

*Telephone: +(371)-67033907. E-mail: artis.kons@lu.lv.

ORCID

Artis Kons: 0000-0002-4055-8442

Notes

The authors declare no competing financial interest.

■ REFERENCES

(1) Hilfiker, R. In *Crystallization*; Beckmann, W., Ed.; Wiley-VCH Verlag GmbH & Co. KGaA: Weinheim, Germany, 2013; pp 85−103.
(2) Brittain, H. G. *J. Pharm. Sci.* **2012**, *101*, 464−484.
(3) Vangala, V. R.; Chow, P. S.; Tan, R. B. H. *CrystEngComm* **2013**, *15*, 878−889.
(4) Zhang, Q.; Lu, L.; Dai, W.; Mei, X. *CrystEngComm* **2014**, *16*, 1919−1926.
(5) Wang, X.; Wu, S.; Dong, W.; Gong, J. *Org. Process Res. Dev.* **2013**, *17*, 1110−1116.
(6) Zeidan, T. A.; Trotta, J. T.; Chiarella, R. A.; Oliveira, M. A.; Hickey, M. B.; Almarsson, Ö.; Remenar, J. F. *Cryst. Growth Des.* **2013**, *13*, 2036−2046.
(7) Yu, L.; Stephenson, G. A.; Mitchell, C. A.; Bunnell, C. A.; Snorek, S. V.; Bowyer, J. J.; Borchardt, T. B.; Stowell, J. G.; Byrn, S. R. *J. Am. Chem. Soc.* **2000**, *122*, 585−591.
(8) Pudipeddi, M.; Serajuddin, A. T. M. *J. Pharm. Sci.* **2005**, *94*, 929−939.
(9) Van Tonder, E. C.; Maleka, T. S. P.; Liebenberg, W.; Song, M.; Wurster, D. E.; de Villiers, M. M. *Int. J. Pharm.* **2004**, *269*, 417−432.
(10) Guo, F.; Harris, K. D. M. *J. Am. Chem. Soc.* **2005**, *127*, 7314−7315.
(11) Trask, A. V.; van de Streek, J.; Motherwell, W. D. S.; Jones, W. *Cryst. Growth Des.* **2005**, *5*, 2233−2241.
(12) Zhou, Y.; Guo, F.; Hughes, C. E.; Browne, D. L.; Peskett, T. R.; Harris, K. D. M. *Cryst. Growth Des.* **2015**, *15*, 2901−2907.
(13) Lim, G. K.; Fujii, K.; Harris, K. D. M.; Apperley, D. C. *Cryst. Growth Des.* **2011**, *11*, 5192−5199.
(14) Fujii, K.; Uekusa, H.; Itoda, N.; Yonemochi, E.; Terada, K. *Cryst. Growth Des.* **2012**, *12*, 6165−6172.

DOI: 10.1021/acs.cgd.6b01534
Cryst. Growth Des. 2017, 17, 1146−1158

(15) Gankina, E. M.; Porodenko, N. V.; Kondratenko, R. Y.; Severin, E. S.; Kaminka, M. E.; Mashkovskii, M. D. *Pharm. Chem. J.* **1992**, *26*, 373−376.
(16) Mashkovsky, M. D.; Yakhontov, L. N. In *Progress in Drug Research/Fortschritte der Arzneimittelforschung/Progrès des Recherches Pharmaceutiques*; Birkhäuser Basel: Basel, 1969; *13*, pp 293−339.
(17) Kons, A.; Rutkovska, L.; Bērziņš, A.; Bobrovs, R.; Actiņš, A. *CrystEngComm* **2015**, *17*, 3627−3635.
(18) Dolomanov, O. V.; Bourhis, L. J.; Gildea, R. J.; Howard, J. A. K.; Puschmann, H. *J. Appl. Crystallogr.* **2009**, *42*, 339−341.
(19) Sheldrick, G. M. *Acta Crystallogr., Sect. A: Found. Crystallogr.* **2008**, *64*, 112−122.
(20) Macrae, C. F.; Bruno, I. J.; Chisholm, J. A.; Edgington, P. R.; McCabe, P.; Pidcock, E.; Rodriguez-Monge, L.; Taylor, R.; van de Streek, J.; Wood, P. A. *J. Appl. Crystallogr.* **2008**, *41*, 466−470.
(21) Greenspan, L. *J. Res. Natl. Bur. Stand., Sect. A* **1977**, *81A*, 89−96.
(22) Altomare, A.; Cuocci, C.; Giacovazzo, C.; Moliterni, A.; Rizzi, R.; Corriero, N.; Falcicchio, A. *J. Appl. Crystallogr.* **2013**, *46*, 1231−1235.
(23) Altomare, A.; Campi, G.; Cuocci, C.; Eriksson, L.; Giacovazzo, C.; Moliterni, A.; Rizzi, R.; Werner, P.-E. *J. Appl. Crystallogr.* **2009**, *42*, 768−775.
(24) Boultif, A.; Louër, D. *J. Appl. Crystallogr.* **2004**, *37*, 724−731.
(25) Le Bail, A.; Duroy, H.; Fourquet, J. L. *Mater. Res. Bull.* **1988**, *23*, 447−452.
(26) Dollase, W. A. *J. Appl. Crystallogr.* **1986**, *19*, 267−272.
(27) March, A. *Z. Kristallogr.* **1932**, *81*, 285−297.
(28) Giannozzi, P.; Baroni, S.; Bonini, N.; Calandra, M.; Car, R.; Cavazzoni, C.; Ceresoli, D.; Chiarotti, G. L.; Cococcioni, M.; Dabo, I.; Dal Corso, A.; de Gironcoli, S.; Fabris, S.; Fratesi, G.; Gebauer, R.; Gerstmann, U.; Gougoussis, C.; Kokalj, A.; Lazzeri, M.; Martin-Samos, L.; Marzari, N.; Mauri, F.; Mazzarello, R.; Paolini, S.; Pasquarello, A.; Paulatto, L.; Sbraccia, C.; Scandolo, S.; Sclauzero, G.; Seitsonen, A. P.; Smogunov, A.; Umari, P.; Wentzcovitch, R. M. *J. Phys.: Condens. Matter* **2009**, *21*, 395502.
(29) Perdew, J. P.; Burke, K.; Ernzerhof, M. *Phys. Rev. Lett.* **1996**, *77*, 3865−3868.
(30) Grimme, S. *J. Comput. Chem.* **2006**, *27*, 1787−1799.
(31) Standard Solid State Pseudopotential Library (http://www.quantum-espresso.org/pseudopotentials).
(32) Lund, A. M.; Orendt, A. M.; Pagola, G. I.; Ferraro, M. B.; Facelli, J. C. *Cryst. Growth Des.* **2013**, *13*, 2181−2189.
(33) Frisch, M. J.; Trucks, G. W.; Schlegel, H. B.; Scuseria, G. E.; Robb, M. A.; Cheeseman, J. R.; Scalmani, G.; Barone, V.; Mennucci, B.; Petersson, G. A.; Nakatsuji, H.; Caricato, M.; Li, X.; Hratchian, H. P.; Izmaylov, A. F.; Bloino, J.; Zheng, G.; Sonnenberg, J. L.; Hada, M.; Ehara, M.; Toyota, K.; Fukuda, R.; Hasegawa, J.; Ishida, M.; Nakajima, T.; Honda, Y.; Kitao, O.; Nakai, H.; Vreven, T.; Montgomery, J. A. J.; Peralta, J. E.; Ogliaro, F.; Bearpark, M.; Heyd, J. J.; Brothers, E.; Kudin, K. N.; Staroverov, V. N.; Kobayashi, R.; Normand, J.; Raghavachari, K.; Rendell, A.; Burant, J. C.; Iyengar, S. S.; Tomasi, J.; Cossi, M.; Rega, N.; Millam, J. M.; Klene, M.; Knox, J. E.; Cross, J. B.; Bakken, V.; Adamo, C.; Jaramillo, J.; Gomperts, R.; Stratmann, R. E.; Yazyev, O.; Austin, A. J.; Cammi, R.; Pomelli, C.; Ochterski, J. W.; Martin, R. L.; Morokuma, K.; Zakrzewski, V. G.; Voth, G. A.; Salvador, P.; Dannenberg, J. J.; Dapprich, S.; Daniels, A. D.; Farkas, O.; Foresman, J. B.; Ortiz, J. V; Cioslowski, J.; Fox, D. J; Montgomery, J. A. J.; Peralta, J. E.; Ogliaro, F.; Bearpark, M.; Heyd, J. J.; Brothers, E.; Kudin, K. N.; Staroverov, V. N.; Kobayashi, R.; Normand, J.; Raghavachari, K.; Rendell, A.; Burant, J. C.; Iyengar, S. S.; Tomasi, J.; Cossi, M.; Rega, N.; Millam, N. J.; Klene, M.; Knox, J. E.; Cross, J. B.; Bakken, V.; Adamo, C.; Jaramillo, J.; Gomperts, R.; Stratmann, R. E.; Yazyev, O.; Austin, A. J.; Cammi, R.; Pomelli, C.; Ochterski, J. W.; Martin, R. L.; Morokuma, K.; Zakrzewski, V. G.; Voth, G. A.; Salvador, P.; Dannenberg, J. J.; Dapprich, S.; Daniels, A. D.; Farkas, Ö.; Foresman, J. B.; Ortiz, J. V; Cioslowski, J.; Fox, D. J. *Gaussian 09, Revision D.01*; Gaussian Inc.: Wallingford, CT, 2009.
(34) Burger, A.; Ramberger, R. *Microchim. Acta* **1979**, *72*, 259−271.
(35) Gelbrich, T.; Hursthouse, M. B. *CrystEngComm* **2005**, *7*, 324−336.
(36) Pina, M. F.; Pinto, J. F.; Sousa, J. J.; Fábián, L.; Zhao, M.; Craig, D. Q. M. *Mol. Pharmaceutics* **2012**, *9*, 3515−3525.
(37) Fujii, K.; Aoki, M.; Uekusa, H. *Cryst. Growth Des.* **2013**, *13*, 2060−2066.
(38) Kiang, Y.-H.; Cheung, E.; Stephens, P. W.; Nagapudi, K. *J. Pharm. Sci.* **2014**, *103*, 2809−2818.

DOI: 10.1021/acs.cgd.6b01534
Cryst. Growth Des. 2017, 17, 1146−1158

V

Kons, A., Rutkovska, L., Bērziņš, A., Bobrovs, R., Actiņš, A.

THREE ANHYDROUS FORMS AND A DIHYDRATE FORM OF QUIFENADINE HYDROCHLORIDE: A STRUCTURAL STUDY OF THE THERMODYNAMIC STABILITY AND DEHYDRATION MECHANISM

CrystEngComm. **2015**, 17, 3627–3635

CrystEngComm

PAPER

View Article Online
View Journal | View Issue

Cite this: *CrystEngComm*, 2015, 17, 3627

Three anhydrous forms and a dihydrate form of quifenadine hydrochloride: a structural study of the thermodynamic stability and dehydration mechanism†

Artis Kons,*[a] Ligita Rutkovska,[a] Agris Bērziņš,[a] Raitis Bobrovs[ab] and Andris Actiņš[a]

Received 2nd March 2015,
Accepted 6th April 2015

DOI: 10.1039/c5ce00426h

www.rsc.org/crystengcomm

Crystal structures of dihydrate (DH) and three anhydrous forms (A, B and C) of quifenadine (1-azabicyclo[2.2.2]oct-8-yl-diphenyl-methanol) hydrochloride are presented, and crystal structure information is used to explain and rationalize the relative stability of polymorphs and observed phase transformations. The dehydration mechanism of the hydrate is provided by interpreting the results obtained in studies of crystal structures, dehydration kinetics and thermal analysis. Structural analysis is used to explain the observed relative stability of the anhydrous phases and the hydrate. The crystal structures have been determined either from single crystal (form DH) or from powder diffraction data (forms A, B and C). All three polymorphs consist of similar hydrogen bonded tetramers, and the structural differences arise due to differences in conformation or/and molecular packing.

Introduction

Polymorphism is the ability of compounds to crystallize into different crystalline modifications. If solvent molecules are incorporated in the crystal lattice along with the host molecules in either stoichiometric or nonstoichiometric ratio, then the resulting phase is called a solvate or pseudopolymorph. Polymorphism and pseudopolymorphism of an active pharmaceutical ingredient (API) have an influence on its solubility, bioavailability and stability. Therefore, identification of polymorphs and pseudopolymorphs, comparison of their physicochemical properties and understanding conditions of transformations between crystalline forms are very important.[1–3]

From pharmaceutical and supramolecular points of view, the knowledge of polymorph and pseudopolymorph crystal structures gives general information about their stability, formation pathways and also physicochemical properties. Moreover, studies on the polymorphism of organic systems can lead to generalization of the fundamental aspects of the structure–property relationship.[4,5] Therefore, crystal structure determination of pharmaceutically active compounds during the crystalline phase screening process is advisable.

Commonly, the crystal structure is determined from single-crystal X-ray diffraction data. However, many crystalline solids cannot be prepared in the form of an appropriate single crystal. In such a case, powder X-ray diffraction methods can be used to extract structural information. The development of direct-space approaches for structure solution has given the opportunity to solve crystal structures even from diffraction data recorded using laboratory X-ray powder diffraction instrumentation.[6,7]

Quifenadine (1-azabicyclo[2.2.2]oct-8-yl-diphenyl-methanol), a quinuclidine derivative, is an antihistaminic agent that decreases the impact of histamine by blocking histamine H1-receptors in the peripheral tissues and activates the enzyme diamine oxidase (histaminase).[8,9] To the best of our knowledge, there are no reports on the existence of polymorphs or solvates of quifenadine hydrochloride.

In the present paper, thermal analytical techniques (differential thermal analysis, thermogravimetric analysis and hot-stage microscopy), powder and single-crystal X-ray diffractometry, and gravimetric moisture sorption studies were employed to characterize the solid state forms of quifenadine hydrochloride. Crystal structures of three anhydrous forms and a hydrate are presented, and crystal structure information is used to explain and rationalize the relative stability of polymorphs and observed phase transformations. Structural transformations during the dehydration process of hydrate

[a] *Faculty of Chemistry, University of Latvia, Kr. Valdemara iela 48, Riga, Latvia. E-mail: artis.kons@lu.lv.*
[b] *Formulation and Drug Delivery Research Group, School of Pharmacy and Biomolecular Sciences, Liverpool John Moores University, Liverpool, UK*

† CCDC 1051731, 1051732, 1051733, and 1051734 contain the supplementary crystallographic data for the structures of DH, A, B, and C, respectively. For crystallographic data in CIF or other electronic format see DOI: 10.1039/c5ce00426h

have been interpreted and the relative stabilities of anhydrous phases and the hydrate have been evaluated.

Experimental section

Materials

Quifenadine hydrochloride (purity >99%) was obtained from JSC Olainfarm (Olaine, Latvia). The sample consisted of a commercial racemic mixture of polymorph A. Inorganic compounds and organic solvents of analytical grade were purchased from commercial sources and used without further purification.

Sample preparation

Dihydrate DH was prepared by recrystallizing quifenadine hydrochloride from water and stored under ambient conditions. Single crystals of DH were obtained by slow evaporation from a mixture of acetonitrile/water (95/5 v/v) and stored in mother liquor under ambient conditions. Anhydrous form B was obtained by dehydration of DH at 80 °C or 0% relative humidity and stored over a desiccant. Anhydrous form C was prepared by recrystallizing from *n*-butanol or iso-butanol and stored under ambient conditions. Anhydrous form A was used without further purification.

Single-crystal X-ray diffraction (SCXRD)

The single-crystal X-ray diffraction data for quifenadine hydrochloride DH was collected at 173 K using a Nonius Kappa CCD diffractometer with Mo K_α radiation (λ = 0.71073 Å) and an Oxford Cryostream open-flow nitrogen cryostat for sample temperature control. The structure was solved by direct methods in OLEX2 (ref. 10) software and refined by full-matrix least-squares on F^2 using SHELXL.[11] All non-hydrogen atoms were refined anisotropically. The most disagreeable reflections with $\Delta(F^2)$ values greater than 5 su were omitted (6 reflections with *hkl* indices: 0 1 2; 2 −3 2; 1 −3 4; 3 −3 2; −2 −2 8 and −2 −1 6). Mercury 3.3 (ref. 12) software was used for crystal structure analysis and simulation of powder X-ray diffraction patterns based on crystal structure data. Crystallographic face indexing of quifenadine dihydrate was done at room temperature. Face indexing was performed using Collect software.[13]

Powder X-ray diffraction (PXRD)

For routine measurements of phase composition, the PXRD patterns were recorded on a Bruker D8 Advance diffractometer using copper radiation (CuK_α λ = 1.54180 Å) with Bragg–Brentano geometry and LynxEye (1D) detector. The tube voltage and current were set to 40 kV and 40 mA, respectively. The divergence and antiscattering slits were set at 0.6 mm, and the receiving slit was set at 8 mm. The patterns were recorded from 3° to 30° on the 2θ scale, using a scan speed of 0.2 s per 0.02°.

For structure determination, PXRD patterns were recorded on a Bruker D8 Discover diffractometer using copper radiation (CuK_α λ = 1.54180 Å) in transmission mode and LynxEye (1D) detector. The tube was employed with voltage and current settings of 40 kV and 40 mA. The sample was loaded into a special glass Nr. 10 capillary (0.5 mm diameter). A capillary spinner (60 rpm) was used to minimize instrumental and sample packing aberrations. The incident beam path of the diffractometer was equipped with a Göbel mirror, Soller slits, and a 0.6 mm divergence slit, while the diffracted beam path was equipped only with Soller slits. The diffraction patterns were recorded from 3 or 5 to 70° on the 2θ scale at a 0.01° step size using a scan speed of 20 s per step.

Structure determination from powder X-ray diffraction data

Indexing of powder diffraction patterns of quifenadine hydrochloride A, B and C forms was carried out with programs Dicvol91 (ref. 14) and X-Cell[15,16] using the first 25 reflections (2θ < 35°). All forms were indexed with a triclinic unit cell. The cell and diffraction pattern profile parameters were refined using the Pawley method[17] (R_{wp} = 2.29%, R_p = 1.40% for A; R_{wp} = 1.09%, R_p = 0.75% for B and R_{wp} = 2.33%, R_p = 1.77% for C). The space group for all forms was assigned to $P\bar{1}$ with Z = 2.

The trial geometry model was generated by optimizing the quifenadine molecule using DFT-D within the DMol^3 module[18] in Materials Studio 7 using the PBE functional[19] and a dispersion correction according to Grimme.[20]

The Monte Carlo/Simulating Annealing search algorithm in the MS Powder Solve package was used to constantly adjust the conformation, position, and orientation of the trial model in the unit cell in order to maximize the agreement between the calculated and the measured diffraction data. The structural solution obtained from the Powder Solve was refined by Rietveld refinement based on the measured powder X-ray diffraction pattern. In the Rietveld refinement, cell parameters, the position and orientation of motion groups, torsion angles, thermal vibration, and preferred orientation parameters (using March–Dollase model[21,22]) were optimized to get the optimum crystal structure. Aromatic rings were treated as rigid groups. The final Rietveld refinement showed a good agreement between the observed and the calculated profiles (Fig. 2). Relevant crystal data and refinement details for A, B, C and DH are summarized in Table 1.

Calculation of lattice and interaction energy in PIXEL

The crystal lattice and interaction energy calculations were performed according to the semiempirical PIXEL methodology (with code provided in the CLP software suite). Empirical parameters were used as provided in the literature.[23] The atom positions for the purposes of this calculation were obtained by a standard procedure using RETCIF and RETCOR modules. The hydrogen atom positions were renormalized. Molecular electron density calculations were performed in Gaussian 09 (ref. 24) at the MP2/6-31G(d,p)

Table 1 Crystal structure data for quifenadine hydrochloride forms

Cell parameters	A form	B form	C form	DH form
Chemical formula	$C_{20}H_{24}NOCl$	$C_{20}H_{24}NOCl$	$C_{20}H_{24}NOCl$	$C_{20}H_{24}NOCl\cdot 2H_2O$
Formula weight	329.86	329.86	329.86	365.88
Sample type	Powder	Powder	Powder	Single crystal
Crystal system	Triclinic	Triclinic	Triclinic	Triclinic
Space group	$P\bar{1}$	$P\bar{1}$	$P\bar{1}$	$P\bar{1}$
Temperature	293(2)	293(2)	293(2)	173(2)
a, Å	6.372(2)	6.408(5)	6.449(2)	6.339(1)
b, Å	12.699(5)	9.281(6)	12.951(3)	8.601(2)
c, Å	10.759(4)	18.356(2)	11.222(2)	18.404(5)
α, °	96.03(2)	113.09(3)	97.60(1)	100.02(2)
β, °	98.88(2)	83.62(3)	106.61(2)	92.32(3)
γ, °	80.68(2)	116.50(3)	75.25(2)	103.45(2)
V, Å^3	845.9(1)	895.8(1)	862.9(1)	957.5(3)
ρ_{calc}, g cm^{-3}	1.295	1.223	1.270	1.269
Z (Z')	2 (1)	2 (1)	2 (1)	2 (1)
R_{wp} (R_p)/R_1 (wR_2), %	2.81 (1.89)	1.41 (0.99)	3.12 (2.32)	4.8 (14.8)

level using standard grid parameters. The condensation level 4 and a calculation cutoff value of 40 Å were used.

Differential thermal analysis/thermogravimetric analysis (DTA/TG)

DTA/TG analysis was performed using an Exstar6000 TG/DTA6300 (SII) instrument. Open aluminium pans were used. Heating of samples from 30 °C to 320 °C was performed at a heating rate of 10 °C min^{-1} under 100 mL min^{-1} nitrogen flow. The sample mass was approximately 5–7 mg.

Gravimetric determination of water content

The water sorption and desorption processes of B and DH were measured in desiccators with controlled relative humidity (RH). To provide a variety of RH values, saturated salt solutions and P_2O_5 were used. The salts used for this experiment and the corresponding RH values were LiBr (6%), LiCl (11%), CH_3CO_2K (23%), $MgCl_2$ (32%), NaBr (56%), KI (68%), NaCl (75%), KCl (84%), K_2SO_4 (97%), and also P_2O_5 (~0%).[25]

Dehydration kinetics

Nonisothermal experiments were performed at heating rates of 0.5, 2, 3, 4, 5 and 10 °C min^{-1}, and isothermal studies were carried out at 30–70 °C using an Exstar6000 TG/DTA6300 (SII) apparatus. For isothermal studies, the heater unit was preset to the required temperature allowing fast stabilization of the necessary temperature at the start of the experiment. The sample mass was 6.0 ± 0.5 mg, and the nitrogen flow rate was 100 ± 10 mL min^{-1}.

Hot stage microscopy (HSM)

For thermo-microscopic investigations, a Laborlux 12 PolS (Leitz) polarized light microscope equipped with a heating stage and a Newtronic heating control module was used. The heating rate was 5° min^{-1}. Images were collected using Leica Application Suite software from a DFC450 (Leica) digital microscope camera.

Results and discussion

An initial polymorph screening of quifenadine hydrochloride was performed by recrystallization from 16 solvents (water, methanol, ethanol, *n*-propanol, iso-propanol, *n*-butanol, iso-butanol, acetone, ethyl acetate, acetonitrile, dichloromethane, chloroform, toluene, 1,4-dioxane, dimethylformamide and dimethyl sulfoxide) at variable temperatures. Through the screening process, quifenadine hydrochloride was found to crystallize in three crystalline modifications: two polymorphs (A and C) and dihydrate (DH). Additional polymorph B was obtained by dehydration of DH.

Thermal analysis

The DTA and TG thermal profiles of all crystalline forms are illustrated in Fig. 3. No thermal event was observed for forms A and C in the temperature range prior to the degradation near 320 °C, confirming that these forms are unsolvated. One small exothermal event (at 168 °C) was observed for form B in the temperature range until the onset of degradation. This exothermal effect is attributed to a solid-state phase transition from form B to A as confirmed by PXRD analysis, which substantiates the monotropic relationship between these polymorphs on the basis of the heat of transition rule.[26]

Dehydration of form DH was observed as an endothermic peak in the DTA over a temperature range from 40 °C to 80 °C and associated weight loss of 9.5% in the TGA. A mass loss of 9.5% corresponds to 1.92 mol of water, which is only slightly below the theoretical value of 2 mol of water per mole of quifenadine hydrochloride. No further weight loss was observed until the material began to degrade at 320 °C. The dehydration product was polymorph B, as confirmed by the PXRD analysis. After the dehydration, an exothermic effect observed at 171 °C corresponds to phase transition from polymorph B to form A.

Thermodynamic stability of quifenadine hydrochloride polymorphs

To better understand the relative thermodynamic relationships of quifenadine hydrochloride polymorphs, solvent-mediated slurry-bridging (SMSB) experiments were carried out at various temperatures. Mixtures of forms A/B, A/C and B/C were slurried in acetone and tetrahydrofuran at 5 and 25 °C, in acetonitrile at 60 °C and in butyl acetate at 120 °C. That resulted in conversion of mixtures of A/B and A/C to pure form A at all temperatures and similarly a mixture of polymorphs B/C converted to form C. These observations

indicate that form A is the most thermodynamically stable form at all studied temperatures and form C is more thermodynamically stable than form B.

On the basis of the density rule,[26] the most stable crystal structure should have the highest density. As shown in Table 1, the density values calculated from crystal structure data for forms A, B, and C indicate that the stability follows the order of A > C > B. Additionally, a comparison of the stability of forms A, B and C was performed using calculation of the crystal lattice energy for these forms with PIXEL software. As expected, form A has the most negative total lattice energy of −382.7 kJ mol^{-1} and therefore is the most stable form at 0 K, followed by form C (−371.4 kJ mol^{-1}) and form B with the highest lattice energy of −361.5 kJ mol^{-1}. Therefore the lattice energy calculations correlate with conclusions obtained from SMSB experiments and crystal density results.

These observations indicate that form A is the most thermodynamically stable form at all temperatures and has a monotropic relationship with both forms B and C. Polymorphs B and C also have a monotropic relationship with form C being thermodynamically more stable than form B.

Moisture sorption experiments

In moisture sorption/desorption experiments, both the weight change and the phase composition of the samples were determined. The moisture sorption/desorption isotherms of quifenadine hydrochloride forms B/DH (Fig. 4) show that the anhydrous form B is stable (*i.e.*, does not absorb water) up to 11% relative humidity (RH). Under higher moisture conditions, the sample takes up water and transforms to DH. The measured mass increase of 9.5% is in agreement with thermogravimetric measurement (1.92 mol of water). By decreasing the humidity, when the RH is less than 6%, the dehydration of DH occurs and polymorph B is obtained. The distinct steps and the presence of hysteresis between the sorption and desorption isotherms are characteristic of stoichiometric hydrates. However, small hysteresis (~5% of RH) shows that this reversible phase transformation has a low energy barrier suggesting that crystal structures of these two forms can be similar. The sorption/desorption isotherms show that DH is a very stable hydrate, which releases water only at very low relative humidity, whereas form B is an unstable anhydrous phase, absorbing water already at 11% RH.

Moisture sorption analysis of form C showed that it was stable up to 89% RH (for 2 months), while at higher RH it transformed to form DH, but form A was stable up to 100% RH and transformation to DH was not observed after 2 months.

Analysis of the crystal structures

Structures of polymorphs A, B, and C were determined using powder X-ray diffraction data, but the structure of DH was determined using single-crystal X-ray diffraction data. Crystallographic data for all forms are shown in Table 1. All these crystalline modifications crystallize in the $P\bar{1}$ space group. The crystal structure of each polymorph contains one quifenadine cation and one chloride anion in the asymmetric unit, whereas dihydrate contains additional two water molecules in the asymmetric unit.

Overlay of powder X-ray diffraction (PXRD) patterns of quifenadine hydrochloride polymorphs and dihydrate is depicted in Fig. 5. Each form has a unique and distinguishable PXRD pattern. A comparison of PXRD patterns shows that forms A and C have similar positions and intensities of first four peaks suggesting structural similarities. The agreement between the experimental and crystal structure simulated PXRD patterns of DH confirms the identity of the polycrystalline phase.

A quifenadine molecule consists of two terminal phenyl groups, one quinuclidine moiety and one hydroxyl group linked together by a quaternary carbon. The conformational state of the quifenadine cation in all four structures is compared in Fig. 6, and the torsion angle values are summarized in Table 2 (numbering of atoms is given in Fig. 1). This analysis was carried out using the molecules of identical enantiomers in a quifenadine hydrochloride racemic mixture. It can be seen that the molecular conformation in all four forms is very similar and only minor conformational differences arise mainly due to rotation of phenyl groups and quinuclidine moiety around C(3)–C(1), C(4)–C(1) and C(2)–C(1) bonds. The torsion angle ∠C2–C1–C3–C8 in the DH structure is closest to the corresponding angle found in the cation of form B, whereas the torsion angles ∠C2–C1–C4–C10 and ∠C3–C1–C2–C6 in the DH structure are closest to the corresponding angles found in the cation of form C.

In quifenadine hydrochloride, the only easily acessible strong hydrogen bond acceptor is the Cl$^-$ anion, and the possible donors allowing the formation of strong hydrogen bonds are the NH$^+$ group and the hydroxyl group. As shown in Fig. 7, all three polymorphs have the same hydrogen bonding pattern where two chloride anions interact with two quifenadine cations through N14–H···Cl24 and O5–H···Cl24 bonds and form a tetramer with the graph set $R_4^2(16)$. Slight differences were observed in the hydrogen bond geometry and interaction energy between hydrogen bond donor and acceptor moieties in each of these three forms (see Table 3). Form A has the most negative interaction energy between cation and anion moieties, but interaction energy in forms B and C is almost equal. The hydrogen bonding pattern in the quifenadine hydrochloride dihydrate structure is more complex due to the presence of two water molecules increasing

Table 2 Torsion angle values describing conformational states of quifenadine cations in crystalline forms A, B, C and DH

	∠C2–C1–C3–C8	∠C2–C1–C4–C10	∠C3–C1–C2–C6
A	−36.9(3)	46.2(3)	174.0(2)
B	−24.0(6)	60.5(10)	179.3(4)
C	−44.1(4)	59.0(4)	172.2(2)
DH	−15.9(2)	61.9(2)	169.88(14)

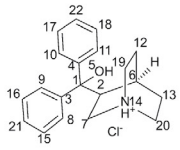

Fig. 1 Molecular structure of quifenadine hydrochloride with the numbering of non-hydrogen atoms.

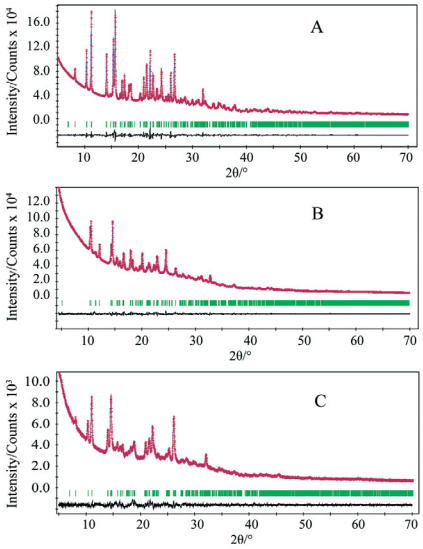

Fig. 2 Final Rietveld fit for quifenadine hydrochloride forms A, B and C: red crosses – measured data points; blue line – calculated profile; black line – difference curve; green tick marks – calculated peak positions.

the number of possible hydrogen bond acceptor and donor sites. In this structure, hydrogen bonds are formed between NH^+ group and water molecules. The Cl^- is involved in

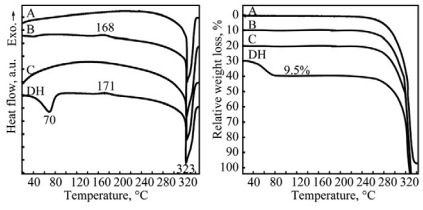

Fig. 3 Stacked plots of the DTA and TG curves of quifenadine hydrochloride forms A, B, C and DH.

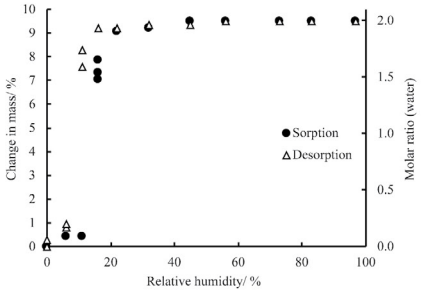

Fig. 4 Moisture sorption and desorption isotherms of quifenadine hydrochloride forms B/DH at 30 °C.

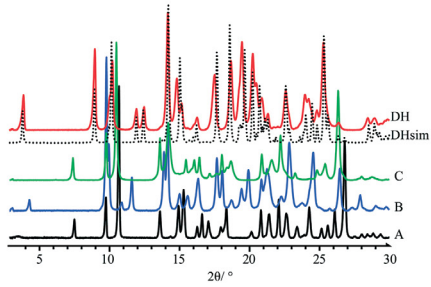

Fig. 5 PXRD patterns of quifenadine hydrochloride forms A, B, C and DH.

H-bonding with the three water molecules and also with the –OH group attached to Cl. H-bonds between water molecules are also observed. Two quifenadine cations, two chloride anions and two water molecules form a hexamer with the graph set $R_6^4(20)$ through N14–H···O25, O5–H···Cl24 and O25–H···Cl24 bonds (see Fig. 7). Two other water molecules

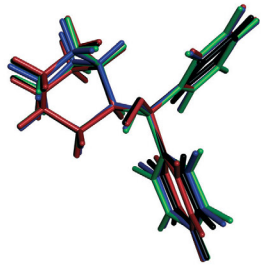

Fig. 6 Overlay of the quifenadine cations extracted from the crystal structures of A (black), B (blue), C (red) and DH (green) with superimposed quifenadine moieties.

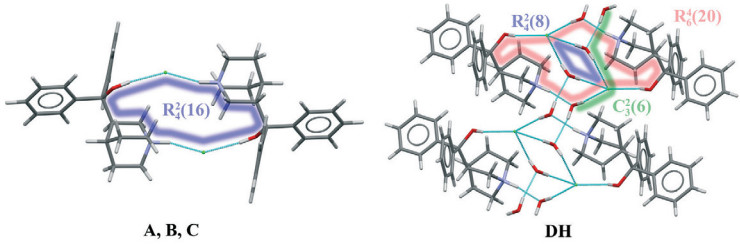

Fig. 7 The hydrogen bonding patterns in quifenadine hydrochloride forms A, B, C and DH.

Table 3 Geometry and energy data for hydrogen bonds in quifenadine hydrochloride forms A, B, C and DH

Interaction	D···A, Å	D–H···A, °	Interaction energy, kJ mol^{-1}
Form A			
O5–H···Cl24	3.096(4)	156	−423.5
N14–H···Cl24	3.010(4)	153	−446.6
Form B			
O5–H···Cl24	3.152(5)	159	−413.9
N14–H···Cl24	3.042(5)	150	−442.2
Form C			
O5–H···Cl24	3.177(7)	151	−411.5
N14–H···Cl24	3.034(7)	151	−444.6
Form DH			
O5–H···Cl24	3.197(2)	165	—[a]
N14–H···O26	2.727(2)	166	—
O25–H48···Cl24	3.171(2)	172	—
O25–H49···Cl24	3.177(2)	179	—
O25–H···O26	2.732(2)	165	—
O26–H···Cl24	3.179(2)	171	—

[a] It was not possible to perform interaction energy calculation using PIXEL code because of four chemical entities in the asymmetric unit.

form a hydrogen bonded ring with chloride anions with the graph set $R_4^2(8)$. All of the water molecules are also involved in the formation of a hydrogen bonded chain including a chloride anion ($C_3^2(6)$) perpendicular to the H-bonded hexamer $R_4^2(8)$ ring. Therefore the dehydration induces breakage of the hydrogen bond network and six hydrogen bonds are replaced with two new ones. Obviously, the water molecules play a stabilizing role in the quifenadine hydrochloride dihydrate structure by forming an efficient hydrogen bonding network, which explains its stability.

As shown in Fig. 8, forms A and C have the same monolayered molecular packing pattern where all neighboring molecules are in antiparallel orientation. The 2D pattern is defined by the same type of layers. However, there are marked differences between the packing of forms A and C and form B. The molecular packing of form B has a bilayered pattern where neighboring molecules are in the same direction and molecules in each layer are in opposite orientation to those in an adjacent layer. The molecular packing of form B has more distinguishable hydrophobic and hydrophilic

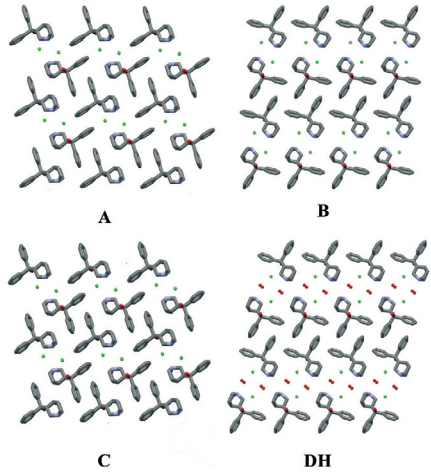

Fig. 8 The molecular packing in quifenadine hydrochloride forms A, B, C and DH (hydrogen atoms have been omitted for clarity).

layers than in forms A and C where tetramers are packed more efficiently.

The molecular packing of form DH shares common features with that of form B. The 2D structural pattern of DH is defined by the same molecular orientation and the same

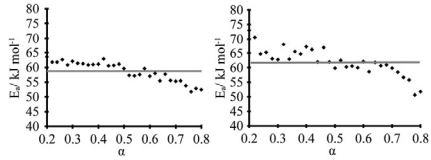

Fig. 9 Dehydration E_a values as a function of fraction dehydrated α in isothermal (left) and non-isothermal (right) modes.

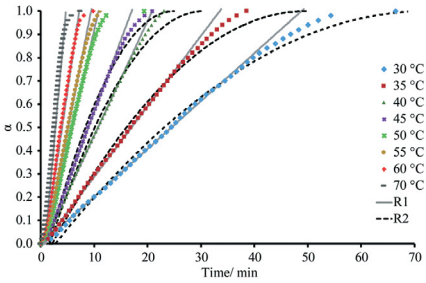

Fig. 10 Experimental and theoretical representation of the dependence of fraction dehydrated (α) on time obtained from TGA at different temperatures in isothermal mode.

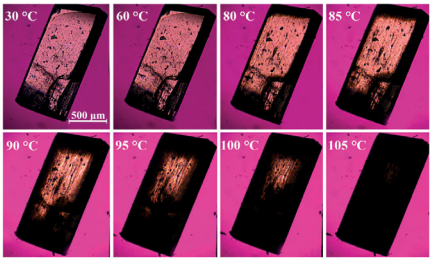

Fig. 11 Photomicrographs of the dehydration process of DH form.

arrangement of the layers with respect to each other. The only difference is the inclusion of water molecules, which are located in structural channels between hydrophilic quinuclidine groups and chloride anions. Therefore DH is a channel hydrate. Besides, water molecules are involved in the main hydrogen bonding network, which makes this hydrate stoichiometric. Due to the high structural packing similarity, it is clear why the dehydration of DH leads to form B instead of A or C. This transition does not change the parallel orientation of quifenadine cations in the crystal structure, and it only decreases the distance between the quifenadine moieties. Transformation of DH to A or C requires a significant amount of molecular reorganization, and therefore, this transition is unfavourable, as is the reverse process, explaining the observations in moisture sorption experiments.

To compare the packing efficiency and therefore the stability in all four forms, calculation of the packing index for these forms has been performed with the PLATON[27] software. PLATON calculations yielded 73.1, 71.7, 69.1 and 68.4% packing indices for forms A, C, B and DH, respectively, which are in agreement with thermodynamic stability results for these polymorphic forms. The lowest packing index of form DH, however, suggests that the presence of water molecule channels does not lead to very efficient packing, but the stability

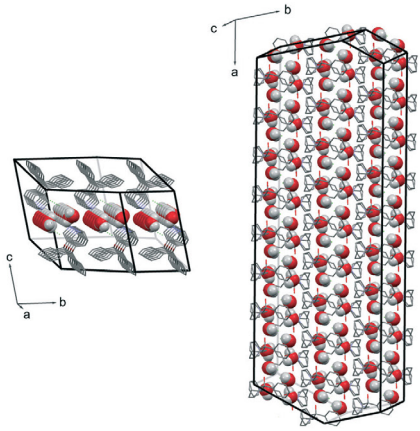

Fig. 12 Determined crystal morphology of DH crystal showing water channels along the *a*-axis.

of this crystal structure is provided by an energetically efficient hydrogen bonding network provided by the insertion of water molecules.

In order to better explore the differences between very similar forms A and C, full geometry optimization of these two crystal structures was performed using the DFT-D method within Quantum Espresso.[28] The obtained results indicated that between forms A and C there is only a small energy barrier because after geometry optimization of both experimental structures an almost identical structure was obtained. Therefore the only explanation why form C was obtained from *n*-butanol or iso-butanol instead of very similar form A can be based on the presence and strength of some specific interactions between the solvent molecules and the quifenadine and chloride moieties during the crystallization, resulting in slightly different molecular packing, which interestingly was not able to regroup to very similar but thermodynamically more stable structure A.

Dehydration kinetics

The dehydration kinetic model and activation energy (E_a) were determined in isothermal and non-isothermal modes to better understand the dehydration mechanism of DH. It is recommended to analyze the solid-state kinetics over selected fraction dehydrated (α) values because errors are usually higher at very low and high fraction dehydrated values;[29] therefore, determination of activation energy and model fitting were performed for the data $0.2 \leq \alpha \leq 0.8$. The isothermal and nonisothermal dehydration kinetics of DH were first analyzed by Friedman's isoconversional method. Fig. 9 gives calculated E_a values as a function of fraction dehydrated

α for dehydration of DH in isothermal (left) and non-isothermal (right) modes. The activation energy was determined to be 59 ± 4 kJ mol^{-1} and 62 ± 5 kJ mol^{-1} in isothermal and non-isothermal modes, respectively. The matching values of E_a calculated for both isothermal and nonisothermal modes suggest that the dehydration mechanism in both modes is the same. To identify an acceptable kinetic model, linear regression correlation coefficient (R^2) for the plot of $g(\alpha)$ *versus* t was calculated for the most common solid state kinetic models. Equally high correlation coefficients were found for both one-dimensional phase boundary reaction model R1 (R^2 = 0.9995) and two-dimensional phase boundary reaction model R2 (R^2 = 0.9994). Then the reconstruction of the dehydration curves was performed to identify the most appropriate reaction model between R1 and R2. Fig. 10 gives the experimental and theoretical dehydration isotherms (fraction dehydrated *versus* time) obtained from TGA in isothermal mode at different temperatures. As shown in Fig. 10, model R1 provides a good description of the isothermal dehydration kinetics over the $0.2 \leq \alpha \leq 0.8$ range of the fraction dehydrated. Besides, R1 is a rational dehydration model for channel type hydrate with structurally close dehydration product, as the dehydration process most likely occurs by the movement of the phase boundary in the direction of the water channels. At $\alpha > 0.8$, experimental isothermal α–time plots deviated from the linear relationship (and therefore from kinetic model R1) because the dehydration process became slower. Although similar deviation is characteristic of kinetic model R2, in this case R2 provides the worse fit to the experimental data (see Fig. 10). Therefore the observed deviation indicated that at the end of the dehydration the mechanism was changing, which probably could be caused by the presence of particles with different sizes, as large particles dehydrate slower than smaller particles.

Hot stage microscopy

The direct microscopic observations can provide useful information to identify and substantiate the best fitting kinetic model obtained from mathematical analysis of the kinetic data. As many solid-state kinetic models are based on geometric model functions, adequacy of these models can be verified by visual observation of the dehydration reaction.[30,31]

Photomicrographs taken during the dehydration of DH using hot stage microscopy are shown in Fig. 11, and crystal morphology determined by single crystal face indexing is shown in Fig. 12. From Fig. 12, it can be seen that there are channels containing water molecules along the *a*-axis in the DH structure, and during the dehydration, water escapes through these channels. This result fits with the observations from hot stage microscopy in Fig. 11, where the dehydration process initiates from both ends of the crystal, and by increasing the temperature, the reaction boundary slowly moves inwards to the center of the crystal. Therefore the microscopic observations confirm the R1 reaction model, where the dehydration process is in one dimension, and water molecules escape through the water channels along the *a*-axis.

Conclusions

Crystallization of quifenadine hydrochloride from 16 different solvents produced two anhydrous forms (A and C) and a dihydrate (DH), while the dehydration of DH produced another new polymorph (B). The same hydrogen bonding pattern (hydrogen bonded tetramer consisting of two quifenadine cations and two chloride anions) was observed in the crystal structures of all three polymorphs. Thermodynamic stability of the polymorphs was established by SMSB experiments and calculation of the crystal lattice energy. These results demonstrated that form A is the most thermodynamically stable form, followed by form C and then form B; besides, all three polymorphs have a monotropic relationship to each other.

In DH, hydrogen bonds form a complex network, with water molecules playing a stabilizing role. Water molecules are located in structure channels and dehydration produces structurally similar polymorph B. Therefore the solid-state hydration/dehydration transformation DH ↔ B is reversible under ambient conditions and depends on the relative humidity.

The dehydration of form DH was studied using various experimental methods. It was determined that the dehydration proceeds by the one-dimensional phase boundary reaction model (R1) in which the water molecules escape through the structure channels along the *a*-axis.

Acknowledgements

We wish to thank Riga Technical University Institute of Polymer Materials for the opportunity to carry out hot-stage microscopy measurements, Inese Sarcevića for the help with single-crystal structure determination and Formulation and Drug Delivery Research Group, School of Pharmacy and Biomolecular Sciences, Liverpool John Moores University for the opportunity to carry out calculations with Materials Studio.

Notes and references

1 S. Ito, M. Nishimura, Y. Kobayashi and S. Itai, *Int. J. Pharm.*, 1997, **151**, 133–142.
2 H. G. Brittain, *J. Pharm. Sci.*, 2012, **101**, 464–484.
3 R. Hilfiker, ed. W. Beckmann, *Crystallization: Basic Concepts and Industrial Applications*, Wiley-VCH Verlag GmbH & Co. KGaA, Weinheim, Germany, 2013.
4 J. Bernstein, *Cryst. Growth Des.*, 2011, **11**, 632–650.
5 G. P. Stahly, *Cryst. Growth Des.*, 2007, **7**, 1007–1026.
6 W. I. F. David, K. Shankland, J. Van De Streek, E. Pidcock, W. D. S. Motherwell and J. C. Cole, *J. Appl. Crystallogr.*, 2006, **39**, 910–915.
7 W. I. F. David and K. Shankland, *Acta Crystallogr., Sect. A: Found. Crystallogr.*, 2008, **64**, 52–64.
8 *United States Patent*, 1978, US4117139A.
9 L. Makarov, L. Balykova, O. Soldatova, V. Komolyatova and V. Serebruany, *Am. J. Ther.*, 2012, **17**, 396–401.

10 O. V. Dolomanov, L. J. Bourhis, R. J. Gildea, J. a. K. Howard and H. Puschmann, *J. Appl. Crystallogr.*, 2009, **42**, 339–341.
11 G. M. Sheldrick, *Acta Crystallogr., Sect. A: Found. Crystallogr.*, 2008, **64**, 112–122.
12 C. F. Macrae, I. J. Bruno, J. A. Chisholm, P. R. Edgington, P. McCabe, E. Pidcock, L. Rodriguez-Monge, R. Taylor, J. van de Streek and P. A. Wood, *J. Appl. Crystallogr.*, 2008, **41**, 466–470.
13 BV Nonius, *Nonius KappaCCD Collect*, 1998.
14 A. Boultif and D. Louër, *J. Appl. Crystallogr.*, 1991, **24**, 987–993.
15 A. Boultif and D. Louër, *J. Appl. Crystallogr.*, 2004, **37**, 724–731.
16 M. A. Neumann, *J. Appl. Crystallogr.*, 2003, **36**, 356–365.
17 G. S. Pawley, *J. Appl. Crystallogr.*, 1981, **14**, 357–361.
18 B. Delley, *J. Chem. Phys.*, 1990, **92**, 508–517.
19 J. Perdew, K. Burke and M. Ernzerhof, *Phys. Rev. Lett.*, 1996, **77**, 3865–3868.
20 S. Grimme, *J. Comput. Chem.*, 2006, **27**, 1787–1799.
21 A. March, *Z. Kristallogr.*, 1932, **81**, 285–297.
22 W. a. Dollase, *J. Appl. Crystallogr.*, 1986, **19**, 267–272.
23 A. Gavezzotti, *New J. Chem.*, 2011, **35**, 1360–1368.
24 M. J. Frisch, G. W. Trucks, H. B. Schlegel, G. E. Scuseria, M. A. Robb, J. R. Cheeseman, G. Scalmani, V. Barone, B. Mennucci, G. A. Petersson, H. Nakatsuji, M. Caricato, X. Li, H. P. Hratchian, A. F. Izmaylov, J. Bloino, G. Zheng, J. L. Sonnenberg, M. Hada, M. Ehara, K. Toyota, R. Fukuda, J. Hasegawa, M. Ishida, T. Nakajima, Y. Honda, O. Kitao, H. Nakai, T. Vreven, J. A. J. Montgomery, J. E. Peralta, F. Ogliaro, M. Bearpark, J. J. Heyd, E. Brothers, K. N. Kudin, V. N. Staroverov, R. Kobayashi, J. Normand, K. Raghavachari, A. Rendell, J. C. Burant, S. S. Iyengar, J. Tomasi, M. Cossi, N. Rega, J. M. Millam, M. Klene, J. E. Knox, J. B. Cross, V. Bakken, C. Adamo, J. Jaramillo, R. Gomperts, R. E. Stratmann, O. Yazyev, A. J. Austin, R. Cammi, C. Pomelli, J. W. Ochterski, R. L. Martin, K. Morokuma, V. G. Zakrzewski, G. A. Voth, P. Salvador, J. J. Dannenberg, S. Dapprich, A. D. Daniels, O. Farkas, J. B. Foresman, J. V. Ortiz, J. Cioslowski, D. J. Fox, J. Montgomery, J. A. J. E. Peralta, F. Ogliaro, M. Bearpark, J. J. Heyd, E. Brothers, K. N. Kudin, V. N. Staroverov, R. Kobayashi, J. Normand, K. Raghavachari, A. Rendell, J. C. Burant, S. S. Iyengar, J. Tomasi, M. Cossi, N. Rega, N. J. Millam, M. Klene, J. E. Knox, J. B. Cross, V. Bakken, C. Adamo, J. Jaramillo, R. Gomperts, R. E. Stratmann, O. Yazyev, A. J. Austin, R. Cammi, C. Pomelli, J. W. Ochterski, R. L. Martin, K. Morokuma, V. G. Zakrzewski, G. A. Voth, P. Salvador, J. J. Dannenberg, S. Dapprich, A. D. Daniels, Ö. Farkas, J. B. Foresman, J. V. Ortiz, J. Cioslowski and D. J. Fox, 2009.
25 L. Greenspan, *J. Res. Natl. Bur. Stand., Sect. A*, 1977, **81A**, 89–96.
26 A. Burger and R. Ramberger, *Microchim. Acta*, 1979, **72**(3–4), 273–316.
27 A. L. Spek, *Acta Crystallogr., Sect. D: Biol. Crystallogr.*, 2009, **65**, 148–155.
28 P. Giannozzi, S. Baroni, N. Bonini, M. Calandra, R. Car, C. Cavazzoni, D. Ceresoli, G. L. Chiarotti, M. Cococcioni, I. Dabo, A. Dal Corso, S. de Gironcoli, S. Fabris, G. Fratesi, R. Gebauer, U. Gerstmann, C. Gougoussis, A. Kokalj, M. Lazzeri, L. Martin-Samos, N. Marzari, F. Mauri, R. Mazzarello, S. Paolini, A. Pasquarello, L. Paulatto, C. Sbraccia, S. Scandolo, G. Sclauzero, A. P. Seitsonen, A. Smogunov, P. Umari and R. M. Wentzcovitch, *J. Phys.: Condens. Matter*, 2009, **21**, 395502.
29 A. Khawam and D. R. Flanagan, *Thermochim. Acta*, 2005, **429**, 93–102.
30 V. Koradia, H. L. D. E. Diego, M. R. Elema and J. Rantanen, *J. Pharm. Sci.*, 2010, **99**, 3966–3976.
31 A. K. Galwey, *Thermochim. Acta*, 2000, **355**, 181–238.